



University of
Sheffield

Impaired mechanoelectrical transduction
drives efferent re-innervation of inner hair
cells

By:

A. O'Connor

The University of Sheffield

Thesis submitted for: PhD

2023



Impaired mechanoelectrical transduction
drives efferent re-innervation of inner hair
cells

By:

Andrew O'Connor

Supervisor: Professor Walter Marcotti

Co-Supervisors: Dr Laura Corns, Dr Mike Bowl

The University of Sheffield

Faculty of Science

Department of Biosciences

May 2023

Acknowledgements

Firstly, I would like to thank my supervisor Professor Walter Marcotti who has been an excellent supervisor. He has been supportive throughout my time in the lab and encouraged me to push myself to achieve the best I can. I am also grateful for his patience when I explored new ideas, and for his constructive feedback when I needed it. Thanks, must also go to my co-supervisor Dr Laura Corns, she has inspired me to think of my work in new ways and helped develop the practicality of any new ideas. Additionally, a large section of this study would not have been possible had it not been for the conditional knockout strains that I was able to use. Therefore, I would like to thank Dr Mike Bowl at MRC Harwell for enabling these sections of my work to take place. I was fortunate enough to be funded by the RNID and BBSRC, who enabled this research project to take place.

The members of the Marcotti lab all deserve my thanks, both members past and present. I would like to thank Dr Federico Ceriani for helping me with any of the problems I encountered during my patch clamp experiments. I must also thank Dr Jing-Yi Jeng and Dr Samuel Webb for selflessly passing on their knowledge of immunolabelling to me, as well as providing me with feedback on my thesis. Once again, my thanks must go to Sam. He consistently encouraged me to develop myself, both as a scientist and as an individual. Whether that be helping me problem solve any issues I had or having a long chat about anything and everything – I truly appreciate it. To all those who I shared the office with whilst writing my thesis, I thank them all for having the patience to put up with me and for the support they provided to me. My thanks must also go to the technicians in the lab, their friendliness and encouragement helped me more than they will realise.

Finally, I must thank all my friends and family. Special thanks go to my mum and dad who have always supported me with whatever I endeavored to do. I am also grateful for them for being so patient and considerate when I spoke to them about my PhD work. Additionally, I would like to thank Arian Bradley, who helped me to remain motivated throughout writing my thesis and supported me in more ways than one, words cannot describe how thankful I am. Lastly, I would like to reserve a word for my ever-loving Granny, Val. She was my greatest supporter and was always so proud of everything I achieved. I know she would be even prouder now that I am completing my thesis and PhD – this is for her.

Abstract

The inner hair cells (IHCs) are the primary sensory cells within the mammalian cochlea and are responsible for detecting acoustic stimuli and converting them into electrical signals for the brain to perceive sound. This conversion is performed by the mechano-electrical transducer (MET) channels that are found on the stereocilia atop IHCs. During postnatal development IHCs receive transient axosomatic (direct) innervation by the efferent fibres which is then lost after the onset of hearing, which in mice is around postnatal day 12. Studies have shown that IHCs become re-innervated by efferent fibres in ageing mice and in mouse models with impaired MET channel function (*Myo7a^{fl/fl};Myo15 cre^{+/-}*). However, the details of how this mechanism takes place remain unclear. It is currently unknown whether the re-innervation of the IHCs occurs as a consequence of general cellular dysfunction or if it is specific to impaired MET function.

Experiments were performed using *Myo7a^{fl/fl};Myo15 cre^{+/-}* mice, and from two additional conditional knockout (cKO) mouse models that specifically disrupted neurotransmitter release in IHCs, whilst maintaining MET functionality (*Otoferlin^{tm1c};Vglut3 cre-ER^{T2}* and *Otof^{fl/fl};Myo15 cre^{+/-}*). *Myo7a* encodes for the unconventional myosin 7a, which is required for MET function, while *Otof* encodes for the Ca²⁺ sensor of neurotransmitter release otoferlin. Immunofluorescence was used to determine the expression profile of the pre- and post-synaptic proteins of the efferent system. *Ex vivo* whole cell patch-clamp electrophysiology was used to identify the function of the re-innervating efferent system.

The results show that IHCs from *Myo7a^{fl/fl} Myo15 cre^{+/-}* mice were re-innervated by the efferent fibres from about P24 onwards. Prior to the efferent re-innervation, the IHCs re-express post-synaptic small conductance Ca²⁺ activated potassium channels (SK2) but IHCs do not show functional efferent synapses until P25. This indicates the IHCs drive the efferent re-innervation. Conversely to the recent literature, the IHCs lose their afferent synapses after the re-innervation of IHCs. In both otoferlin cKO mice, there was no visible return of axosomatic efferent innervation on IHCs, indicating that the re-innervation is likely to be driven by impaired mechano-electrical transduction.

Contents

Acknowledgements	i
Abstract	ii
Contents	iii
List of Figures	vii
List of Tables	x
Abbreviations	xi
Chapter 1 – General Introduction	1
1.1 Development and function of the cochlea	2
1.1.1. The mammalian auditory system	3
1.1.2. Structure of the mammalian cochlea	5
1.1.3. IHC postnatal development.....	9
1.1.3.1 Basolateral membrane channels: pre-hearing and post-hearing changes	9
1.1.3.2. IHC stereocilia and the mechano-electrical transducer channel	13
1.1.4. IHC Afferent Innervation	20
1.1.4.1. Postnatal development of IHC afferent innervation.....	23
1.1.4.2. Ribbon synapses in the IHCs	26
1.1.5. IHC Efferent Innervation	31
1.1.5.1. Postnatal development of IHC efferent innervation.....	32
1.2. Age-related hearing loss	38
1.2.1. Pathophysiology of ARHL	40
1.2.2. Risk factors of age-related hearing loss.....	43
1.2.3. Mouse models of age-related hearing loss.....	49
1.2.4. Efferent re-innervation of mature IHCs in ageing.....	51
1.2.4.1. Efferent re-innervation in 6J mouse models	51
1.2.4.2. Biophysical and morphological changes in IHCs during ageing.....	57

1.2.4.3. Efferent re-innervation of aged IHCs can be induced by MET silencing.....	61
1.3. Inflammation in the cochlea	64
1.4. Aims and hypotheses of the present study.....	68
Chapter 2 – Methods and Materials	70
2.1. Ethics statements	71
2.1.1. Animal strains	71
2.1.2. Tamoxifen injections	73
2.2. Auditory brainstem responses	74
2.3. Single-cell electrophysiology.....	75
2.3.1. Electrophysiology set up	76
2.3.2. Tissue preparation	78
2.3.3. Experimental solutions.....	80
2.3.4. Recording pipettes	82
2.3.5. Cleaning pipettes	83
2.3.6. Whole cell patch-clamp recordings	83
2.3.7. Extracellular superfusion.....	83
2.4. Immunofluorescence microscopy	84
2.5. Analysis of immunofluorescence images	87
2.6. Genotyping	89
2.7. Statistical analysis	90
Chapter 3 - Efferent re-innervation of IHCs is caused by disrupted MET function	91
3.1. Introduction	92
3.2. Results	95
3.2.1. Axosomatic efferent innervation returns to IHCs from around P24	95
3.2.2. Progressive biophysical changes in IHCs from <i>Myo7a^{fl/fl} Myo15 cre^{+/-}</i>	102
3.2.3. ABR thresholds in <i>Myo7a^{fl/fl} Myo15 cre^{+/-}</i> mice	108

3.2.4. IHCs from <i>Myo7a^{fl/fl} Myo15 cre^{+/-}</i> mice lose ribbon synapses after the axosomatic efferent-IHC innervation has returned	112
3.2.5. The efferent innervation of IHCs lacking the harmonin protein never matures	118
3.3. Discussion	120
3.3.1. Initial changes in IHCs as axosomatic efferent innervation returns ...	120
3.3.2. Progressive physiological changes in IHCs	122
3.3.3. Efferent re-innervation returns prior to afferent synapse loss	123
3.3.4. Efferent innervation of IHCs from <i>Ush1c^{fl/fl} Myo15 cre^{+/-}</i> mice does not mature normally	124
3.3.5. Future directions for axosomatic efferent innervation studies	125
Chapter 4 – Disrupting the IHC afferent synapse does not result in efferent re-innervation	126
4.1. Introduction	127
4.2. Results	128
4.2.1. Characterising tamoxifen injections in otoferlin conditional knockout mice	128
4.2.2. IHCs from otoferlin conditional knockout mice do not have a return of axosomatic efferent innervation	139
4.3. Discussion	144
4.3.1. Tamoxifen injections from P10 induce the best knockout of otoferlin in IHCs.....	144
4.3.2. Progressive loss of otoferlin in IHCs following tamoxifen injections..	145
4.3.3. The return of axosomatic efferent innervation on IHCs was not seen in otoferlin conditional knockout mice	147
Chapter 5 - Increased immune response in the cochlea following the loss of Myo7a	149
5.1. Introduction	150
5.2. Results	153
5.2.1. Changes in the number of macrophages in the cochlea after the loss of Myo7a.....	153

5.3. Discussion	160
5.3.1. Macrophages numbers increase with age in <i>Myo7a^{fl/fl} Myo15 cre^{+/-}</i> mice	160
5.3.2. Future directions for investigating macrophages in sterile inflammation mouse models	163
Chapter 6 - General Discussion	164
6.1. The return of axosomatic efferent innervation on IHCs is driven by MET dysfunction	165
6.2. Efferent synapses return to IHCs prior to a loss of afferent synapses ..	168
6.3. Is the returning efferent innervation a result of IHC and OHC dysfunction, or IHC dysfunction alone?	169
6.4. Could neurotrophins be attracting efferent fibres to the IHCs?	170
6.5. What role is inflammation playing in hearing loss?	170
6.6. Future work	171
6.7. Conclusions	173

List of Figures

Figure 1. 1. Anatomy of the outer, middle, and inner ear.	4
Figure 1. 2. Cross section diagrams of the cochlea.	8
Figure 1. 3. Diagram showing the development of key basolateral membrane properties for IHCs.	12
Figure 1. 4. Scanning electron microscopy images of the IHC and OHC stereocilia.	14
Figure 1. 5. Diagram showing the composition of the tip link and the associated proteins at the upper tip link density.	17
Figure 1. 6. Schematic showing the 3 rows of stereocilia and the MET channels at rest, during activation and during adaptation of the MET channels.	18
Figure 1. 7. Schematic of an IHC displaying the modiolar and pillar synapses with type I SGN fibres.	22
Figure 1. 8. Diagrams depicting the innervation of the IHCs and OHCs, including an overview for the developmental timeline of the afferent innervation.	25
Figure 1. 9. Postnatal maturation of the IHC ribbon synapse and synapse morphology.	28
Figure 1. 10. Diagram indicating the IHC ribbon synapse, focusing on otoferlin and the synaptic vesicles.	30
Figure 1. 11. Schematics of the immature and mature organ of Corti, demonstrating the development of the afferent and efferent innervation.	33
Figure 1. 12. Organisation of the mammalian olivocochlear efferent system.	36
Figure 1. 13. Age-related hearing loss changes in audiogram hearing thresholds.	39
Figure 1. 14. Principle intrinsic, extrinsic and genetic factors that affect ARHL.	44
Figure 1. 15. Diagrams to show the effect of age-related hearing loss.	46
Figure 1. 16. Diagram showing the effect of NIHL and the synaptopathy that occurs in the same manner as ARHL synaptopathy.	48
Figure 1. 17. Transmission electron microscopy showing the efferent re-innervation of aged IHCs.	53
Figure 1. 18. Efferent re-innervation of aged IHCs in ARHL have functional efferent synapses.	55
Figure 1. 19. Evidence of nAChRs and SK2 channel expression in re-innervated aged IHCs.	56
Figure 1. 20. An overview of how IHCs change in ageing.	58
Figure 1. 21. Changes in ribbon synapses in age-related hearing loss strains.	60
Figure 1. 22. Efferent re-innervation of Myo7a ^{fl/fl} Myo15-cre ^{+/-} following MET silencing.	62
Figure 1. 23. Location of macrophages in the normal and insulted cochlea.	66

Figure 2. 1. Schematic of the Cre-loxP system and how it enables conditional knockouts.	73
Figure 2. 2. Auditory brainstem response experimental set up.	75
Figure 2. 3. Photo of the electrophysiology rig used for experiments.	77
Figure 2. 4. Tissue preparation for whole cell patch-clamp electrophysiology.	79
Figure 3. 1. Characterising the loss of Myo7a from IHCs.	96
Figure 3. 2. IHCs re-express SK2 channels at P24 in Myo7a ^{fl/fl} Myo15 cre ^{+/-} mice.	99
Figure 3. 3. Axosomatic efferent synapses on IHCs in Myo7a ^{fl/fl} Myo15 cre ^{+/-} mice are functional.	101
Figure 3. 4. The number of SK2 channels expressed in IHCs is larger in P39 in Myo7a ^{fl/fl} Myo15 cre ^{+/-} mice.	104
Figure 3. 5. IHCs from Myo7a ^{fl/fl} Myo15 cre ^{+/-} underwent biophysical changes over time.	107
Figure 3. 6. ABR thresholds in Myo7a ^{fl/fl} Myo15 cre ^{+/-} mice from P20-35.	111
Figure 3. 7. Ribbon synapse number is reduced in IHCs from Myo7a ^{fl/fl} Myo15 cre ^{+/-} mice at P50.	115
Figure 3. 8. Quantification of ribbon synapses in Myo7a ^{fl/fl} Myo15 cre ^{+/-} mice.	117
Figure 3. 9. IHCs from Ush1c ^{fl/fl} Myo15 cre ^{+/-} mice express continue to express SK2 channels after the onset of hearing.	119
Figure 4. 1. Characterising the conditional knockout of otoferlin from IHCs in tamoxifen inducible mice.	130
Figure 4. 2. Otoferlin is progressively knocked out of IHCs after two tamoxifen injections from P10.	133
Figure 4. 3. The conditional knockout rate of otoferlin from IHCs was not linear in tamoxifen injected Otof ^{fl/fl} Vglut3 cre ^{+/-} mice.	135
Figure 4. 4. Histogram plots showing the distribution of IHCs that had otoferlin knocked out.	138
Figure 4. 5. IHCs from Otof ^{fl/fl} Myo15 cre ^{+/-} mice begin to lose otoferlin expression at P8 and is completely lost at P16.	140
Figure 4. 6. IHCs from otoferlin conditional knockout mice do not have a return axosomatic efferent innervation.	143

Figure 5. 1. The number of Iba1+ macrophages increase in Myo7a^{fl/fl} Myo15 cre^{+/-} mice with age.
..... 156

**Figure 5. 2. Differences in inflammation between aged Myo7a^{fl/fl} Myo15 cre^{+/-} mice and aged 6N
and 6N-repaired mice.** 159

List of Tables

Table 1. 1. The typologies of presbycusis along with the histopathologic and audiometric changes seen in each type.	42
Table 2. 1. Composition of extracellular solution.	80
Table 2. 2. Composition of high K⁺ (40mM) extracellular solution.	81
Table 2. 3. Composition of intracellular solution.	82
Table 2. 4. Primary Antibodies used for immunofluorescence.	87
Table 2. 5. Genotyping information for the different strains used.	89

Abbreviations

ABRs – Auditory brainstem responses

ACh – Acetylcholine

AMPA - α -amino-3-hydroxy-5-methyl-4-isoxazolepropionic acid

APs – Action potentials

ARHL – Age-related hearing loss

ATP - Adenosine 5'-triphosphate

BDNF – Brain derived neurotrophic factor

BK – Large conductance Ca^{2+} -activated potassium channel

BM – Basilar membrane

CAP – Compound action potential

CBA – CBA/CaJ

CDH23 – Cadherin 23

CGRP - calcitonin gene related peptide

ChAT – Choline acetyltransferase

CN – Cochlear nucleus

CtBP2 - C-terminal-binding protein 2

C3H – C3H/HeJ

DA – Dopamine

DAMPs – Damage-associated molecular patterns

EP – Endocochlear potential

FOV – Field of view

GABA - Gamma aminobutyric acid

XII

GLAST - Glutamate-aspartate transporter

HSR – High spontaneous discharge rate

Iba1 – Ionised calcium binding adapter molecule 1

IC – Inferior colliculus

IL-1 β – Interleukin-1 beta

IL-6 – Interleukin-6

IHCs – Inner hair cells

LOC – Lateral olivocochlear fibres

LSR – Low spontaneous discharge rate

LSO – Lateral superior olive

LTLD – Lower tip link density

MCP-1 (CCL2) – Monocyte chemoattractant protein-1

MET – Mechanoelectrical transducer

MOC – Medial olivocochlear fibres

MSO – Medial superior olive

Myo7a – Myosin VIIa

Myo15 – Myosin XVa

nAChRs - α 9 α 10 nicotinic acetylcholine receptors

NIHL – Noise-induced hearing loss

NO – Nitric oxide

NT-3 – Neurotrophin-3

OHCs – Outer hair cells

OSL – Osseous spiral lamina

XIII

PCDH15 – Protocadherin 15

PRRs – Pattern recognition receptors

PSD – Post-synaptic density

PVCN – Postero-ventral cochlear nucleus

qPCR – Quantitative polymerase chain reaction

RRP – Readily releasable pool

RT-qPCR – Real time qPCR

SGNs – Spiral ganglion neurons

SK2 – Small conductance Ca²⁺-activated potassium channel

SNHL – Sensory-neural hearing loss

SOC – Superior olivary complex

TEM – Transmission electron microscopy

Tlr4 – Toll-like receptor 4

TNF α – Tumour necrosis factor alpha

USH1C/D/F – Usher syndrome type 1 C/D/F

UTLD – Upper tip link density

Vglut3 – Vesicular glutamate transporter 3

6J – C57BL/6J

6N – C57BL/6N

6N-repaired – C57BL/6NTac^{Cdh23⁺}

Chapter 1 – General Introduction

1.1 Development and function of the cochlea

An animal's sense of hearing is crucial. Whether said animal is using their sense of hearing to hunt prey, or if the prey is using their hearing to avoid a predator, hearing is essential to survival. Over millions of years, countless animal species' hearing has evolved to become fine-tuned and exquisitely sensitive to both low and high frequency sounds. In humans, we rely less intensely on our sense of hearing for survival compared to our ancestors. Instead, in modern society we rely heavily on our sense of hearing for taking in external acoustic stimuli and analysing it so we can understand what is happening in the environment around us. The benefits of our complex auditory system allow us to process speech efficiently and learn rapidly in order to communicate effectively.

As the quality of medical care improves, the human population reaps the benefits of longer lifespans and cutting-edge technologies to help treat a plethora of diseases and conditions that threaten us. One major obstacle that is quickly approaching us, with an ever growing, ageing population, are the changes occurring in the vital sense of hearing due to age-related hearing loss. Here, we will take a detailed look at how the auditory system functions, with a particular focus on the organ of Corti, before discussing our current knowledge regarding the pathophysiology of age-related hearing loss.

1.1.1. The mammalian auditory system

The auditory system plays an integral role in animals and humans' ability to perceive and interact with the environment. The mammalian ear is divided into three different regions: the outer, middle, and inner ear (Figure 1.1); each region is highly specialised in order to efficiently convert external acoustic stimuli into electrical signals for the brain to perceive. The outer ear funnels the sound waves down the ear canal to the tympanic membrane, also known as the eardrum. The tympanic membrane vibrates and transfers the auditory stimuli to the three bones of the middle ear: the ossicles – malleus, incus and stapes. The ossicles stimulate the cochlear sensory epithelium in the inner ear by transmitting vibrations through the oval window and causing the fluid in the cochlea to move. Within the cochlea the mechanical auditory stimulus is converted into an electrical stimulus by the inner hair cells and is sent to the brain via the afferent spiral ganglion neurons for processing. The inner ear also contains the vestibular system (balance organ) and is embedded into the base of the skull, with the temporal bone providing stability and protection (Hribernik and Volavšek, 2016).

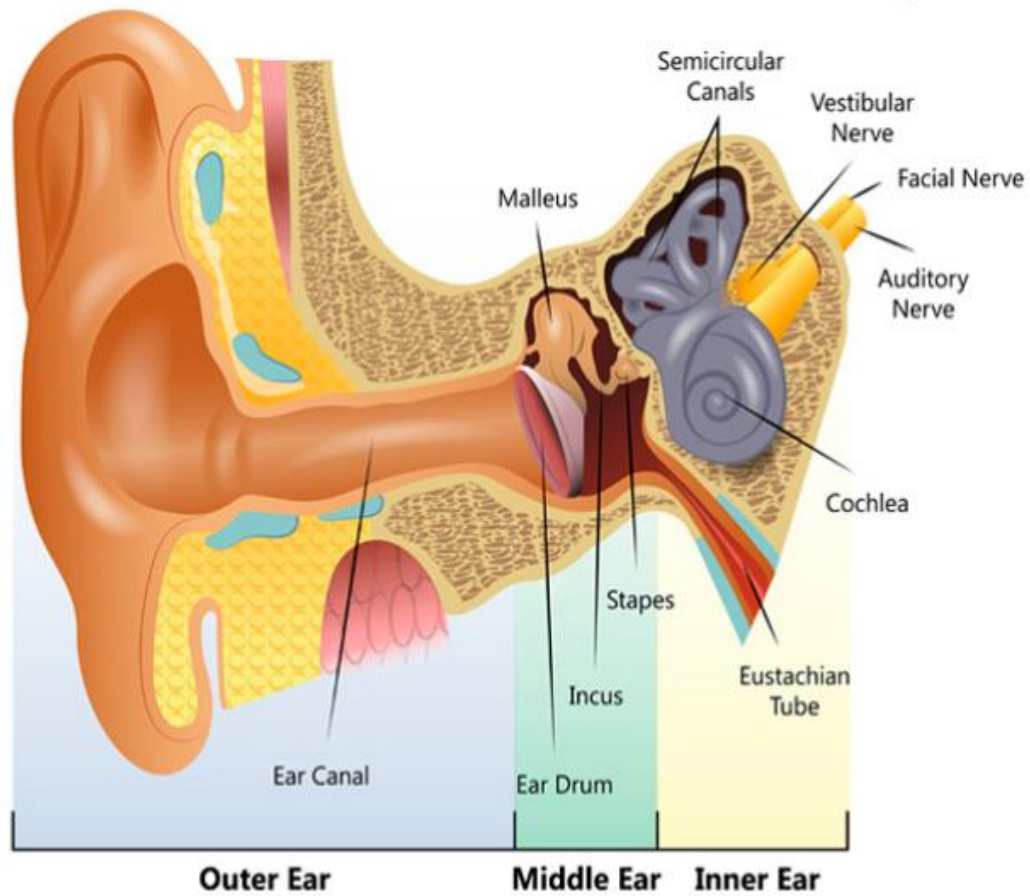


Figure 1. 1. Anatomy of the outer, middle, and inner ear.

The outer ear contains the ear canal, the middle ear contains the ear drum (tympanic membrane) and 3 ossicles - malleus, incus and stapes. The inner ear contains the spiral cochlea (auditory organ) and vestibular system (balance organ), which can be identified by the semi-circular canals. It is innervated by cranial nerve VIII – the vestibulocochlear nerve. Figure from (Services, 2022).

1.1.2. Structure of the mammalian cochlea

The human cochlea is highly sensitive and can detect a range of hearing frequencies from 20-20,000 Hz, in addition to a large range of sound intensities (Purves et al., 2001). In order to achieve these precise levels of sound encoding, the cochlea is specialised in a multitude of different ways.

The cochlea is a coiled labyrinth that is comprised of three fluid filled chambers (scalae): scalae tympani, vestibuli and media (Figure 1.2A), all of which are filled with lymph and run along the length of the cochlea (Boron and Boulpaep, 2012). The scala vestibuli is the upper chamber and contains perilymph, which is similar in composition to extracellular fluid: 140 mM Na⁺, 5.8 mM K⁺ and 1.3 mM Ca²⁺ (Wangemann and Schacht, 1996). The scala tympani is the lower chamber and contains perilymph. The two perilymph fluids link through the opening at the apex of the cochlea, the helicotrema (Boron and Boulpaep, 2012). The scala media is the middle compartment and is filled with endolymph, containing 155 mM K⁺, 1 mM Na⁺ and 20-40 μM Ca²⁺ (Wangemann and Schacht, 1996). It also has a voltage of +80 mV compared to the perilymph chambers, which have a voltage of 0 mV (Tasaki et al., 1954). This creates the endolymphatic potential (+80mV) which is due to the difference between the perilymph and endolymph (Steel and Barkway, 1989, Fettiplace and Kim, 2014). The scala media is enclosed from the perilymph containing chambers by two membranes. It is separated from the scala vestibuli by the Reissner's membrane, whilst being separated from the scala tympani by the basilar membrane (BM) (Figure 1.2A & B) (Elliott and Shera, 2012). Additionally, the scala media forms the cochlear duct and contains the organ of Corti, the neurosensory epithelium which sits on the basilar membrane, and contains the sensory inner hair cells (IHCs) and outer hair cells (OHCs) (Slepecky, 1996).

The scalae chambers also help to optimise the cochlear hair cells in their respective role of sensory reception (IHCs) and cochlear amplification (OHCs) (these are described later in this section). The IHCs and OHCs have stereocilia (microvilli) projections that form hair bundles. The stereocilia hair bundles are surrounded by endolymph, whereas the basolateral parts of the hair cells are surrounded by perilymph. This separation of the lymph fluids is achieved by the reticular lamina, located at the apical part of the IHCs and OHCs. The stria vascularis (Figure 1.2A) is responsible for producing the endocochlear potential (EP) (+80 mV) within the

scala media (v. Békésy, 1952). The EP is produced and maintained by the intermediate cells within the stria vascularis via a K^+ recycling mechanism (Takeuchi et al., 2000, Wangemann, 2002).

The sensory epithelium sits on top of the BM, which has a specialised function that is linked to the hair cells detection of mechanical stimuli and conversion to electrical signals. The BM is a collagenous sheet and vibrates in response to sound inducing waves produced from the moving cochlear fluids (Slepecky, 1996). The BM's function is frequency analysis and it achieves this by being tonotopically organised along the length of the cochlea (von Békésy and Wever, 1960). Tonotopic organisation of the cochlea results in different regions of the BM preferentially responding to either high (basal region) or low frequency (apical region) sounds (Humphries et al., 2010). Békésy and Wever (1960) showed that travelling sound waves increased in amplitude along the BM, reaching a peak at a specific frequency before declining in amplitude afterwards. From this, it was determined that the BM has characteristic frequencies – regions along the BM that will get a maximal response to a certain frequency (Russell and Sellick, 1977). Moreover, the BM has a gradient in its stiffness, with the base being stiffer compared to the apex, this helps to fine tune frequency analysis and results in accurate responses to different sound frequencies (Emadi et al., 2004).

The organ of Corti that sits upon the BM contains the sensory hair cells; the IHCs and OHCs, as well as the surrounding non-sensory (supporting) cells. The sensory hair cells are in four rows in the organ of Corti, with one row of IHCs and three rows of OHCs (Figure 1.2B). The IHCs are the primary sensory receptors and are responsible for converting the mechanical stimuli into electrical signals that will be sent to the brain for processing. The process that converts the mechanical stimuli into electrical signals (mechano-electrical transduction (MET)) is key for sound perception and will be covered later in the introduction (see section 1.1.3.2). Like the rest of the cochlea, the IHCs are specialised to be as efficient as possible for their role, the process of mechano-electrical transduction, as well as transmission of the electrical signals to the brain. Some of these specialisations will be covered more thoroughly throughout this thesis. Similar to how the BM has differences across the length of the cochlea, the sensory hair cells also have distinct differences between the apex and base. For example, stereocilia that are found atop IHCs and OHCs and are crucial for mechano-electrical transduction. The IHC stereocilia that are found in the apex of the cochlea are often longer than those found at

the base, these are adaptations that allow the stereocilia to respond more optimally to either low or high frequency sounds (Fettiplace and Hackney, 2006). Another specialisation within the cochlea is a positive driving force (+140 mV) that aids the influx of K^+ and Ca^{2+} into the hair cells via the MET channels (Corey and Hudspeth, 1983, Crawford et al., 1991). The driving force is due to the difference between the endolymph (+80 mV) that the hair bundles are found in and the hair cells resting membrane potential (-60 mV) (Marcotti et al., 2003a).

The OHCs also have their own specialisations that separates them functionally from the IHCs. OHCs are electromotile, which means that they can shorten or elongate their shape in response to depolarisation or hyperpolarisation (Brownell, 1983, Brownell et al., 1985, Ashmore, 1987). OHCs are able to do this due to the presence of the motor protein prestin – which is densely localised to the basolateral (beneath the cuticular plate that stereocilia are embedded into) part of the OHC membrane (Zheng et al., 2000). This electromotility enables OHCs to act as a sound amplifier (Ryan and Dallos, 1975, Dallos and Harris, 1978, Harrison and Evans, 1979). The OHCs role is linked to that of the BM, in that the BM will vibrate at specific frequencies depending on the sound stimuli, this will then result in the shortening or elongation of the OHC which helps with sound amplification and frequency selectivity (Ryan and Dallos, 1975, Dallos and Harris, 1978, Harrison and Evans, 1979). Additionally, the OHCs amplification of the BM can be highly important at low sound pressures (Ashmore, 2008, Dallos, 2008).

A brief overview for the inner ear has been discussed so far. The mammalian inner ear undergoes many embryonic and postnatal developmental changes before the auditory system becomes fully mature around postnatal day 21 (P21). This thesis is interested only in the postnatal development as well as the mature organ of Corti, so embryonic changes will not be discussed. Additionally, for the remainder of this thesis there will be a focus on the IHCs, as the project is IHC specific. OHCs may be mentioned during some sections for additional information, however, the IHCs will be predominantly discussed.

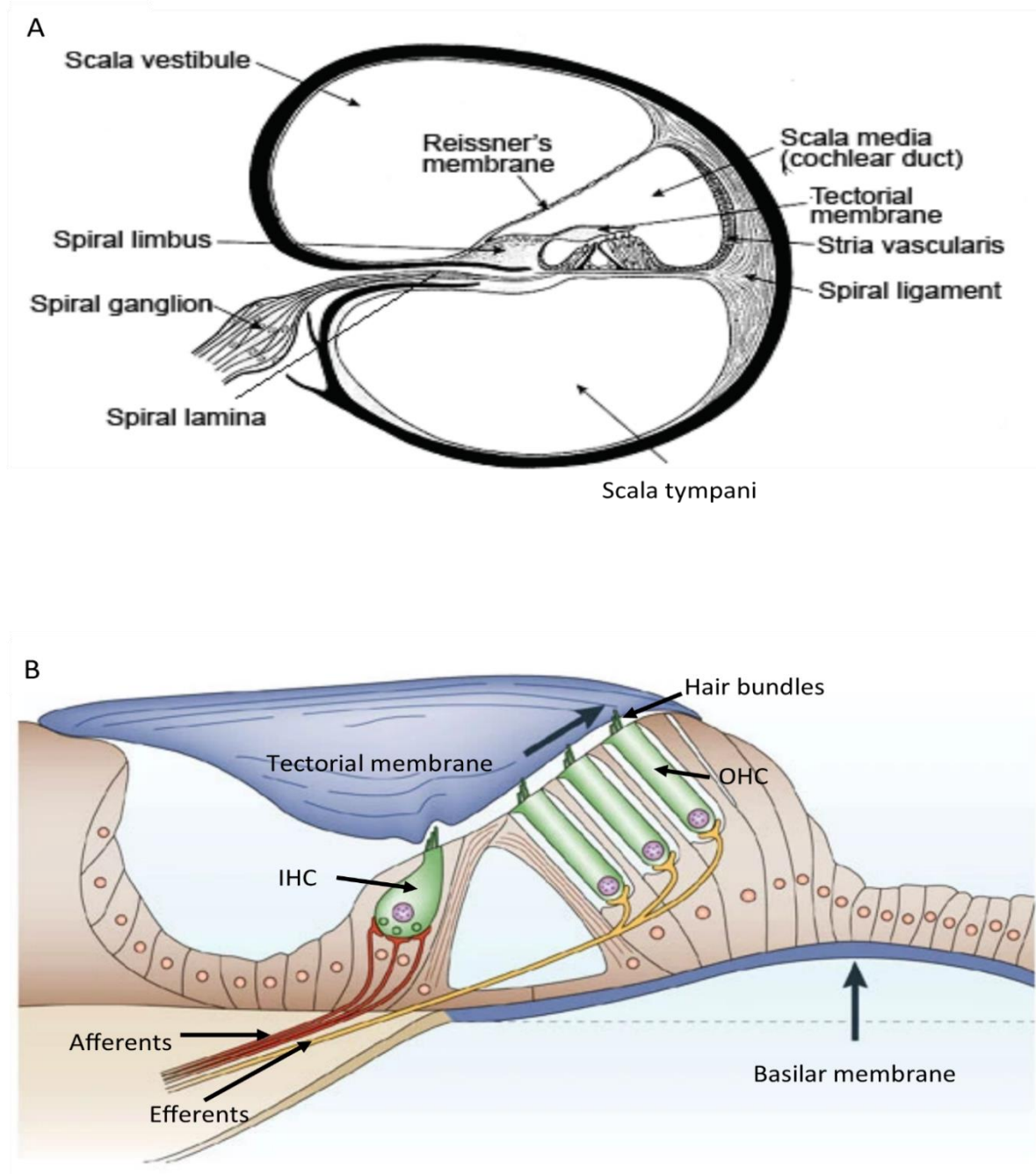


Figure 1. 2. Cross section diagrams of the cochlea.

A: depicting the 3 chambers of the cochlea, the scalae vestibuli, media and tympani, the organ of Corti and its innervating spiral ganglion, as well as the stria vascularis. **B:** illustrating the upward displacement (upward arrow) of the basilar membrane during stimulation of the cochlea caused by movement of fluid in the scala media. The IHCs hair bundles are not fixed into the tectorial membrane, whereas the outer hair cell hair bundles are fixed into the tectorial membrane. Figures and figure legends adapted from (Turunen-Taheri et al., 2017, Fettiplace and Hackney, 2006) respectively.

1.1.3. IHC postnatal development

As mentioned above, the organ of Corti undergoes progressive developmental changes before achieving functional maturation. When mice are born (postnatal day 0, P0) they are unable to hear. Mice remain deaf for the early time points of development and can only hear once they have reached postnatal day 12 (P12) (Mikaelian and Ruben, 1965, Ehret, 1983, Romand, 1983, Kros et al., 1998). There are many developmental changes that take place up to the onset of hearing in mice, as well as further changes that continue after. The remainder of this thesis introduction will focus on IHCs, covering some of the key changes in their development and innervation up to the onset of hearing (developmental) and beyond (mature / adult). There are many differences that enable for identifying whether IHCs are still developmental or if they are functionally mature (adult). Typically, it takes around 3 postnatal weeks (~P21) for all the key developmental changes to take place within the mammalian cochlea.

1.1.3.1 Basolateral membrane channels: pre-hearing and post-hearing changes

Before the onset of hearing at P12 the IHCs have several different ion channels that are expressed when compared to after the onset of hearing. These ion channel changes result in different biophysical profiles that can be used to categorise whether an IHC expresses a developmental profile or mature (adult) profile (Figure 1.3). For example, IHCs fire spontaneous action potentials before birth up until P12. These spontaneous action potentials (APs) are fired intrinsically, the $Ca_v1.3$ Ca^{2+} channels being involved before the onset of hearing (typically in the first postnatal week) (Figure 1.3) (Marcotti et al., 2003c, Tritsch et al., 2010, Johnson and Marcotti, 2008, Johnson et al., 2013a). Additionally, the spontaneous APs can be induced via the spontaneous release of ATP by non-sensory supporting cells (in the second postnatal week) (Tritsch et al., 2010, Wang et al., 2015, Johnson et al., 2017). The function of the spontaneous APs is to help the IHCs undergo functional development, and if the IHCs cannot fire spontaneous APs then mice often remain deaf after P12 and IHCs fail to mature correctly (Johnson et al., 2007, Johnson et al., 2013a). Therefore, the spontaneous APs that fire during the first postnatal week are crucial for the developing innervation of the IHCs during development (Johnson et al., 2017).

For IHCs to be able to fire spontaneous APs there is a function for both I_{Ca} and I_{Na} currents (Figure 1.3). Like spontaneous APs, the I_{Ca} currents (driven by $Ca_v1.3$ channels) in IHCs can be found embryonically, this is because the I_{Ca} current is essential for the IHCs ability to generate spontaneous APs and if the current is not present then IHCs degenerate rapidly after P12 (Platzer et al., 2000, Marcotti et al., 2003b). Moreover, the I_{Ca} current is maintained in IHCs after the onset of hearing. The I_{Na} current (carried via $Na_v1.1$ and $Na_v1.6$ channels) can also be found before birth in IHCs, due to its involvement with IHC APs. The I_{Na} function is to speed up the time it takes the IHCs membrane potential to reach threshold when firing spontaneous APs (Marcotti et al., 2003b). Similar to spontaneous APs, the I_{Na} current is lost from IHCs around P12, indicating that its function is tied to the development of the IHCs biophysical profile (Marcotti et al., 2003b).

Throughout all stages of development, IHCs require K^+ currents to be present. One such K^+ current is the strong inward rectifier I_{K1} , which is known to be involved in regulating the resting membrane potential of the IHCs, and together with I_{Ca} work to depolarise the IHCs in generating spontaneous APs (Marcotti et al., 1999, Marcotti et al., 2003a). The I_{K1} current is only present in IHCs until P12 (Figure 1.3), at which point the expression of $I_{K,f}$ becomes one of the predominant K^+ currents expressed (Figure 1.3), highlighting the strictly prehearing developmental role for I_{K1} . After the onset of hearing at P12, the IHCs no longer fire spontaneous APs and have matured into being high frequency sensory receptors that fire graded potentials (see section 1.1.4.2) (Johnson et al., 2013a, Johnson et al., 2017, Johnson et al., 2019). The $I_{K,f}$ current, is driven via a large conductance Ca^{2+} -activated K^+ channel (BK) (Appenrodt and Kros, 1997, Kirkwood and Kros, 1997, Kros et al., 1998). As the $I_{K,f}$ current is fast activating, its function is to prevent the IHCs from being able to generate any APs, even if current is injected into the IHC – allowing the IHCs to perform their mature function of mechano-electrical transduction (Marcotti et al., 2003a). Additionally, there is a delayed rectifier (slowly activated) K^+ current (I_{Ks} that is expressed in mature IHCs at P12 after I_{K1} is no longer expressed).

Another K^+ current that is only expressed after P12 when the IHCs are mature is the $I_{K,n}$, which is driven via the KCNQ4 channels (Marcotti et al., 1999, Marcotti et al., 2003a). The $I_{K,n}$ current is active around resting membrane potentials in the mature IHCs ($\sim -70mV$), therefore it is proposed to be involved with determining the membrane potential of the IHC (Marcotti et

al., 2003a, Dominik et al., 2003). Furthermore, if KCNQ4 is not present in IHCs (or OHCs, where it was discovered first (Housley and Ashmore, 1992, Marcotti and Kros, 1999)) then mice remain deaf (Kubisch et al., 1999). It was suggested that the lack of KCNQ4 channels results in K^+ that enters the IHCs through MET channels accumulate within the cell, inducing excitotoxicity as the IHC remains depolarised, enabling increased activation of Ca^{2+} channels and afferent nerve fibres (Moser and Beutner, 2000, Beutner and Moser, 2001, Marcotti et al., 2003a). From these findings, the presence of different K^+ currents can be used to determine whether an IHC has a developmental or mature biophysical profile, with developmental profiles typically including I_{K1} whereas mature IHCs have $I_{K,f}$, $I_{K,s}$ and $I_{K,n}$ present (Marcotti et al., 2003a).

The prehearing, developmental IHCs also express $\alpha 9\alpha 10$ nicotinic acetylcholine receptors (nAChRs) from birth until after the onset of hearing (Figure 1.3) (Elgoyhen et al., 1994, Elgoyhen et al., 2001, Katz et al., 2004, Roux et al., 2011). The nAChRs allow Ca^{2+} to flow into the IHCs when the efferent fibres that transiently innervate the developing IHCs (see section 1.1.5 on efferent innervation) release acetylcholine (ACh). The Ca^{2+} that flows into the IHCs activate the small conductance Ca^{2+} activated K^+ channels (SK2). The SK2 channels are expressed by IHCs just after birth (Figure 1.3), and are functionally coupled to the nAChRs (Glowatzki and Fuchs, 2000, Katz et al., 2004, Marcotti et al., 2004). Together, the nAChRs and SK2 channels form synapses with the efferent fibre terminals at the developing IHCs. When SK2 channels are activated by Ca^{2+} , there is a efflux of K^+ out of the IHCs, resulting in the IHC becoming hyperpolarised (Evans, 1996, Marcotti et al., 2004). Therefore, the SK2 channels help regulate the spontaneous APs during the first postnatal week by hyperpolarising the IHCs, and if SK2 channels are not present then the IHCs fail to functionally mature (Johnson et al., 2007). As IHCs lose their transient efferent innervation after the onset of hearing, the nAChRs and SK2 channels become downregulated, with IHCs no longer responding to ACh at P18 – whilst SK2 channels are no longer expressed by IHCs around P20-21 (Glowatzki and Fuchs, 2000, Katz et al., 2004, Marcotti et al., 2004).

The MET channels (see section 1.1.3.2) are crucial to both prehearing IHCs, as well as functionally mature IHCs after P12. The presence of the MET channel can be seen in apical IHCs around P2-3 (Crawford et al., 1991). The function of the MET channel in the first postnatal week is to aid with spontaneous APs, allowing Ca^{2+} into the IHCs through the MET

channels that are open at rest (see section 1.1.3.2) (Johnson et al., 2012). The MET channels become functionally mature towards the end of the first postnatal week, and from the onset of hearing at P12, become responsible for sound induced mechano-electrical transduction, which coincides with the functional maturation of the IHCs (Cody and Russell, 1987, Crawford et al., 1991, Kros et al., 1992). Furthermore, once the MET channel and IHCs are functionally mature, the IHCs no longer fire spontaneous or induced APs, instead firing highly sensitive graded receptor potentials that are stimulated by the process of MET (see section 1.1.4.2) (Johnson et al., 2012). Once IHCs are functionally mature at P12, the MET channels have also been shown to be crucial in the IHCs maintaining this mature biophysical profile. If the MET channel is dysfunctional in mature IHCs then the IHCs have been shown to return to their developmental, immature biophysical profile (Corns et al., 2018).

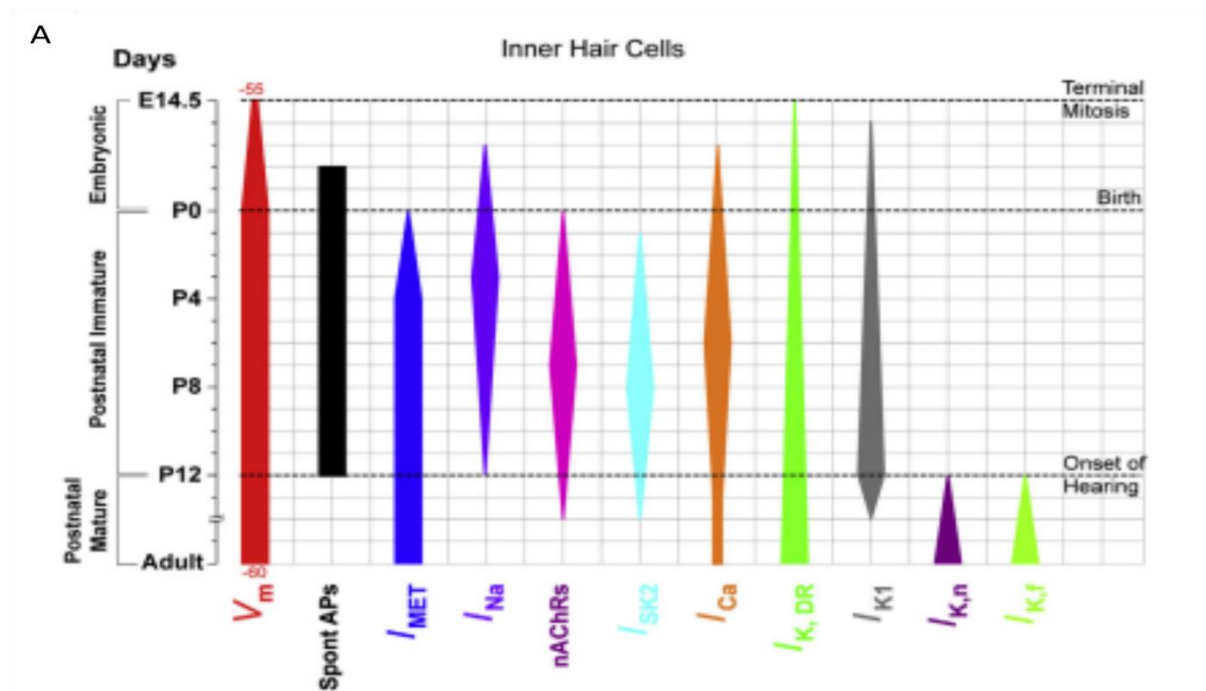


Figure 1. 3. Diagram showing the development of key basolateral membrane properties for IHCs.

A: timeline for basolateral ion channel changes in mouse apical IHCs. The bars indicate the overlap between different sodium, potassium and calcium currents that are required for the functional maturation of IHCs (postnatal day 12, P12). After the onset of hearing at P12 and IHCs are mature, the biophysical profile changes and can be identified by the presence of $I_{K,n}$ and $I_{K,f}$ carried by KCNQ4 and BK channels, respectively. Width of the vertical bars indicates

size of the currents or resting membrane potential (V_m) during development. Figure adapted from (Corns et al., 2014a).

1.1.3.2. IHC stereocilia and the mechano-electrical transducer channel

The stereocilia that are found atop the IHCs and OHCs (Figure 1.4 A, B & C) are essential for normal functional hearing. Like the basolateral region of the IHC and its innervation (see section 1.1.4, 1.1.5), the stereocilia and MET channels undergo many developmental changes from birth up to the onset of hearing in the mammalian cochlea. However, the focus of this thesis is based on the changing biophysical profile of the IHC and innervation, therefore, the stereocilia and MET channels will not be covered extensively and only the relevant proteins / mechanisms that are essential for this thesis will be discussed.

Stereocilia enable the conversion of mechanical (sound) stimuli into electrical signals to be sent to the brain and the MET channels that are found at the tips of stereocilia are responsible for this conversion. The stereocilia hair bundles become displaced by the mechanical stimuli, this deflection of the stereocilia enables the opening of the MET channels and conversion of acoustic information. For this to be possible, the stereocilia are organised into three rows, in a staircase structure that increase in height and form a hair bundle (Figure 1.4) (Tilney et al., 1992). The stereocilia have filamentous tip links that connect the shorter rows of stereocilia to the side of the neighbouring taller row (Pickles et al., 1984, Assad et al., 1991). If the hair bundle is deflected in the direction of the tallest stereocilia row (excitatory), this opens the MET channel (and depolarises the IHCs) (Figure 1.6), which are located at the tips of the two shorter rows of stereocilia (Corey and Hudspeth, 1983, Howard and Hudspeth, 1987, Assad et al., 1991, Gillespie et al., 1993, Beurg et al., 2009a, Pan et al., 2013, Zhao et al., 2014, Beurg et al., 2015). On the other hand, when the hair bundles deflect towards the shorter rows of stereocilia (inhibitory), the MET channels close. When the MET channels are open, they are non-selective for cations such as Ca^{2+} and K^+ , however, they have a greater permeability for Ca^{2+} (Corey and Hudspeth, 1979, Ohmori, 1985, Ricci and Fettiplace, 1998, Beurg et al., 2009b).

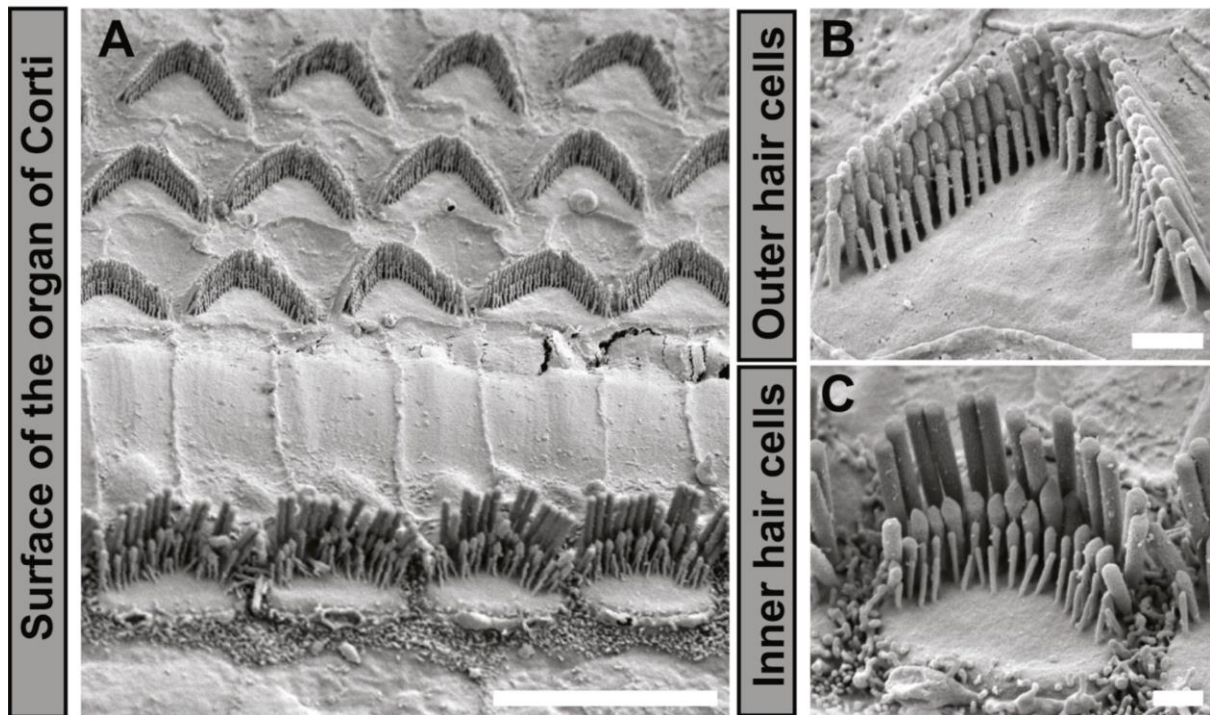


Figure 1. 4. Scanning electron microscopy images of the IHC and OHC stereocilia.

A: scanning electron microscopy image of a mature mouse organ of Corti with the tectorial membrane removed, showing three rows of OHCs located on the lateral side (top image), and one row of IHCs located on the medial side (bottom image). Scale bar: 10 μm **B:** higher magnification image of an OHC, showing the three rows of stereocilia and the staircase structure; scale bar is 1 μm . **C:** higher magnification image of an IHC, showing the staircase structure and three rows of stereocilia; scale bar is 1 μm . Figure and figure legends adapted from (Schwander et al., 2010).

IHC stereocilia have a single tip link that connects to the neighbouring taller stereocilia, and they are essential in the process of MET. The MET channels are always open at rest, allowing a small influx of Ca^{2+} into the IHCs, even in the absence of excitatory or inhibitory stimulation (Corns et al., 2018). To achieve this partial opening at rest, the tip links maintain a tension between the MET channels and the hair bundles, a process that requires multiple different proteins working together in a complex (Kachar et al., 2000, Furness et al., 2008, Pan et al., 2009, Caberlotto et al., 2011a, Fettiplace and Kim, 2014, Beurg et al., 2015). However, only the proteins relevant for the key understanding of MET and have functional relevance for this thesis will be discussed further.

The tip links themselves are made up of two protofilaments that form a right-handed, coiled double helix (Kachar et al., 2000). As the tip links insert into the tip of the shorter stereocilia as well as the side of the neighbouring, taller stereocilia, there are two insertion sites present at the tip links (Assad et al., 1991). The insertion regions of the upper and lower tip links are electron dense regions that lie between the stereocilia membrane and the actin filaments that stereocilia are comprised of (Furness and Hackney, 1985). One of the protofilaments that make up the tip links was identified using electron microscopy and revealed to be Cadherin 23 (CDH23) (Figure 1.5) (Siemens et al., 2004). CDH23 is essential for the tip links and normal functional hearing, if it is mutated – such as in the human deafness condition Ushers syndrome (USH) type 1D, then patients have profound deafness, vestibular problems as well as blindness in the form of retinitis pigmentosa (Bolz et al., 2001, Bork et al., 2001). The second protofilament that makes up the tip links is protocadherin 15 (PCDH15) (Ahmed et al., 2006), a member of the cadherin superfamily. PCDH15 was subsequently identified to interact with CDH23 and forms the lower third of the tip link (Figure 1.5), whereas CDH23 makes up the upper two thirds (Kazmierczak et al., 2007). Similarly, to mutations in CDH23, if PCDH15 is mutated then it results in Ushers syndrome, albeit, type 1F, which also results in deafness and vestibular problems (Ahmed et al., 2001, Alagramam et al., 2001, Ahmed et al., 2003). The function of the tip link in the process of MET is to mechanically gate the ion channel, this includes aiding the opening of the MET channels upon excitatory stimulation (hair bundle moving towards taller stereocilia) as the tip link gets stretched (Goodyear et al., 2005, Kazmierczak et al., 2007).

At the upper tip link density there is a complex of proteins that are involved in the normal MET function for the IHCs, as well as maintaining the tension in the tip links (Figure 1.5). One protein that is crucial for the functioning of the MET channel is unconventional myosin VIIa (Myo7a) (Kros et al., 2002). Myo7a is localised at the upper tip link density and is involved in forming a complex with adaptor proteins known as harmonin and sans (Verpy et al., 2000, Grati and Kachar, 2011). Moreover, mutations in Myo7a were one of the first genetic causes of Ushers syndrome identified (Ushers syndrome type 1B, USH1B) (Weil et al., 1995, Self et al., 1998). Myo7a plays a role in embryonic development of hair cells in mice, with its expression being reported as early as embryonic day 9 (E9) (Sahly et al., 1997, Boëda et al., 2001). This indicates that Myo7a is needed to be expressed during development, otherwise deafness and other defects occur such as in USH1B. Furthermore, as Myo7a is a myosin motor, it has been reported to be essential for maintaining the resting tension of the tip link, enabling the MET channels to be partially open at rest (Kros et al., 2002). If Myo7a is mutated then MET currents become smaller and the IHCs lose the open resting state of the MET channels (Kros et al., 2002).

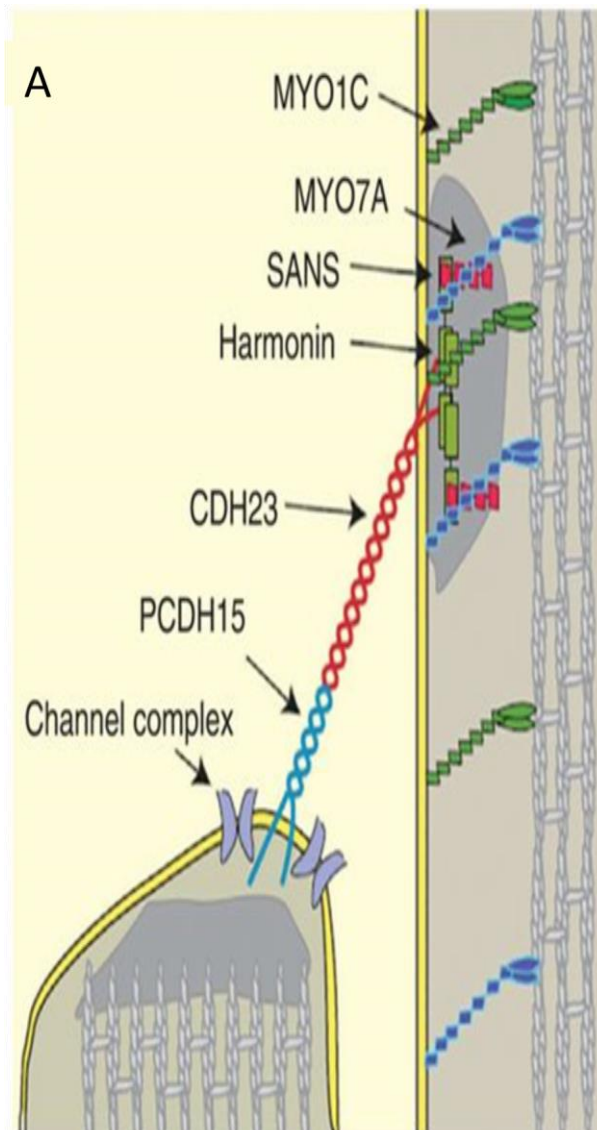


Figure 1. 5. Diagram showing the composition of the tip link and the associated proteins at the upper tip link density.

The MET channels (channel complex) can be seen at the tip of the shorter row of stereocilia. Attached to the MET channel is the tip link, that connects the two stereocilia together, the lower third of the tip link is comprised of protocadherin 15 (PCDH15), whilst the upper two thirds are made up of cadherin 23 (CHD23). The tip link inserts into the upper tip link density (UTLD) on the side of the taller row of stereocilia. The UTLD consists of multiple proteins, including unconventional myosins' 1c and 7a (Myo1c, Myo7a) in addition to the sans and harmonin proteins. Figure from (Richardson and Petit, 2019).

Myo7a is also involved in the process of adaptation of the MET channel (Figure 1.5) (Kros et al., 2002, Stepanyan and Frolenkov, 2009, Corns et al., 2014b). Adaptation is when the MET channels are open in an excitatory stimulation and comes in two forms – fast and slow adaptation (Figure 1.6) (Howard and Hudspeth, 1987, Crawford et al., 1989, Crawford et al., 1991, Wu et al., 1999, Holt and Corey, 2000, Ricci et al., 2000, Fettiplace and Hackney, 2006). The purpose of the adaptation is to enable MET channel to optimally respond to a sustained stimulus (Fettiplace and Kim, 2014). Both types of adaptation are influenced by Ca^{2+} entering the open MET channel during excitation, with Ca^{2+} then functioning to close the channel by interacting with the channel itself (Kennedy et al., 2003, Lelli et al., 2009) or via accessory proteins (Fettiplace and Kim, 2014). The Ca^{2+} then interacts over a short period of time (fast) or a slightly slower time period (slow) to close the MET channels, resulting in adaptation of the channel (Crawford et al., 1989, Crawford et al., 1991, Ricci et al., 2000, Cheung and Corey, 2006, Stepanyan and Frolenkov, 2009, Corns et al., 2014b). Myo7a has been shown to specifically have a role in slow adaptation of the MET current (Crawford et al., 1989, Crawford et al., 1991, Choe et al., 1998, Kros et al., 2002, Cheung and Corey, 2006).

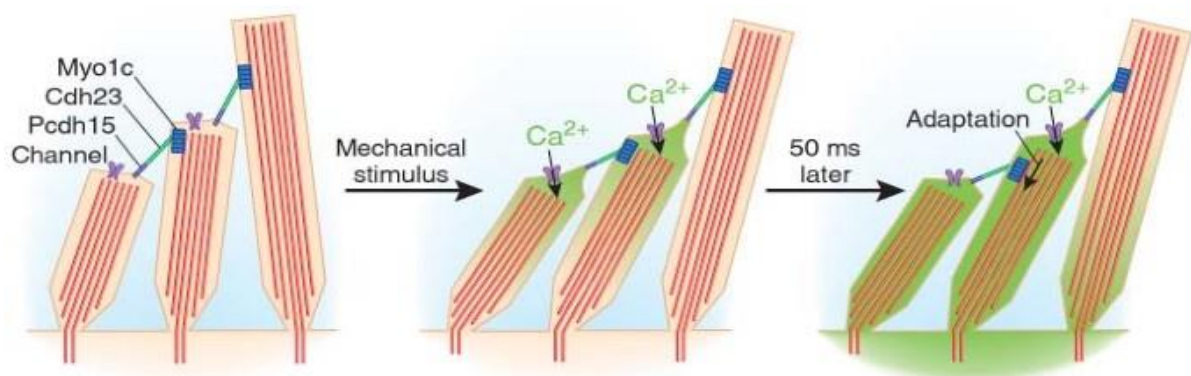


Figure 1. 6. Schematic showing the 3 rows of stereocilia and the MET channels at rest, during activation and during adaptation of the MET channels.

At rest the tip links have a rest tension that enables the MET channels to be partially open. Upon activation (mechanical stimulus, deflects to hair bundle towards the tallest stereocilia, middle panel), the tip links become stretched and the MET channels open, allowing Ca^{2+} and K^+ (not shown in schematic) into the hair cell. The right hand panel shows the adaptation that occurs 50ms after excitatory stimulation, which includes Ca^{2+} directly interacting with the MET

channel, to maintain optimal sensitivity to sustained stimuli. Figure from (Spinelli and Gillespie, 2009).

There is also the expression of another unconventional myosin in the stereocilia – myosin XV (Myo15). Myo15 is found in the tips of the stereocilia and has functional roles in stereocilia elongation, as well as maintenance of the staircase structure (Gillespie et al., 1993, Anderson et al., 2000, Belyantseva et al., 2003, Delprat et al., 2004). Likewise, to mutations in Myo7a, if Myo15 is mutated then IHCs have dysfunctional MET currents and results in deafness in both mice (Probst et al., 1998) and humans (Wang et al., 1998) due to the stereocilia being shorter and losing the typical staircase structure (Belyantseva et al., 2003). Myo15 also has been implicated to have a role in slow adaptation of the MET channels, along with Myo7a (Fang et al., 2015). However, unlike Myo7a, Myo15 is not expressed in stereocilia tip until P2 in the basal coil of the cochlea, and P4 in the apical coil (Caberlotto et al., 2011b).

The maturation of the basolateral ions, and the stereocilia as well as the MET channels are sufficient to understand the core parts of this thesis, which will predominantly be focusing on changes in the efferent innervation in age-related hearing loss mouse models (see section 1.2.4). The following sections will now cover the development of the afferent and efferent innervation, as well as how the electrical signals that the MET channels convert are passed through to the afferent fibres (see section 1.1.4.2).

1.1.4. IHC Afferent Innervation

The innervation of the mammalian cochlea undergoes many developmental changes from embryonic stages until around three weeks postnatally. Both the IHCs and OHCs are innervated by afferent and efferent fibres throughout development, however, the focus will predominantly be on the innervation of the IHCs.

IHCs are innervated by type I spiral ganglion neurons (SGNs), which function to send the acoustic information that the IHCs detect and convert into an electrical signal to the brain for processing. There are two types of SGNs (type I and type II) (Kiang et al., 1982) and 90-95% (Spoendlin, 1972) of the total SGN population is made up of type I SGNs – with the remainder being type II SGNs that innervate the OHCs. In the mature cochlea the IHCs have synapses with around 10-20 type I SGN afferent fibres (Liberman, 1980, Meyer et al., 2009), with the highest number of synapses relating to the tonotopic map of the cochlea. This results in the highest number of afferent synapses in 3-4 kHz frequency in humans, which is the frequency that is used in everyday conversations (Meyer et al., 2009). IHCs have afferent synapses on both the modiolar and pillar side of the cells (Figure 1.7), with the modiolar being the side that is closest to where the bundles of SGNs are located, whereas the pillar side is the part of the IHCs that face towards the OHCs (Liberman, 1980). Depending on whether an afferent synapse is located in either the modiolar or pillar side of the IHC demonstrates a heterogeneity within the SGN population, with synapses on either side having slightly different functions (Kiang et al., 1982, Liberman, 1980, Liberman, 1982a).

SGNs that synapse on the modiolar side of the IHCs are categorised by having high thresholds with a low spontaneous discharge rate (LSR), whereas on the pillar side the SGNs have low thresholds with high spontaneous rates (HSR) (Liberman, 1982a, Liberman, 1982b). It is believed that the 49-67% of the SGNs are high threshold and LSR fibres (modiolar), whilst 33-51% are low threshold and HSR fibres (pillar) (Taberner and Liberman, 2005). The heterogeneity in the SGN subtypes enables the cochlea to encode and respond to a wide range of sound frequencies and intensities. In addition to the position that the SGN is found on the IHC, the SGNs characteristic frequency (frequency that the SGN maximally responds) varies along the length of the cochlea (Liberman, 1982a, Liberman, 1982b). There are morphological differences between the modiolar and pillar SGN synapses, which helps them

to be optimised for their functions. For example, modiolar afferent synapses have larger pre-synaptic ribbon synapses (see section on ribbon synapses, 1.1.4.2), with an increased number of $Ca_v1.3$ channels, accompanied by a smaller post-synaptic patch of AMPA receptors (Liberman et al., 2011, Wong et al., 2013). Alternatively, SGNs that synapse on the pillar side of the IHCs have smaller pre-synaptic ribbons with a lower density of $Ca_v1.3$ channels, but a larger post-synaptic patch of AMPA receptors – this is due to there being opposing gradients of ribbon synapse size and AMPA receptors in IHCs (Liberman et al., 2011). SGNs are often lost in age-related as well as in noise-induced hearing loss (Barclay et al., 2011, de Graaf et al., 2013), with a recent report showing that there was more pre-synaptic loss of pillar side SGN synapses in IHCs compared to modiolar, however, there is loss in both regions (Jeng et al., 2020a).

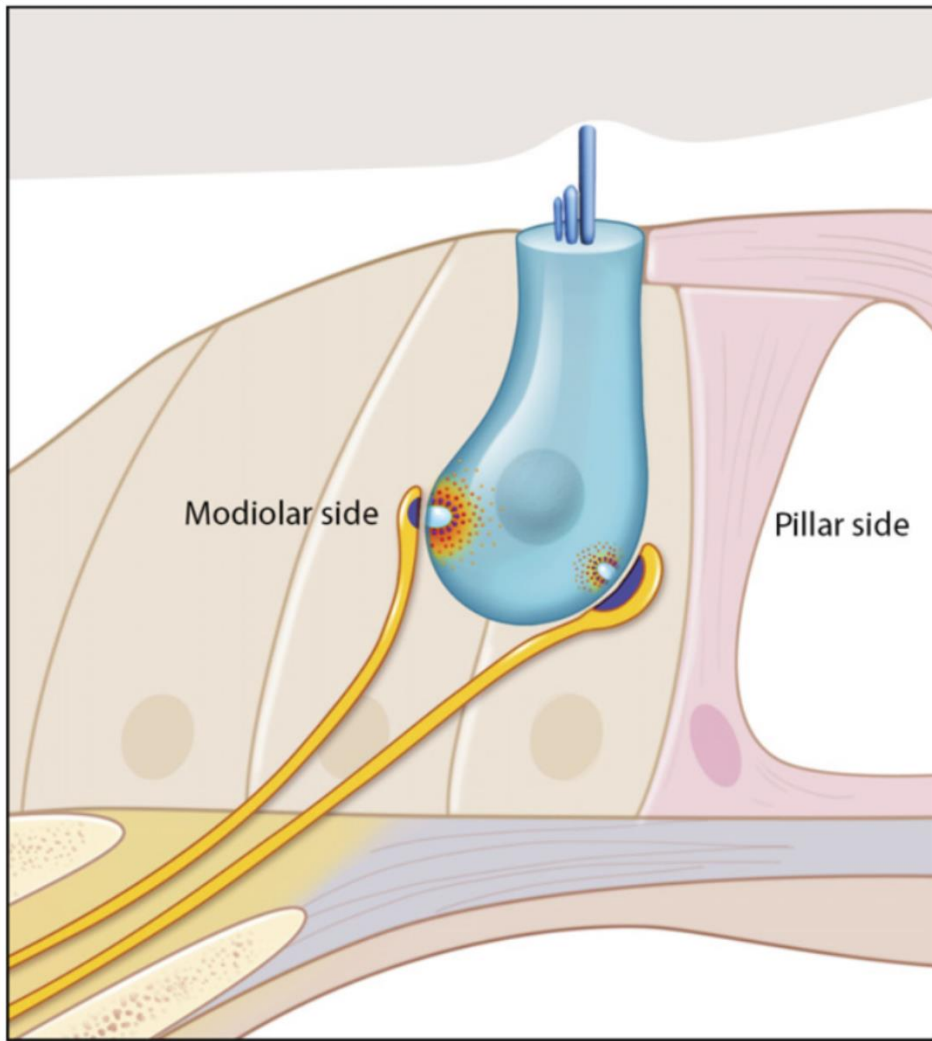


Figure 1. 7. Schematic of an IHC displaying the modiolar and pillar synapses with type I SGN fibres.

The schematic demonstrates the differences in location and morphology of the types of afferent innervation of IHCs. On the modiolar side the IHCs express larger pre-synaptic densities, with smaller post-synaptic densities whereas on the pillar side the IHCs have smaller pre-synaptic densities and larger post-synaptic densities. Figure from (Niwa et al., 2021).

Afferent synapses are excitatory, as the IHCs pre-synaptic ribbons have vesicles filled with glutamate (see section), and in mature IHCs the accompanying post-synaptic density (PSD) is filled with AMPA receptors, some of which include: GluR2 and GluR3 (Usami et al., 1995, Niedzielski and Wenthold, 1995, Matsubara et al., 1996, Eybalin et al., 2004). Upon glutamate release from the IHC pre-synapse, the AMPA receptors become activated, which results in an excitatory post synaptic current in the type I SGN (Ruel et al., 1999, Ruel et al., 2000, Glowatzki and Fuchs, 2002, Keen and Hudspeth, 2006, Grant et al., 2010). Loss of the post-synaptic AMPA receptors commonly results in deafness due to the type I SGNs not transmitting the electrical signal to the auditory nerve and through the auditory pathway (Grant et al., 2010, Matsubara et al., 1996, Niedzielski and Wenthold, 1995, Usami et al., 1995). There is also a function for the non-sensory supporting cells that surround the IHCs, whose function is to help prevent saturation in currents and excitotoxicity caused by an accumulation of glutamate by expressing glutamate-aspartate transporter (GLAST). These cells achieve this function by taking up the excess glutamate that is found at the synaptic density.

1.1.4.1. Postnatal development of IHC afferent innervation

At birth, both IHCs and OHCs are transiently innervated by type I and type II SGNs (Figure 1.8A) (Perkins and Morest, 1975, Echteler, 1992, Simmons, 1994), however, in the mature cochlea, the IHCs are only innervated by type I SGNs and OHCs are only innervated by type II SGNs. To achieve the mature innervation of the cochlea, there is a refinement and retraction of afferent fibres (Pujol et al., 1998, Sobkowicz et al., 2002, Sobkowicz et al., 2004).

The synaptic afferent terminals that innervate the IHCs begin to alter their localisation between P0-P3, with the synapses being predominantly found at the base of the cells, as opposed to found more sporadically across the IHC length. Between P3-P6 there is the retraction of type I SGNs from OHCs (Figure 1.8B) (Huang et al., 2007). For the accurate refinement and retraction of afferent fibres, neurotrophic factors such as brain derived neurotrophic factor (BDNF) have been shown to be essential (Ernfors et al., 1995, Fritzsche et al., 2004, Wiechers et al., 1999). BDNF is expressed across the organ of Corti and there is increase in SGN loss if BDNF is not present during development, resulting in IHC innervation not maturing properly (Ernfors et al., 1995, Fritzsche et al., 2004, Wiechers et al., 1999).

Furthermore, BDNF has also been implicated for therapeutic treatments for hearing loss, with studies showing it to have hearing restorative potentials via gene therapy treatment (Blakley et al., 2020, Fukui et al., 2012). Spontaneous APs are also involved in the refinement and retraction of SGN fibres by helping send signals to the SGNs, influencing tonotopic differentiation of the afferent pathway (Johnson et al., 2011). By the onset of hearing at P12, the IHC afferent innervation has matured.

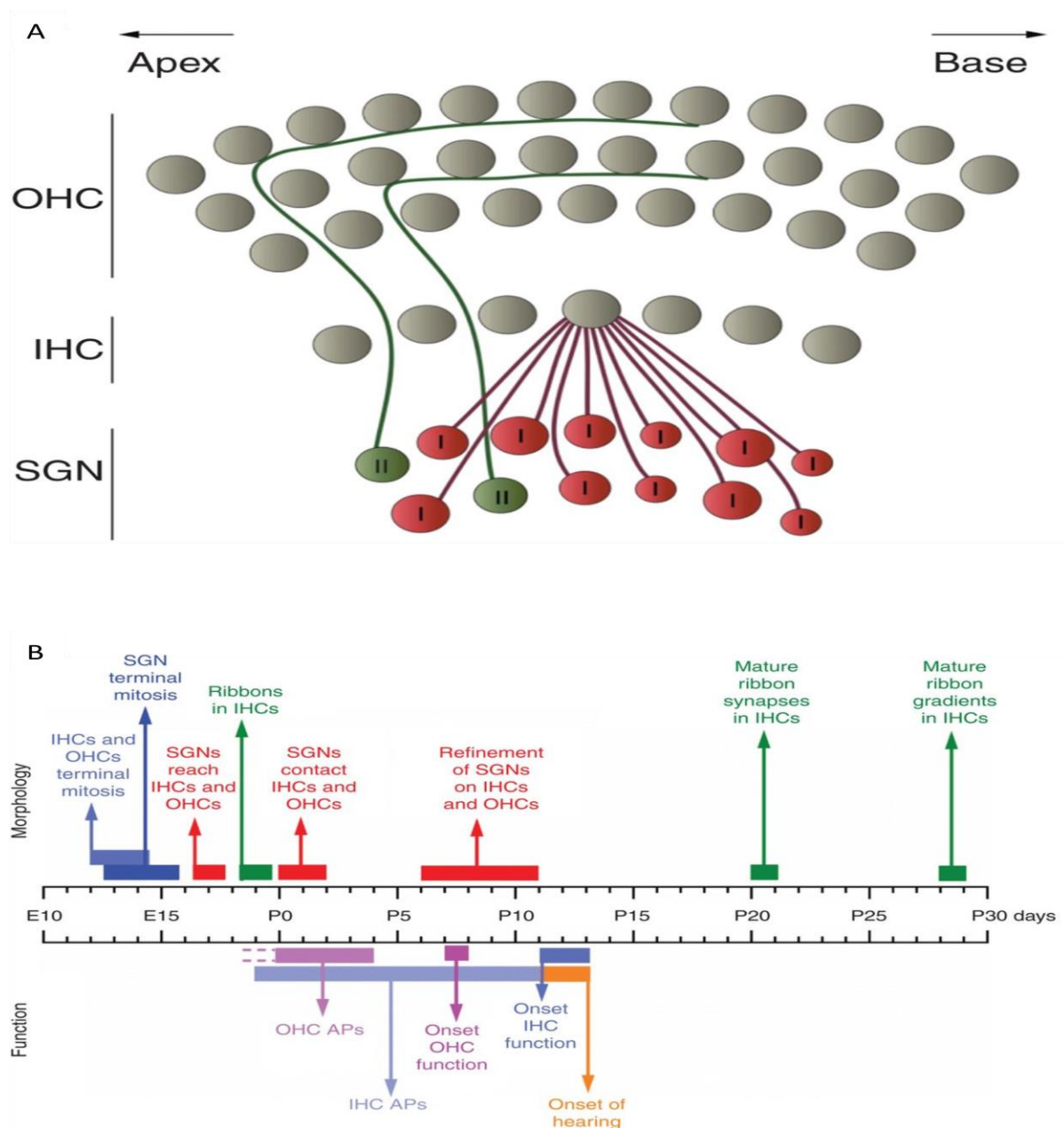


Figure 1. 8. Diagrams depicting the innervation of the IHCs and OHCs, including an overview for the developmental timeline of the afferent innervation.

A: diagram illustrating the innervation of IHCs and OHCs by SGNs in the adult cochlea. Mature IHCs are innervated by ~95% of the type I SGN fibres. In mice, about 10–20 unbranched myelinated SGNs connect with a single IHC while each neuron receives input from only one IHC. The remaining ~5% of SGNs are type II unmyelinated neurons that project toward the OHCs and spiral toward the base of the cochlea contacting multiple OHCs. **B:** diagram showing the functional and morphological maturation of SGNs and hair cells in the mouse cochlea. Figures and figure legends adapted from (Johnson et al., 2019) respectively. For a full list of references relating to information in **B**, see (Johnson et al., 2019).

1.1.4.2. Ribbon synapses in the IHCs

This thesis has currently delved into some of the key differences between the developing IHCs and the mature function IHCs after the onset of hearing at P12. As mentioned previously, when the IHCs are developing they fire spontaneous APs in the first postnatal week, and can fire exogenously induced APs up to P12, at which point the IHCs instead fire sound-induced graded receptor potentials (Cody and Russell, 1987). How these changes are achieved will be covered in this section, firstly by covering the morphology of ribbon synapse and developmental changes from immature to mature.

Ribbon synapses are crucial for transmitting the acoustic information that is converted into electrical signals by the MET channels. The ribbon synapses are excitatory and release glutamate as their neurotransmitter (Kataoka and Ohmori, 1994). After IHCs are depolarised by the opening of the MET channels, L-type $\text{Ca}_v1.3$ channels located near the pre-synaptic region (Figure 1.10) (Platzer et al., 2000, Brandt et al., 2003, Brandt et al., 2005) at the basal pole of the IHCs become activated. The influx of Ca^{2+} triggers the fusing and release of glutamate from vesicles onto the post-synaptic density at the ribbon synapse, inducing excitatory post-synaptic currents in the type I SGNs via the AMPA receptors, sending the signal up the ascending auditory pathway (Sobkowicz et al., 1982, Glowatzki and Fuchs, 2002, Brandt et al., 2005, Keen and Hudspeth, 2006).

Ribbon synapses are the pre-synaptic component that IHCs form with the axosomatic type I SGN innervation mentioned above. The ribbon synapses are characterised by having a large pre-synaptic electron dense structure, which is the central region that synaptic vesicles tether to (Figure 1.9, 1.10) (Smith and Sjöstrand, 1961). However, as mentioned earlier, the ribbon synapse size varies on whether the type I SGN synapse on either the modiolar or pillar side of the IHC. In pre-hearing, developing IHCs, the ribbon synapses are spherical in shape that changes to become more oval/ellipsoid in shape in mature IHCs shape (Figure 1.9) (Sobkowicz et al., 1982, Khimich et al., 2005). Moreover, in development, there are many ribbon synapses within the IHCs (over 30), which decreases to between 10-20 ribbons as IHCs mature – this is concurrent with pruning and refinement of type I SGNs synapsing onto the IHCs, resulting in 1:1 connections between ribbon synapses and SGNs terminals (Michanski et al., 2019, Johnson et al., 2019). The decrease in the number of ribbon synapses in development

(Sobkowicz et al., 1986, Sendin et al., 2007, Huang et al., 2012) is due to the IHCs shifting from firing spontaneous APs and instead firing graded receptor potentials, with reducing Ca^{2+} currents (Johnson et al., 2005, Marcotti et al., 2003b, Zampini et al., 2010). A key component of the ribbon synapse is the readily releasable pools (RRPs) of glutamate filled vesicles found at the base of the ribbon synapse and surrounding the pre-synaptic membrane (Khimich et al., 2005, Johnson et al., 2005). By P6, there are between 600-800 vesicles in a single IHCs RRP, whilst each individual ribbon synapses have a RRP containing 40-50 vesicles (Kantardzhieva et al., 2013), with these numbers being maintained in the mature IHCs. Interestingly, the ribbon synapse lacks typical components for neurotransmitter release that would be found at conventional synapses, such as synaptophysins (Safieddine and Wenthold, 1997, Eybalin et al., 2002), synapsins (Mandell et al., 1990) and synaptotagmin 1 and 2 (Safieddine and Wenthold, 1999).

To understand how the ribbon synapse functions, the molecular composition of the synapse was investigated. The synapse is comprised of several key proteins, one of which is the protein RIBEYE (Figure 1.10). RIBEYE is a scaffold protein at the pre-synaptic terminal and is largely responsible for stabilising the synapse (Magupalli et al., 2008). Mice that have RIBEYE knocked out of their IHCs do not form as many ribbon synapses and have reduced exocytosis (release of glutamate from the synapse), as well as hearing impairments – indicating the importance of RIBEYE in developing mice (Becker et al., 2018, Xiong et al., 2020). The B domain of RIBEYE is identical to the N-terminal of the transcriptional co-repressor; C-terminal-binding protein 2 (CtBP2) a nuclear protein, moreover, RIBEYE and CtBP2 are transcribed from the same gene (Schmitz et al., 2000).

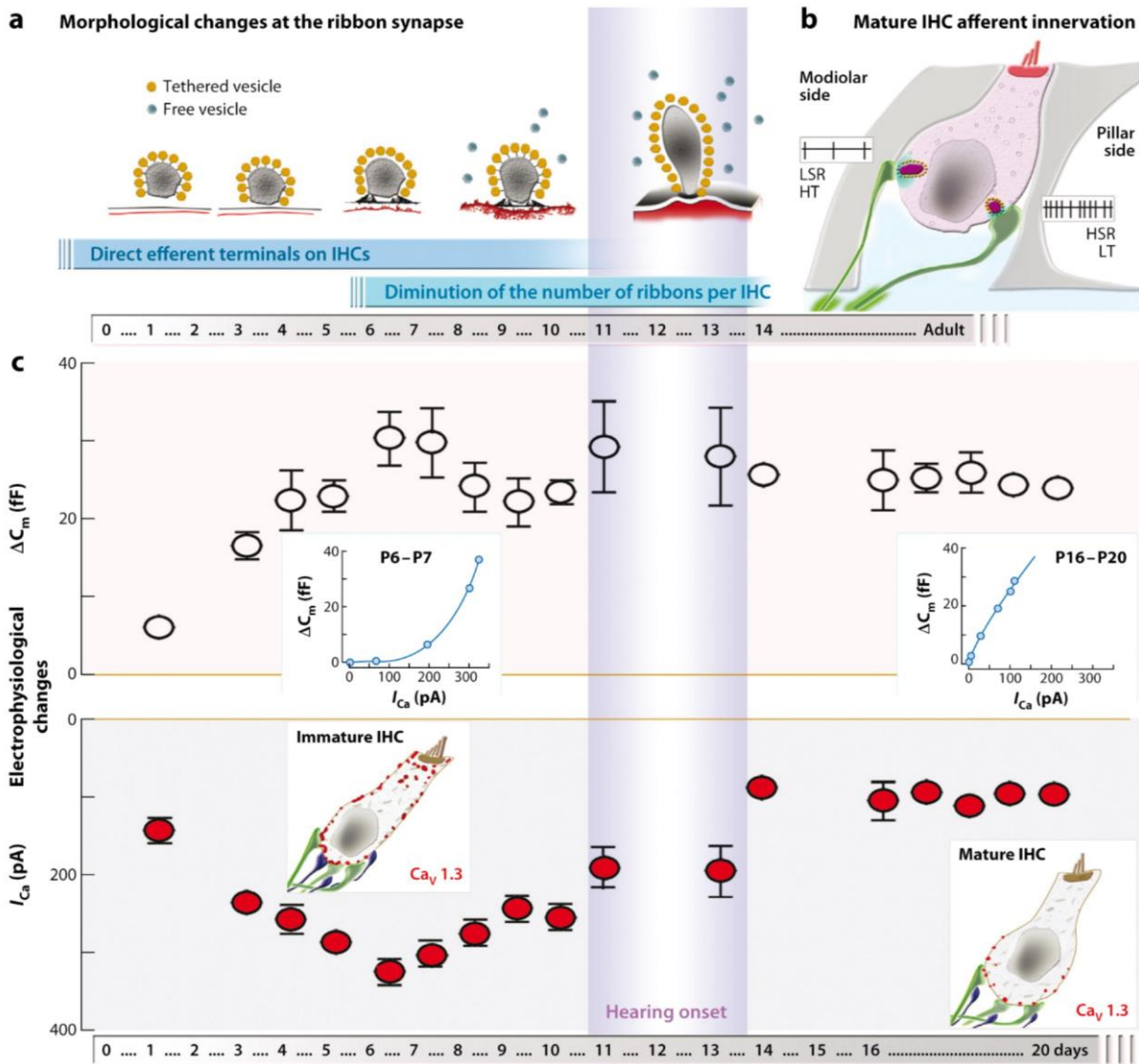


Figure 1. 9. Postnatal maturation of the IHC ribbon synapse and synapse morphology.

A: morphological maturation of the mouse IHC ribbon. **B:** characteristics of afferent innervation at the mature IHC ribbon synapse. Synapses at the modiolar side of the IHC involve afferent neurons that have smaller diameters, higher-threshold (HT) sensitivity, and lower spontaneous rate firing (LSR), and the pre-synaptic regions have larger ribbons (violet) and display higher Ca^{2+} inputs (light green). At the pillar side, the synapses display opposite characteristics. **C:** developmental changes in ΔC_m and I_{Ca} , the top panel shows the relation between I_{Ca} (pre-synaptic Ca^{2+} entry) and vesicle exocytosis, and IHC innervation. Figure from (Safieddine et al., 2012).

Another protein that is essential for functional ribbon synapses in developing IHCs and mature IHCs is the protein otoferlin. Otoferlin is involved with exocytosis at the ribbon synapse as it is a Ca^{2+} sensor in IHCs during the late step of exocytosis, triggering membrane fusion of the vesicles (Figure 1.10) (Roux et al., 2006). To do this role, otoferlin interacts with the SNARE protein SNAP25 at the ribbon synapse (Roux et al., 2006). Mutations in the *OTOF* gene, encoding the otoferlin protein has been implicated in human deafness (inherited recessive profound prelingual deafness, DFNB9) (Roux et al., 2006, Yasunaga et al., 1999), as well as deafness in mice (Dulon et al., 2009, Johnson et al., 2009, Roux et al., 2006, Stalmann et al., 2021, Strenzke et al., 2016, Takago et al., 2019). If otoferlin is knocked out of IHCs in mice, the IHCs have impaired exocytosis as well as there being reduced numbers of type I SGNs and the mice having profound deafness (Roux et al., 2006). Otoferlin can be detected in IHCs from embryonic day 16 and is maintained throughout development and into adulthood (Roux et al., 2006). Otoferlin is such a crucial component of the ribbon synapse and functional hearing, that there has been multiple recent studies that have utilised gene therapy to restore partial hearing function in otoferlin mutant mice (Akil et al., 2019, Al-Moyed et al., 2019).

The vesicular glutamate transporter 3 (Vglut3) is also involved in the ribbon synapse and exocytosis. Vglut3 is responsible for the transport and repackaging of glutamate into vesicles for secretion during exocytosis (Ruel et al., 2008, Seal et al., 2008). Moreover, if Vglut3 is mutated or absent then it results in dominant inherited progressive non-syndromic deafness in humans (DFNA25) (Ruel et al., 2008). The expression of Vglut3 is limited to the IHCs ribbon synapse and when it is knocked out then exocytosis is impaired in IHCs from these mice (Seal et al., 2008). Similar to otoferlin, there have been studies trying to restore hearing function by targeting Vglut3 in IHCs via gene therapy (Akil et al., 2012). Both otoferlin and Vglut3 are relevant for this thesis as a conditional knockout mouse strain targeting otoferlin and using a Vglut3 cre driver was used in the study (see Chapter 4).

In age-related hearing loss and noise-induced hearing loss, there has been historical reports that the ribbon synapses and type I SGNs are preferentially lost on the modiolar side of the IHC (Kujawa and Liberman, 2009, Kujawa and Liberman, 2015, Liberman and Kujawa, 2017). Furthermore, the loss of type I SGNs and ribbon synapses was coined 'hidden hearing loss' (also known as cochlear synaptopathy) due to its difficulty to explain with common hearing diagnostic tests in humans (Kujawa and Liberman, 2015).

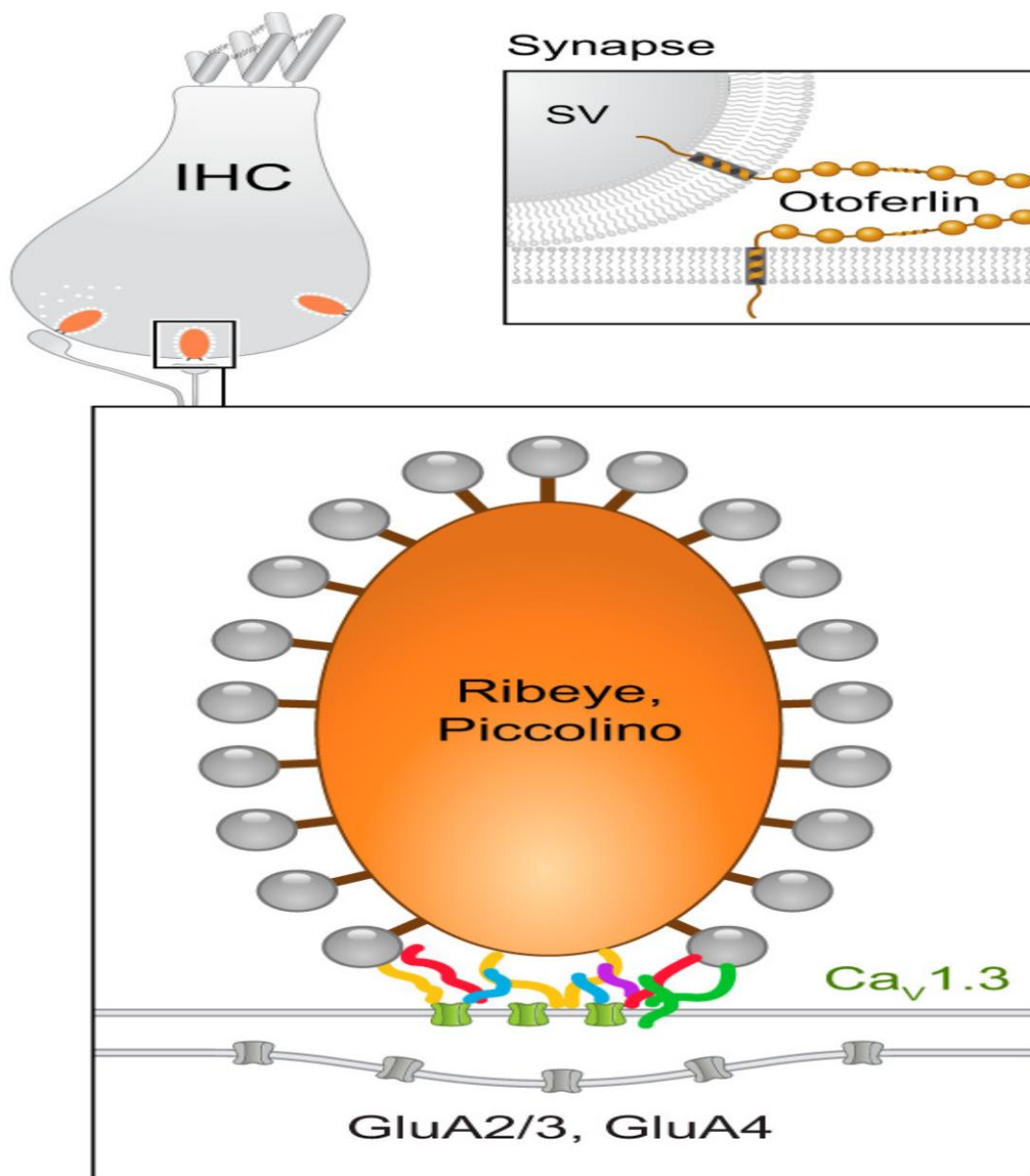


Figure 1. 10. Diagram indicating the IHC ribbon synapse, focusing on otoferlin and the synaptic vesicles.

At the IHC ribbon synapse otoferlin has a function as a Ca²⁺ sensor and is critical for the release of glutamate from vesicles. The lower panel shows the central ribbon that is attached to the pre-synaptic membrane by the Ribeye and Piccolino scaffold proteins. Ca_v1.3 channels are located near to the ribbon synapse and are involved with exocytosis. The glutamate that is released from synaptic vesicles is detected by post-synaptic AMPA receptors, such as GluA2/3 and GluA4. Figure from (Moser et al., 2019).

1.1.5. IHC Efferent Innervation

The efferent system in the cochlea is inhibitory and the efferent innervation of IHCs undergoes a profound change from developmental stages to the mature innervation that is found after the onset of hearing. The efferent fibres predominantly innervate the OHCs, however, as they transiently innervate the IHCs during development, the focus will be on the developmental innervation and why this changes as the cochlea develops.

The auditory efferent system, known as the olivocochlear system, was first discovered in 1946 (Rasmussen, 1946) and its functional inhibition on the auditory system was found a decade later (Galambos, 1956). The efferent system is subdivided into two types of efferent fibres, determined by their origin within the superior olivary complex (SOC), as well as their termination at the target cochlear hair cells (Warr, 1975, Warr and Guinan, 1979). There are the medial olivocochlear efferent fibres (MOC), originating in the medial and rostral nuclei of the SOC and terminating directly (axosomatic) on the mature OHCs. However, during development, the IHCs are transiently innervated by the MOCs up to the onset of hearing (Figure 1.11A) (Guinan and Stankovic, 1996, Guinan, 2006, Guinan et al., 2011). The lateral olivocochlear efferent fibres (LOC) originate in the lateral nuclei of the SOC, and terminate on the dendrites (axodendritic) of the type I SGNs beneath the basal pole of the mature IHCs (Figure 1.11B) (Bruce et al., 2000, Simmons, 2002). Both the MOC and LOC fibres have ipsilateral and contralateral projections, however, the LOC fibres project predominantly to the ipsilateral cochlea, whereas the MOC fibres project predominantly to the contralateral cochlea (Guinan Jr et al., 1983, Robertson and Gummer, 1985). The MOC innervation of the cochlea is highly branched and myelinated, and the region of the cochlea innervated by an efferent fibre matches that of an afferent fibre with the same characteristic frequency, thus, the efferent innervation is tonotopically organised, as is the afferent innervation (Liberman and Brown, 1986, Brown, 2014).

1.1.5.1. Postnatal development of IHC efferent innervation

At birth, efferent fibres have been labelled and visualised near the IHCs, with an indication that the membranes form synapses, but not near OHCs (Figure 1.11A) (Bruce et al., 1997, Bruce et al., 2000). By P2, there is a diffuse efferent innervation of the first row of OHCs, however the efferent fibres begin to form spiral bundles; dense bundles of multiple efferent fibres and are localised mostly to supporting OHCs. The inner spiral bundle is distinct by P4 as it innervates the immature IHCs, whereas there is only sparse innervation of the OHCs (Sobkowicz and Emmerling, 1989, Bruce et al., 2000). At P6, the transient innervation of immature IHCs is still present and the radial efferent fibres pass between the supporting OHCs and innervate the Deiter's cells - supporting cells in the OHC region. Between P8-10, the inner spiral bundle increases in size, especially on the modiolar side of IHCs and the efferent fibres are localised to the base of OHCs (Bruce et al., 2000). The transient innervation of immature IHCs by efferent fibres progressively disappears from around the onset of hearing in mice (Figure 1.10A); by P21, there is no response at all to exogenous application of ACh (Glowatzki and Fuchs, 2000, Marcotti et al., 2004). Because of this transient innervation, it was postulated that ACh and efferent feedback play a role in the maturation of IHCs by reducing their activity (Uziel et al., 1981, Glowatzki and Fuchs, 2000). On the other hand, OHCs gain axosomatic efferent innervation between P4-6 (Figure 1.11B) and show sensitivity to ACh by P8 (Dulon and Lenoir, 1996, He and Dallos, 1999), which coincides with their onset of electromotility (He et al., 1994) and maturation (Marcotti and Kros, 1999).

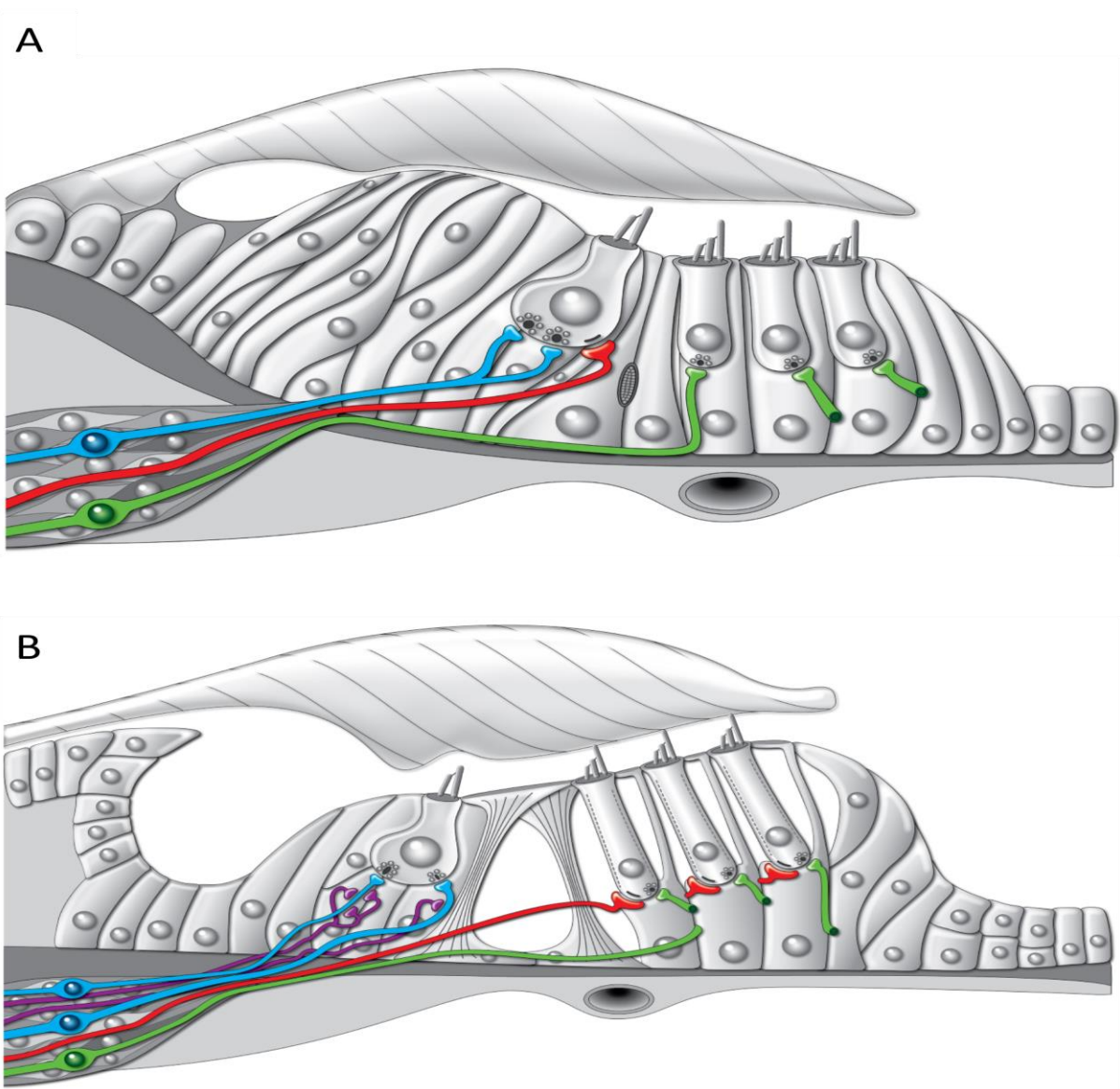


Figure 1. 11. Schematics of the immature and mature organ of Corti, demonstrating the development of the afferent and efferent innervation.

A: immature organ of Corti in the first postnatal week. IHCs have transient afferent (blue) and efferent (red) axosomatic (direct) synapses. The IHCs are innervated by type I spiral ganglion neuron (SGNs) fibres through postnatal life. The immature IHCs have immature ribbon synapses that are more spherical in shape. The OHCs are sparsely innervated by type II SGN fibres. **B:** mature organ of Corti. IHCs lose the axosomatic efferent innervation, with the lateral olivocochlear fibres (purple) forming axodendritic synapses with the type I SGN fibres beneath the IHC. The ribbon synapses also mature to have a more oval / elliptical shape after the onset of hearing at P12. The OHCs have axosomatic efferent innervation from medial olivocochlear fibres (red) throughout adulthood.

Building upon the findings from the Uziel et al., 1981, the functional role of the IHC MOC axosomatic efferent innervation was shown to modulate the IHCs as they fire spontaneous APs during development, and during IHC maturation (Glowatzki and Fuchs, 2000, Goutman et al., 2005, Johnson et al., 2013b, Moglie et al., 2018, Wedemeyer et al., 2018). This is crucial, because if the efferent innervation of IHCs in development is lost, then there is a resulting loss of tonotopic organisation associated with hearing loss in the frequencies effected (Clause et al., 2014, Clause et al., 2017). The main neurotransmitters for MOC fibres include ACh, GABA, CGRP (calcitonin gene related peptide), ATP, enkephalins and NO (nitric oxide), however, the predominant neurotransmitter is ACh, as the efferent fibres are cholinergic inhibitors (Safieddine and Eybalin, 1992, Eybalin, 1993, Schrott-Fischer et al., 2007). As mentioned previously, the nAChRs and SK2 channels are found in the efferent synapse in IHCs during development (see section 1.1.3.1). The inhibitory mechanism of the efferent fibres for hyperpolarising the IHC functions via nAChRs stimulation allowing Ca^{2+} to enter the IHC, which activates the SK2 channels and results in K^+ leaving the IHC (Marcotti et al., 2004, Glowatzki and Fuchs, 2000, Katz et al., 2004).

As the IHCs lose their MOC efferent innervation during development of the IHCs, the MOC fibres innervate the OHCs in the mature cochlea. Once the cochlea is mature, the MOC fibres have a plethora of functions, most of which act to change cochlear mechanisms in order to prevent overstimulation (Patuzzi and Thompson, 1991, Maison and Liberman, 2000, Maison et al., 2002, Taranda et al., 2009). The identification of MOC functions was originally performed in non-mammalian vertebrates such as fish, frogs and turtles. The findings similarly showed that stimulation of the MOC fibres induced an inhibitory post-synaptic potential, hyperpolarising the hair cells and reducing the excitatory post-synaptic currents recorded from SGNs (Flock and Russell, 1973, Art et al., 1984, Art et al., 1985). In the mammalian cochlea the efferent inhibition reduces the electromotility of mature OHCs (Brown et al., 1983, Brown and Nuttall, 1984). Moreover, the MOC system aids with selective attention (Oatman, 1976, Delano et al., 2007, Terreros et al., 2016), as well as signal detection within noisy environments (Nieder and Nieder, 1970a, Nieder and Nieder, 1970b, Winslow and Sachs, 1987, Dolan and Nuttall, 1988, Kawase et al., 1993).

The LOC fibres do not form direct synapses with the IHCs during development, or in the mature cochlea, instead, they form synapses onto the type I SGN fibres (axodendritic) that innervate the IHCs. Similar to how the MOC fibres modulate the spontaneous APs that developing IHCs fire, the LOC fibres modulate the spiking activity of the type I SGNs directly, demonstrating an inhibitory function (Hossain et al., 2005). The LOC fibres have been less extensively studied compared to MOC fibres, mainly due to the fibres being thin and unmyelinated, making them more difficult to electrically stimulate in studies (Ranck Jr, 1981, Gifford and Guinan, 1987). As the LOC fibres are also inhibitory, their neurotransmitters are similar to those mentioned earlier for MOCs, such as ACh, GABA and CGRP, however, LOC fibres also release dopamine (DA), serotonin and opioids such as dynorphin or enkephalin (Altschuler et al., 1985, Altschuler et al., 1988, Safieddine and Eybalin, 1992, Eybalin, 1993).

Studies have indirectly activated the LOC fibres via stimulation of the inferior colliculus (IC), which is upstream of the LOC fibres in the hearing pathway, revealing that LOC efferents have two functional subdivisions; either increasing or decreasing the magnitude of responses in the type I SGNs, with a proposed importance for aiding the accuracy of binaural comparisons, which is possible due to the variety of neurotransmitters released (Groff and Liberman, 2003). Early studies of LOC efferent inhibition required different approaches in order to elucidate how the inhibition works. One method focused on chronic or acute impacts upon the SGNs following de-efferentation (Liberman, 1990). Alternatively, targeting the various neurotransmitters of LOC synapses gained insight into how the system works, whether that be focusing on ACh, GABA, opioid agonists or CGRP (Sahley et al., 1991, Felix and Ehrenberger, 1992, Arnold et al., 1998, Bailey and Sewell, 2000). Some of the neurotransmitters have also been the focus of targeted deletion and analysing the effect on the LOC system – such as CGRP (Maison et al., 2003).

The origins of the MOC and LOC neurons varies slightly, with the place of origin influencing their functions. The MOC neurons are found in the ventral nucleus of the trapezoid body (VNTB) and have a relatively uniform population of neurons, whereas the LOC neurons are located within the lateral superior olive (LSO) - both the LSO and VNTB are located in the SOC of the brainstem (Figure 1.12) (Frank and Goodrich, 2018). The LOC neurons that the LSO contains have two subtypes 'shell' neurons that are found in the periphery of the LSO, as well as the 'intrinsic' neurons found centrally within the LSO (Brown, 1987, Vetter and Mugnaini,

1992, Warr et al., 1997). The two subtypes of LOC neurons also differentially innervate the type I SGNs, as the shell neurons bifurcate and sparsely innervate the SGNs along the cochlea, alternatively, the intrinsic neurons form high density patches along the cochlea (Brown, 1987, Vetter and Mugnaini, 1992, Warr et al., 1997). The variability in LOC neuron morphology, innervation pattern of type I SGNs and neurotransmitter release is believed to enable the neurons to have both inhibitory and excitatory impacts on the SGN firing activity (Brown, 1987, Warr et al., 1997, Darrow et al., 2006, Elgoyhen et al., 2018).

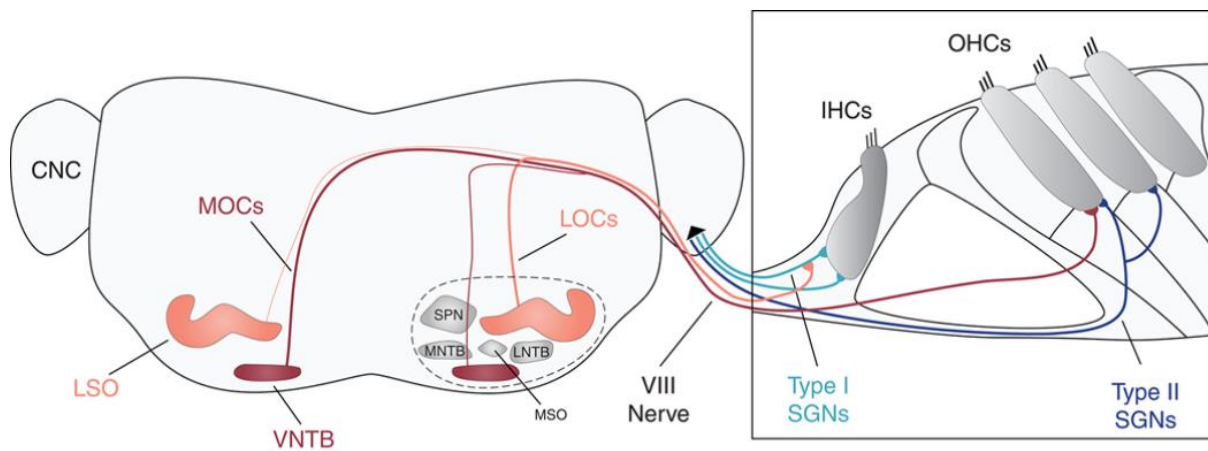


Figure 1. 12. Organisation of the mammalian olivocochlear efferent system.

Auditory information transduced by inner (IHCs) and outer hair cells (OHCs) is conveyed to the auditory brainstem via Type I and Type II spiral ganglion neurons (SGNs), respectively. SGNs project into the brain via the VIII nerve and synapse onto neurons in the cochlear nuclear complex (CNC). The superior olivary complex (SOC, dashed circle) contains multiple nuclei involved in sound localization, including the medial superior olive (MSO), lateral superior olive (LSO), ventral nucleus of the trapezoid body (VNTB), lateral nucleus of the trapezoid body (LNTB), medial nucleus of the trapezoid body (MNTB), and the superior periolivary nucleus (SPN). Medial (MOCs) and lateral (LOCs) olivocochlear neurons reside primarily in VNTB and LSO, respectively, and project back to the sensory epithelium via the VIII nerve. Other types of neurons are also housed in VNTB and LSO, including the neurons that mediate afferent responses, but only MOCs and LOCs are indicated for simplicity. Within the cochlea, LOCs form synapses with Type I SGNs, whereas MOCs terminate on OHCs. Figure and figure legend from (Frank and Goodrich, 2018).

The MOC and LOC neurons are both susceptible to damage related loss, as well as age-related loss. In age-related hearing loss (ARHL), there seemingly is a greater loss of MOC neurons as opposed to LOC neurons, which may be due to the differences in their mechanisms of action on modulating either hair cell or SGN activity (Liberman, 2017, Liberman and Liberman, 2019, Kobrina et al., 2020). Interestingly, in ARHL there has been reports of the IHCs being re-innervated by efferent fibres (Lauer et al., 2012, Zachary and Fuchs, 2015, Jeng et al., 2021). The remainder of this thesis introduction will now focus on age-related hearing loss and expand more on how the efferent re-innervation of IHCs was discovered, as this is crucial for this study.

1.2. Age-related hearing loss

One of the key studies of this thesis is using an age-related hearing loss mouse model to study the efferent re-innervation of IHCs (see section 1.2.4). Therefore, this section will introduce age-related hearing loss, as well as highlighting what is currently known about the efferent re-innervation, in addition to what is still yet to be discovered about the process.

Amongst the various sensory deficits that humans can potentially encounter, age-related hearing loss (ARHL) and its progression is one of the most common (Howarth and Shone, 2006). ARHL is the most common cause of hearing loss and in 1955 it was termed presbycusis (Schuknecht, 1955). Presbycusis encompasses all aspects and aetiologies that cause hearing loss in elderly people (Figure 1.13) (CHABA, 1988). The condition results in a deterioration in hearing sensitivity and speech understanding in noisy environments, in addition to slowed central processing of acoustic information and impairments in sound localisation capabilities (Gates and Mills, 2005). ARHL is estimated to affect approximately two thirds of people over the age of 70 in the United States, and in 2020 half of the people with ARHL were expected to be over 70 years old (Tu and Friedman, 2018). Interestingly, males have shown to be more susceptible to ARHL (Figure 1.13B) (Jerger et al., 1993). In the UK, more than 40% of people over 50 have hearing loss, increasing to <71% of people over 70 years old (Action on hearing loss, (2019). Additionally, it is expected that by 2060, the number of people with moderate to profound hearing loss will be more than those who have mild hearing loss, showing the upward struggle that many people will have to overcome in the future (Goman et al., 2017).

ARHL does not affect the auditory system alone, it impacts an individual's physical and social life, as well as being involved with a plethora of systemic complications and cognitive disorders (Gates and Mills, 2005, Howarth and Shone, 2006, Liu and Yan, 2007, Van Eyken et al., 2007b, Sprinzl and Riechelmann, 2010, Lee, 2013). Therefore, ARHL impacts on many different areas of an individual's life, thus decreasing the quality of life, as depression, social isolation and low self-esteem are often stimulated by ARHL (Mulrow et al., 1990).

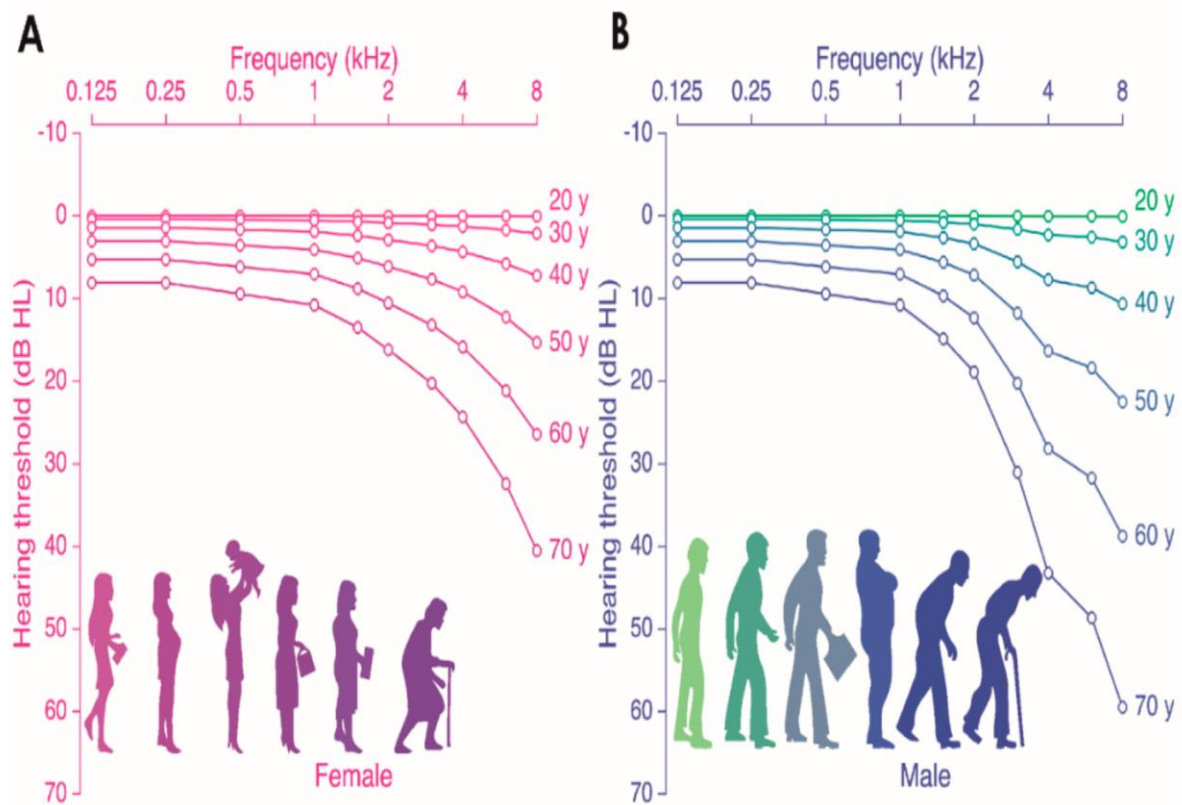


Figure 1. 13. Age-related hearing loss changes in audiogram hearing thresholds.

A: audiograms for females, with the x-axis displaying the pure tone frequency (Hz) and the y-axis the hearing thresholds (dB HL). **B:** audiogram for males. Each individual graph is representative of the median audiogram at a specific age (from 20 to 70 years old, with increments of 10 years). Figure and figure legend from (Wang and Puel, 2020).

1.2.1. Pathophysiology of ARHL

ARHL is a progressive and bilateral sensory-neural hearing loss (SNHL). The hearing loss associated is often mild-moderate, with decreases in audiometric mid-high frequencies (2-8 kHz) (Jafari et al., 2019). However, the pathophysiology of presbycusis is multifactorial, complex and has been divided into different types and categories. Initially there were the sensory, neural and stria (metabolic) categories of presbycusis, until this was expanded into a potential six different categories in 1993 (Table 1.1) (Schuknecht, 1955, Schuknecht, 1964, Schuknecht and Gacek, 1993). However, of the six different types; sensory, neural, stria (metabolic) and cochlear conductive are the most common.

Sensory presbycusis stems from degeneration primarily of the OHCs in the organ of Corti (Crowe et al., 1934), usually in the basal turn of the cochlea and expanding progressively toward the apex, initially inducing high frequency hearing loss (Hansen and Reske-Nielsen, 1965, Johnsson and Hawkins, 1972, Dublin, 1976, Schuknecht and Gacek, 1993). The progression of degeneration from sensory presbycusis was found to be the same in mammalian animal studies and in humans (Suga and Lindsay, 1976, Wright et al., 1987, Bhattacharyya and Dayal, 1989). Sensory presbycusis, however, has a relatively low incidence rate as claimed by Schuknecht, with future studies corroborating the claim that only 5% of total presbycusis cases are likely to be of the sensory type (Schuknecht and Gacek, 1993, Gates et al., 2002).

Likewise, neural presbycusis results in a downward slope in pure tone thresholds towards high frequencies and subsequent severe difficulties with speech discrimination when compared to pure tone thresholds (Schuknecht and Gacek, 1993). Furthermore, in order to be categorised as neural presbycusis, there must be a <50% loss of neurons, from the total 35,500 afferent neurons (Lee, 2013). Previously it has been shown that there is a loss of approximately 2100 neurons every 10 years in humans (Otte et al., 1978). The resulting loss of 50% or more of the afferent neurons is responsible for the difficulties in speech discrimination and when up to 90% of neurons are lost, there is a shift in the auditory threshold (Pauler et al., 1986, Makary et al., 2011). Moreover, there seems to be a heightened loss of modiolar SGN neurons that are lost, as opposed to pillar neurons (Liberman and Kiang,

1978, Stamatakis et al., 2006, Kujawa and Liberman, 2009, Kujawa and Liberman, 2015, Liberman and Liberman, 2019).

Strial presbycusis, also known as metabolic, is characterised by hearing loss across all frequencies of the audiogram as well as atrophy of the stria vascularis (Pauker et al., 1988), thus decreasing the endocochlear potential that is generated via the normal K^+ recycling function of the stria vascularis (Review section 1.1. for more details). The dysfunctional K^+ recycling affecting the endocochlear potential is the underlying mechanism that is responsible for the cochlea-wide hearing loss across all frequency ranges (Pauker et al., 1988). Furthermore, studies in gerbils have shown that high frequency hearing loss is associated with the loss of the endocochlear potential and the degree of hearing loss will vary with the severity of disruption to the EP (Schulte and Schmiedt, 1992, Gratton et al., 1996, Gratton et al., 1997a, Gratton et al., 1997b, Spicer and Schulte, 2005). Additionally, strial/metabolic presbycusis is the most common form of ARHL in humans (Mills and Schmiedt, 2004).

The other main type of presbycusis that will be discussed briefly is cochlear conductive. This type is more elusive compared to the other three main types mentioned above as it is difficult to conclusively classify the forms of degeneration (Schuknecht and Gacek, 1993). The proposal of a cochlear conductive form of presbycusis was suggested a few years before its inclusion as one of the six types (Ramadan and Schuknecht, 1989). Cochlear conductive presbycusis presents itself as a degeneration as a result of the stiffening of the basilar membrane and basal regions of the cochlea, with linear decreasing audiograms (Schuknecht, 1964, Ramadan and Schuknecht, 1989, Schuknecht and Gacek, 1993, Lee, 2013). The other two forms of presbycusis: mixed and indeterminate, as well as summaries of the six types can be seen in Table 1.1.

Type of Presbycusis	Histopathologic change	Audiometric change
Sensory	Sensory cell loss within the organ of Corti at the base of the cochlea, typically OHC.	Problems with amplification of the high frequency sounds encoded at the 4 kHz frequency (Keithley, 2019), which equates to high frequency hearing loss.
Neural	Loss of type I SGNs.	Progressive loss in word discrimination in the presence of stable pure tone thresholds.
Strial (Metabolic)	Atrophy of the stria vascularis.	Problems with amplification of high frequency sounds in the >2 kHz region, hearing loss in all frequencies.
Cochlear conductive (mechanical)	Stiffening of the basilar membrane.	Linear descending audiograms.
Mixed	Combination of different pathologies.	Down-slope hearing loss towards high frequency and abrupt increases in the threshold at high frequencies. Different changes seen depending on the combination of pathologies.
Indeterminate	No consistent pathology.	Abrupt high tone hearing loss but with no consistent pathology to correlate to audiometric findings.

Table 1. 1. The typologies of presbycusis along with the histopathologic and audiometric changes seen in each type. Table adapted from (Schuknecht and Gacek, 1993).

Ageing of the auditory system is more often than not, manifested with a loss of receiving inputs from the periphery, but it can also occur from damage to the central components of auditory processing (Jafari et al., 2019). Central presbycusis often results in speech discrimination difficulties that cannot be explained by the peripheral (cochlear) hearing loss and typically do not improve when using hearing amplification systems such as hearing aids (Gates, 2012). However, it has also been proposed that central presbycusis could progress independently of the peripheral forms of degeneration (Gates and Mills, 2005, Ouda et al., 2015). The conversion of auditory stimuli, such as vocal sounds and speech comprehension, and subsequent processing that occurs within the brain is exceedingly complex. Both peripheral and central auditory systems are necessary, in addition to multiple interactions with other brain regions (Hickok and Poeppel, 2007, Hickok et al., 2011, Ouda et al., 2015, Skipper et al., 2017). Thus, any defects and deterioration within the peripheral or central auditory systems drastically decreases the accuracy of speech recognition, as well as impacting the overall acuity of auditory neural processing (Lin et al., 2011, Basner et al., 2014, Bilodeau-Mercure et al., 2015).

1.2.2. Risk factors of age-related hearing loss

In addition to the pathologies for ARHL, there are mechanistic risk factors that underlie the degeneration of hearing. As alluded to earlier, the complexity of ARHL is vast, and the disorder is multifactorial, with intrinsic, extrinsic and genetic factors (Figure 1.14).

Genetic risk factors for ARHL have been established, with varying severity distinct between the different types of ARHL. For example, one study showed that inheritability is greater for strial/metabolic presbycusis (Gates et al., 1999). Moreover, in humans there is an estimated 25% to 75% variability in the pathological types of presbycusis that have been linked to a genetic component (Gates et al., 1999, Christensen et al., 2001, Viljanen et al., 2007). Multiple genes have been identified in causing a predisposition towards ARHL, affecting different aspects of the cochlea. Genetic polymorphisms were found in genes encoding antioxidant enzymes, such as glutathion S-transferase (*GSTM1* and *GSTT1* – null genotype) and N-acetyltransferase (*NAT2*6A*) showing links to ARHL (Ünal et al., 2005, Van Eyken et al., 2007a, Bared et al., 2010).

There are not just genetic and intrinsic risk factors effecting ARHL, as with most diseases there are different environmental factors that effect it also. Some environmental factors include lifestyle choices such as alcohol consumption and cigarette smoking, whereas others could come from noise exposure or ototoxic medications (aminoglycosides, cisplatin, salicylate and loop diuretics) (Cruickshanks et al., 1998a, Cruickshanks et al., 1998b, Dalton et al., 1998, Fransen et al., 2003).

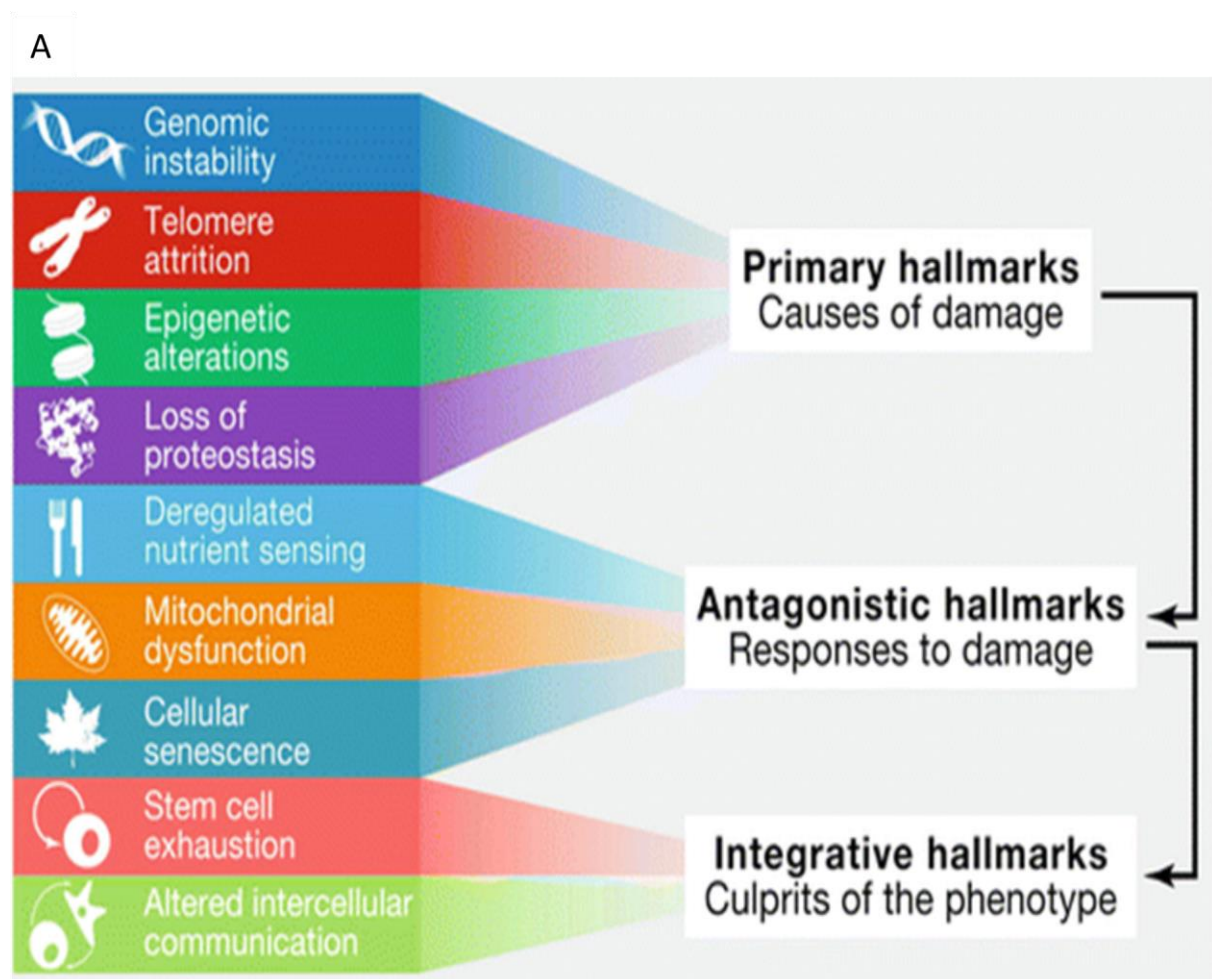


Figure 1. 14. Principle intrinsic, extrinsic and genetic factors that affect ARHL.

An overview of the multifactorial and complex mechanisms that effect ARHL in different ways. Figure and figure legend from (Melgar-Rojas et al., 2015).

A common environmental risk factor for ARHL can come from noise overexposure, which in turn results in noise-induced hearing loss (NIHL). Noise-induced hearing loss is characterised by either permanent or reversible (temporary) shifts in auditory thresholds following overexposure to loud noise (Figure 1.15A) (Clark and Bohne, 1999, Rabinowitz, 2012). There is a relationship between ARHL and NIHL which has been the focus of a large body of studies since the millennium. The ageing processes within the cochlea could be accelerated over time due to noise exposure inducing malfunctioning homeostasis and protective mechanisms (Gates et al., 2000, Ohlemiller, 2006). There were two hypotheses relating to the interactions between NIHL and ARHL in the last decade, one proposed that there is an age-noise interaction which would exacerbate ARHL in previously noise damaged ears (Gates and Mills, 2005). Conversely, the second hypothesis proposed that noise history had no significant impact on the threshold changes rate, in a study performed in elderly patients (Lee et al., 2005). The interactions between NIHL and ARHL in humans are still under some debate today. Multiple studies have shown that noise exposure in ARHL mouse models triggers widespread, progressive neuronal loss within the cochlea (Figure 1.15B & C) and exacerbates ARHL (Kujawa and Liberman, 2006). Expanding upon this, a study showed that an acute synaptopathy (preferential loss of modiolar type I SGNs) occurs in NIHL even after hair cells recover from damage and thresholds return to normal, therefore accelerating ageing (Fernandez et al., 2015). Overall, there are common pathologies for NIHL, ARHL and hidden hearing loss (HHL), such as the loss of type I SGNs and ribbon synapses (Kujawa and Liberman, 2015).

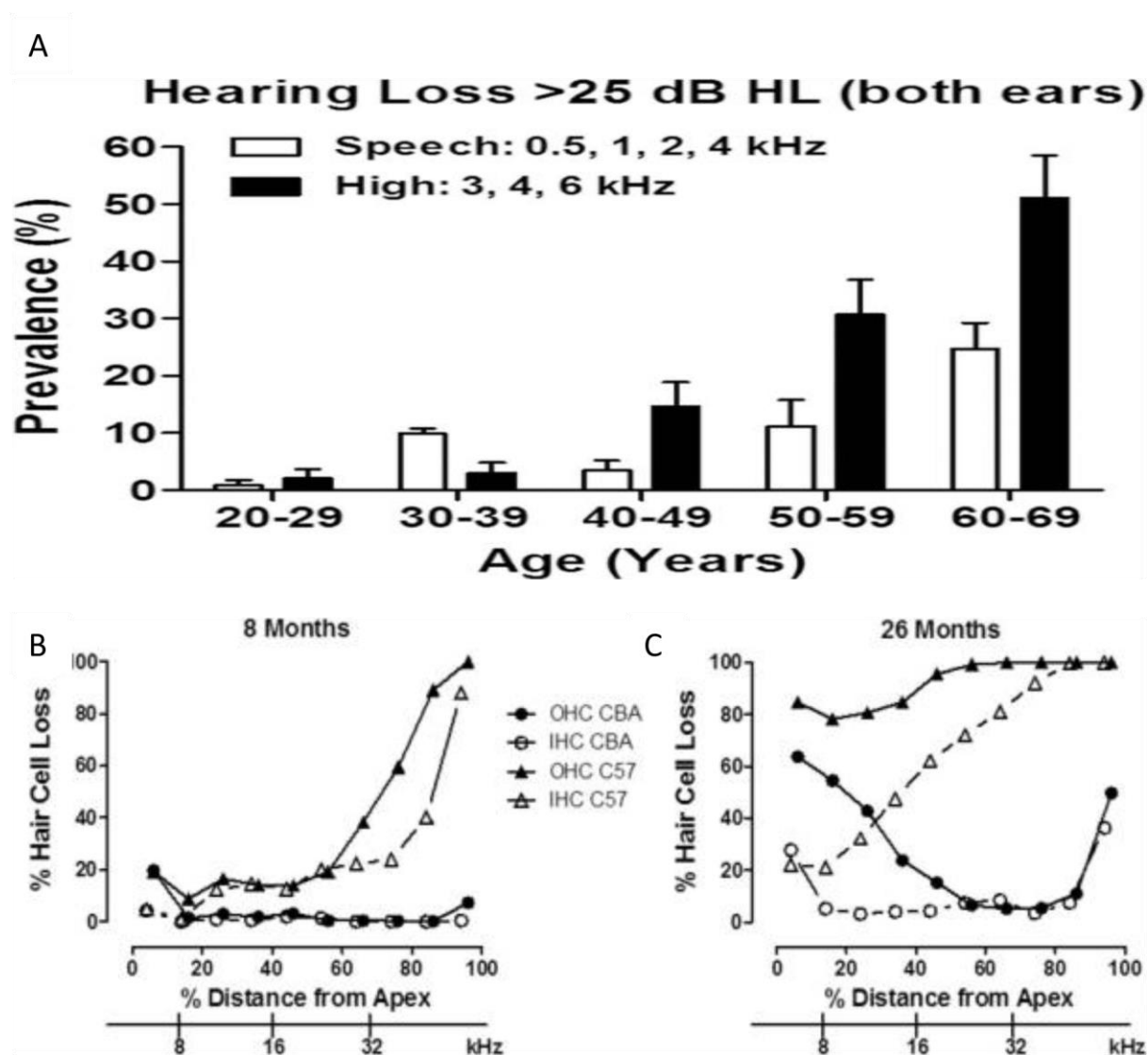


Figure 1. 15. Diagrams to show the effect of age-related hearing loss.

A: prevalence of Speech-Frequency and High-Frequency, bilateral hearing impairment in United States women and men from US National Health and Nutrition Examination Survey, 2011–2012. Bilateral impairment defined as pure tone average in both ears > 25 dB HL. **B & C:** cochleograms that show the percentage of OHC and IHC loss as a function of percentage distance from the apex of the cochlea in CBA and C57BL/6 mice at 8 months and 26 months of age (ARHL mouse models). Frequency vs. place map shown on lower x-axis. Figure and figure legend adapted from (Salvi et al., 2018).

Additionally, other studies revealed that long term effects of noise on young ears could be detrimental, following early onset NIHL cases (Wallhagen et al., 1997). Moreover, NIHL can cause temporary or permanent shifts in auditory thresholds, depending on the duration and intensity level (loudness) of noise exposure; these reversible threshold shifts are common within a human's lifespan (Rabinowitz, 2012). Inducing a temporary NIHL is sufficient to result in cochlear synaptopathies in mice (Kujawa and Liberman, 2009, Sergeyenko et al., 2013). Studies in rats discovered that repetitive exposure to a short duration sound over a long time period induces early onset ARHL, compared to non-exposed control rats (Alvarado et al., 2014, Alvarado et al., 2016, Alvarado et al., 2019). However, it is possible that due to the studies design, repetitive exposure to NIHL could accumulate and induce hearing loss. It has been proposed that NIHL and ARHL share 'common pathogenic pathways' and there are synergistic interactions between the two processes. These interactions involving coincident, overlapping or independent mechanisms ultimately result in sensorineural hearing loss (Alvarado et al., 2015, Tavanai and Mohammadkhani, 2017, Alvarado et al., 2018). Overall, whilst studies aim to further the understanding of the connection between NIHL and ARHL, the concepts and understanding is relatively poor (Fetoni et al., 2011). Whilst some findings point towards the suggestion that long-term noise exposure could modify the onset of ARHL, particularly in neural presbycusis (Wang and Puel, 2020).

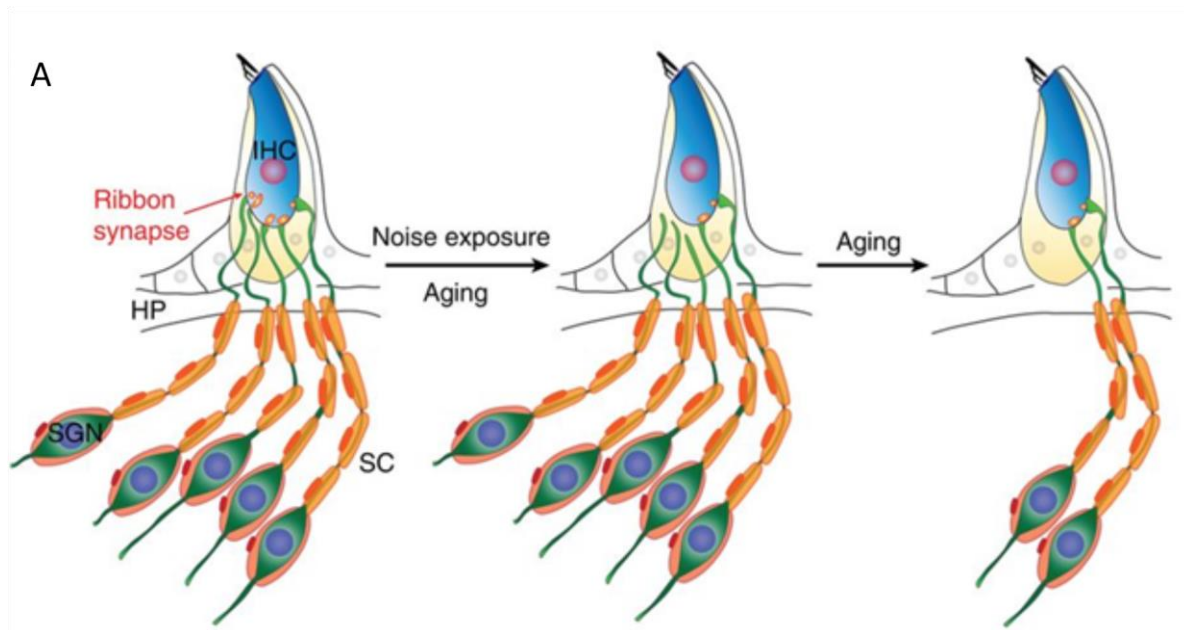


Figure 1. 16. Diagram showing the effect of NIHL and the synaptopathy that occurs in the same manner as ARHL synaptopathy.

A: model for HHL caused by cochlear synaptopathy. Noise exposure and ageing result in preferential synaptic degeneration of modiolar type I SGNs. Figure from (C Kohrman et al., 2020).

1.2.3. Mouse models of age-related hearing loss

There are similarities in the onset and progression of ARHL in both humans and mice, therefore, for many decades' mouse models have been used to study the disease. The subsequent sections will focus on mouse models of ARHL as the mouse cochlea is anatomically similar to humans, and the hereditary abnormalities are also comparable (Steel and Bock, 1983, Brown and Steel, 1994, Steel and Brown, 1996). Past genetic analysis focused on mouse models, revealing nearly 100 naturally occurring mutations that could form the basis of human hearing deafness studies (Lyon and Searle, 1989, Steel, 1995, Steel and Brown, 1996). A prime example is the shaker-1 mice (*sh1*) which have characteristic hyperactivity, head shaking and circling behaviours, the mutation was identified to be within the *myo7a* gene via positional cloning (Gibson et al., 1995). Subsequently, mutations in the homologous human *myo7a* gene were revealed to underlie non-syndromic hearing impairments such as autosomal dominant 11 (DFNA11) and autosomal recessive 2 (DFNB2) (Well et al., 1995, Liu et al., 1997a, Liu et al., 1997b).

There are also many different inbred mouse strains which can be specific for different forms of hearing loss, with at least 10 out of ~80 strains showing the *Ahl* (age-related hearing loss) locus found on chromosome 10 that impacts ARHL (Erway et al., 1993, Johnson et al., 1997, Fetoni et al., 2011). The C57BL/6J (6J) mouse strain is frequently used for early-onset ARHL studies since the cochleae show sensory and neural presbycusis typologies, as defined by Schuknecht, together with progressive hearing loss (Church and Shucard, 1986, Hunter and Willott, 1987b, Shone et al., 1991, Schuknecht and Gacek, 1993, Erway et al., 1993, McFadden and Willott, 1994, Walton et al., 1995, Johnson et al., 1997, Willott et al., 1995, Parham, 1997). The 6J strain exhibits rapid ARHL, by 6 months of age there is significant hearing loss at high frequencies (>20 kHz) and hearing loss at low frequencies by 12 months of age. In addition, by 15 months of age, the 6J mice have profound hearing loss (Li and Borg, 1991). The 6J mice are homozygous for the defective *Ahl1* (*or 753A*) allele of the gene encoding CDH23 involved in the tip link complex and MET (Johnson et al., 2000, Bowl and Dawson, 2015).

As opposed to the widely used 6J mouse model of ARHL there is also the CBA mouse strain – which is a good hearing strain. The CBA strain has consistently shown that it is resistant to the progressive deterioration caused by ARHL, with mice retaining their hearing sensitivity until

around 18 months of age (Willott, 1986, Hunter and Willott, 1987a, Willott and Bross, 1990, Jacobson et al., 2003). However, the CBA mice have peripheral neuronal loss and following 18 months of age, there is a progressive decline in hearing sensitivities, starting at high frequencies and progressing to low frequencies (Li and Borg, 1991, Jacobson et al., 2003). This results in the CBA mice being a late-onset hearing loss strain. Additionally, after 18 months there is progressive IHC and OHC loss occurring in a basal-apical gradient, corresponding to the high-low frequency loss of hearing sensitivity (Spongr et al., 1997).

An alternative mouse model for hearing loss studies have utilised the C3H/HeJ (C3H) mouse strain. The C3H mouse strain has many different inbred sub strains and have been found to have good hearing for up to 14 months (Trune et al., 1996, Jeng et al., 2020a, Jeng et al., 2021). Moreover, the C3H mice have comparable hearing thresholds to CBA mice up to 12 months (Henry and Chole, 1980, Erway et al., 1993). Thus, the C3H/HeJ mouse strain can be used as a mouse model of good hearing.

Therefore, age-related hearing loss strains have been utilised for age-related studies, such as identifying changes in the IHCs and OHCs with age (Jeng et al., 2020b, Jeng et al., 2020a). However, there are mouse models that present the age-related hearing loss phenotypes seen in 6J mice, but at a much younger age – such as the conditional knockout of the MET protein Myo7a ($Myo7a^{fl/fl} Myo15^{cre+/-}$ strain, see section) (Corns et al., 2018). Additionally, the phenomenon of IHCs becoming re-innervated by efferent fibres has been reported in age-related hearing loss strains, as well as in mice with conditional knockout Myo7a mice, which will be covered in the next sections of this thesis (Lauer et al., 2012, Zachary and Fuchs, 2015, Corns et al., 2018, Jeng et al., 2021).

1.2.4. Efferent re-innervation of mature IHCs in ageing

In the last decade, a small number of studies have shown that the mature IHCs have a somewhat inherent plasticity relating to the efferent innervation, something which had not previously been shown or even considered. The mature IHC stops responding to ACh around P18 in mice (Glowatzki and Fuchs, 2000), a time when the MOC efferent fibres only form axosomatic synapses with OHCs. Subsequently nAChRs and SK2 channels are down regulated in IHCs (Glowatzki and Fuchs, 2000, Simmons, 2002, Marcotti et al., 2004, Katz et al., 2004).

1.2.4.1. Efferent re-innervation in 6J mouse models

Efferent re-innervation of IHCs is when the efferent fibres that only form axosomatic (direct) synapses onto the IHCs during development return in ageing, in what was not known or seen until 2012 when the first study reported this phenomenon in early onset, age-related hearing loss 6J mice.

This study by Lauer et al., 2012, 6J mice that were either one year of age, or older and demonstrated that the IHCs become re-innervated by efferent fibres. As mentioned above, IHCs no longer have axosomatic efferent innervation after the onset of hearing – with the post-synaptic nAChRs and SK2 channels being downregulated by P21 (Glowatzki and Fuchs, 2000, Simmons, 2002, Marcotti et al., 2004, Katz et al., 2004). By the IHCs becoming re-innervated by efferent fibres, this revealed the potential for the cochlea to return to a pre-hearing, developmental stage of innervation, including cholinergic efferent inhibition (Glowatzki and Fuchs, 2000, Lauer et al., 2012). The aged IHCs had fewer afferent synapses compared to one month old mice, indicating a progressive loss with age. Moreover, the young (one month) IHCs did not have axosomatic efferent synapses, whereas the aged IHCs (one year or more) did, demonstrating that the re-innervation takes place naturally with age (Lauer et al., 2012). Additionally, the aged IHCs had fewer axodendritic efferent synapses onto the type I SGNs – indicating that there is fewer LOC fibres synapsing onto the type I SGNs. This finding confirmed the findings of an older study showing that there is a progressive loss of type I SGNs with age (Stamatakis et al., 2006).

There may be a potential connection between the degeneration of mature SGNs during ageing, which induces the efferent re-innervation of the IHCs. The efferent re-innervation of mature IHCs has been seen previously, but following AMPA induced excitotoxicity inside the cochlea (Ruel et al., 2007). Nonetheless, 5 days after AMPA induced excitotoxicity there was a return of functional compound action potentials, however, the direct efferent contacts with IHCs retracted and normal adult axodendritic synapses with SGNs were seen (Ladrech et al., 2003). It was proposed that more work would be required to prove whether these efferent terminal synapses contacting IHC in old 6J mice were functional (Lauer et al., 2012). Moreover, the re-innervation could be dependent on the *cadherin 23* mutation underlying ARHL in 6J mice, therefore studying some other models of ARHL or good hearing models such as CBA or C3H would be interesting.

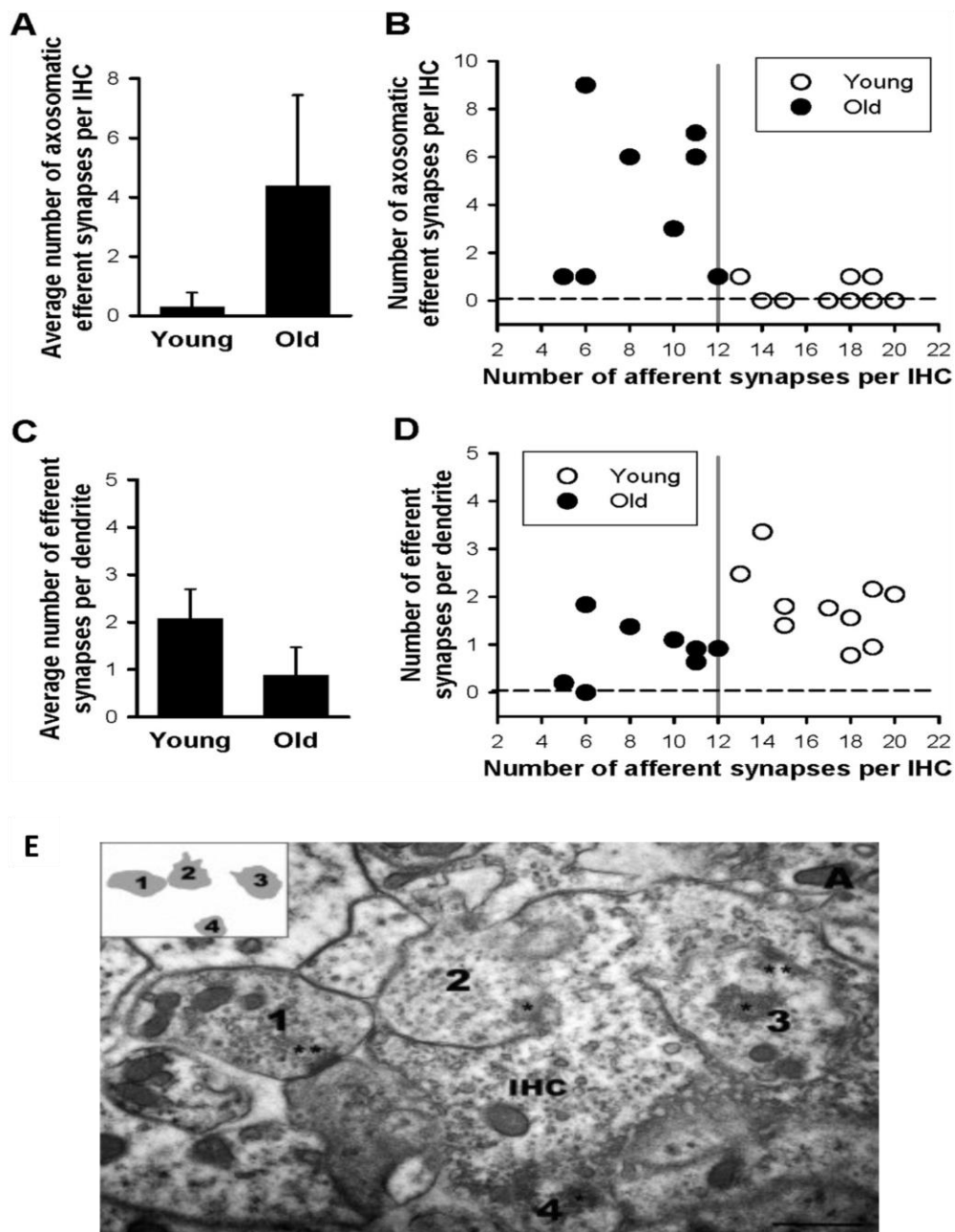


Figure 1. 17. Transmission electron microscopy showing the efferent re-innervation of aged IHCs.

A: number of axosomatic efferent synapses per IHC, with aged mice having more efferent synapses. **B:** axosomatic efferent synapses were associated with fewer synapses between IHCs and afferent fibres. **C:** number of efferent synapses per dendrites in IHCs. **D:** aged mice had fewer efferent synapses per dendrite which were associated with fewer afferent synapses per IHC. **E:** multiple efferent terminals (numbered 1-4) contacting the basal pole of an IHC of an older mouse (11 months old). Figures and figure legends adapted from (Lauer et al., 2012).

A follow up study aimed to answer the question proposed at the end of the initial study (Lauer et al., 2012) which was: are the axosomatic efferent synapses contacting aged IHCs functional? To test this, electrophysiology was used to target the IHCs with axosomatic efferent synapses in aged 6J mice. One method that has been extensively used to target the efferent system when studying OHCs used a solution that contained a high concentration of K^+ (40mM) (Oliver et al., 2000). The high K^+ solution, when locally perfused over the IHCs and potential efferent synapses, will depolarise the efferent synaptic terminals – inducing the release of their neurotransmitter, ACh. If the IHCs are re-innervated by efferent fibres and form functional synapses, then the IHCs will re-express nAChRs and SK2 channels, therefore, if nAChRs are present then the IHCs will respond to the induced ACh release from efferent terminals and Ca^{2+} will enter the IHCs, stimulating the SK2 channels and causing an efflux of K^+ out of the IHC. Experimentally, the efferent re-innervation can be seen by inhibitory post-synaptic currents upon perfusion of high K^+ solution, indicating the presence of a functional efferent synapse. This technique was utilised in this study to investigate if the efferent re-innervation of aged IHCs in 6J mice resulted in functional synapses, or just axosomatic efferent contacts (Zachary and Fuchs, 2015).

Efferent induced post-synaptic currents were present in apical IHCs at P7-P10, but not in 1 month old mice (Zachary and Fuchs, 2015). However, the current was found in 20% of the IHCs from 8.5-9.5 months old mice, and by 12 months about 50% IHCs produced post-synaptic currents (Figure 1.18A-C) (Zachary and Fuchs, 2015). Thus, the synaptic currents which are typically seen in early immature IHCs up to P18 (Glowatzki and Fuchs, 2000, Glowatzki and Fuchs, 2002) were seen in aged IHCs from 6J mice that had efferent re-wiring. It could be suggested that the aged IHCs are potentially trying to revert to an immature, pre-hearing innervation in a form of plasticity to slow the progression of hearing loss.

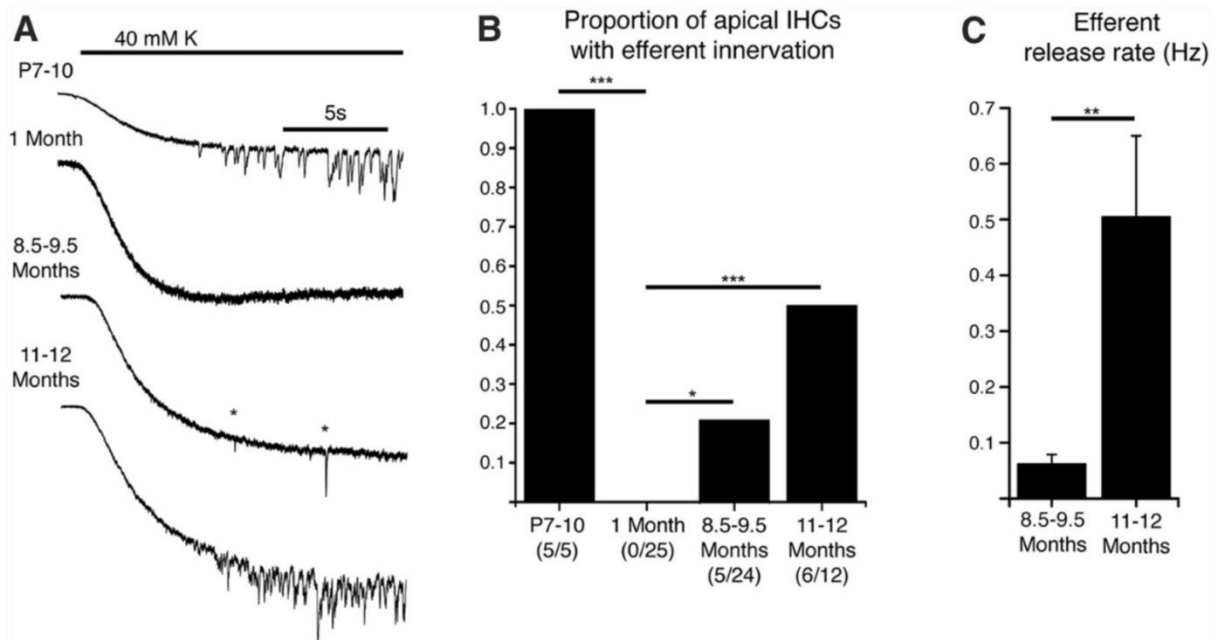


Figure 1. 18. Efferent re-innervation of aged IHCs in ARHL have functional efferent synapses.

A: examples of IHC membrane current responses evoked by 40 mM external K^+ at P7–P10, 1 month, 8.5–9.5 months, and 11–12 months. Two synaptic events are marked with asterisks at 8.5 months. **B:** for the same ages, the proportion of apical IHCs with efferent activity in 40 mM K^+ . **C:** efferent release rates increase from 8.5–9.5 to 11–12 months of age. Data are means \pm SEM of the first 10 release events across all recordings in 40 mM K^+ . Figures and figure legends from (Zachary and Fuchs, 2015).

The authors had shown that the efferent re-innervation of IHCs had functional synapses, however, it was necessary to confirm that the nAChRs and SK2 channels were responsible for the currents seen. This would confirm that the re-innervation returned to recapitulate the developmental innervation pattern. Although perfusing the IHCs and efferent terminals with high K^+ solution showed the presence of nAChRs, it would have been better to try and block the inhibitory post-synaptic currents with strychnine, a potent blocker of $\alpha 9\alpha 10$ nAChRs. To determine whether there was the presence of SK2 channels at the efferent synapse, Zachary & Fuchs 2015, demonstrated that the induced current can be blocked when apamin, a potassium channel blocker, was applied (Zachary and Fuchs, 2015).

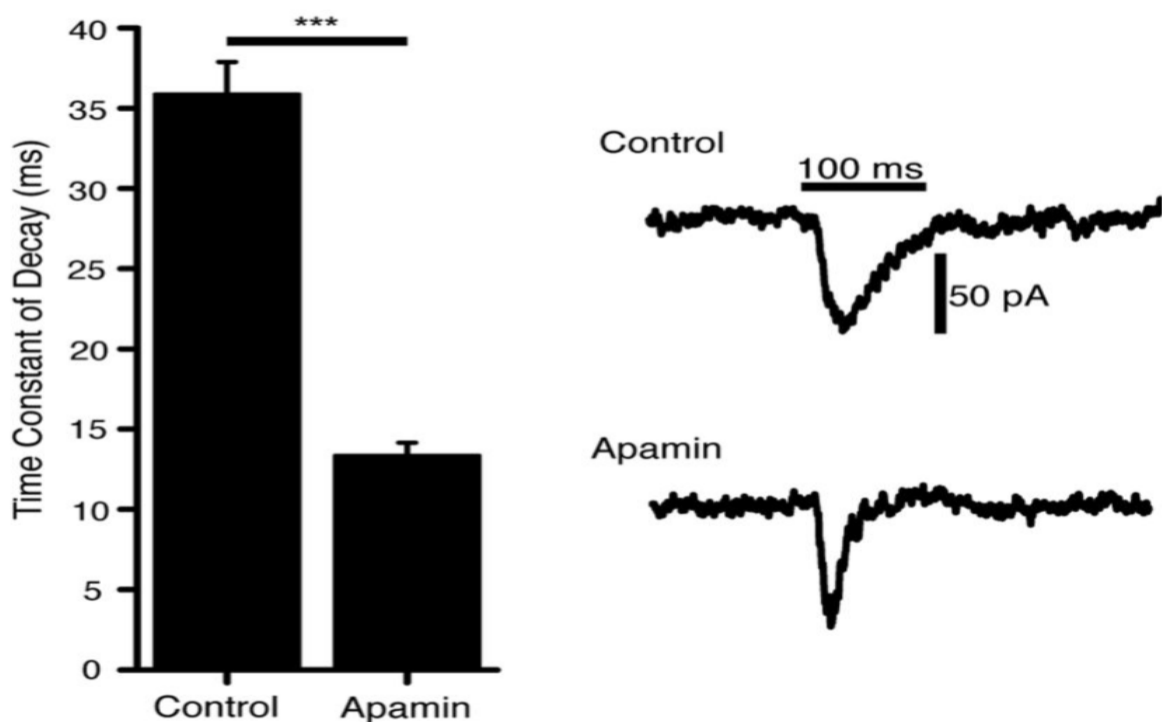


Figure 1. 19. Evidence of nAChRs and SK2 channel expression in re-innervated aged IHCs.

Apamin at 400 nM reduced the time constant of decay for inward synaptic currents recorded in 80 mM external K^+ (***) $p < 0.001$, $n = 67$ events across 2 recordings, 14- to 15-month-old cells). Figure and figure legend from (Zachary and Fuchs, 2015).

1.2.4.2. Biophysical and morphological changes in IHCs during ageing

A more recent set of studies has profiled the biophysical, morphological and pathophysiological changes that occur in cochlea IHCs utilising different age-related and good hearing mouse models, which had not been done previously. The studies used four different mouse strains, early onset ARHL strains C57BL/6J (6J) and C57BL/6N (6N) mice that have the mutation in *Cdh23*, and late-onset C3H/HeJ. Additionally, the genome edited C57BL/6NTac^{*Cdh23*⁺} (6N-Repaired) mice (Jeng et al., 2020a, Jeng et al., 2020b, Jeng et al., 2021), which was repaired by CRISPR-Cas9 (Mianné et al., 2016) were used as a good hearing control, due to the gene editing repairing the early onset hearing loss phenotype.

These studies revealed the biophysical and morphological changes that occur in apically located aged IHCs in the four mouse strains. Auditory brainstem recordings (ABR) showed that aged 6J and 6N had the highest threshold shift compared to young adults, whereas aged C3H had no hearing threshold shift and 6N-repaired had a minimal threshold shift (Figure 1.20A). Although there was hearing loss in the early-onset strains, IHC degeneration was not seen the apical coil of the cochlea until 17 months of age (Jeng et al., 2021). However, all four strains had a progressive decrease in the size of the IHC surface area (Jeng et al., 2021). As a result of the reduced surface area size the $I_{K,f}$ (BK) current size was smaller, whereas $I_{K,n}$ (KCNQ4) was not, showing that the reduction in surface area occurs in the upper region (neck) of the IHCs (Figure 1.20B-D) (Jeng et al., 2021).

Interestingly, the resting membrane (V_m) potential of the aged IHCs was not affected by a reduced surface area in any of the four strains. Furthermore, it was proposed by Jeng et al., (2021) that the reduction of surface area in aged IHCs could be to maintain an optimal working condition by reducing their energy consumption and metabolic stress. There was also a reduction in the size of the MET currents in mice with the *Cdh23*^{*ahl*} mutation (6J and 6N) (Figure 1.20E-G), this reduction was not seen in the 6N-repaired mice until 9 months of age, suggesting that a reduction in MET apparatus function plays a pivotal role in the progression of ARHL (Jeng et al., 2021).

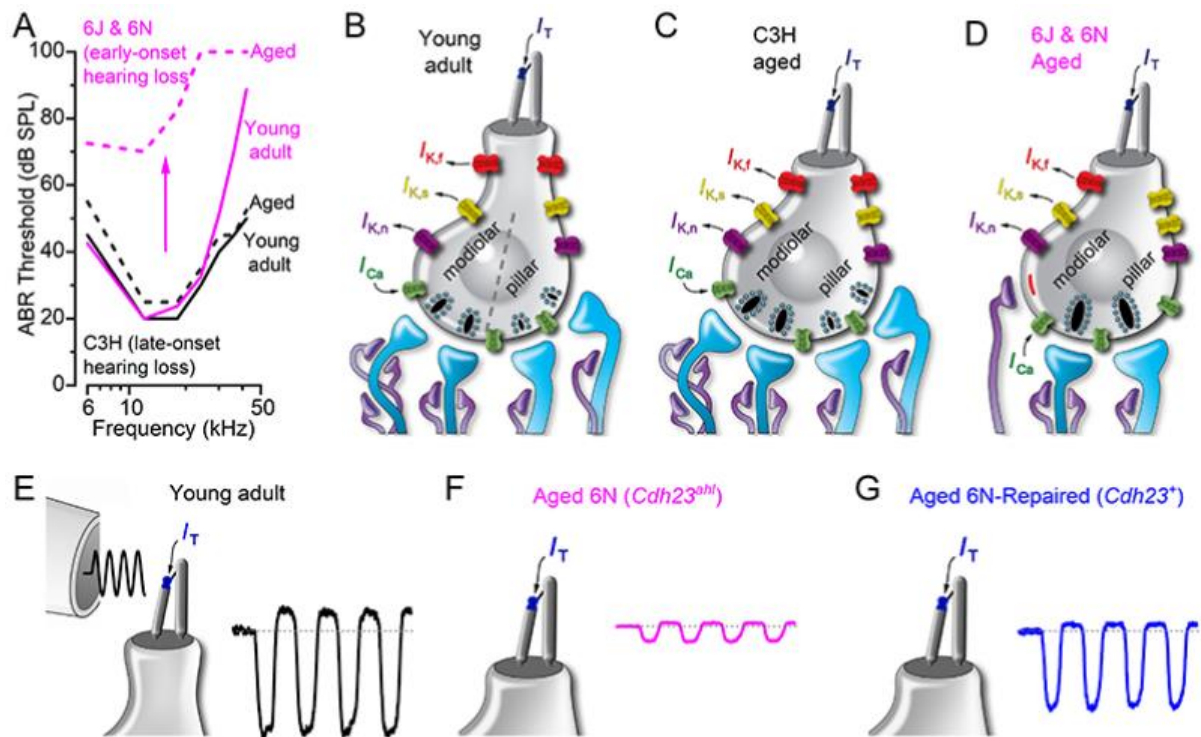


Figure 1. 20. An overview of how IHCs change in ageing.

A: auditory brainstem response (ABR) thresholds for frequency-specific pure-tone stimulation from 6 kHz to 42 kHz recorded from C3H (black, late-onset hearing loss) and both 6N and 6J (magenta, early-onset hearing loss) mice at 1–3 months (young adult) and 14–18 months (aged). **B-D:** schematic representation of the basolateral membrane protein profile and innervation pattern of IHCs from young adult (**B**) and aged C3H (**C**) and from 6J and 6N (**D**) mice. With age, the number of BK channels (red, carrying $I_{K,f}$) is reduced in early-onset hearing loss mice (**D**) but not in C3H mice (**C**). KCNQ4 channels (purple: $I_{K,n}$) are unchanged in all strains. Channels carrying $I_{K,s}$ (yellow) appear to increase only in early-onset hearing loss mice. The afferent (blue) and efferent (light purple) fibres are present at both ages but are highly reduced in number only in aged IHCs from 6J and 6N mice (**D**). Direct axosomatic efferent synapses, most likely LOC fibres, primarily target IHCs from early-onset hearing loss mice at least up to 15 months of age. The number of ribbon synapses is largely unaffected in C3H mice, but substantial changes are present in 6J and 6N mice. **E-G:** schematic representation of the apical portion of IHCs with the MET apparatus being stimulated by the piezo-driven fluid jet (**E**). The MET current was reduced in size with age in IHCs from mice carrying the *Cdh23^{ahl}* allele (**F**), but not in 6N-Repaired mice (**G**). Figure and figure legend adapted from (Jeng et al., 2021).

Moreover, at 15 months there is a reduced number of ribbon synapses in 6J and 6N strains (Figure 1.21A-E), correlating with more severe hearing loss, whereas the 6N-repaired strain had more ribbon synapses than 6J and 6N mice, which correlated with only partial hearing loss in 9-12kHz regions. The good hearing C3H mice did not lose ribbon synapses with age, but had fewer at younger ages compared to the other strains (Jeng et al., 2020a). Furthermore, the reduction in ribbon synapses occurs on both the modiolar and pillar side of the IHCs but is only evident after 6 months of age. This data is different from previous studies (Sobkowicz et al., 1982, Kujawa and Liberman, 2009, Kujawa and Liberman, 2015), that reported there is a preferential loss of modiolar SGNs and ribbon synapses, however, due to the extensive research in the Jeng et al., 2021 study and finding the same results in the early onset ARHL strains, this is a key result that furthers our understanding of synapse loss in ageing. Although there are morphological changes in IHC ribbon synapses that occur with age, surprisingly, the functionality of the ribbon synapses did not significantly change (Jeng et al., 2020a). The size and kinetics of synaptic exocytosis and the replenishment of the synaptic vesicles were not affected by age, however, these results suggest a significant reorganisation of the aged IHCs that is similar to the pre-hearing stages of development, and proposed as a compensatory method for a loss of afferent fibres (Michanski et al., 2019, Jeng et al., 2020a). This proposed compensatory method is due to the previous suggestions that the efferent re-innervation of IHCs is possible due to the loss of type I SGNs leaving the LOC fibres without any afferent fibres to form the axodendritic synapses on (Lauer et al., 2012, Zachary and Fuchs, 2015). This degeneration of afferent fibres would then free up the LOC fibres to re-innervate the IHCs.

An interesting finding in relation to this thesis was that direct re-innervation of aged IHCs occurred by LOC fibres in all strains except C3H (however, C3H did sporadically show re-innervation after 15 months of age) (Jeng et al., 2021). The difficulty of showing whether the LOC or MOC fibres re-innervate the IHCs is due to the limitations in the antibodies that are available for immunofluorescence experiments. Jeng et al., 2021, used a combination of the efferent fibre marker choline acetyltransferase (ChAT) with the antibody that labels both afferent and efferent fibres (ATP1A3). Together, with SK2 antibodies the re-innervation could show that it is specifically the LOC efferent fibres that re-innervate the IHCs. This work answers an important question as to whether the re-innervation of aged IHCs was dependent

on the *Cdh23^{ahl}* allele, found in 6J and 6N mice. However, as 6N-repaired IHCs also had axosomatic synapses with LOC fibres, it can be concluded that the re-innervation is not specific to the *Cdh23^{ahl}* allele. It is also interesting to note that there were occasional re-innervated IHCs in C3H mice at 15 months of age, showing that the efferent re-innervation is scaled to the degree of hearing loss (Jeng et al., 2021). Additionally, the LOC fibres re-innervating IHCs were predominantly located on the modiolar side of the IHCs (Figure 1.20D). Moreover, some IHCs had post-synaptic expression of SK2 channels present prior to the re-innervation, this could be that IHCs have an active role in attracting LOC fibres (Jeng et al., 2021).

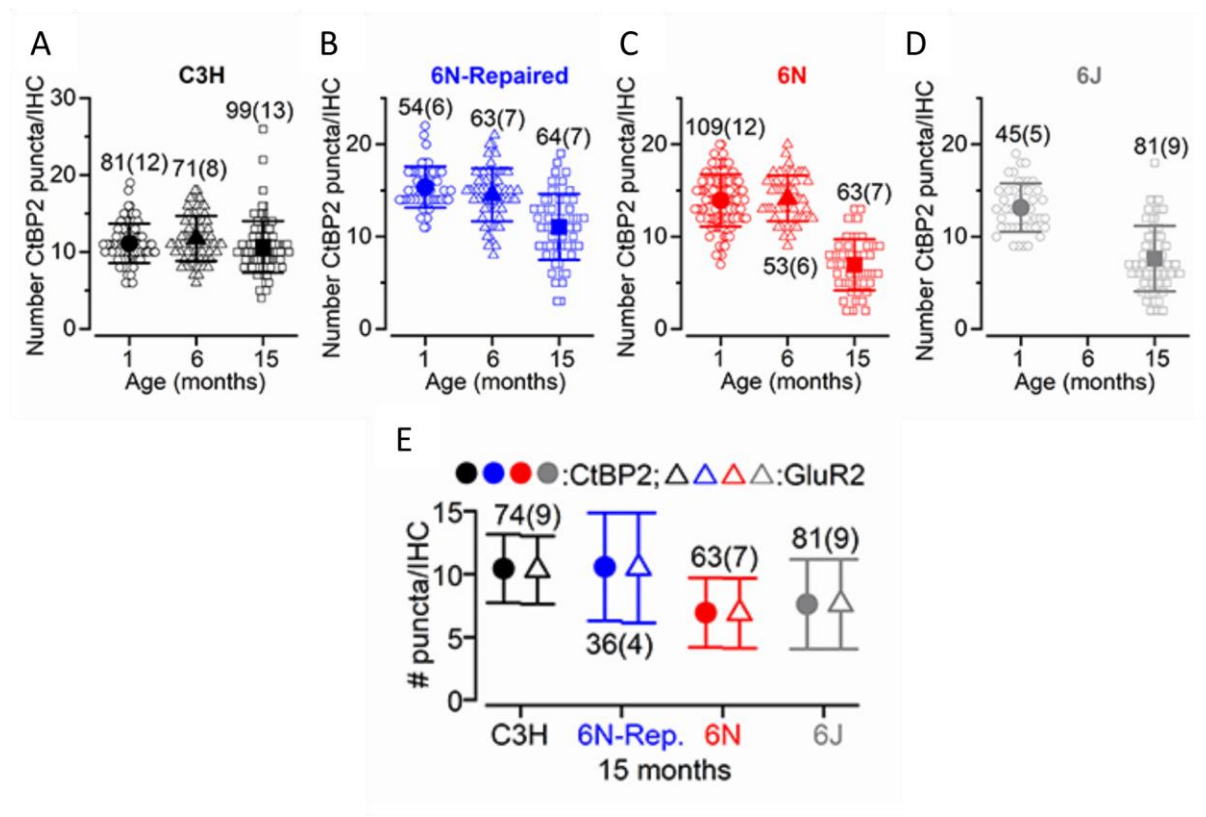


Figure 1. 21. Changes in ribbon synapses in age-related hearing loss strains.

A-D: number of CtBP2 puncta as a function of age in IHCs from C3H (**A**), 6N-Repaired (**B**), 6N (**C**) and 6J (**D**) mice. Data are plotted as mean values (larger closed symbols) and individual CtBP2 counts (smaller open symbols). **E:** number of CtBP2 and GluR2 puncta in IHCs from 15-month-old mice (C3H, 6N-Repaired, 6N and 6J). Numbers above or below the data in **A-E** represent the IHCs (and mice) used for each time point. Average values are mean \pm SD. Figure and figure legend adapted from (Jeng et al., 2020a).

1.2.4.3. Efferent re-innervation of aged IHCs can be induced by MET silencing

As briefly mentioned before, a conditional knockout mouse model for Myo7a (*Myo7a^{fl/fl} Myo15-cre^{+/-}*) can be used as an alternative model for early onset age-related hearing loss, due to the IHCs returning to a developmental like biophysical profile. In addition, to the return to an immature phenotype, the IHCs are also re-innervated by efferent fibres, like in 6J, 6N and 6N-repaired mice (Corns et al., 2018, Jeng et al., 2021). The *Myo7a^{fl/fl} Myo15-cre^{+/-}* mice have Myo7a conditionally knocked out from P2-P4 onwards, which is the age that Myo15 is expressed in IHCs and OHCs. The *Myo7a^{fl/fl} Myo15-cre^{+/-}* mice develop normally in the absence of Myo7a, as the IHCs did not respond to external application of ACh at P22, whilst having no axosomatic efferent synapses at P20 (Corns et al., 2018). Surprisingly, from P33 onwards the IHCs in *Myo7a^{fl/fl} Myo15-cre^{+/-}* mice became re-innervated by efferent fibres – significantly younger than in 6J, 6N and 6N-repaired mice, whereas the littermate wildtype mice remained insensitive to ACh. Additionally, the typical ACh dependent currents, which are usually carried out by the nAChRs and SK2 channels in pre-hearing IHCs, were seen in the *Myo7a^{fl/fl} Myo15-cre^{+/-}* mice. Therefore, abolishing the MET current, and affecting the ability of IHCs to transduce acoustic stimuli, causes the efferent terminals return to innervate IHCs directly in about two-weeks (~P33) after they are lost in normal development. A specific $\alpha 9\alpha 10$ nAChR blocker (strychnine) was used to confirm that the nAChR channels had been re-expressed in the aged *Myo7a^{fl/fl} Myo15-cre^{+/-}* mice. Furthermore, transmission electron microscopy (TEM) revealed that in P37 *Myo7a^{fl/fl} Myo15-cre^{+/-}* mice, the mature IHC had undergone re-innervation and the efferent terminals formed direct axosomatic synapses (Figure 1.22H & I) (Corns et al., 2018).

Both male and female mice were used in these studies, showing that the re-innervation of aged IHCs is not sex specific. Hence, this *Myo7a^{fl/fl} Myo15-cre^{+/-}* mouse model is extremely beneficial for the re-innervation phenomenon in ageing, and could be used in future studies to further elucidate the understanding of the mechanisms of the re-innervation – in a two-week time frame, instead of waiting a year for re-innervation to occur, as in 6J, 6N or 6N-repaired mice (Lauer et al., 2012, Zachary and Fuchs, 2015, Jeng et al., 2021).

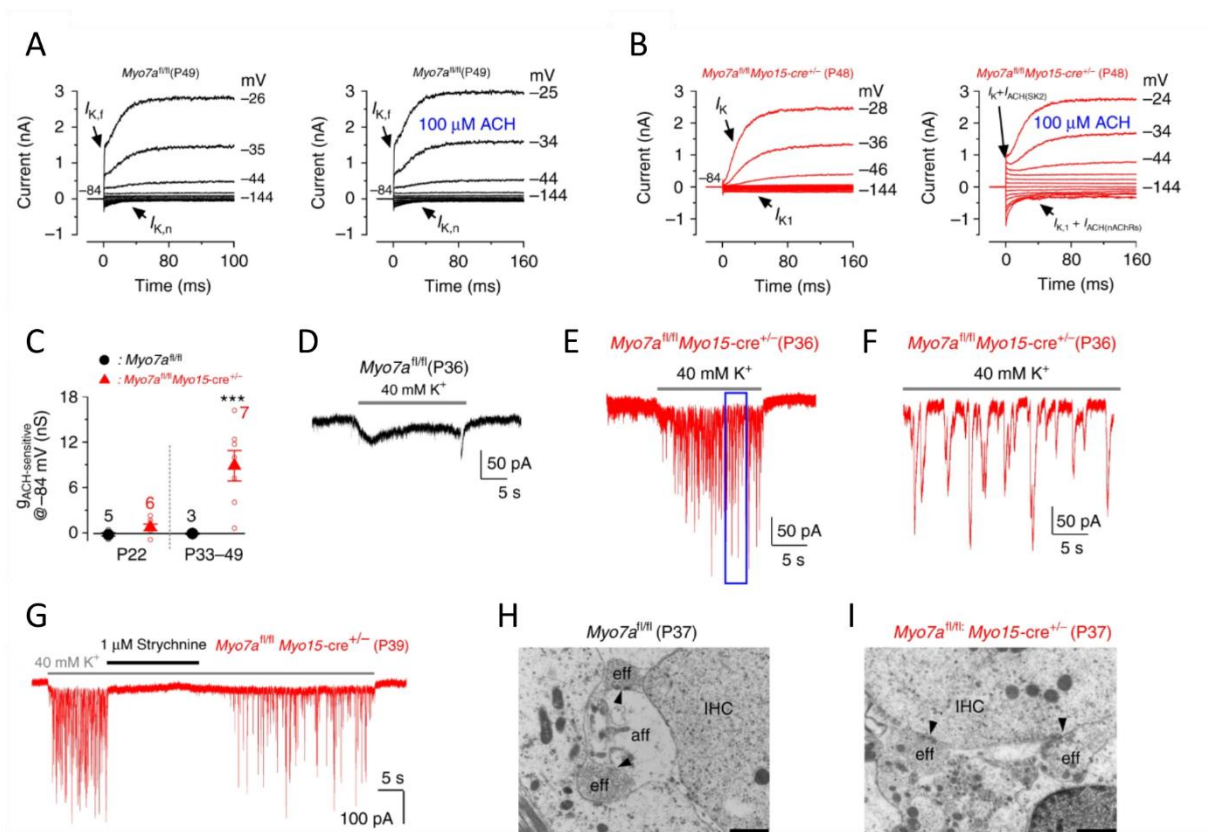


Figure 1. 22. Efferent re-innervation of *Myo7a^{fl/fl}Myo15-cre^{+/-}* following MET silencing.

A, B: currents recorded from adult IHCs of control *Myo7a^{fl/fl}* (**A**) and *Myo7a^{fl/fl}Myo15-cre^{+/-}* mice before (left panels) and during superfusion of ACh (right panels). ACh-induced current was only present in the *Myo7a^{fl/fl}Myo15-cre^{+/-}* IHC. **C:** steady-state slope conductance of the ACh-sensitive current (g_{ACh} -sensitive) at different age ranges in the two genotypes. For more details see: Corns et al., 2018. **D-G:** voltage-clamp recordings obtained from adult IHCs of control *Myo7a^{fl/fl}* (**D**) and *Myo7a^{fl/fl}Myo15-cre^{+/-}* **E, F, G** mice during the superfusion of 40mM extracellular K^+ . Synaptic currents were only evoked in *Myo7a^{fl/fl}Myo15-cre^{+/-}* IHCs. **F:** expanded time scale of the blue area shown in **E**. **G:** effect of 1 μ M strychnine on the ACh-induced synaptic currents. **H, I:** TEM showing the IHC synaptic region from control *Myo7a^{fl/fl}* (**H**) and *Myo7a^{fl/fl}Myo15-cre^{+/-}* (**I**) mice. IHCs from *Myo7a^{fl/fl}* mice showed the characteristic efferent terminals forming axodendritic contact with type I SGNs. In *Myo7a^{fl/fl}Myo15-cre^{+/-}* mice efferent fibres make direct axosomatic contact with the IHC (**I**), which is characteristic of pre-hearing IHCs. Scale bars: 1 μ m. Figure and legend adapted from (Corns et al., 2018).

The studies that have been discussed here are the only literature reporting the efferent re-innervation of IHCs. The finding that the disruption of the MET channel also has the re-innervation of IHCs in the Corns et al., 2018, enables the mechanism to be studied in a time dependent manner. This forms the foundation for this thesis, which aims to investigate the time dependent changes of the efferent re-innervation, to answer some of the key questions that were raised by the previous studies, such as whether the IHCs are driving the mechanism and whether there is a loss of afferent synapses and type I SGNs after the MET channels become dysfunctional.

1.3. Inflammation in the cochlea

The last part of this introduction takes a slight turn in relation to the rest of the thesis. This is because the results for this chapter (Chapter 5) were a side project that was explored following some of the ideas and findings when using the *Myo7a^{fl/fl} Myo15-cre^{+/-}* mice and studying efferent re-innervation of IHCs (Chapter 3). The original idea was that during the efferent re-innervation of IHCs, the environment is changing within the organ of Corti, as neurotrophic factors are involved in the developing innervation, this was one idea but instead I decided to explore whether the changes in the *Myo7a* knockout resulted in larger environmental changes (eg, an inflammatory response).

The cochlea was thought to be an immune privileged environment for many years (McCabe, 1989), this was after the blood labyrinth barrier was discovered (Juhn and Rybak, 1981). However, it was discovered that the cochlea has a number of different immune cell types, ranging from granulocytes, T cells, B cells, natural killer cells and macrophages, showing that it is not immune privileged (Matern et al., 2017). Of these immune cells, macrophages make up the greatest proportion (~80%) of immune cells within the cochlea (Matern et al., 2017). Macrophages are present within the cochlea and they function to maintain the homeostasis, as well as to phagocytose the dying cells in the environment (Aderem and Underhill, 1999). Moreover, the cochlea has a resident population of macrophages that are present during embryonic development and into postnatal maturity (Fredelius and Rask-Andersen, 1990, Ginhoux et al., 2010, Davies and Taylor, 2015, Ginhoux and Guilliams, 2016, Liu et al., 2018, Hoeffel and Ginhoux, 2018). Although the resident macrophages are known to be present within the cochlea, little is known about them, and they have not been extensively studied.

For macrophages to perform their functional roles, they are located in different regions of the cochlea, mostly the stria vascularis (lateral wall) (Jabba et al., 2006, Ito et al., 2022), the SGNs (Kaur et al., 2015) and the osseous spiral lamina (OSL) (Figure 1.22A-D) (Wake et al., 2009, Hirose et al., 2017). Surprisingly, macrophages are not found in the organ of Corti, with it being suggested that they cannot survive in the high K^+ concentration (Warchol, 2019). The only time that macrophages have been seen penetrating the sensory neuroepithelium is in response to ototoxic compounds during live imaging (Xu et al., 2020). Cochlea that had been

exposed to different types of insult have inflammatory responses, often detected by changes in macrophage number and morphology (Figure 1.23B & D). Insults such as noise-exposure (Mizushima et al., 2017, He et al., 2020, Rai et al., 2020), ototoxic aminoglycosides (Wang et al., 2003, Ladrech et al., 2007, Sato et al., 2010, Hirose and Sato, 2011, Kaur et al., 2015), induced hair cell death via: diphtheria toxin (Kaur et al., 2015) and tamoxifen injections (Xu et al., 2020), as well as ageing (Noble et al., 2019) and stress (Liu et al., 2018) have all shown immune responses. Although macrophages have been shown to be responding to age-related hearing loss and the death of OHCs, it is still unknown if the macrophages are actively influencing the process (Frye et al., 2017).

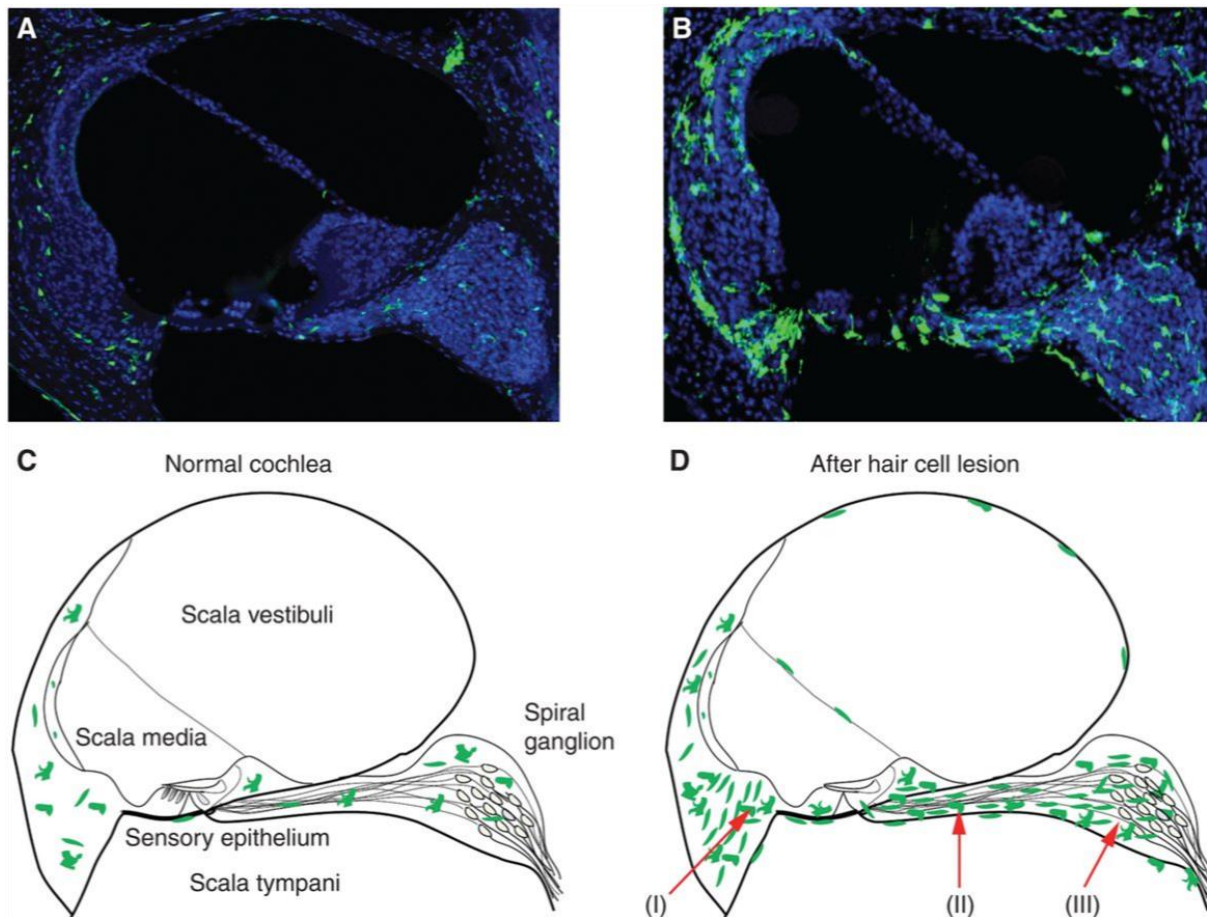


Figure 1. 23. Location of macrophages in the normal and insulted cochlea.

A & B: frozen sections of cochleae from transgenic mice, expressing green fluorescent protein (GFP) (green) in all macrophages, monocytes, and microglia. Sections were also labelled with DAPI (blue). **A & C:** uninjured cochlea contains resident macrophages, which are distributed throughout the nonsensory supporting tissues. **B & D:** after loss of cochlear hair cells, increased numbers of macrophages are present in all regions of the cochlea. Arrows indicate locations where macrophage numbers are particularly enhanced after acoustic trauma or aminoglycoside ototoxicity: (I) lateral wall, (II) osseous spiral lamina, and (III) the spiral ganglion. Figure and figure legend from (Warchol, 2019).

Sterile inflammation can occur when there is an absence of infection and is associated with intracellular components of dying cells being recognised by inflammatory signalling receptors (Chen and Nuñez, 2010, Rock et al., 2010, Shen et al., 2013). There are also pattern recognition receptors (PRRs), which are molecules that are sensitive to pathogens and pathogenic material, the PRRs can then become activated by non-infectious stimuli and mediate / initiate inflammatory responses (Chen and Nuñez, 2010) by inducing macrophages to release pro-inflammatory cytokines and chemokines (Frye et al., 2019). One PRR, Toll-like receptor 4 (Tlr4) activates inflammatory signalling pathways and has been shown to be constitutively expressed within the cochlea and becomes upregulated after cochlea insult (Hirose et al., 2014). Moreover, Tlr4 has been shown to be an upstream regulator of inflammatory responses within the cochlea (Patel et al., 2013, Cai et al., 2014). Currently there has been no reports in the literature showing an inflammatory response to a protein being knocked out of the IHCs (such as a conditional knockout of Myo7a), as all studies induce stress of trauma to the cochlea via different methods mentioned above. From this it is hypothesised that the *Myo7a^{fl/fl} Myo15-cre^{+/-}* mouse model could be a model of sterile inflammation (as there is no injections or trauma to the cochlea, only the loss of Myo7a) and Tlr4 could be the PRR that initiates the immune response within the cochlea following a loss of MET channels and Myo7a from IHCs, the results of this are reported in Chapter 5.

1.4. Aims and hypotheses of the present study

This introduction has detailed some of the key aspects for the development of the IHCs as they mature. As the innervation, IHCs ion channel profile and synaptic machinery matures, the IHCs become adapted to be efficient sensory cells that enable us to be able to hear. Additionally, some of the changes that take place to these systems with ageing have been highlighted, focusing on the phenomenon of the IHCs becoming re-innervated with in age related hearing loss. As alluded to in the sections above, there are still many unknowns about the mechanism of IHC efferent re-innervation. Therefore, the aim of this thesis is to answer some of these questions to further our understanding of this mechanism.

The first aim (see Chapter 3) is to answer whether the IHCs are driving the efferent re-innervation (changing first) or the efferent fibres innervate the IHC first, which causes the IHC to adapt in order to accommodate for the change in innervation. Furthermore, I will try to identify if there is a critical time frame for the re-innervation to take place and can any molecular markers be used to determine what comes first? To answer this aim there will be multiple techniques used. As the re-innervation of IHCs is also seen in the conditional knockout of *Myo7a* (*Myo7a^{fl/fl}Myo15-cre^{+/-}*: Corns et al., 2018), albeit at much younger ages than in ARHL mouse models, this enables the mechanism to be studied in a temporal manner to identify the workings of the mechanism. Additionally, whether the IHCs lose afferent synapses in the (*Myo7a^{fl/fl}Myo15-cre^{+/-}* mice has not been investigated, so this will be studied to see if the efferent re-innervation of IHCs could influence any potential afferent synapse loss. Therefore, using this conditional knockout, whole cell patch-clamp electrophysiology and immunofluorescence experiments will be performed to study the efferent re-innervation of IHCs. It is hypothesised that the IHCs are the ones driving the efferent re-innervation, which was suggested by Jeng et al., 2021, however, when using ARHL mouse models the innervation is either there at old ages or it is not, the advantage of the *Myo7a* conditional knockout is that I can study the changes that the IHCs undergo as the re-innervation begins and try to profile this.

The second aim (see Chapter 4) is to identify whether the efferent re-innervation of IHCs is a response to the IHCs becoming dysfunctional. Currently, the ARHL mouse models and a

mouse model with dysfunctional MET currents show re-innervation, therefore, I aim to identify whether disrupting neurotransmitter release at the ribbon synapse but maintaining functional MET currents would instigate the efferent re-innervation. To do this multiple conditional knockout mouse models targeting otoferlin (see section 1.1.4.2 for more information on otoferlin) will be used for this aim. Immunofluorescence and electrophysiology will also be used to answer this research question. It is hypothesised that disrupting neurotransmitter release in the IHCs will result in the efferent re-innervation, similar to if the MET channels are disrupted and in ARHL.

The last aim is related to the side project that was explored during this thesis (see Chapter 5), will disrupting the MET channels by knocking out *Myo7a* result in an inflammatory response? Once again, the *Myo7a^{fl/fl}Myo15-cre^{+/-}* mice will be used for these experiments, utilising immunofluorescence to visualise if there is an inflammatory response, and if it is specifically located to regions of the cochlea – e.g., does it preferentially occur around the organ of Corti, or is it located to the osseous spiral lamina where the innervating afferent and efferent fibres are projecting? It is hypothesised that knocking out *Myo7a* and disrupting MET channels will result in an inflammatory response, and that this will reveal that the mouse model can also be a model for sterile inflammation, which as currently not been reported in the literature. If there is an inflammatory response in the conditional knockout of *Myo7a*, then this would be a novel finding in the field of cochlea inflammatory research.

Chapter 2 – Methods and Materials

2.1. Ethics statements

The animal studies performed in the UK were licenced by the Home Office under the Animals (Scientific Procedures) Act 1986 and were approved by the University of Sheffield Ethical Review Committee. Mice were housed in the University of Sheffield according to Home Office guidelines with 12-hour light/dark cycles. Additionally, the completion of the Home Office modules 1,2 and 3 were performed before any animal work was performed. The cochleae were removed from the mice that were culled by a Schedule 1 method (cervical dislocation) performed by a registered Schedule 1 practitioner. For in vivo measurements, mice were anaesthetised using intraperitoneal injections of ketamine (100mg/Kg, Fort Dodge Animal Health) and xylazine (10mg/Kg, Rompun 2%, Bayer), injections were performed as previously described (Ingham et al., 2011). At the end of the procedure mice were killed by cervical dislocation.

2.1.1. Animal strains

For conditional knockout mice, the targeted *tm1a* allele for both *Myo7a* (*Myo7a^{tm1a(EUCOMM)Wtsi}* allele ID: 4431921) and *Ush1C* (*Ush1c^{tm1a(KOMP)Wtsi}* allele ID: 4363497) were generated by the Mouse Genetics Programme at the Wellcome Trust Sanger Institute (Cambridge, UK). In the *Myo7a* conditional knockout, critical exons 10 and 11 were floxed, whereas exons 5-8 were floxed for the *Ush1c* mice. The *tm1d*-alleles (conditional knockout), which were used for the experiments, were obtained by crossing the *tm1c* mouse (*Myo7a^{fl/fl}* and *Ush1c^{fl/fl}*) with the *Myo15-cre* mice. The reason for crossing the floxed *Myo7a* and *Ush1c* mice with the *Myo15 cre* mice allowed the normal embryonic development of the IHCs and OHCs MET channels. Furthermore, as *Myo15* is expressed around P4 in the apex of the cochlea (see section 1.1.3.2), the genes would be conditionally knocked out from this time point onwards.

Additionally, a tamoxifen inducible conditional knockout strain was generated, targeting otoferlin: *Otoferlin^{tm1c}; Vglut3 cre-ER^{T2}; td-tomato (Otof^{fl/fl} Vglut3 cre^{+/-})*. The otoferlin mice were generated from '*Otof^{tm1a(KOMP)Wts}*' cryo-sperm by MRC Harwell (Oxford, UK). The *Otof* mice were crossed with the tamoxifen inducible *Vglut3-creER^{T2}* (Li et al., 2018), enabling the otoferlin gene to be conditionally knocked out once the mice were injected with

tamoxifen. By using tamoxifen inducible Vglut3 cre, the otoferlin was only knocked out of IHCs, as that is where Vglut3 is expressed (see section 1.1.4.2). The tamoxifen inducible cre was designed so that otoferlin could be knocked out at different ages – with the aim to allow the innervation of IHCs to mature fully (which takes around three postnatal weeks, ~P21) before knocking out otoferlin and then investigating whether this would instigate the efferent re-innervation of IHCs. Furthermore, td-tomato mice (strain number: 007909) from the Jackson Laboratory were used as a Cre reporter strain. The td-tomato mice were produced by insertion of a Lox-P-Stop-LoxP-td tomato sequence into the genome. As the td tomato mice were crossed with the otoferlin conditional knockout mice, to generate the *Otoferlin^{tm1c}; Vglut3 cre-ER^{T2}; td-tomato* strain – this results in td tomato being expressed only when the Vglut3 cre is expressed (Figure 2.1) (after tamoxifen injections), this would then label which IHCs have expressed the cre and therefore should have otoferlin knocked out and have no neurotransmitter release. The reason for adding the reporter to this strain was so that during electrophysiology experiments it would be easier to determine whether an IHC has the cre expressed, this is because the cre expression is not 100% in all IHCs (Li et al., 2018).

As the *Otoferlin^{tm1c}; Vglut3 cre-ER^{T2}; td-tomato* strain would not have 100% efficiency of the cre, the *Otoferlin^{tm1c}* mice were also crossed with the *Myo15-cre* mice, to identify whether a non-tamoxifen inducible cre would have any differences in the potential changes in the IHCs or potential efferent re-innervation.

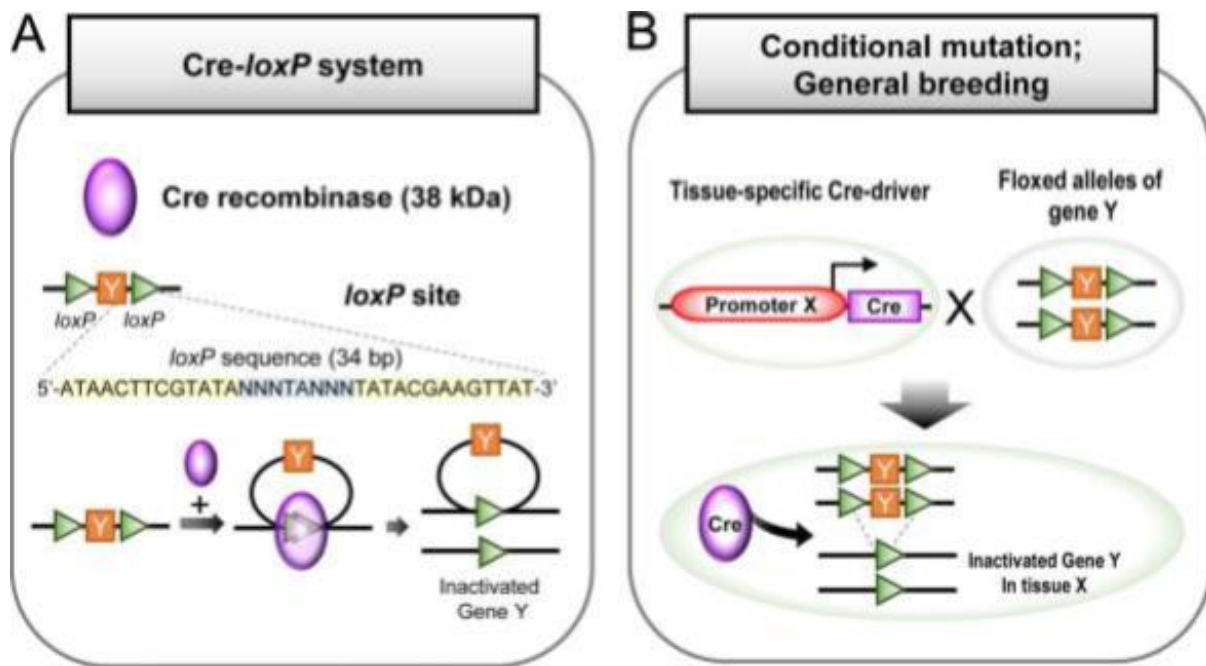


Figure 2. 1. Schematic of the Cre-loxP system and how it enables conditional knockouts.

A: An overview of Cre-loxP system. 38 kDa Cre recombinase recognizes the loxP sites of specific 34 bp DNA sequences. **(B)** General breeding strategy for conditional mutation using loxP and Cre driving mouse line. In principle, one mouse must have a tissue-specific driven cre gene and another mouse have loxP flanked (floxed) alleles of interest gene Y. Expression of Cre recombinase excises floxed loci and inactivates the gene Y. Figure and figure legend adapted from (Kim et al., 2018).

2.1.2. Tamoxifen injections

Tamoxifen (T5648-1G, Sigma-Aldrich) induces cre-recombinase activation, resulting in a conditional knockout of the target gene. Tamoxifen is a reagent that can be injected, it is then metabolised in the liver and its metabolites then bind to oestrogen receptors (Jahn et al., 2018). This is why the tamoxifen inducible cre mice have ER^{T2} added to the cre, enabling the tamoxifen to bind to the cre and induce the knockout of the floxed target gene. A tamoxifen solution with a concentration of 20µg/µl was produced, to achieve this 1ml of tamoxifen solution was made up in corn oil (C8267-500ML, Sigma-Aldrich) and 100% ethanol (E/0650DF/17, Fisher Scientific), 0.02g of tamoxifen was dispersed in 920µl corn oil, with 80µl 100% ethanol added. The solution was sonicated at 30°C for 15-20 minutes until all the

powder had dispersed and the solution was clear. If the solution turned cloudy then this was interpreted as water entering the solution and the tamoxifen forming a precipitate, therefore, if the solution was cloudy then a fresh solution was produced. Tamoxifen is light sensitive so the solution was covered with foil. Tamoxifen was made fresh on the day of injections. Mice were weighed and the tamoxifen doses calculated appropriately and the mice were injected via the intraperitoneal route.

All mice received two injections of tamoxifen, with the first injection being performed on either: P10, P14 or P21, with the second injection being performed 24 hours later. After tamoxifen injections the mice were weighed daily and monitored for any adverse effects prior to culling for experimental use. The humane endpoint for the tamoxifen injections was weight loss over 20% of the animals starting body weight.

Doses for injections were calculated with the following equation:

A: target concentration ___ $\mu\text{g/g}$; **B:** TAM concentration ___ $\mu\text{g}/\mu\text{l}$

Injection volume = $(\text{A} * \text{animal weight}) / \text{B}$; units = μl

2.2. Auditory brainstem responses

Auditory brainstem responses (ABR) experiments and analysis were performed by Professor Walter Marcotti, who also produced Figure 3.6 (found in Chapter 3). ABRs were recorded from either male or female knockout mice as well as littermate control mice between P20 and P35, to detect neural activity along the auditory pathway in response to acoustic stimuli. Mice had electrodes placed subcutaneously on their head, with an active electrode on the vertex, a second active electrode (reference) on the left bulla, whereas the ground electrode was placed on the right (Figure 2.1 Left) bulla. Anaesthetised mice were placed inside a soundproof chamber (MAC3, IAC, UK) on a heated pad at 35-37°C (Figure 2.1 Right). Stimuli were delivered to both ears by calibrated loudspeakers (MF1-S, Multi Field Speaker, Tucker-Davis Technologies, USA) placed 10cm from the animal's pinnae. Sound pressure was calibrated with a low-noise microphone probe system (ER10B+, Etymotic, USA). Experiments were performed using customised software (Ingham et al., 2011) driving an RZ6 auditory processor (Tucker-Davis Technologies).

Response thresholds were estimated from the resulting ABR waveform, defined as the lower sound level at which any recognisable feature of the waveform was visible. Responses were for pure tones of frequencies at 3, 6, 12, 18, 24, 30, 36 and 42 kHz as well as clicks. Stimulus sound pressure levels were 0-95 dB SPL which were presented in steps of 5 dB SPL, brainstem response signals were averaged over 256 repetitions. Tone bursts were 5ms in duration with a 1 ms on/off ramp time, presented at a rate of 42.6/sec.

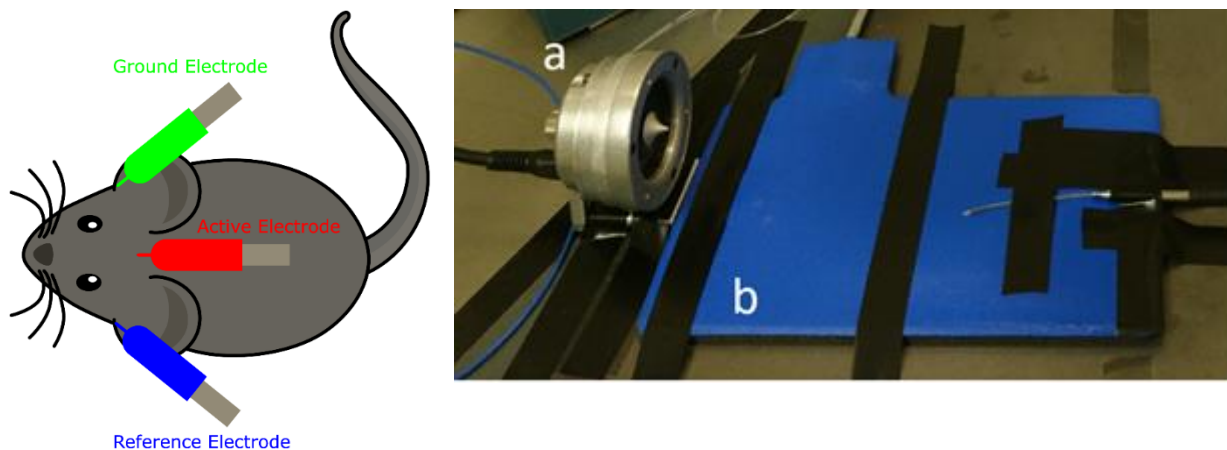


Figure 2. 2. Auditory brainstem response experimental set up.

A: schematic showing the position of the electrodes, the activate electrode (red) is placed on the vertex. A reference electrode is placed on the left bulla (blue) and the ground electrode is placed on the right bulla. **B:** different components of the set-up in a sound proof chamber, **A** is the speaker, whilst **B** is the heat-pad. The head of the mouse was placed facing the speaker.

2.3. Single-cell electrophysiology

Single cell electrophysiology was used to identify the biophysical changes in the IHCs during the process of efferent re-innervation. Using whole cell patch clamp methods, specific experiments were performed to identify whether the IHCs re-express nAChRs and SK2 like the developing, immature IHCs do. By performing these experiments over a time period from P24-42, this allowed the mechanistic changes to be identified in the IHCs as they become re-innervated.

2.3.1. Electrophysiology set up

A dissected apical coil of the cochlea was fixed in place under a nylon mesh grid in a specially made chamber (see section 2.3.2), the chamber was then placed onto a custom made rotating stage which was fixed to an upright microscope (Figure 2.2) (Olympus BX51, Japan). The organ of Corti was visualised using a 60x water immersion objective (LUMPlanFL, Olympus, Japan). The microscope was on an anti-vibration table (TMC, USA) within a Faraday cage to isolate the set-up from external electrical noise (Figure 2.2). A peristaltic pump (Cole-Parmer, USA) was used to provide a continuous flow of extracellular solution across the chamber at a speed of 9ml/min and the pump was connected to a ground with a 65 μ F capacitor to prevent noise contaminating recordings. The peristaltic pump enabled the IHCs in dissected apical coil to remain healthy and single cell electrophysiology recordings to be taken. On average a single preparation had viable cells for around 30-40 minutes with the peristaltic pump being used. All recordings were performed at room temperature.

The recording (patch) pipette position was positioned using a micromanipulator (PatchStar, Scientifica, UK) and attached to a head-stage of an amplifier (Optopatch, Cairn Research Ltd, UK). Recorded signals were filtered at 2.5 kHz with a Bessel low-pass filter. The signals were converted into digital signals by the Digidata 1440A (Molecular Devices, USA) and were sampled at 5 kHz by the pClamp10 software (Molecular Devices, USA). Recordings were stored on a computer for off-line analysis which was performed in Clampfit software and Origin (Origin Lab, USA).

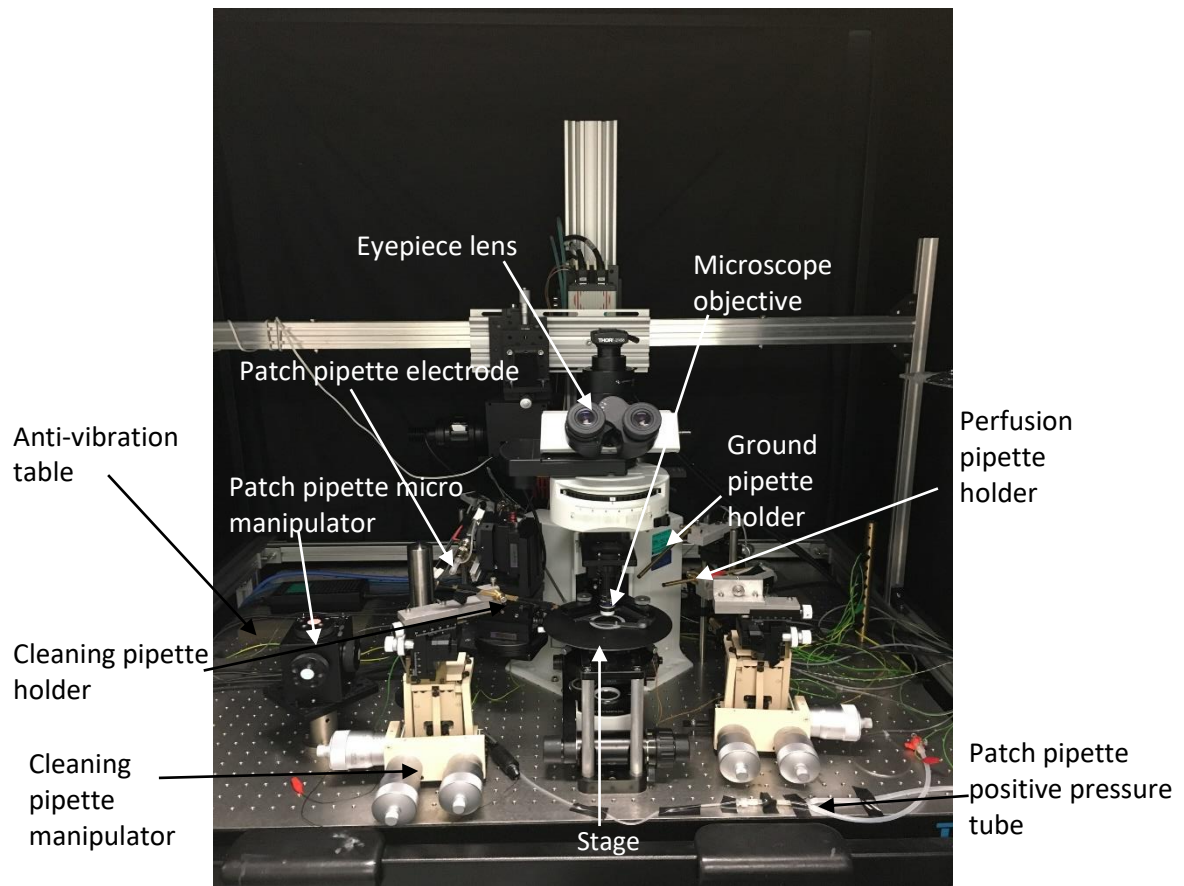


Figure 2. 3. Photo of the electrophysiology rig used for experiments.

Labels indicate the separate parts that make up the rig.

2.3.2. Tissue preparation

Ex vivo recordings were performed on apical-coil IHCs (~9-12 kHz, low frequency region found in apex) of acutely dissected organs of Corti from adult mice. Mice of either sex were killed by cervical dislocation and the inner ear placed in a small Petri dish filled with ice cold extracellular solution (see section 2.4.3 for more details). Isolation of the organ of Corti was performed under a dissecting microscope, beginning with the connective tissue and surrounding muscles in the inner ear being removed.

The cleaned inner ear was moved to a debris free Petri dish with fresh ice-cold extracellular solution. The whole inner ear was held by the vestibular system using a pair of forceps (Figure 2.3A), this enabled the bone covering the apical-coil cochlea turn to be removed using another pair of forceps (Dumont #3 or #4, followed by further refinement on a sharpening stone). Removal of the bone in this region exposes the cochlea nerve which can be carefully cut away using fine forceps, allowing the bone covering the entire apical cochlear coil to be removed. Very fine forceps were used to delicately cut the auditory nerve before removing the apical region of the organ of Corti, which was placed into a recording chamber with fresh extracellular solution using a custom made small (4 mm diameter) stainless steel spoon.

In the recording chamber, the apical region of the organ of Corti is immobilised using a nylon mesh fixed to a stainless-steel ring and the tectorial membrane removed (Figure 2.3B).

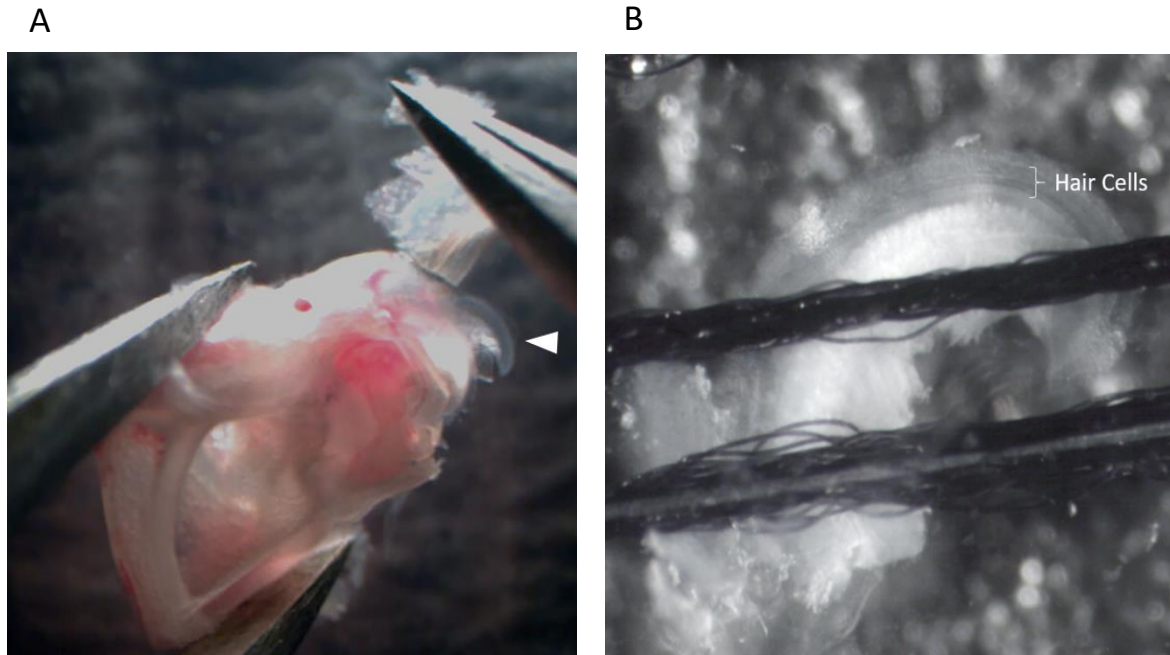


Figure 2. 4. Tissue preparation for whole cell patch-clamp electrophysiology.

A: The cochlea of a one-month old mouse. The vestibular region was held with forceps whilst the bone was removed from the apex of the cochlea, exposing the apex (white arrowhead).

B: the apical coil of the cochlea was affixed underneath a nylon mesh grid. The hair cells within the organ of Corti are labelled.

2.3.3. Experimental solutions

Extracellular solution was made to have a physiological composition like the perilymph found surrounding the basolateral parts of the hair cells (Table 1). Amino acids (11130-036, Gibco, USA) and vitamins (11120-037, Gibco, USA) were added as supplements to the extracellular solution. The osmolality of the solution was 306-308 mOsm/kg, whilst the pH was adjusted to 7.48 using 4M NaOH.

Chemical	Final Concentration (mM)
NaCl	135
MgCl₂	0.9
KCl	5.8
CaCl₂	1.3
HEPES	10
Glucose	5.6
NaH₂PO₄	0.7
NaPyruvate	2

Table 2. 1. Composition of extracellular solution.

A high K^+ extracellular solution was also used during experiments to test whether the re-innervated IHCs expressed SK2 and nAChR channels (see section 2.3.7 for methods). The composition of the high K^+ solution can be seen in Table 2. The osmolality of the solution was 306 mOsm/kg, whilst the pH was adjusted to 7.48 using 4M NaOH.

Chemical	Final Concentration (mM)
NaCl	113
KCl	40
MgCl₂	0.9
CaCl₂	1.3
HEPES	10
Glucose	5.6
NaH₂PO₄	0.7

Table 2. 2. Composition of high K^+ (40mM) extracellular solution.

For whole cell electrophysiology current and voltage clamp recordings, KCl based intracellular solution was used to fill patch pipettes (Table 3). The osmolality of the solution was adjusted to 293 mOsm/kg, and the pH was adjusted to 7.28 using 1M KOH.

Chemical	Final Concentration (mM)
Na₂Phosphocreatine	10
Na₂ATP	5
HEPES	5
KCl	131
MgCl₂	3
KOH-EGTA	1

Table 2. 3. Composition of intracellular solution.

2.3.4. Recording pipettes

Recording patch pipettes were produced from soda glass capillaries (1413027, Hilgenberg, Germany) using a pipette puller (Model PP-830, Narishige Instruments, Japan). Patch pipette shanks were then coated in wax (Mr Zoggs Sex Wax, CA, USA) to reduce the electrode capacitance. Pipettes were filled with intracellular solution (see Table 3) and had a resistance of 2-3 MΩ for IHC recordings.

2.3.5. Cleaning pipettes

Cleaning pipettes were pulled from borosilicate glass capillaries (30-0062, Harvard Apparatus, UK) and had a tip diameter of 3 μm . Cleaning pipettes were filled with extracellular solution and used to create a tear in the sensory epithelium. The pipettes were connected to a 10 ml syringe, which was used to apply suction to clean supporting cells away from target IHCs.

2.3.6. Whole cell patch-clamp recordings

Once IHCs were exposed, patch pipettes were lowered into the chamber. Positive pressure was applied to the patch pipette whilst being lowered into the solution to prevent debris build up in the pipette tip. Positive pressure was maintained as the patch pipette tip approached the IHC membrane, upon contact with the IHC, negative suction was applied until a $>1\text{ G}\Omega$ resistance was achieved, producing a seal. IHCs were held at a membrane potential of -80 mV for recordings. Whole cell patch-clamp configuration was achieved by applying sharp negative suction, a decrease in resistance and large current seen was indicative of the IHC entering whole cell patch clamping. Membrane potentials were corrected for residual series resistance (R_s), after compensation (usually 80%) and the liquid junction potential of -4 mV , measured between the electrode and bath solutions.

Whilst investigating basolateral membrane properties the size of $I_{K,f}$ was measured at -25 mV and 1.0 ms after the start of the voltage step. This is required due to the nature of the $I_{K,f}$ current, which is a fast activating outward K^+ current that functions to prevent spontaneous APs in the mature IHCs (see section). Steady-state total currents were measured at 160ms, at a potential of 0 mV (extrapolated from the current-voltage curves).

2.3.7. Extracellular superfusion

A high K^+ solution (Table 2.2) was superfused over the IHCs whilst the cells were being voltage clamped. High K^+ solution depolarises the efferent fibre terminals, inducing the release of ACh, if IHCs were re-innervated then they would be re-expressing nAChRs and SK2 channels, as well as having the efferent synapses. The stimulated release of ACh from the efferent terminals would be detected by nAChRs and cause Ca^{2+} to enter the IHCs, this Ca^{2+} would activate the SK2 channels and result in K^+ leaving the cell, hyperpolarising it. This process can

be visualised in voltage clamp recordings in the form of inhibitory post-synaptic currents. The local superfusion utilised gravity to enable the flow of the extracellular solutions into the recording chamber via a multi-barrel pipette. Using gravity to control the flow of solution prevented background noise being produced as well as reducing any debris interference. Typically, the IHCs were locally perfused with the high K^+ solution, an extracellular solution containing $100\mu\text{M}$ acetylcholine or $1\mu\text{M}$ strychnine (Sigma-Aldrich, Gillingham, UK) to identify if IHCs re-expressed nAChRs. If inhibitory post-synaptic currents were induced and blocked by strychnine (a potent nAChR blocker), then this would indicate the re-expression of nAChRs in IHCs. Additionally, voltage clamp recordings were taken when perfusing control (normal extracellular solution, Table 2.1), followed by perfusion of the ACh containing solution, with a control wash afterwards. This was to identify if IHCs responded to ACh and if the currents responsible could be seen in the recordings. To analyse whether IHCs responded to ACh, the control recording trace was subtracted from the ACh perfusion trace, if the IHCs responded to ACh then the currents would be larger – following the (Marcotti et al., 2004) analysis. The ACh sensitivity was then measured at -84mV , which is the voltage that nAChRs become active in IHCs.

2.4. Immunofluorescence microscopy

Immunolabelling was used to visualise the efferent synaptic machinery on IHCs, this was to provide confirmation for the functional electrophysiology experiments that were also performed.

Dissected inner ears from the aforementioned mouse strains were fixed with 4% paraformaldehyde in phosphate-buffered saline (PBS, pH 7.4) (OXOID, BR0014G) for 20 minutes at room temperature. After fixation, cochlea had three PBS washes at room temperature, each for 10 minutes. Subsequently, the organ of Corti were dissected and transferred into Eppendorf caps for future steps. The dissected cochleae were incubated for an hour at room temperature in PBS supplemented with 5% normal horse serum (Sigma, H0146) and 0.5% Triton-X-100 (T9284, Sigma-Aldrich, UK). The samples were then incubated overnight at 37°C with the primary antibodies (Table 2.4) in PBS supplemented with 1%

normal horse serum. The samples were washed three more times with PBS before being appropriately labelled with species specific Alexa Fluor secondary antibodies (all used at 1:1000 concentration) for one hour at 37°C. After which, the samples had three more PBS washes before being manually mounted onto glass slides using a custom made stainless steel spoon and forceps in VECTASHEILD (H-1000, Vector Laboratories). The z-stack (either 0.1µm or 0.2µm steps) images were captured on either a Zeiss LSM 880 with AiryScan for super-resolution confocal microscopy (Plan-Apochromat 63x/ Oil DIC M27 objective, numerical aperture: 1.4) or on a Nikon CSU-W1 Spinning disk confocal microscope (BBSRC ALERT2021 award BB/V019368/1) with either a 25µm or 50µm pinhole size (either: Plan-Apochromat 20x, numerical aperture: 0.75; 40x oil, numerical aperture: 1.3; 100x oil, numerical aperture: 1.45). Images shown in the results chapters are maximum intensity projections of all the z-stack images, whilst the 3D projections shown at the full z-stack images that were interpolated using Fiji ImageJ software. Images were taken at the Wolfson Light Microscope Facility at the University of Sheffield. Image stacks were processed with Fiji ImageJ analysis software, Arivis software or Nikon W1 analysis software.

Primary Antibody	Species isotope	Concentration	Company	Catalogue no.
ChAT	Goat-IgG	1:500	Merck Millipore	AB144P
CtBP2	Mouse-IgG1	1:200	BD	612044
GluR2	Mouse-IgG2a	1:200	Merck Millipore	MAB397
Iba1	Rabbit-IgG	1:1000	Synaptic systems	234 003
Myo7a	Rabbit-IgG	1:200	Proteus BioSciences	25-6790
Myo7a	Mouse-IgG1	1:100	DSHB	No. 138-1-s
Otoferlin	Mouse-IgG1	1:2000	Abcam	ab53233
SK2	Rabbit-IgG	1:100	Merck Sigma	P0483

--	--	--	--	--

Table 2. 4. Primary Antibodies used for immunofluorescence.

2.5. Analysis of immunofluorescence images

Analysis for SK2 puncta and afferent ribbon synapse puncta was performed on the entire z-stack images. Using the commercial Arivis software an analysis pipeline was created (arivis Vision4D version 3.4.0, Arivis AG, Germany), the 'Blob Finder' segmentation tool was used to identify individual puncta. After this, the 'Distances' metric was used with a parameter of $<2\mu\text{m}$ to determine if the puncta were colocalised / in close proximity. If the puncta were $<2\mu\text{m}$ apart then this was used to determine that they were close enough to be forming a synapse. The measurements were then exported to an excel spreadsheet and analysed using GraphPad Prism (GraphPad Software, USA).

To analyse the macrophages, I encompassed the growing method of training an artificial intelligence (AI) /deep learning to aid with the image analysis. The Segment.AI tool from the Nikon software (NIS-Elements AR v5.41.02) was used. For the segment.AI algorithm to accurately detect the macrophages it was trained using over 10 different z-stack images from different genotypes and ages. For each of the training images multiple macrophages were manually binarised – this was to define the difference between real labelling and background, up to 20 macrophages were manually identified on around 5 different z-stack slices for each of the training data set. It was important to identify the different macrophage morphologies, so that amoeboid and ramified macrophages would both be detected, as well as macrophages that followed the afferent and efferent fibres from the modiolus to the sensory epithelium. After this, the manually identified training images were then used to train the AI, with the number of iterations used dependent on the accuracy of the macrophage detection. It was determined that 100 iterations enabled the AI to accurately detect the various morphologies as well as distinguish between any macrophages that may have been stacked on one another. Once the AI was trained, the 'General Analysis 3' analysis tool was used to create an analysis pipeline that had multiple measurements and would export the data into an excel sheet for

future analysis. Some of these measurements included macrophage volume, orientation, sphericity, elongation and macrophage counts. As the macrophage project was a preliminary study and the AI and analysis was still in optimisation, only the number of macrophages was used for quantification. Moreover, there were limitations to the Nikon analysis software, as the region of interest (ROI) option in the analysis pipeline would not actually be incorporated into the analysis. What this practically meant is that it was not possible to focus on specific regions of the cochlea for analysis, eg the OSL or outer sulcus, to then identify any changes in these regions. Additionally, this meant that the analysis could not be controlled for a defined size ROI, and numbers are taken from the entire cochlea, however, due to variability in the size of the apex that was dissected means that the preliminary quantification from this needs to be improved and not over interpreted.

2.6. Genotyping

For conditional knockout mice, genomic DNA was amplified under standard conditions using Promega Taq DNA polymerase (Invitrogen, UK). The reaction mix was incubated at 94°C for 5 minutes followed by 35 cycles of 94 °C for 30 s, 58 °C for 45 s and 72 °C for 90 s, followed by 72 °C for 5 min. The genotyping for the *Otof^{fl/fl} Vglut3 cre^{+/-}*, *Otof^{fl/fl} Myo15 cre^{+/-}* and *Ush1c^{fl/fl} Myo15 cre^{+/-}* mice were performed by research technicians. Primers pairs and products are shown in Table 5.

Gene	Forward primer	Reverse primer	Base pair products
<i>Myo7a</i>	5' GGG AGA GAA AGC AGG GTG TG 3'	5' AAG CTG GAC TCT CTG GTG GC 3'	WT ~ 360 bp Mut ~ 460 bp
<i>Myo15-cre</i>	5' AGG GAC CTG ACT CCA CTT TGG G 3'	5' TGG TGC ACA GTC AGC AGG TTG G 3'	Myo15-cre ~ 500 bp
<i>Otof-tm1c</i>	5' TCC CAG GTA GCA CTT GGT TT 3'	5' GTG TAG AAG AAC CCC GAC CA 3'	WT ~ 230 bp Mut ~ 150 bp
<i>Td-tomato (WT)</i>	5' AAG GGA GCT GCA GTG GAG TA 3'	5' CCG AAA ATC TGT GGG AAG TC 3'	~ 300 bp
<i>Td-tomato (Mut)</i>	5' GGC ATT AAA GCA GCG TAT CC 3'	5' CTG TTC CTG TAC GGC ATG G 3'	~ 200 bp
<i>Ush1C</i>	5' ACA GAG CCG TGG GTT CAT TC 3'	5' GTA ATG GAG CTG AGG CAG GG 3'	WT ~ 326 bp Mut ~ 430 bp

Table 2. 5. Genotyping information for the different strains used.

2.7. Statistical analysis

Statistical analysis was performed on Prism software (GraphPad Software, USA). Statistical comparisons between multiple data-sets were made by either one-way or two-way ANOVA, followed by Tukey's multiple comparison tests or Šidák post-test. Additionally, Students t test were also used. The criterion for statistical significance was set at 0.05 and data are shown as mean values \pm SD.

Chapter 3 - Efferent re-innervation of IHCs is caused by
disrupted MET function

3.1. Introduction

The axosomatic efferent innervation of IHCs is typically only seen in development, and after the onset of hearing at P12 (Kros et al., 1998), the IHCs start to lose the axosomatic efferent innervation. By P21 IHCs no longer have axosomatic efferent innervation (Glowatzki and Fuchs, 2000, Katz et al., 2004, Marcotti et al., 2004). The function of the efferent innervation is to hyperpolarise the hair cells. For the hyperpolarisation to occur there are a combination of ion channels and receptors that work together. The pre-synaptic efferent fibre terminals release the neurotransmitter ACh, which is detected by the IHCs that express post-synaptic $\alpha 9\alpha 10$ nicotinic acetylcholine receptors until P18 (Elgoyhen et al., 1994, Elgoyhen et al., 2001, Glowatzki and Fuchs, 2000, Katz et al., 2004). This allows the influx of Ca^{2+} into the IHC which stimulates the small conductance calcium activated potassium channels (SK2), once SK2 channels are open there is a subsequently efflux of K^+ from the IHC, resulting in its hyperpolarisation (Evans, 1996, Marcotti et al., 2004, Katz et al., 2004).

When the IHCs stop responding to ACh and lose their axosomatic efferent innervation, the IHCs display a 'mature' adult biophysical profile. To determine whether an IHC has 'mature' (adult) and 'immature' (developmental) current profile, outward potassium currents are used. IHCs have outward potassium currents that have both a fast and slow component that are carried with two different potassium channels. During development, the slow component of the outward current is known as $I_{k,neo}$ and is present after birth up until the onset of hearing at P12 (Kros et al., 1998). After the onset of hearing at P12, IHCs express the fast activating large conductance Ca^{2+} -activated K^+ current ($I_{k,f}$: (Kros et al., 1998)) and the slow delayed rectified K^+ current. Therefore, the absence of $I_{k,f}$ and the presence of the $I_{k,neo}$ can be used to define an immature IHC current profile, and vice versa for the mature profile (Kros et al., 1998).

In age-related hearing loss mouse models such as C57BL/6J and 6N, harbouring the *Cdh23^{ahl}* mutation that impacts the stereocilia atop the IHCs and OHCs, there is a return of axosomatic efferent innervation to IHCs after one year of age (Lauer et al., 2012, Zachary and Fuchs, 2015, Jeng et al., 2021). Additionally, in the good hearing strain 6N-repaired, where the *Cdh23^{ahl}*

mutation was repaired by CRISPR-Cas9 (Mianné et al., 2016), the IHCs also become re-innervated by efferent fibres, albeit, later than in 6N and 6J mice.

The IHCs that become re-innervated express functional efferent synapses with both SK2 channels and $\alpha 9\alpha 10$ nAChRs expressed (Zachary and Fuchs, 2015, Jeng et al., 2021). Moreover, it has also been shown that the lateral olivocochlear (LOC) efferent fibres that re-innervate the IHCs (Jeng et al., 2021). The LOC fibres form axodendritic synapses onto the afferent fibres that innervate the IHCs (Simmons, 2002). It has been proposed that the degeneration of afferent fibres in age-related hearing loss leaves the LOC fibres without afferents to synapse on, resulting in the LOC fibres re-innervating the IHCs to stay alive (Lauer et al., 2012, Zachary and Fuchs, 2015, Jeng et al., 2021). Supporting this proposal, there is a reduction in the number of afferent synapses in IHCs from 6J, 6N and 6N-repaired mice with age (Jeng et al., 2021). Although the loss of afferent synapses and fibres seemingly comes prior to the efferent re-innervation of IHCs with ageing, identifying the exact mechanism of re-innervation has not been found in ageing mouse models.

The mechano-electrical transducer channels (MET) are responsible for converting acoustic stimuli into electrical signals which will be sent to the brain for auditory processing. If the MET channels become dysfunctional then the IHCs become re-innervated by efferent fibres, similar to in age-related hearing loss strains (Corns et al., 2018). Interestingly, when the MET channels do not function properly, the re-innervation of IHCs takes place at much younger ages compared to age-related mouse models. A conditional knockout mouse model disrupting the MET channels by targeting unconventional myosin VIIa (Myo7a), a protein that maintains tension at the MET channels and is involved in the open probability (Verpy et al., 2000, Kros et al., 2002, Senften et al., 2006, Grati and Kachar, 2011), was shown to have IHCs that became re-innervated (Corns et al., 2018). The re-innervation of IHCs in the Myo7a conditional knockout was shown to have taken place by P36 (Corns et al., 2018), as opposed to after one year of age in age-related 6J, 6N and 6N-repaired mouse strains (Lauer et al., 2012, Zachary and Fuchs, 2015, Jeng et al., 2021). This finding enables the mechanistic changes of efferent re-innervation to be studied over a short time-period, by using the conditional knockout mouse model of Myo7a (*Myo7a^{fl/fl} Myo15 cre^{+/-}*).

The conditional knockout mouse model for Myo7a (*Myo7a^{fl/fl} Myo15 cre^{+/-}*) was used in this study. By using a Myo15-cre driver for this study, Myo7a will be knocked out of IHCs and OHCs

only, resulting in dysfunctional MET channels (Corns et al., 2018). Myo15 is expressed between P2-4 in postnatal development, meaning that Myo7a is present for normal development within the embryo. The aim for this study was to investigate the discrete mechanistic changes that take place during efferent re-innervation of IHCs – to identify if the IHCs are driving the efferent re-innervation, as well as whether the afferent synapses are lost before or after the re-innervation.

The efferent re-innervation of IHCs is driven by changes in the IHCs. This is shown by the IHCs re-expressing SK2 channels from P24, whereas functional synapses were only seen from P25 onwards. Following the re-innervation of IHCs, the IHCs undergo progressive biophysical changes and revert to an 'immature' like current profile, with a reduction in the $I_{k,f}$ current. Surprisingly, there was only a loss of afferent synapse after the efferent re-innervation of IHCs, with both pre- and post- synaptic components of the afferent synapse being lost at P50. This finding indicates that the efferent re-innervation is not a survival response after the loss of afferent fibres (Lauer et al., 2012, Zachary and Fuchs, 2015, Jeng et al., 2021). However, it may be that the efferent re-innervation could influence the loss of afferent synapses in IHCs.

3.2. Results

3.2.1. Axosomatic efferent innervation returns to IHCs from around P24

Firstly, a timeline investigating the level of Myo7a knocked out in IHCs was established by using immunofluorescence. Both *Myo7a^{fl/fl} Myo15 cre^{+/-}* and littermate control *Myo7a^{fl/fl}* mice were used. This was not established in the Corns et al., (2018) study, as immunolabelling data only showed the loss of Myo7a in the stereocilia at P10. In control *Myo7a^{fl/fl}* mice there was no loss of Myo7a in any IHCs (Figure 3.1A). In *Myo7a^{fl/fl} Myo15 cre^{+/-}* mice, Myo7a was present in the large majority of IHCs at P4 and P7 (Figure 3.1B & C), but by P12 only a few cells showed Myo7a (Figure 3.1D) and by P22 it was knocked out in all IHCs (Figure 3.1E).

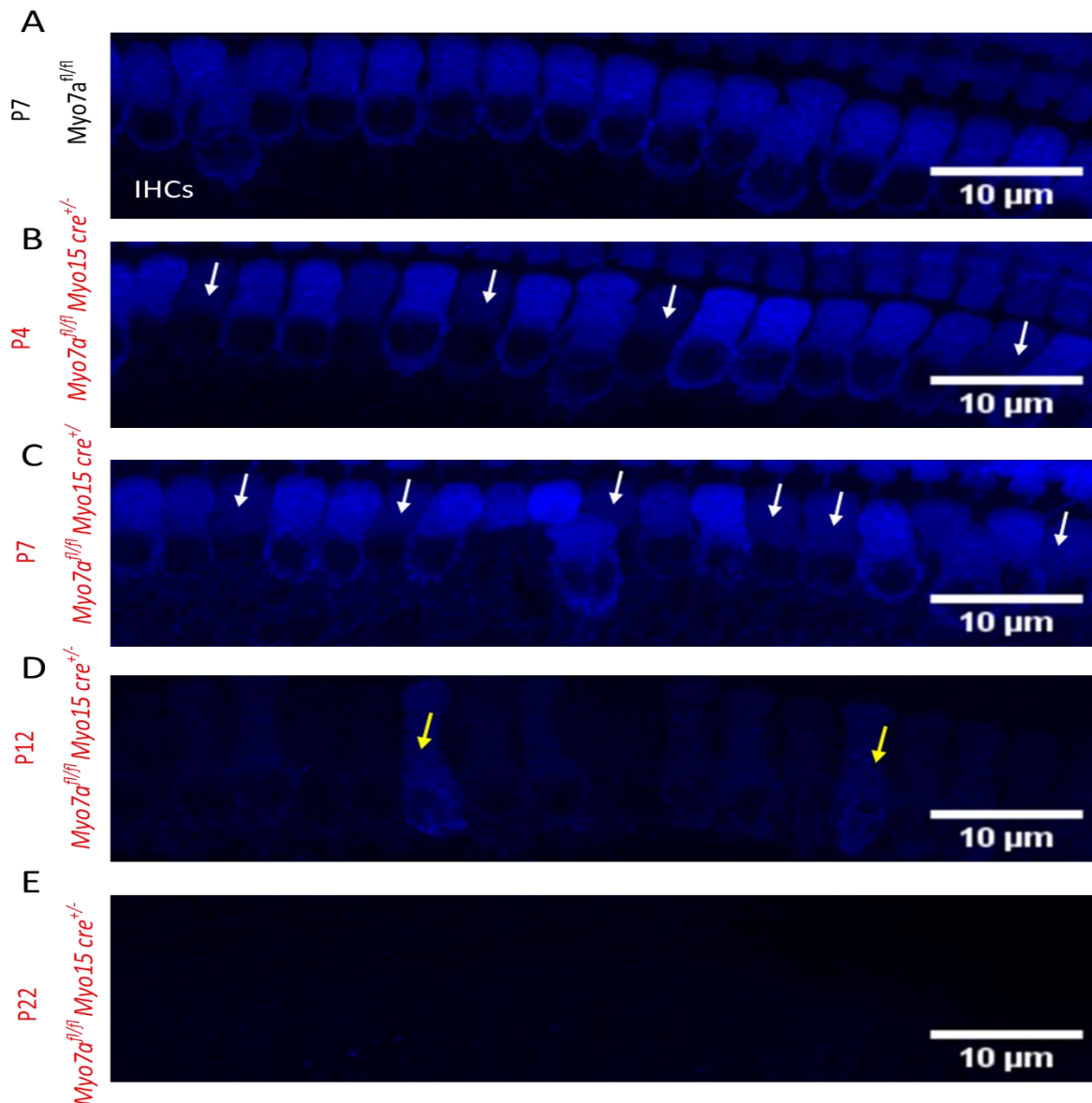


Figure 3. 1. Characterising the loss of Myo7a from IHCs.

A-E: maximum intensity projections of confocal z-stacks of the apical coil of the cochlea (85µm) at the 9-12 kHz region. IHCs were labelled with an anti-Myo7a antibody (blue), scale bars: 10µm. **A:** shows the expression of Myo7a in IHCs from control *Myo7a^{fl/fl}* mice. **B:** shows that some IHCs started to lose their Myo7a labelling at P4 (white arrows), soon after Myo15 cre was expressed during development in *Myo7a^{fl/fl} Myo15 cre^{+/-}* mice. **C, D:** images showing that the number of IHCs with a lower or no expression of Myo7a in P7 and P12 *Myo7a^{fl/fl} Myo15 cre^{+/-}* mice is progressively increasing (white arrows). The yellow arrows in **D** shows the two IHCs that still express Myo7a. **E:** shows that no IHCs express Myo7a at P22 in *Myo7a^{fl/fl} Myo15 cre^{+/-}* mice.

To determine the age at which the efferent innervation re-establish axosomatic contact with IHCs following a loss of *Myo7a*, immunofluorescence and confocal microscopy was used to label the pre- and post-synaptic proteins ChAT and SK2 (see methods). An example of axosomatic efferent innervation can be seen in Figure 3.2A-F, at a time point (P10) that is representative of the IHC during development. Figure 3.2B shows an example of a single IHC zoomed in, showing the high level of SK2 labelling located near the base of the IHC. Figure 3.2C shows the same IHCs as in Figure 3.2A but rotated to the Z, Y plane to provide a better view of the localisation of the SK2 channels. The process of zooming in to a single IHC and rotating the initial image to the Z, Y plane was applied to all images in Figure 3.2. Furthermore, Figure 3.2A-F shows the characteristic colocalisation of either SK2 and ChAT (Figure 3.2C) in developing cochlea, highlighting the axosomatic efferent synapse at the base of the IHCs.

The IHCs from control *Myo7a^{fl/fl}* mice did not express SK2 channels at P24 (Figure 3.2D-F), indicating that in the presence of *Myo7a* the efferent innervation matured normally. On the other hand, IHCs from *Myo7a^{fl/fl} Myo15 cre^{+/-}* mice at P24 had SK2 channels re-expressed (Figure 3.2G-I), albeit only in one IHC in the image shown. Figure 3.2I shows a lateral view of the IHCs, and it is not clear that any of the SK2 puncta are colocalised with the pre-synaptic ChAT efferent synaptic terminals (colocalization would appear yellow). Therefore, to identify whether IHCs at P24 in *Myo7a^{fl/fl} Myo15 cre^{+/-}* mice expressed functional efferent synaptic machinery (presence of both nAChRs and SK2 channels), whole cell patch-clamp electrophysiology was performed in *Myo7a^{fl/fl} Myo15 cre^{+/-}* and control mice. Perfusion of an extracellular solution containing a high K⁺ (40mM) concentration (see methods, 2.3.3) was locally perfused over the IHCs during patching experiments. High K⁺ solution depolarises any efferent synaptic terminals that may be forming synapses at the IHC, if present, the synaptic terminals will release ACh which will be detected by nAChRs if the IHCs are re-expressing them. The IHCs re-expressing nAChRs would detect the ACh and allow Ca²⁺ to enter the IHC, stimulating the SK2 channels and resulting in K⁺ leaving the cell, hyperpolarising it (Glowatzki and Fuchs, 2002, Marcotti et al., 2004). The hyperpolarisation can be seen in recordings as inhibitory post-synaptic currents. This method has been previously used to determine whether efferent synapses are functional in IHC re-innervation studies (Zachary and Fuchs, 2015, Corns et al., 2018, Jeng et al., 2021).

IHCs from control mice did not have any induced post-synaptic currents at either P24 (Figure 3.2J) or P25 (Figure 3.2K). Similarly, IHCs from *Myo7a^{fl/fl} Myo15 cre^{+/-}* mice at P24 did also not have any induced post-synaptic currents (Figure 3.2L), however, at P25, IHCs from *Myo7a^{fl/fl} Myo15 cre^{+/-}* mice did express post-synaptic currents that were driven by nAChRs due to the current being readily blocked by a potent nAChR blocker strychnine (Figure 3.2M). These results indicate that the IHCs are driving the efferent re-innervation mechanism by re-expressing the post-synaptic SK2 channels prior to the synapses becoming fully functional at P25.

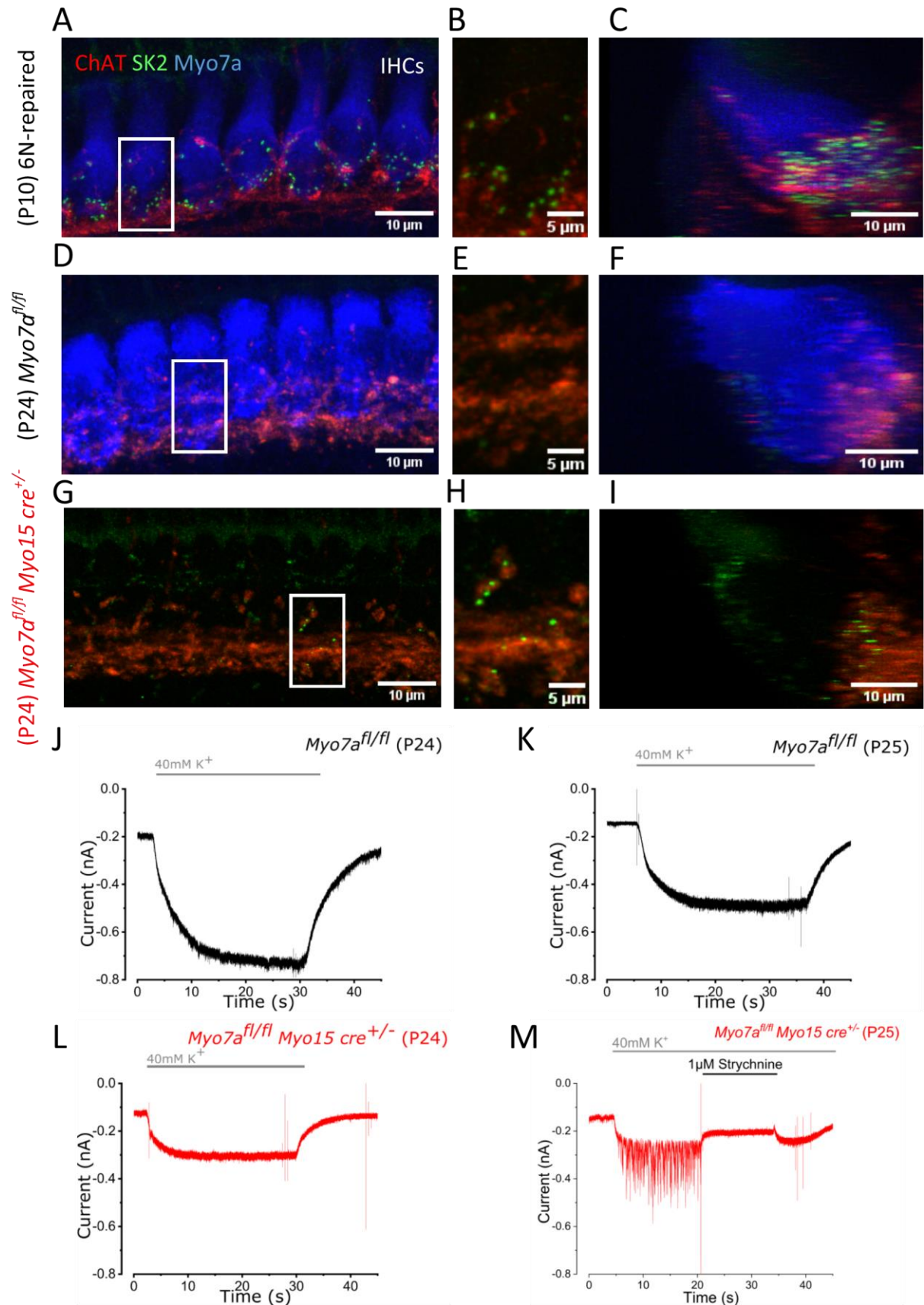


Figure 3. 2. IHCs re-express SK2 channels at P24 in *Myo7a^{fl/fl} Myo15 cre^{+/-}* mice but don't form functional synapses until P25.

A-I: maximum intensity projections of confocal z-stacks of the apical coil of the cochlea (85µm) at the 9-12 kHz region. IHCs were labelled with antibodies against SK2 channels (green), myosin 7a (blue) as well as the efferent terminal markers ChAT (red). Scale bars for the outer column images: 10µm, scale bar for the middle column images: 5µm. **A:** the characteristic expression of SK2 channels at P10 in 6N-repaired mice. **B:** a zoomed in image of the IHC highlighted with the white box in panel **A**, showing the expression of SK2 channels in relation to ChAT positive efferent terminals. **C:** the IHCs from **A** were rotated to the Y, Z plane, enabling a lateral view of the IHCs to see where SK2 channels were expressed on the IHCs. **D-F:** IHCs from control *Myo7a^{fl/fl}* mice did not express SK2 channels at P24. **G-I:** at P24 the IHCs from *Myo7a^{fl/fl} Myo15 cre^{+/-}* mice re-expressed SK2 channels with **I** showing SK2 channels were only expressed at the basal pole of IHCs. SK2 and either ChAT labelling that were in close proximity appeared yellow, as can be seen in **C**, indicating the presence of both pre- and post-synaptic terminals. **J-M:** inward post-synaptic currents in IHCs (**M**) evoked with high K⁺ (40mM) extracellular KCl during long lasting recordings at -84 mV in control *Myo7a^{fl/fl}* and *Myo7a^{fl/fl} Myo15 cre^{+/-}* mice at P25. Post-synaptic currents were blocked with 1µM strychnine in *Myo7a^{fl/fl} Myo15 cre^{+/-}* mice.

Figure 3.3A shows the percentage of IHCs from *Myo7a^{fl/fl} Myo15 cre^{+/-}* mice that had the return of axosomatic efferent innervation with functional synapses. To categorise whether IHCs had the return of efferent innervation, they were split into if they displayed post-synaptic currents when perfused with high K⁺ solution that was blocked by 1µM strychnine, or if they did not show any post-synaptic currents. 51.06% (24 out of 47 IHCs) did not show any post-synaptic currents whereas 48.94% (23 out of 47 IHCs) showed post-synaptic currents that was blocked by 1µM strychnine. Therefore, about half of the IHCs from *Myo7a^{fl/fl} Myo15 cre^{+/-}* mice had a return of axosomatic efferent innervation during the early age range (P25-31).

Figure 3.3B & C show that IHCs from control *Myo7a^{fl/fl}* mice remained insensitive to the perfusion of 100µM ACh during depolarising voltage steps to -24mV from a holding of -84mV. Figure 3.3D & E show that at P25 IHCs from *Myo7a^{fl/fl} Myo15 cre^{+/-}* mice minimally respond when 100µM ACh was perfused, supporting that IHCs re-express nAChRs.

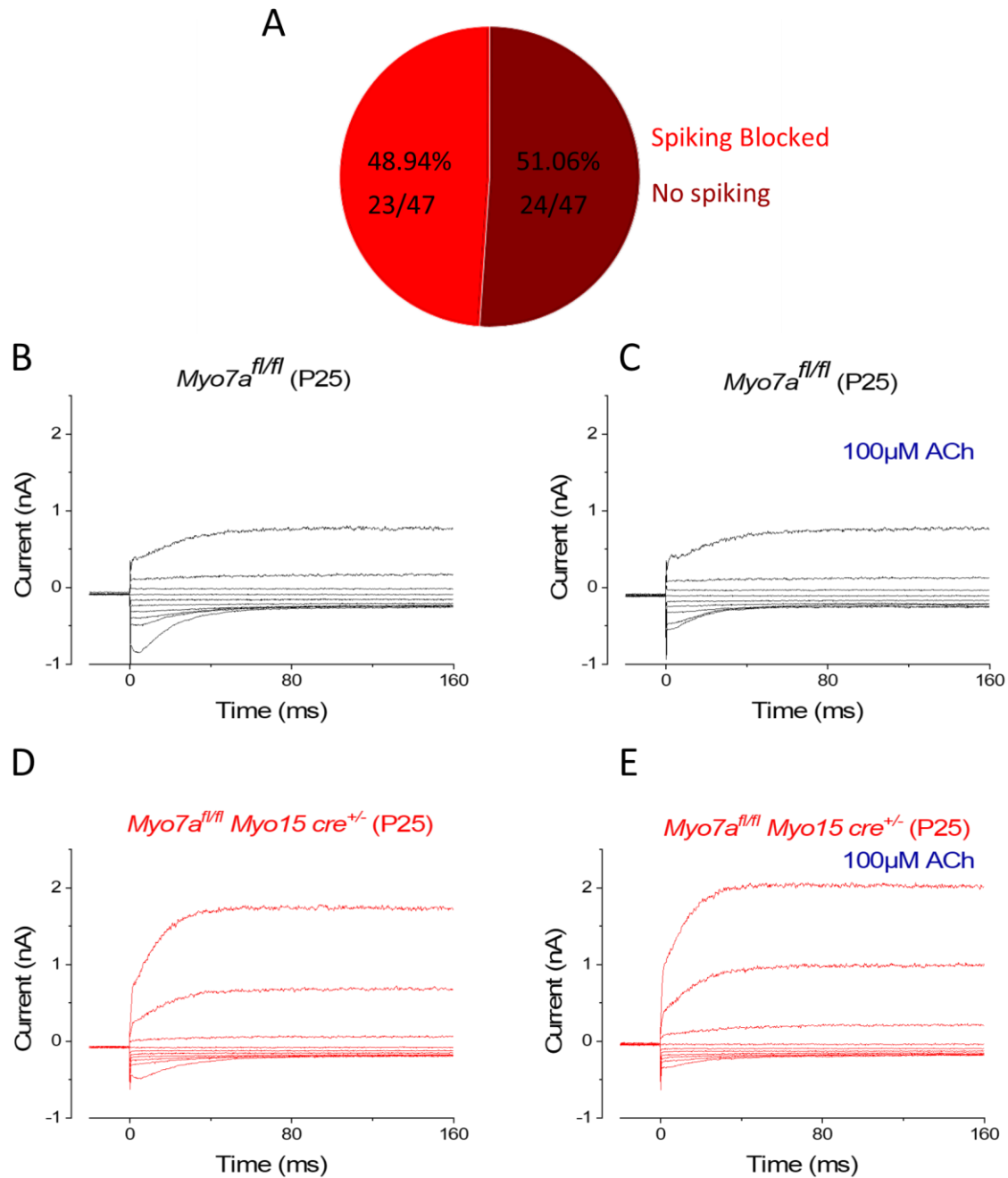


Figure 3. 3. Axosomatic efferent synapses on IHCs in *Myo7a^{fl/fl} Myo15 cre^{+/-}* mice are functional.

C: the percentage of IHCs that had a return of axosomatic efferent innervation was 48.94% (23 out of 47 IHCs). **B-E:** current traces from IHCs that were depolarised with voltage steps from -124 mV to +24 mV before (control) and after the extracellular application of 100 μ M ACh. The IHCs from *Myo7a^{fl/fl} Myo15 cre^{+/-}* mice did not instantaneously respond to ACh at P25.

3.2.2. Progressive biophysical changes in IHCs from *Myo7a^{fl/fl} Myo15 cre^{+/-}*

The return of axosomatic efferent innervation to IHCs in *Myo7a^{fl/fl} Myo15 cre^{+/-}* mice has previously been reported to take place as the IHCs basolateral membrane channel profile return to a developmental-like configuration (Corns et al., 2018). Here, it is shown that most of the IHC biophysical characteristics return to a developmental state after the return of axosomatic efferent innervation.

Figure 3.4A-C shows that at older ages (P39) the IHCs from control *Myo7a^{fl/fl}* mice no longer express SK2 channels, as previously shown (Glowatzki and Fuchs, 2000, Katz et al., 2004, Marcotti et al., 2004). Figure 3.4D-F reveals that seemingly more IHCs from *Myo7a^{fl/fl} Myo15 cre^{+/-}* mice re-express SK2 channels by P39. Moreover, at P39 the expression of SK2 channels in *Myo7a^{fl/fl} Myo15 cre^{+/-}* mice was still only seen at the basal pole of the IHCs (Figure 3.4L).

SK2 labelling quantified based on two-day intervals from P24-P39, and when looking for genotype differences there were significantly more SK2 puncta expressed in *Myo7a^{fl/fl} Myo15 cre^{+/-}* mice compared to control mice (Figure 3.3G) ($P = <0.0001$, *Students T-test*). To identify if there was a progressive increase in SK2 puncta in IHCs with age (Figure 3.3H), a two-way ANOVA Šidák post-test and multiple comparisons was performed. There were significant increases for each age tested apart from P24, which likely doesn't show significance due to being underpowered. The two-way ANOVA revealed a genotype, but not genotype and age effect on the number of SK2 puncta seen in IHCs ($P = 0.7060$), although to get a true representation more N numbers may change this result. There was an increase in the number of SK2 puncta seen at each age in *Myo7a^{fl/fl} Myo15 cre^{+/-}* mice between P24 and P30, to identify the change in the expression of SK2 puncta in IHCs, a linear regression was plotted (Figure 3.3I). The linear regression showed an average, the IHCs in *Myo7a^{fl/fl} Myo15 cre^{+/-}* mice expressed 8.34% more SK2 puncta than the previous two days, up to P30 where the results began to plateau. Together, this data demonstrates that IHCs from *Myo7a^{fl/fl} Myo15 cre^{+/-}* mice have a progressive increase in SK2 channels with age, increasing from singular IHCs at P24 to most of the IHCs in the apical region of the cochlea.

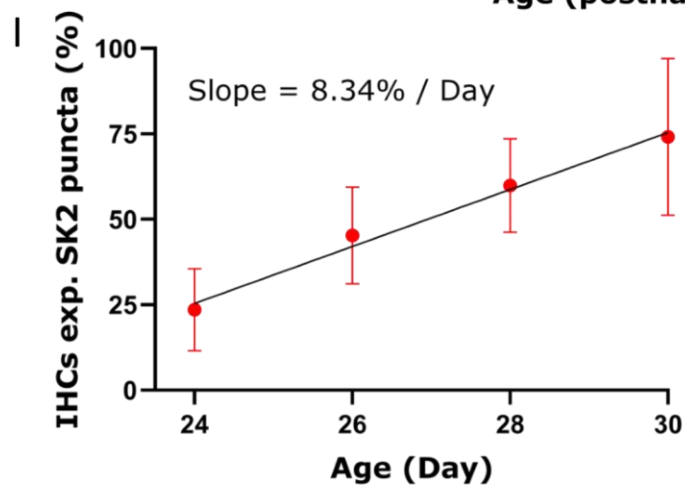
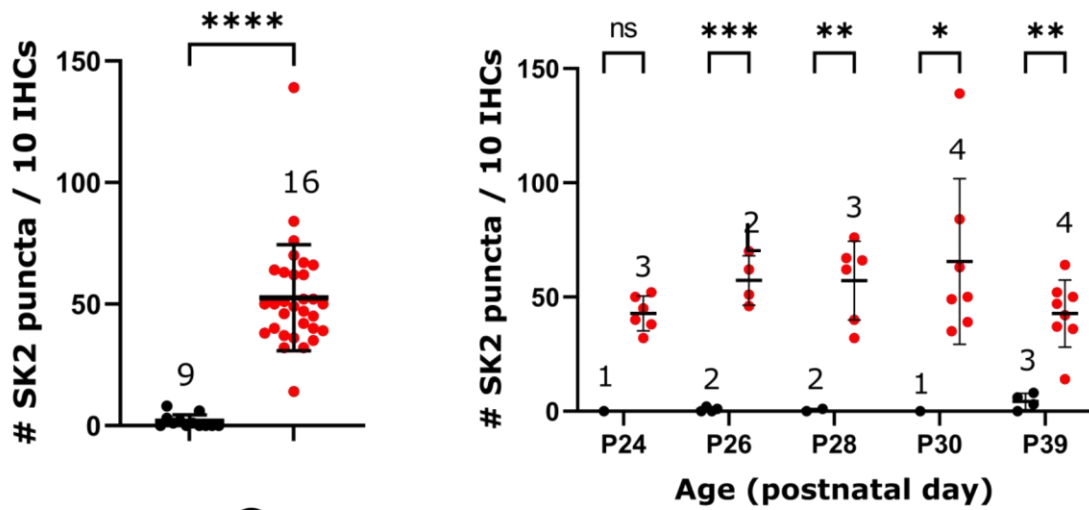
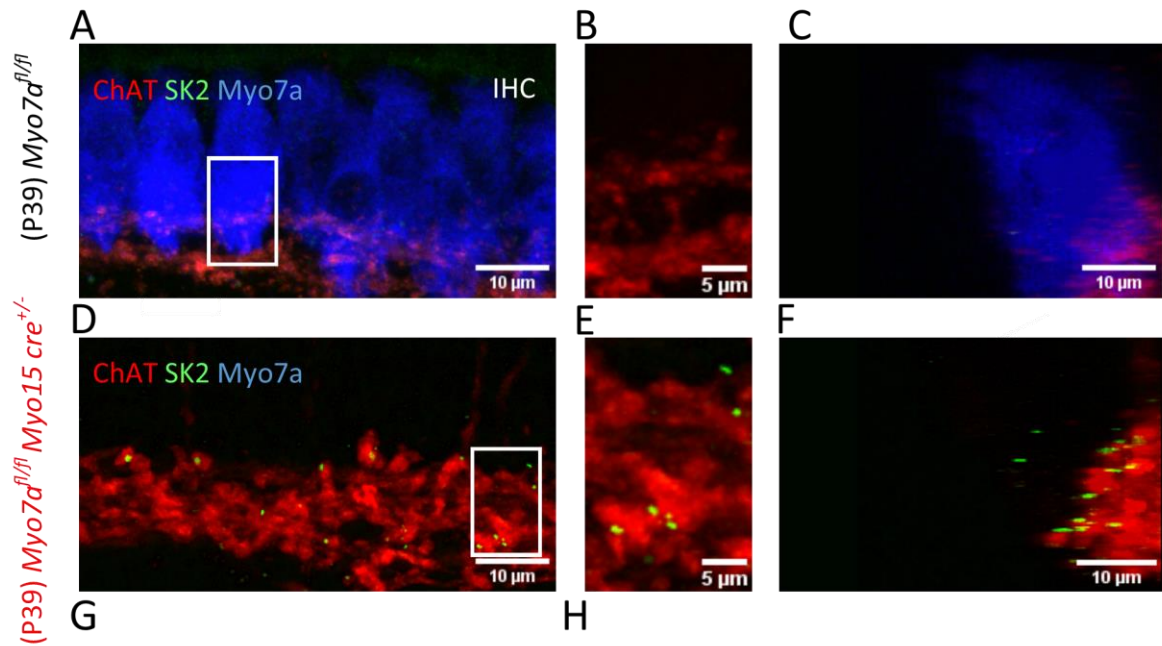


Figure 3. 4. The number of SK2 channels expressed in IHCs is larger in P39 in *Myo7a^{fl/fl} Myo15 cre^{+/-}* mice.

A-L: maximum intensity projections of confocal z-stacks of the apical coil of the cochlea (85 μ m) at the 9-12 kHz region. IHCs were labelled with antibodies against SK2 channels (green), myosin 7a (blue) as well as the efferent terminal markers ChAT (red). Scale bars for the outer column images: 10 μ m, scale bar for the middle column images: 5 μ m. **A-C:** IHCs from control *Myo7a^{fl/fl} Myo15 cre^{+/-}* mice do not express SK2 channels at P39. **D-F:** IHCs from *Myo7a^{fl/fl} Myo15 cre^{+/-}* mice express SK2 channels in IHCs and the expression of SK2 channels was still only seen at the basal pole of IHCs at P39 (**F**). SK2 channels were seen in close proximity to either ChAT efferent terminals (**I**) as labelling appeared yellow. **G:** *Myo7a^{fl/fl} Myo15 cre^{+/-}* mice express more SK2 puncta per 10 IHCs compared to control mice ($P < 0.0001$, Students T-test). **H:** the number of SK2 puncta in *Myo7a^{fl/fl} Myo15 cre^{+/-}* mice increases with age, whereas the IHCs from control mice did not increase. **I:** the expression of SK2 channels in IHCs from *Myo7a^{fl/fl} Myo15 cre^{+/-}* mice increased at a linear rate of 8.34% every two days, demonstrating a progressive increase in re-innervation with time. Average data is shown as mean \pm SD.

Whole cell patch-clamp recordings were taken from IHCs of *Myo7a^{fl/fl} Myo15 cre^{+/-}* mice and control *Myo7a^{fl/fl}* mice across ages ranging from P25-42. IHCs from control *Myo7a^{fl/fl}* mice remained insensitive to 100 μ M ACh at older ages (P39-42: Figure 3.5B & C) whilst also having their typical 'adult' current profile (Figure 3.5A) (Kros et al., 1998, Marcotti et al., 2003a). On the other hand, Figure 3.5D show that IHCs from *Myo7a^{fl/fl} Myo15 cre^{+/-}* mice express an immature current profile and continued to respond to 100 μ M ACh at older ages (P42), supporting previous findings (Corns et al., 2018). Figure 3.5E-F shows that IHCs from control *Myo7a^{fl/fl}* mice did not show post-synaptic currents at older ages when perfused with high K⁺ solution (Figure 3.5G), whereas the IHCs from *Myo7a^{fl/fl} Myo15 cre^{+/-}* mice continued to show post-synaptic currents that was readily blocked by strychnine (Figure 3.5H). Using the aforementioned categorisation of whether an IHC had the return of axosomatic efferent innervation showed that at older ages (P32-42) 38 out 55 (69.09%) IHCs had the presence of functional efferent synapses (Figure 3.5I).

The results from a two-way ANOVA revealed that there was no interaction between age and genotype on the slope conductance at -84mV ($F(1, 102) = 0.855, P = 0.3572$, two-way ANOVA). Furthermore, the IHCs that had the return of efferent innervation at younger ages (P25-31) did not show a significant increase in their slope conductance compared to IHCs from control *Myo7a^{fl/fl}* mice (Figure 3.5J) ($F(102) = 1.345, P = 0.330$, Šidák post-test, two-way ANOVA). On the other hand, Figure 3.5J shows that the older (P32-42) IHCs that had a return of axosomatic efferent innervation showed a significant increase in their slope conductance at -84mV to 2.71 nS compared to 0.93nS in IHCs from control *Myo7a^{fl/fl}* mice ($F(102) = 2.730, P = 0.0149$, Šidák post-test, two way ANOVA).

Figure 3.5K shows that IHCs from *Myo7a^{fl/fl} Myo15 cre^{+/-}* mice did not have a significant decrease in their $I_{k,f}$ current at younger ages compared to control mice (P25-31), whereas at older ages (P32-42) there was a significant decrease ($F(54) = 2.420, P = <0.0001$, Šidák post-test, two way ANOVA). Furthermore, a two-way ANOVA revealed that both age and genotype influence the size of $I_{k,f}$ currents ($F(1, 218) = 22.04, P = <0.0001$, two way ANOVA).

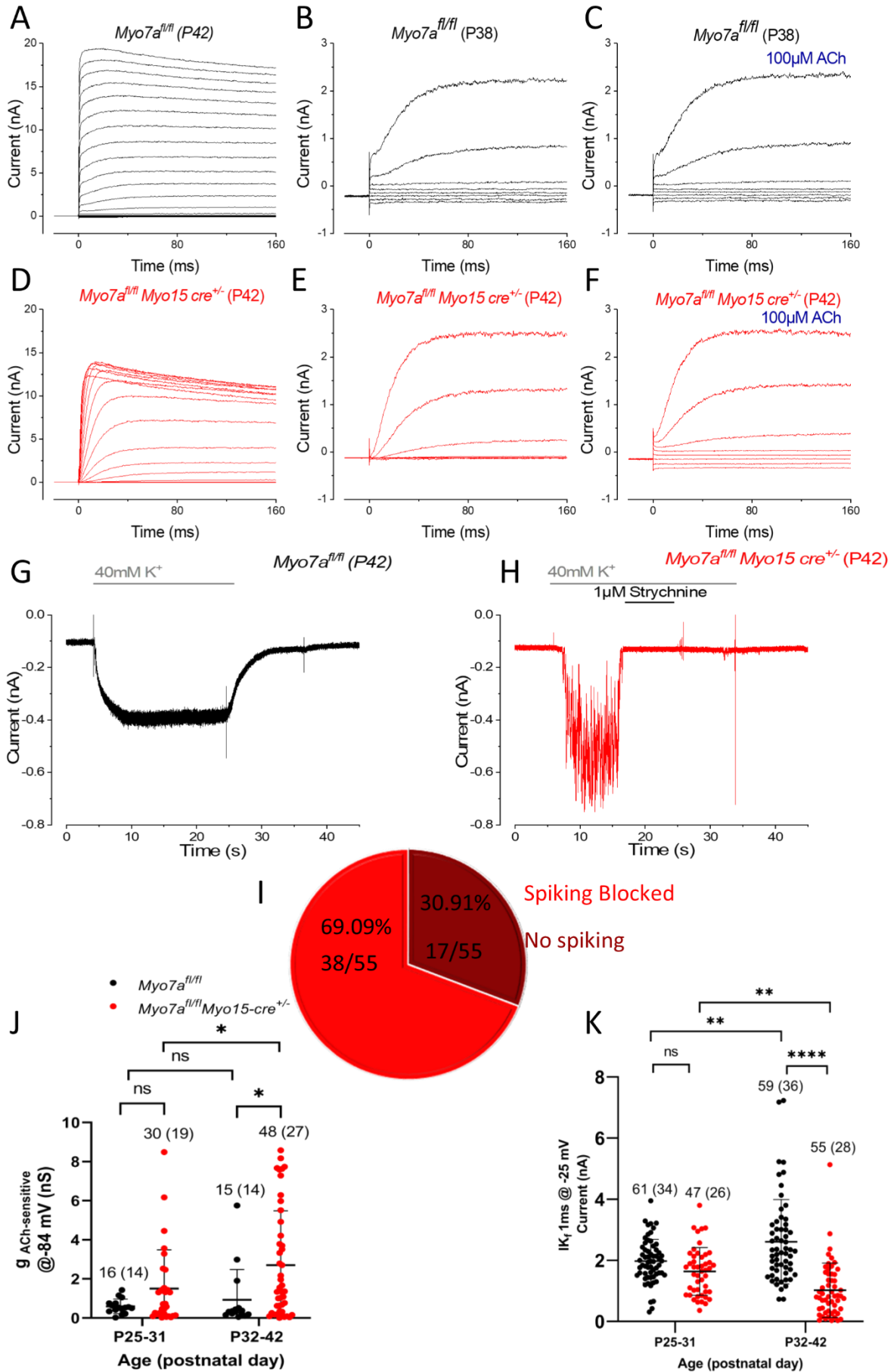


Figure 3. 5. IHCs from *Myo7a^{fl/fl} Myo15 cre^{+/-}* underwent biophysical changes over time.

A-F: current voltage recordings from IHCs of control *Myo7a^{fl/fl}* mice (A-C) or *Myo7a^{fl/fl} Myo15 cre^{+/-}* mice (D-F). **A:** control IHCs display normal mature 'adult' type current profile responses when depolarised with voltage steps from -124 mV to +84 mV (Kros et al., 1998). **B-C:** IHCs from control mice did not respond before (control, **B**) or during (**C**) the perfusion of 100µM ACh when depolarised with voltage steps from -124 mV to +24 mV. **D:** displays the IHCs from *Myo7a^{fl/fl} Myo15 cre^{+/-}* mice after the return of axosomatic efferent innervation that had returned to a developmental phenotype, displaying slower current activation during depolarisation steps. **E-F:** IHCs that had the return of axosomatic efferent innervation readily responded to 100µM ACh upon local perfusion. **G-H:** inward post-synaptic currents in IHCs (**G**) evoked with high K⁺ (40mM) extracellular KCl during long lasting recordings at -84 mV in control *Myo7a^{fl/fl}* and *Myo7a^{fl/fl} Myo15 cre^{+/-}* mice at P42. Post-synaptic currents were blocked with 1µM strychnine in *Myo7a^{fl/fl} Myo15 cre^{+/-}* mice (**H**). **I:** the percentage of IHCs that had a return of axosomatic efferent innervation was 69.09% (38 out of 55 IHCs) **J:** the IHCs sensitivity to 100µM ACh, as determined by the slope conductance at -84 mV (Marcotti et al., 2004) comparing the P25-31 and P32-42 age ranges in control and *Myo7a^{fl/fl} Myo15 cre^{+/-}* mice. **K:** the size of $I_{K,f}$ currents in the P25-31 and P32-42 age ranges in control and *Myo7a^{fl/fl} Myo15 cre^{+/-}* mice. The number above the data points represents the IHCs (and mice) used for each age group. Average data is shown as mean ± SD.

3.2.3. ABR thresholds in *Myo7a^{fl/fl} Myo15 cre^{+/-}* mice

Auditory brainstem responses (ABRs) are a technique used to investigate the hearing ability of the mice by measuring the activity of the afferent auditory pathway downstream of the IHCs.

To investigate whether the changes that occur in IHCs impact the hearing ability of the *Myo7a^{fl/fl} Myo15 cre^{+/-}* mice, ABRs were performed at three different ages, before the return of axosomatic efferent innervation at P20, during the early time points as efferent innervation returns at P25-26 and as the IHCs return to the developmental state between P31-35.

Figure 3.6A shows the ABR threshold of control *Myo7a^{fl/fl}* mice and *Myo7a^{fl/fl} Myo15 cre^{+/-}* mice at each of the ages studied. A two-way ANOVA revealed that both age and genotype influenced the ABR threshold for click stimuli ($F(2, 47) = 59.09$, $P < 0.0001$). At P20 the *Myo7a^{fl/fl} Myo15 cre^{+/-}* mice had no changes in their hearing thresholds compared to control mice. By P25-26 the *Myo7a^{fl/fl} Myo15 cre^{+/-}* mice had raised thresholds compared to control mice indicating some degree of hearing loss ($F(47) = 8.257$, $P < 0.0001$, Šidák post-test, two way ANOVA). However, by P31-35 the *Myo7a^{fl/fl} Myo15 cre^{+/-}* mice all had raised thresholds above 95dB, which was the absolute threshold for determining whether the mice were deaf, whereas control mice still had no raised thresholds ($F(47) = 816.73$, $P < 0.0001$, Šidák post-test, two way ANOVA).

Figure 3.6B shows the ABR threshold for tone burst stimuli ranging from low to high frequencies. At P20, there was no difference between control mice or *Myo7a^{fl/fl} Myo15 cre^{+/-}* mice hearing ability at low or high frequencies. At P25-26 the *Myo7a^{fl/fl} Myo15 cre^{+/-}* mice show variability in their hearing ability, with mice displaying raised ABR thresholds at all frequencies. By P31-35 the *Myo7a^{fl/fl} Myo15 cre^{+/-}* mice had raised ABR thresholds above the absolute threshold at 95dB in all frequencies tested, whereas control mice did not have raised ABR thresholds.

Examining the ABR waveform taken during ABR measurements at 12 kHz (Figure 3.6C) revealed that at P20 the amplitude and latency were no significant differences between both control and *Myo7a^{fl/fl} Myo15 cre^{+/-}* mice ($F(26) = 9.021$, $P = 0.1458$, Šidák post-test, two-way ANOVA) (Figure 3.6D). However, at P25 there were significant differences in wave 1

amplitudes in *Myo7a^{fl/fl} Myo15 cre^{+/-}* mice compared to control mice ($F(26) = 9.021$, $P = 0.0005$, Šidák post-test, two-way ANOVA). By P35 the waveform had flat-lined in the *Myo7a^{fl/fl} Myo15 cre^{+/-}* mice compared to control mice, however, there was no significant differences ($F(26) = 9.021$, $P = 0.0997$, Šidák post-test, two-way ANOVA) (Figure 3.6D). The reason for there being no significant differences may be due to the *Myo7a^{fl/fl} Myo15 cre^{+/-}* mice only having three amplitude responses at the higher sound intensities (Figure 3.6D).

Figure 3.6E shows that the wave 1 latency increased progressively with age in the *Myo7a^{fl/fl} Myo15 cre^{+/-}* mice, whereas it was unchanged in control *Myo7a^{fl/fl}* mice. There were significant differences between *Myo7a^{fl/fl} Myo15 cre^{+/-}* mice and control mice at P20, P25 and P35 ($F(26) = 45.22$, $P = 0.0010$ (P20), $P = 0.0091$ (P25), $P = <0.0001$ (P35) respectively, Šidák post-test, two-way ANOVA).

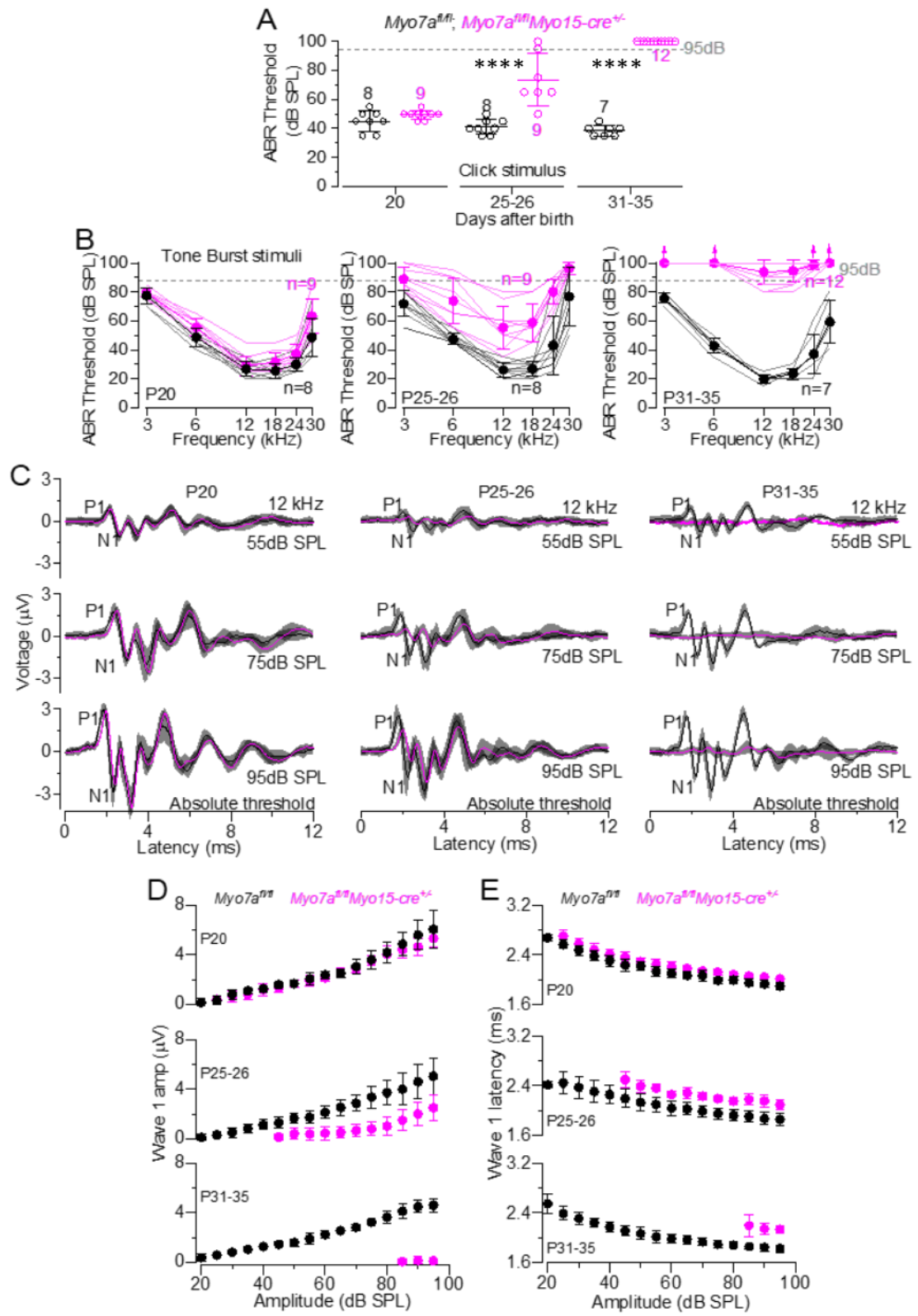


Figure 3. 6. ABR thresholds in *Myo7a^{fl/fl} Myo15 cre^{+/-}* mice from P20-35.

A: average ABR thresholds for clicks recorded from control *Myo7a^{fl/fl}* mice and *Myo7a^{fl/fl} Myo15 cre^{+/-}* mice at P20, P25-26 and P31-35. The number of mice tested for each age/ strain are shown above or below the average data points. **B:** ABR thresholds for frequency specific pure tone stimulation from 3 kHz to 42 kHz from control and *Myo7a^{fl/fl} Myo15 cre^{+/-}* mice. **C:** the size of the different ABR waves recorded during ABR measurements from 12 kHz showing the difference in wave forms at 55dB SPL (top row), 75 dB SPL (middle row) and 95 db SPL (bottom row) for each of the three ages tested. **D-E:** comparing the wave 1 amplitude (**D**) and the wave 1 latency (**E**) at the three different ages tested. **** = $P < 0.0001$.

3.2.4. IHCs from *Myo7a^{fl/fl} Myo15 cre^{+/-}* mice lose ribbon synapses after the axosomatic efferent-IHC innervation has returned

Throughout development IHCs are innervated by type I afferent fibres, which transmit the electrical signal generated during mechano-electrical transduction to the brain, enabling sound to be perceived (Sobkowicz et al., 1982, Sobkowicz et al., 2002, Sobkowicz et al., 2004). There are around 10-13 afferent (ribbon) synapses present in developing IHCs which increases to around 20 after development (Safieddine and Wenthold, 1999, Moser et al., 2006, Safieddine et al., 2012). Ribbon synapses form at the basal pole of the IHCs and contain many highly refined proteins, which allow the synapse to provide a high-fidelity transmission of acoustic information to the afferent fibres. A pre-synaptic component of the afferent fibre terminal expressed in IHCs is the protein RIBEYE (Schmitz et al., 2000, tom Dieck et al., 2005, Magupalli et al., 2008). One post-synaptic component of the ribbon synapse is the expression of AMPA-type glutamate receptors and a subtype of these is the glutamate ionotropic receptor AMPA type subunit 2 (GluR-2) (Lieberman et al., 2011, Furman et al., 2013).

Immunofluorescence and confocal microscopy were used to investigate whether the loss of *Myo7a* in IHCs impacted the number of their afferent synapses. The visualisation of the afferent ribbon synapses was performed using antibodies against GluR2 and the ribeye protein C-terminal binding protein 2: CtBP2. Figure 3.7A shows the IHCs from control *Myo7a^{fl/fl}* mice at P22 had the presence of both pre- and post-synaptic components.

Figure 3.7B shows a zoomed in IHC and highlighting the colocalisation between CtBP2 and GluR2. Figure 3.7C & D revealed that CtBP2 and GluR2 also colocalised in IHCs from P22 *Myo7a^{fl/fl} Myo15 cre^{+/-}* mice. The afferent synapses were also visualised at P50, to identify if ribbon synapses were lost after the return of the axosomatic efferent innervation in *Myo7a^{fl/fl} Myo15 cre^{+/-}* mice was established. The data in Figure 3.7E & F shows that IHCs from control *Myo7a^{fl/fl}* mice at P50 did not show a decrease in CtBP2 or GluR2, whereas in Figure 3.7G & H revealed a decrease in the expression of both CtBP2 and GluR2 *Myo7a^{fl/fl} Myo15 cre^{+/-}* mice at P50.

The expression of CtBP2 and GluR2 was quantified before and during the return of axosomatic efferent innervation in IHCs and a two-way ANOVA revealed that both age and genotype influences the number of GluR2 puncta expressed per IHC ($F(1, 300) = 27.29, P < 0.0001$). Figure 3.8A shows there was a significant decrease in the number of GluR2 puncta expressed per IHC between control *Myo7a^{fl/fl}* and *Myo7a^{fl/fl} Myo15 cre^{+/-}* mice at P50 ($F(300) = 1.883, P < 0.0001$, Šidák post-test, two-way ANOVA). Additionally, there was a significant decrease in the number of GluR2 puncta per IHC in *Myo7a^{fl/fl} Myo15 cre^{+/-}* mice between P22 and P50 (Figure 3.8A) ($F(116) = 27.87, P < 0.0001$, Šidák post-test, two-way ANOVA). However, there was no difference in the number of GluR2 puncta in control *Myo7a^{fl/fl}* mice between P22 and P50.

Like GluR2, a two-way ANOVA showed that age and genotype influence the number of CtBP2 puncta expressed ($F(1, 300) = 21.32, P < 0.0001$). Figure 3.8B shows a significant decrease in the number of CtBP2 puncta expressed per IHC in *Myo7a^{fl/fl} Myo15 cre^{+/-}* mice compared to control mice at P50 ($F(300) = 8.653, P < 0.0001$, Šidák post-test). Moreover, there was a significant decrease in the number ribbon synapses as the number of colocalised CtBP2 and GluR2 puncta decreased at P50 in *Myo7a^{fl/fl} Myo15 cre^{+/-}* mice compared to control mice ($F(1, 300) = 21.32, P < 0.0001$, Šidák post-test, two-way ANOVA). This data indicates that both pre- and post-synaptic components of ribbon synapses were lost in *Myo7a^{fl/fl} Myo15 cre^{+/-}* mice, instead of having a decrease in either the pre- or post-synapse.

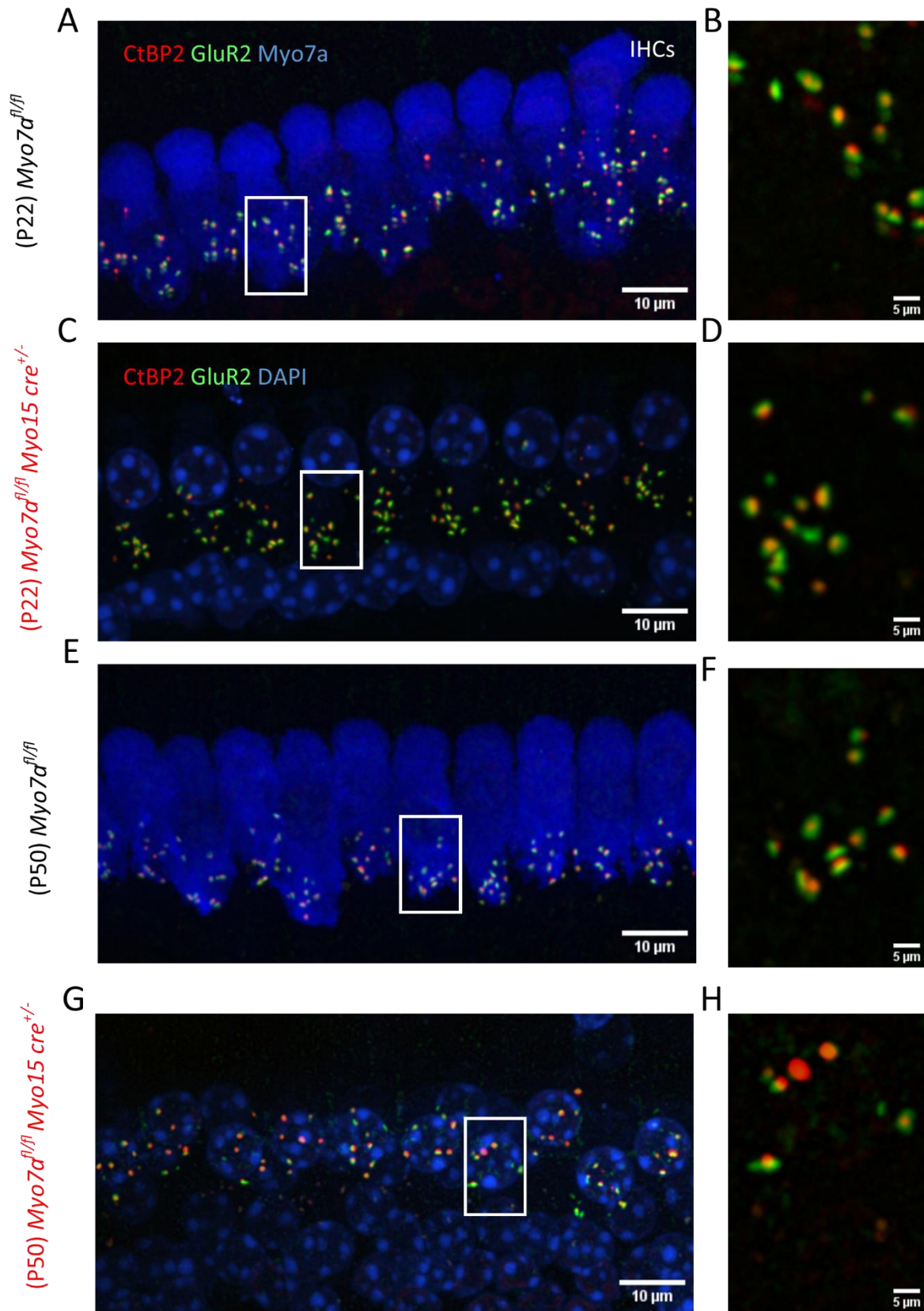


Figure 3. 7. Ribbon synapse number is reduced in IHCs from *Myo7a^{fl/fl} Myo15 cre^{+/-}* mice at P50.

A-H: maximum intensity projections of IHCs from confocal z-stack images taken from the 9-12 kHz region of the cochlea at either P22 or P50 in control and *Myo7a^{fl/fl} Myo15 cre^{+/-}* mice. IHCs were labelled with antibodies against Myo7a (blue) (**A & E**) or DAPI for *Myo7a^{fl/fl} Myo15 cre^{+/-}* mice (**C & G**), the pre-synaptic ribbon marker CtBP2 (red) and post-synaptic GluR2 (green). Scale bars on the left columns are 10µm and 5µm on the right column. **B, D, F, H:** zoomed in images of the IHCs from the white boxes in the images from the left column.

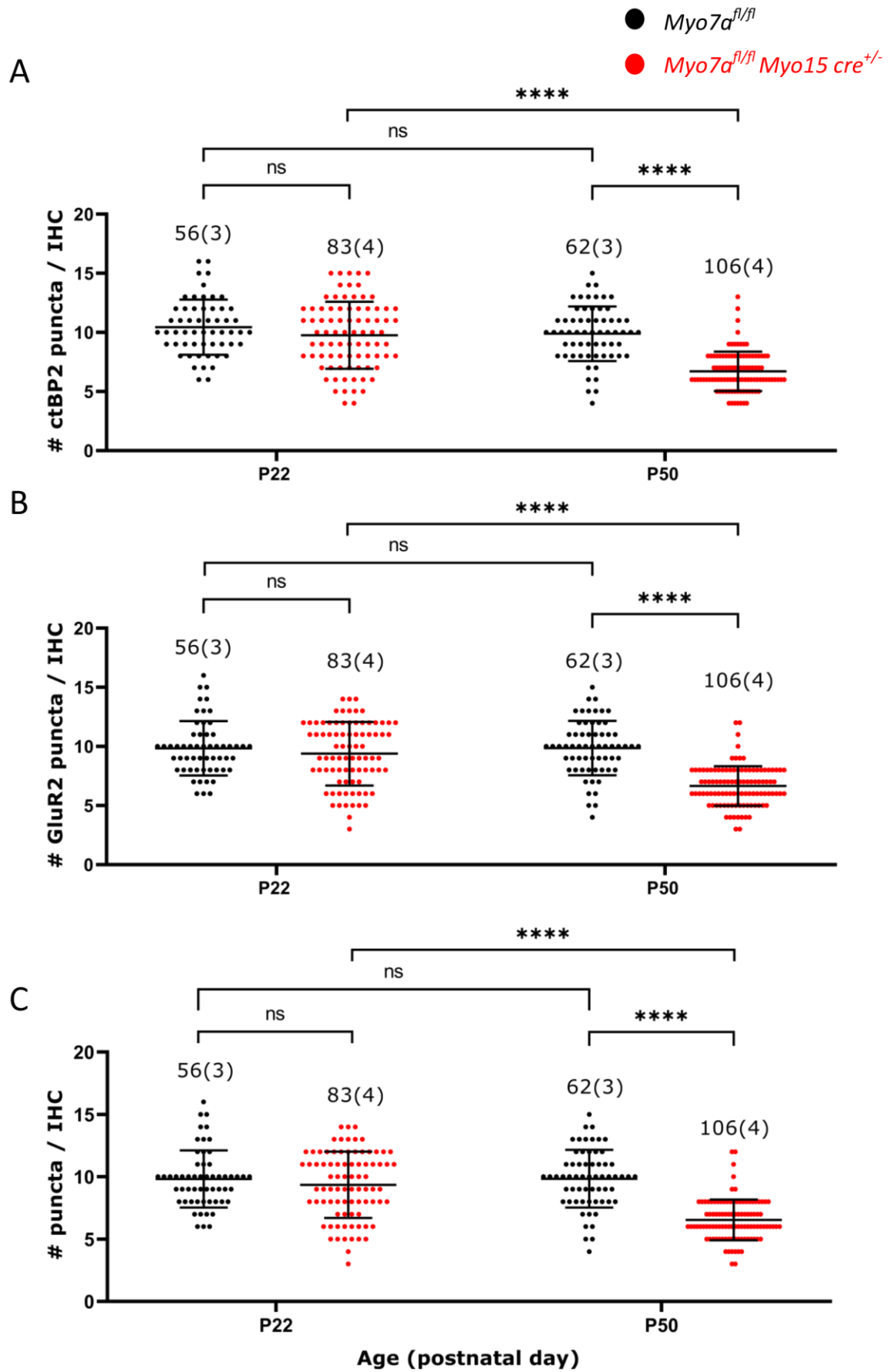


Figure 3. 8. Quantification of ribbon synapses in *Myo7a^{fl/fl} Myo15 cre^{+/-}* mice.

A: the number of GluR2 puncta expressed per IHC at P22 and P50 in control and *Myo7a^{fl/fl} Myo15 cre^{+/-}* mice. **B:** the number of pre-synaptic CtBP2 puncta expressed per IHC at P22 and P50. **C:** the number of ribbon synapses, determined by the colocalisation of pre-synaptic CtBP2 and post-synaptic GluR2 puncta. The number above the data points represents the IHCs (and mice) used for each time point. Averages are shown as mean \pm SD.

3.2.5. The efferent innervation of IHCs lacking the harmonin protein never matures

To confirm if the return of axosomatic efferent innervation on IHCs was driven by the impaired MET currents the *Ush1c Myo15 cre* strain were used for immunofluorescence experiments. *Ush1c* encodes the hair bundle protein harmonin, which is essential for the MET channel complex (Verpy et al., 2000, Boëda et al., 2002, Siemens et al., 2002, Weil et al., 2003, Adato et al., 2004) and if it is lost then IHCs become defective and the mice have profound hearing loss (Lefèvre et al., 2008, Grillet et al., 2009, Bahloul et al., 2010, Grati and Kachar, 2011, Corns et al., 2018).

Ush1c^{fl/fl} Myo15 cre^{+/-} mice and littermate control *Ush1c^{fl/fl}* mice were immunolabelled for pre- and post-synaptic proteins ChAT and SK2, as well as Myo7a to label IHCs to identify if there was a return of axosomatic efferent innervation at P21 and P38. Figure 3.9A-C shows that IHCs from control *Ush1c^{fl/fl}* mice did not express SK2 channels at P21, with Figure 3.9B showing a zoomed in IHC and Figure 3.9C showing the IHCs from Figure 3.9A rotated on the Z, Y plane.

Conversely, IHCs from *Ush1c^{fl/fl} Myo15 cre^{+/-}* mice expressed SK2 channels at P21 (Figure 3.9D-F), which were located at the basal pole of the IHCs (Figure 3.9F). Moreover, the SK2 channels and ChAT were colocalised as the labelling appeared yellow at the base of the IHCs, indicating the presence of axosomatic efferent synapses. Figure 3.9G-I further confirms that control *Ush1c^{fl/fl}* mice lose the expression of SK2 channels like in normal development. At P38 the IHCs from *Ush1c^{fl/fl} Myo15 cre^{+/-}* mice had SK2 channels expressed (Figure 3.9J-L) and the SK2 channels were still expressed at the basal pole of the IHCs (Figure 3.9L). From this data it cannot be concluded that *Ush1c^{fl/fl} Myo15 cre^{+/-}* mice had SK2 channels re-expressed as early as P21 or if the efferent innervation of these mice never matures and the axosomatic efferent synapses were never lost in development.

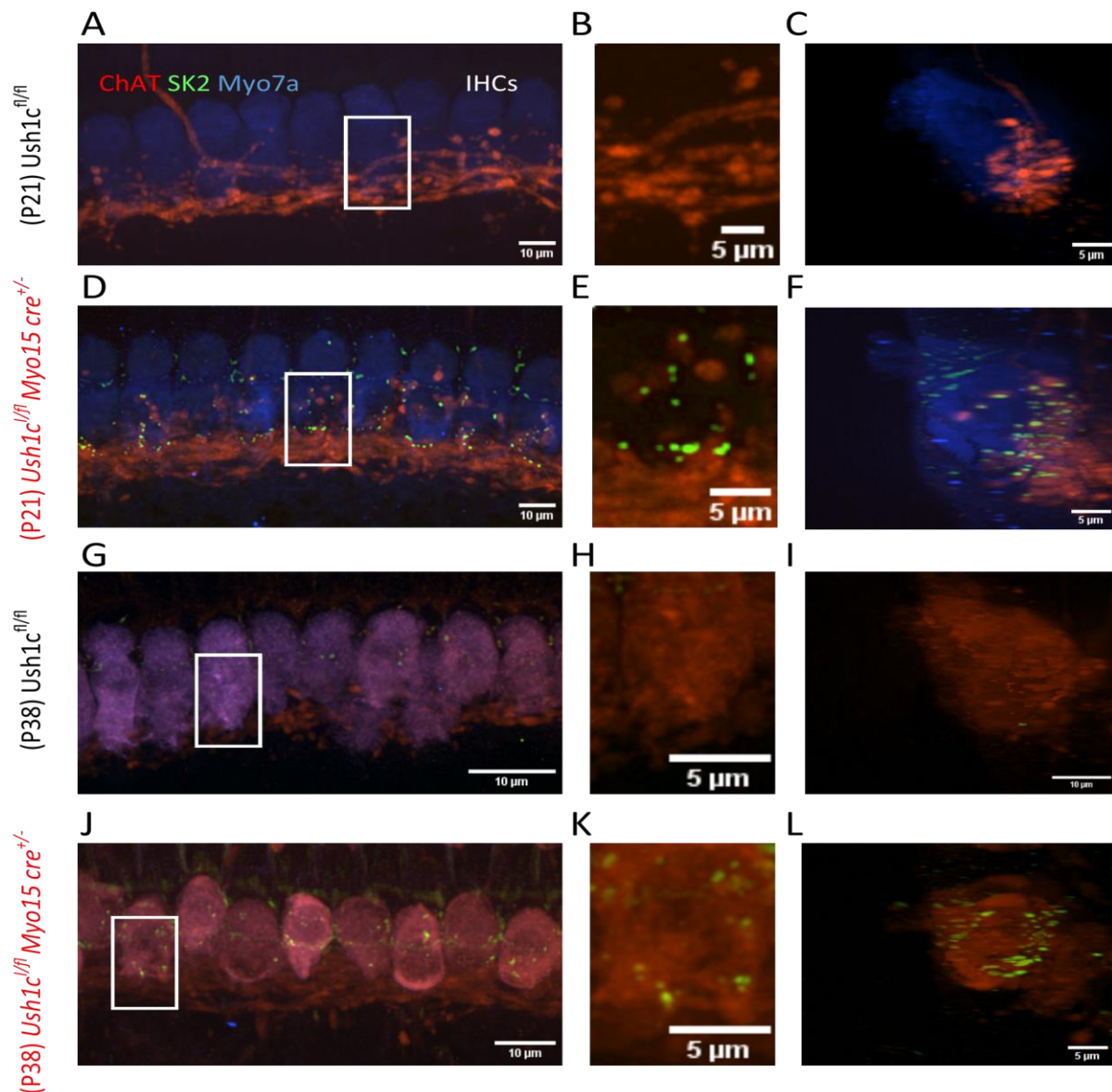


Figure 3. 9. IHCs from $Ush1c^{fl/fl}$ $Myo15 cre^{+/-}$ mice express continue to express SK2 channels after the onset of hearing.

A-L: maximum intensity projections of confocal z-stacks of the apical coil of the cochlea (85 μ m) at the 9-12 kHz region. IHCs were labelled with antibodies against SK2 channels (green), myo7a (blue) and the efferent terminal markers ChAT (red). **A-C:** At P21 IHCs from control $Ush1c^{fl/fl}$ mice did not express SK2 channels. **D-F:** IHCs from $Ush1c^{fl/fl}$ $Myo15 cre^{+/-}$ mice expressed SK2 channels at P21. The SK2 channels were colocalised with ChAT positive efferent terminals at the basal pole of the IHCs (**F**). **G-I:** control $Ush1c^{fl/fl}$ mice did not express SK2 channels in IHCs at P38. **J-L:** IHCs from $Ush1c^{fl/fl}$ $Myo15 cre^{+/-}$ mice also expressed SK2 channels at P38, with the channels expressed at the basal pole of the IHCs. Scale bars for the left column images: 10 μ m and for the middle and right column images: 5 μ m.

3.3. Discussion

In the absence of a functional mechano-electrical transducer current, axosomatic efferent innervation returning to apical coil IHCs (9-12 kHz frequency range) was already evident in some P24 IHCs, but it became more prominent from about P31 onwards. In addition, the IHCs underwent progressive biophysical and morphological changes that resulted in the acquisition of an immature-like profile.

Myo7a^{fl/fl} Myo15 cre^{+/-} mice are a conditional knockout mouse model for the loss of Myo7a, as Myo15 is expressed from early time points in development (P2-4), which enabled the IHCs to develop normally at least initially. In these mice, Myo7a started to be lost from a few IHCs at P4-7, whereas multiple IHCs had lost Myo7a at P12 and all IHCs had lost all expression of Myo7a by P22 (Figure 3.1E). The immunofluorescence confirms that the knockout was working and provides context for previous studies showing that MET currents were reduced in IHCs from P14 onwards in *Myo7a^{fl/fl} Myo15 cre^{+/-}* mice (Corns et al., 2018).

3.3.1. Initial changes in IHCs as axosomatic efferent innervation returns

The earliest age at which IHCs had the re-expression of SK2 in *Myo7a^{fl/fl} Myo15 cre^{+/-}* mice was at P24 (Figure 3.2D-F). The IHCs that re-expressed functional efferent synapses at P25, which was shown by inducing synaptic currents with high K⁺ solution that was blocked by strychnine (Figure 3.2M). This data shows that there was a return of functional axosomatic efferent synapses on IHCs from *Myo7a^{fl/fl} Myo15 cre^{+/-}* mice up to nine days earlier than previously reported (P33) (Corns et al., 2018). Additionally, it shows that the IHCs drive the re-innervation by re-expressing SK2 channels before functional efferent synapses were evident at P25, supporting the theory that the IHCs are driving this mechanism (Jeng et al., 2021). Therefore, some IHCs in *Myo7a^{fl/fl} Myo15 cre^{+/-}* mice have functional axosomatic efferent synapses only a few days after losing them during the normal maturation of innervation, indicating that the mechanism is initiated quickly.

In normal development the IHCs lose their sensitivity to ACh around P18 and by P21 and no longer express $\alpha 9\alpha 10$ nAChRs, SK2 channels or have axosomatic efferent innervation (Glowatzki and Fuchs, 2000, Katz et al., 2004, Marcotti et al., 2004). The Corns et al., 2018

paper showed via transmission electron microscopy images that there was no axosomatic efferent innervation on IHCs at P22 in *Myo7a^{fl/fl} Myo15 cre^{+/-}* mice, demonstrating the maturation of IHC innervation matured normally in these mice.

Therefore, the re-expression of SK2 channels and functional synapses on IHCs shown from P24 onwards in this chapter was a consequence of losing Myo7a expression and not due to the delayed maturation of IHC innervation. Furthermore, the SK2 channels did not colocalise with the efferent terminal markers (ChAT) at this age (Figure 3.2I), indicating the IHCs re-express SK2 channels prior to the return of efferent terminals. Similarly, when testing for the presence of $\alpha 9\alpha 10$ nAChRs in IHCs from P24 *Myo7a^{fl/fl} Myo15 cre^{+/-}* mice there was no induced synaptic currents upon local perfusion of a high K^+ solution (Figure 3.2L). Figure 3.2 revealed that the expression of SK2 channels at P10 in 6N-repaired mice was not spatially restricted to the very basal pole of the IHCs (Figure 3.2C), however, in the SK2 channels re-expressed in IHCs from *Myo7a^{fl/fl} Myo15 cre^{+/-}* mice were only seen at the very basal pole of the IHCs. Interestingly the SK2 channels remained spatially restricted in their expression in IHCs over time, as immunolabelling data showed the same expression at the basal pole of IHCs at P39 (Figure 3.4I).

The ACh dependent current responses in developmental IHCs is driven by Ca^{2+} entering the cell via $\alpha 9\alpha 10$ nAChRs and activating the Ca^{2+} sensitive SK2 channels (Marcotti et al., 2004, Katz et al., 2004), which were absent in control IHCs (Figure 3.3B & C). During the same time P25-31-time window, IHCs from *Myo7a^{fl/fl} Myo15 cre^{+/-}* mice showed a large variability in their responses (Figure 3.3E), with some cells displaying instantaneous responses to ACh at -84mV, as well as having dramatically reduced $I_{k,f}$ currents. On the other hand, around half of the IHCs (Figure 3.3A) from *Myo7a^{fl/fl} Myo15 cre^{+/-}* mice did not show any post-synaptic currents upon stimulation from high K^+ solution and remained insensitive to 100 μ M ACh.

Myo7a^{fl/fl} Myo15 cre^{+/-} mice had a progressive loss of hearing from P20-P35 which was concurrent with the morphological and physiological changes reported. ABRs revealed that between P20 and P25-26 there was a shift in the *Myo7a^{fl/fl} Myo15 cre^{+/-}* mice hearing thresholds (Figure 3.4A & B). It is known that if Myo7a is lost then mice become profoundly deaf (Self et al., 1998, Kros et al., 2002, Grati and Kachar, 2011), however, in this conditional knockout model of Myo7a the hearing loss shown here is the earlier than what was reported by Corns et al., 2018. The function of axosomatic efferent innervation has been shown to

hyperpolarise IHCs during development (Glowatzki and Fuchs, 2000, Marcotti et al., 2004, Goutman et al., 2005). Therefore, as the IHCs have dysfunctional MET channels and the *Myo7a^{fl/fl} Myo15 cre^{+/-}* mice become deaf, it is possible that the return of functional inhibitory axosomatic efferent innervation from P25 could be to reduce any spontaneous firing activity at the afferent synapse.

3.3.2. Progressive physiological changes in IHCs

By P42 the IHCs from *Myo7a^{fl/fl} Myo15 cre^{+/-}* mice no longer showed 'typical' mature current responses (Kros et al., 1998) and instead displayed developmental immature current profiles (Figure 3.5D). Moreover, at this age the IHCs instantaneously responded to locally perfused 100 μ M ACh and displayed the characteristic current components that α 9 α 10 nAChRs and SK2 channels are responsible for (Figure 3.5D & E). The slope conductance of ACh sensitivity at -84mV was significantly increased in *Myo7a^{fl/fl} Myo15 cre^{+/-}* mice compared to control mice in the P32-42 age range. On the other hand, in the P25-31 age range there was no significant increase, indicating that the IHCs responsiveness to ACh increased with age in *Myo7a^{fl/fl} Myo15 cre^{+/-}* mice. This increase also demonstrates that there were progressive changes over time in the IHCs from *Myo7a^{fl/fl} Myo15 cre^{+/-}* mice, as more IHCs in the 9-12 kHz region had a return of axosomatic efferent innervation.

Further progressive changes in the IHCs became evident in the P32-42 age as the $I_{k,f}$ currents were significantly smaller in the *Myo7a^{fl/fl} Myo15 cre^{+/-}* mice compared to control mice (Figure 3.5K). The $I_{k,f}$ currents are driven by BK channels, which are expressed in the neck region of IHCs (Kros et al., 1998). From this reduction in $I_{k,f}$ currents in IHCs from *Myo7a^{fl/fl} Myo15 cre^{+/-}* mice it could be that there is a loss of BK channels and that the IHCs are reducing in cell size in the neck region. However, for this to be confirmed and quantified, future experiments could be to perform immunolabelling to investigate whether there is a loss of BK channels in the IHCs in *Myo7a^{fl/fl} Myo15 cre^{+/-}* mice. Conversely, the IHCs from control *Myo7a^{fl/fl}* mice had an increased $I_{k,f}$ current between P32-42 (Figure 3.5K), potentially indicating that the IHCs continue to become larger in size or number. Additionally, cell membrane capacitance can be used as a measurement for cell size. The Corns et al., 2018 study showed that the IHCs from *Myo7a^{fl/fl} Myo15 cre^{+/-}* mice did not have a reduced cell membrane capacitance at P22, but did at P30 (Corns et al., 2018). This data, together with the results showing the reduced $I_{k,f}$

currents in the P32-42 age range in this study support the claim that the IHCs from *Myo7a^{fl/fl} Myo15 cre^{+/-}* mice are reducing in cell size in the neck region. The smaller cell size, loss of BK channels and reduction of $I_{k,f}$ currents has been shown to take place in the early onset age-related hearing loss mouse strains 6J, 6N as well as in 6N-repaired and the late onset hearing loss strain C3H at 15 months of age, in which the return of axosomatic efferent innervation was prevalent in 6J, 6N and 6N-repaired mice (Jeng et al., 2021).

ABR data revealed that the *Myo7a^{fl/fl} Myo15 cre^{+/-}* mice were profoundly deaf at P35 (Figure 3.6A & B) which is when the IHCs consistently began to show a developmental phenotype as described above, as well as more IHCs having a return of axosomatic efferent innervation. The ABRs also showed that the wave 1 amplitude and latency were impacted in *Myo7a^{fl/fl} Myo15 cre^{+/-}* mice (Figure 3.6D & E), indicating that the IHCs ability to activate the afferent synapses was impaired. Immunolabelling was used to identify if IHCs from *Myo7a^{fl/fl} Myo15 cre^{+/-}* mice had lost their afferent synapses and the data revealed that by P50 IHCs had a significant reduction in both the pre- and post-synaptic components, as well as a reduction in the number of synapses (Figure 3.7 & 8). The reduced number of afferent synapses could explain why there is a reduced wave 1 amplitude and increased latency seen in the *Myo7a^{fl/fl} Myo15 cre^{+/-}* mice. However, as the IHCs in *Myo7a^{fl/fl} Myo15 cre^{+/-}* mice have impaired MET channel functionality, this will also impact the wave 1 amplitude and latency and could be another explanation for the differences observed.

3.3.3. Efferent re-innervation returns prior to afferent synapse loss

Studies have shown that afferent synapse loss has been seen in ageing studies and when mice have been subject to noise overexposure (Stamatakis et al., 2006, Kujawa and Liberman, 2009, Sergeyenko et al., 2013, Fernandez et al., 2015, Hu et al., 2015, Johnson et al., 2019, Jeng et al., 2020a). From these studies, it was proposed that the return of axosomatic efferent innervation on IHCs was possible because of the retraction of type I afferent fibres following afferent synapse loss. The loss of afferent fibres would result in LOC efferent fibres losing their axodendritic connections, leaving the free efferent fibres to form axosomatic efferent synapses on the IHCs (Stamatakis et al., 2006, Lauer et al., 2012, Sergeyenko et al., 2013, Zachary and Fuchs, 2015, Corns et al., 2018, Jeng et al., 2021). Here, it is shown for the first time that the axosomatic efferent re-innervation of IHCs occurs prior to the loss of any

afferent synapses, as there wasn't a decrease in the number of afferent synapses in *Myo7a^{fl/fl} Myo15 cre^{+/-}* mice until P50, whereas the efferent re-innervation occurs from P24 onwards. It is possible that the return of efferent innervation on IHCs and the progressive biophysical changes induces the loss of afferent synapses.

3.3.4. Efferent innervation of IHCs from *Ush1c^{fl/fl} Myo15 cre^{+/-}* mice does not mature normally

To investigate whether efferent re-innervation takes place in a different mouse model in which the hair bundle is disrupted, MET currents are reduced and the IHCs have a developmental phenotype (Corns et al., 2018), the *Ush1c Myo15 cre* mice were investigated at two different ages, P21 and P38. Immunolabelling data showed that IHCs from *Ush1c^{fl/fl} Myo15 cre^{+/-}* mice expressed SK2 channels at both P21 and P38 (Figure 3.9D & J), whereas control *Ush1c^{fl/fl}* mice did not express SK2 channels at either age. In development the loss of SK2 channels and axosomatic efferent contacts onto IHCs takes around three weeks to occur (Glowatzki and Fuchs, 2000, Marcotti et al., 2004, Katz et al., 2004). Therefore, by the IHCs expressing SK2 channels in *Ush1c^{fl/fl} Myo15 cre^{+/-}* mice it cannot be concluded from the immunofluorescence images in this study whether the SK2 channels were remaining from development, or a re-expression. Future electrophysiology experiments to test if the SK2 channels are part of functional synapses would be required to provide further answers for this question.

However, it is possible that losing harmonin expression from the hair bundles of IHCs prevents the axosomatic efferent innervation from developing properly, resulting in the pre- and post-synaptic terminals remaining on IHCs into adulthood. On the other hand, if the IHCs efferent innervation does develop properly, then the re-expression of SK2 channels on IHCs would be taking place three days' sooner than in *Myo7a^{fl/fl} Myo15 cre^{+/-}* mice (which occurs at P24). If this were to be the case, then it could be proposed that the loss of harmonin from IHCs induces the return of axosomatic efferent innervation and re-expression of SK2 channels quicker than in mice where Myo7a is lost from the hair bundles. Moreover, previous studies have shown that *Ush1c^{fl/fl} Myo15 cre^{+/-}* mice are profoundly deaf by P16 (Corns et al., 2018),

from this, it could be suggested that a mutation in the harmonin protein results in MET channel defects and hearing loss more rapidly than disrupting Myo7a.

3.3.5. Future directions for axosomatic efferent innervation studies

There are multiple questions that still need to be answered relating to the return of axosomatic efferent innervation both in ageing and in the *Myo7a^{fl/fl} Myo15 cre^{+/-}* mice. As ageing studies have looked at mouse models of early onset hearing loss harbouring the *Cdh23^{ahl}* mutation, which results in reduced MET currents with age and the *Myo7a* also have reduced MET currents, all these strains proceed to have a return of axosomatic efferent innervation. Moreover, data from the *Ush1c^{fl/fl} Myo15 cre^{+/-}* mice revealed that the IHCs express SK2 channels at P21 and P38, however, it could not be confirmed whether the SK2 channels expressed were due to re-innervation, or the efferent innervation never maturing correctly. However, this data taken with the *Myo7a^{fl/fl} Myo15 cre^{+/-}* re-innervation of IHCs demonstrates the importance of functional MET currents in order to have the proper innervation of the efferent system.

Some of the other questions to be answered when studying the changes in the IHCs after the return of axosomatic efferent innervation. For example, investigating how Ca^{2+} is handled by IHCs after they return to developmental states. Would the adult *Myo7a^{fl/fl} Myo15 cre^{+/-}* mice have spontaneous Ca^{2+} waves like during development? Moreover, it would be interesting to identify if spontaneous action potentials return in *Myo7a^{fl/fl} Myo15 cre^{+/-}* mice similar to in development, which are known to help refine the innervation of the IHCs (Marcotti et al., 2003b, Johnson et al., 2009, Johnson et al., 2011, Johnson et al., 2013a, Johnson et al., 2013b).

However, one question relating to re-innervation of IHCs that is answered in the next chapter of this thesis is whether impacting the IHCs and not disrupting the MET channels would result in re-innervation of IHCs. To achieve this, impacting neurotransmitter release will be used to investigate if this causes a re-innervation of IHCs. The data from the next chapter will further our understanding of whether the re-innervation of IHCs is likely driven by dysfunctional MET channels, or whether the mechanism can be driven by impairing the exocytosis of the IHCs.

Chapter 4 – Disrupting the IHC afferent synapse does not result in efferent re-innervation

4.1. Introduction

The return of axosomatic efferent innervation was seen in the *Myo7a^{fl/fl} Myo15 cre^{+/-}* mice that have dysfunctional MET channels (Corns et al., 2018).

To investigate whether this re-wiring of the IHCs was due to dysfunctional MET currents or due to the malfunctioning of the IHCs, a mouse model was used in which only the release of neurotransmitter from the IHCs was dysfunctional. The conditional knockout mouse model was an *Otoferlin^{tm1c};Vglut3 cre-ER^{T2}; td-Tomato (Otof^{fl/fl} Vglut3 cre^{+/-})* strain, with otoferlin being the target for the conditional knockout. Otoferlin is a protein that is crucial for exocytosis at the IHC ribbon synapses (Roux et al., 2006, Takago et al., 2019). Moreover, otoferlin has been shown to have a key role in vesicle replenishment (Pangršič et al., 2010, Michalski et al., 2017). The absence of otoferlin leads to hearing loss in mice and humans (Yasunaga et al., 1999, Roux et al., 2006).

The otoferlin gene was genetically altered to be flanked by two loxP sites and this is controlled by Cre recombinase (Metzger et al., 1995, Feil et al., 1996, Zhang et al., 1996, Feil et al., 1997). For the Cre recombinase to work, ligand dependent chimeric Cre recombinases (CreER) are present, which are mutated hormone binding domains of the oestrogen receptor (Feil et al., 2009). The Cre is then activated by the synthetic oestrogen receptor ligand 4-hydroxytamoxifen (Metzger et al., 1995, Feil et al., 1996, Zhang et al., 1996, Feil et al., 1997). Therefore, this allows the temporal control of when the otoferlin gene will be knocked out from the IHCs in *Otof^{fl/fl} Vglut3 cre^{+/-}* mice. In addition, the *Otof^{fl/fl} Vglut3 cre^{+/-}* mice had the red fluorescent tag td-tomato genetically added to the Vglut3 cre, therefore when the Cre was expressed in IHCs the IHCs would fluoresce red.

By inducing the loss of otoferlin in IHCs via a conditional mouse model it can be identified if the return of axosomatic efferent innervation is driven by MET channel dysfunction, or more generally to the inability of IHCs to release neurotransmitter.

4.2. Results

4.2.1. Characterising tamoxifen injections in otoferlin conditional knockout mice

Two tamoxifen injections were performed over 24 hours, starting at three different ages: P10, P14 and P21 in *Otof^{fl/fl} Vglut3 cre^{+/-}* and littermate control *Otof^{fl/fl} Vglut3 cre^{-/-}* mice. Immunofluorescence and multichannel confocal microscopy were used to visualise the apical coil of the cochlea and to identify if otoferlin was knocked out of IHCs four weeks post injections. Antibodies against otoferlin and Myo7a were used, whilst td-tomato was used to visualise the IHCs.

Figure 4.1A-C shows control *Otof^{fl/fl} Vglut3 cre^{-/-}* mice that had the first tamoxifen injection at P10 and there was no loss of otoferlin in IHCs four weeks post injection (Figure 4.1A). Figure 4.1B shows that the IHCs from control mice did not express the Vglut3 cre driven td-tomato fluorescent tag, additionally, there was no IHC death after tamoxifen injections (Figure 4.1C). On the other hand, when *Otof^{fl/fl} Vglut3 cre^{+/-}* mice were injected at P10 around half of the IHCs did not express otoferlin (Figure 4.1D & F), whereas all the IHCs in the apical coil expressed td-tomato (Figure 4.1E). IHCs from control mice that were injected at P14 or P21 never had any loss of otoferlin (Figure 4.1G, I, M & O) or expressed td-tomato (Figure 4.1 H, N).

Otof^{fl/fl} Vglut3 cre^{+/-} mice that were injected at P14 appeared to have more IHCs expressing otoferlin (Figure 4.1J & L) compared to *Otof^{fl/fl} Vglut3 cre^{+/-}* mice that were injected at P10. Moreover, all the IHCs expressed td-tomato when the mice were injected at P14 (Figure 4.1K). Interestingly, the IHCs of *Otof^{fl/fl} Vglut3 cre^{+/-}* mice that were injected at P21 did not express td-tomato in all the IHCs in the apical coil (Figure 4.1Q), whilst only a couple of IHCs did not express otoferlin (Figure 4.1P & R). The quantification of the data from the *Otof^{fl/fl} Vglut3 cre^{+/-}* mice seen in Figure 4.1 can be found later in this chapter in Figure 4.3.

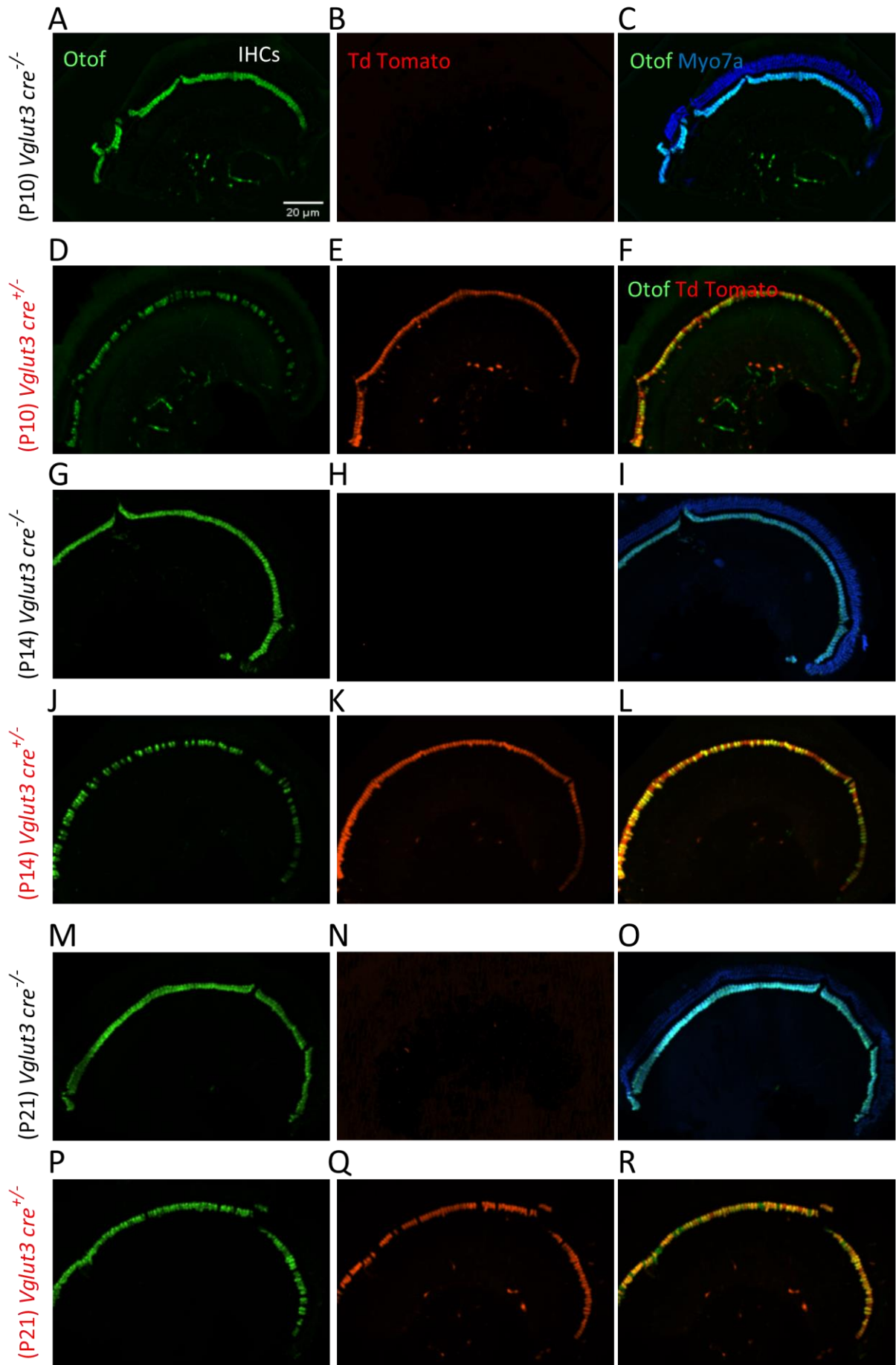


Figure 4. 1. Characterising the conditional knockout of otoferlin from IHCs in tamoxifen inducible mice.

A-R: maximum intensity projections from confocal z-stack images taken of the apical coil of the cochlea. Antibodies against otoferlin (green) and myo7a (blue) were used to visualise the loss of otoferlin from IHCs and myo7a was used as a hair cell marker whereas td tomato (red) was a fluorescent tag that would be expressed in IHCs that expressed *Vglut3 cre*. Immunofluorescence experiments were performed four weeks post tamoxifen injections. **A-C:** control *Otof^{fl/fl} Vglut3 cre^{-/-}* mice injected at P10 expressed otoferlin in all IHCs (**A**) and the IHCs did not express td tomato (**B**), whilst there was no hair cell loss post injection (**C**). **D-F:** *Otof^{fl/fl} Vglut3 cre^{+/-}* mice injected at P10 had reduced expression of otoferlin in their IHCs (**A**) and all IHCs expressed td tomato (**E**). **F:** juxtaposed otoferlin and td tomato labelling shows the IHCs that did not express otoferlin appear red, whereas IHCs that still express otoferlin appear yellow. **G-I:** Control mice did not lose the expression of otoferlin in the IHCs when injected at P14 (**G & I**) and did not express td-tomato in any cells (**H**). **J-L:** fewer IHCs lost the expression of otoferlin when *Otof^{fl/fl} Vglut3 cre^{+/-}* mice were injected at P14 (**J & L**) and all IHCs expressed td-tomato (**K**). **M-O:** control *Otof^{fl/fl} Vglut3 cre^{-/-}* mice injected at P21 did not lose expression of otoferlin in IHCs (**M & O**) or express td tomato (**N**). **P-R:** *Otof^{fl/fl} Vglut3 cre^{+/-}* mice injected at P21 had very few IHCs that lost the expression of otoferlin four weeks post tamoxifen injection (**P & R**) and not every IHC expressed td tomato (**Q**). Scale bar: 20µm

It was determined that two tamoxifen injections starting from P10 resulted in the greatest reduction of otoferlin expression in IHCs from *Otof^{fl/fl} Vglut3 cre^{+/-}* mice. Following this, to characterise the earliest time point that IHCs had reduced otoferlin expression post injections, immunolabelling was performed from one to four weeks post injection.

Figure 4.2A-C show control *Otof^{fl/fl} Vglut3 cre^{-/-}* mice one-week post injection, with all the IHCs expressing otoferlin (Figure 4.2A) and not expressing td tomato (Figure 4.2B), whilst also showing there was no loss of hair cells caused by tamoxifen injections (Figure 4.2C). *Otof^{fl/fl} Vglut3 cre^{+/-}* mice that were immunolabelled one-week post injection showed that a few IHCs did not express otoferlin (Figure 4.2D & F), whilst td tomato was expressed in all IHCs after one week (Figure 4.2E). Mice that were left for two weeks showed that more IHCs had lost otoferlin (Figure 4.2G & I). Interestingly, the *Otof^{fl/fl} Vglut3 cre^{+/-}* mice that were left for three weeks post injection seemingly had fewer IHCs that had lost otoferlin compared to two weeks (Figure 4.2J & L). From this it could be suggested that the knockout rate of otoferlin did not increase in a linear manner. However, four weeks post injection revealed that seemingly over a third of the IHCs in the apical coil did not express otoferlin when *Otof^{fl/fl} Vglut3 cre^{+/-}* mice were injected at P10 (Figure 4.2M & O).

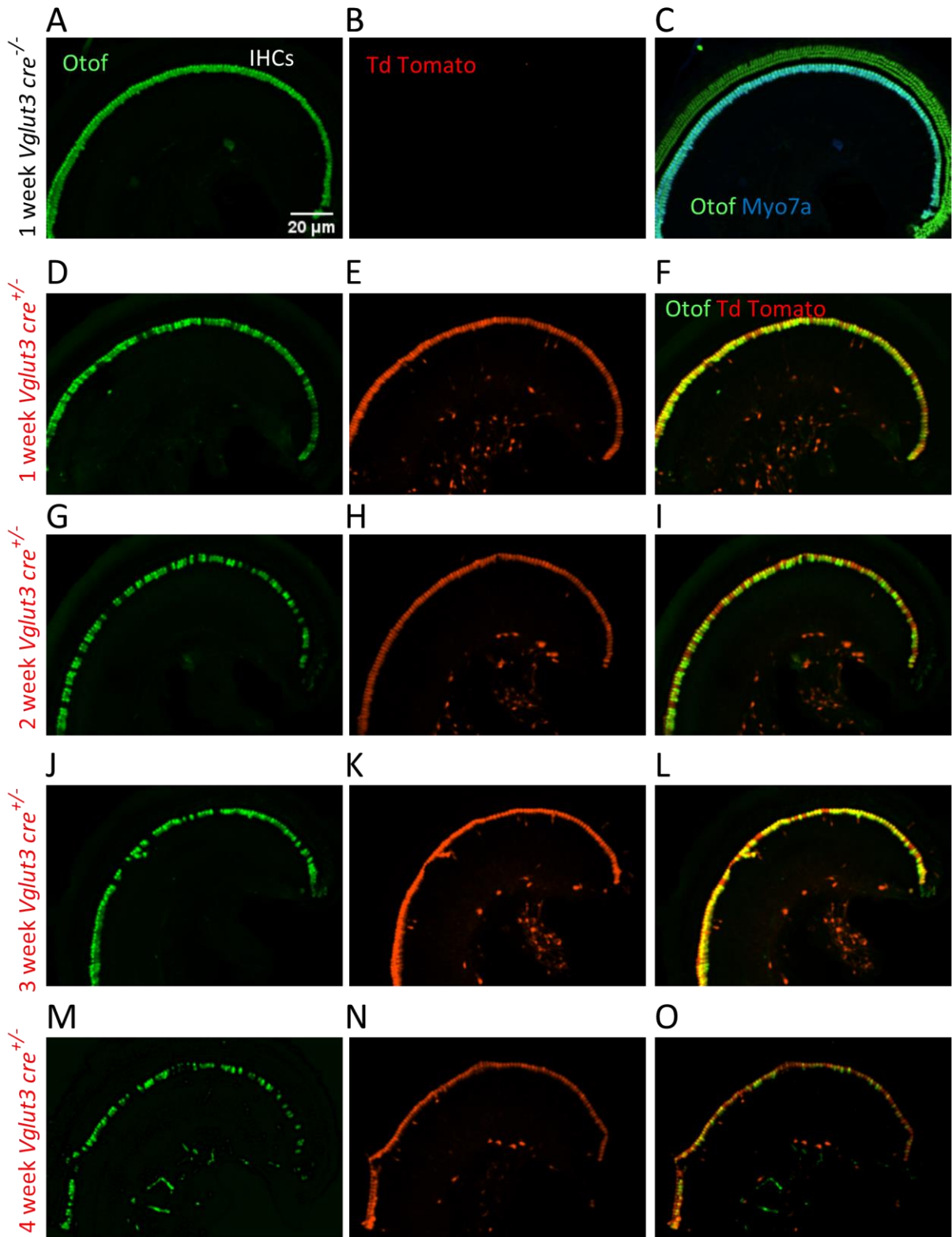


Figure 4. 2. Otoferlin is progressively knocked out of IHCs after two tamoxifen injections from P10.

A-O: maximum intensity projection images taken from confocal z-stack images of the apical coil of the cochlea. Immunolabelling was performed from one to four weeks post two tamoxifen injections from P10 with a 24-hour gap. Antibodies against otoferlin (green) and myo7a (blue) were used to visualise the loss of otoferlin from IHCs and Myo7a was used as a hair cell marker. Td-tomato (red) shows the expression the *Vglut3 cre* in the IHCs. **A-C:** IHCs from control *Otof^{fl/fl} Vglut3 cre^{-/-}* mice had no loss of otoferlin 1 week post injection (**A**) and did not express td-tomato (**B**), in addition, no hair cell loss occurred post injection (**C**). **D-F:** a few IHCs from *Otof^{fl/fl} Vglut3 cre^{+/-}* mice showed a loss of otoferlin one week post injection. **G-I:** an increasing number of IHCs from *Otof^{fl/fl} Vglut3 cre^{+/-}* mice had lost otoferlin expression two weeks post injections. **J-L:** shows the IHCs that had lost otoferlin expression in *Otof^{fl/fl} Vglut3 cre^{+/-}* mice three weeks post tamoxifen injection. **M-O:** around half of the IHCs did not express otoferlin four weeks post injections. Scale bars: 20µm.

The expression and knockout rate of otoferlin (data can be seen in Figure 4.1) was quantified from the immunolabelling images. As all images were taken with the same microscope settings, the images could be quantified to determine the knockout rate / reduction of otoferlin in IHCs.

Figure 4.3A shows the pixel intensities for each IHC within the apical coil of the cochlea to determine if there was a decreased expression of otoferlin within IHCs when the mice were left for different lengths of time post injection. A one-way ANOVA revealed that the average expression of otoferlin (Figure 4.3A) (pixel intensity) within each IHC significantly decreased over time ($F(1854) = 68.34$, $P < 0.0001$, one way ANOVA), decreasing from 1491 (pixel intensity) at one week post injection to 857.3 at four weeks ($P < 0.0001$, Tukey's post-test, one way ANOVA). Following this, the pixel intensities were normalised against the IHC with the highest pixel intensity (strongest otoferlin expression) for each immunolabelling image (Figure 4.3B). This was to encounter for the variability between animals and background auto fluorescence in the images. Figure 4.3B shows that there was a significant decrease in the expression of otoferlin in IHCs when the data was normalised ($F(1854) = 50.99$, $P < 0.0001$, Tukey's post-test, one way ANOVA). To determine whether an IHC had otoferlin knocked out following tamoxifen injections, background auto fluorescence was measured for each image in the OHC region, where otoferlin was not expressed, with this data also being normalised to the IHC with the greatest pixel intensity. The background auto fluorescence was shown to be consistently $< 10\%$ of the normalised data, therefore, this was used as a criterion for whether the IHCs had otoferlin knocked out and is indicated by the dotted black line at 10% in Figure 4.3B.

Figure 4.3C shows the number of IHCs that had otoferlin knocked out post tamoxifen injections using the criterion described above, compared to the total number of IHCs. This data reveals the proportion of IHCs that had otoferlin knocked out increased when mice were left for a longer period after tamoxifen injections. Surprisingly, the quantification reveals the differences in knockout rates, as more IHCs had otoferlin knocked out two weeks post injection compared to three weeks (Figure 4.3C). This difference may be due to variable quality of tamoxifen injections. Moreover, Figure 4.3D shows the percentage of IHCs that had otoferlin knocked out, which significantly increased as mice were left from either one to four weeks ($F(13) = 23.00$, $P < 0.0001$, Tukey's post-test, one way ANOVA). The percentage of

knocked out IHCs increased from 2.03% at one-week post injection to 34.88% at four weeks ($P = <0.0001$, Tukey's post-test, one way ANOVA).

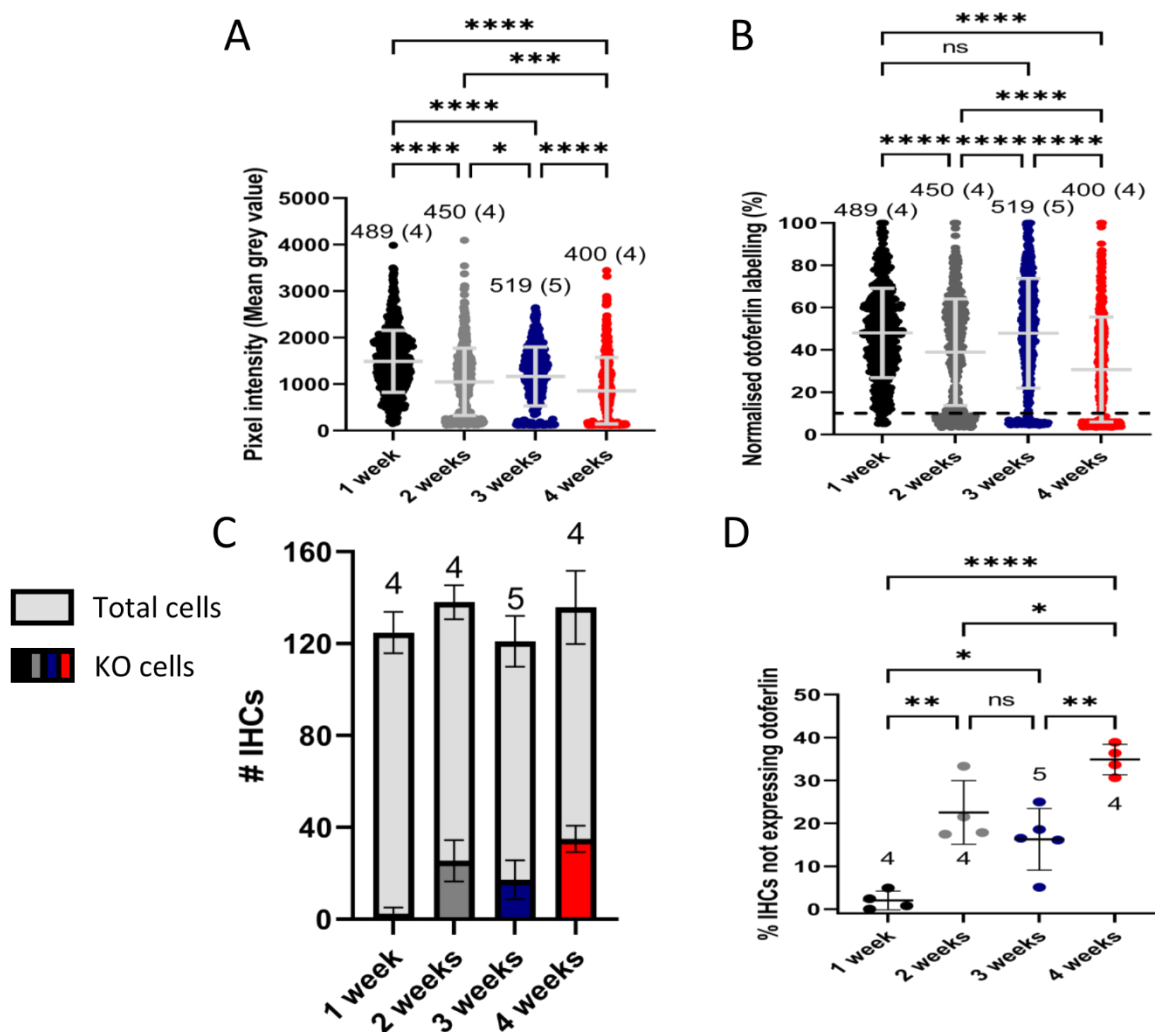


Figure 4. 3. The conditional knockout rate of otoferlin from IHCs was not linear in tamoxifen injected *Otof^{fl/fl} Vglut3 cre^{+/-}* mice.

A: the pixel intensities were measured for each IHC within the apical coil of the cochlea at one, two, three- and four-weeks post tamoxifen injections to determine the expression of otoferlin. **B:** pixel intensities were normalised to the brightest IHC for each image, accounting for any differences in the auto fluorescence across images. **C:** the proportion of IHCs that had no expression of otoferlin shown in relation to the total number of IHCs measured in the apical coil of the cochlea. **D:** the percentage of IHCs that had otoferlin knocked out for one to four weeks post tamoxifen injection. Numbers above the data are the number of IHCs (and

mice) used for each time point (**A-B**), whereas the numbers above the data in **C & D** are the number of mice used. * = $P < 0.05$, ** = $P < 0.01$, *** = $P < 0.001$, **** = $P < 0.0001$. Averages shown as means \pm SD.

Figure 4.4A-D shows histogram plots of the normalised data from Figure 4.3B for each time point post tamoxifen injection. Upon quantification a Kolmogorov-Smirnov test revealed that the number of IHCs that had otoferlin knocked out was normally distributed at one-week post injections (Figure 4.4A) ($P = >0.1$, Kolmogorov-Smirnov test). On the other hand, for two, three- and four-weeks post injections the data was not normally distributed (all $P = <0.0001$, Kolmogorov-Smirnov test). Overall, Figures 4.3 & 4.4 demonstrate that the rate of otoferlin knockout from IHCs after tamoxifen injection was not linear, however, the greatest number of IHCs that did not express otoferlin was four weeks post injections. Ultimately, even four weeks post tamoxifen injection showed that the number of IHCs with otoferlin knocked out was only around a third of all IHCs, indicating that the use of the *Otof^{fl/fl} Vglut3 cre^{+/-}* tamoxifen inducible mice does not have a very good knockout efficiency.

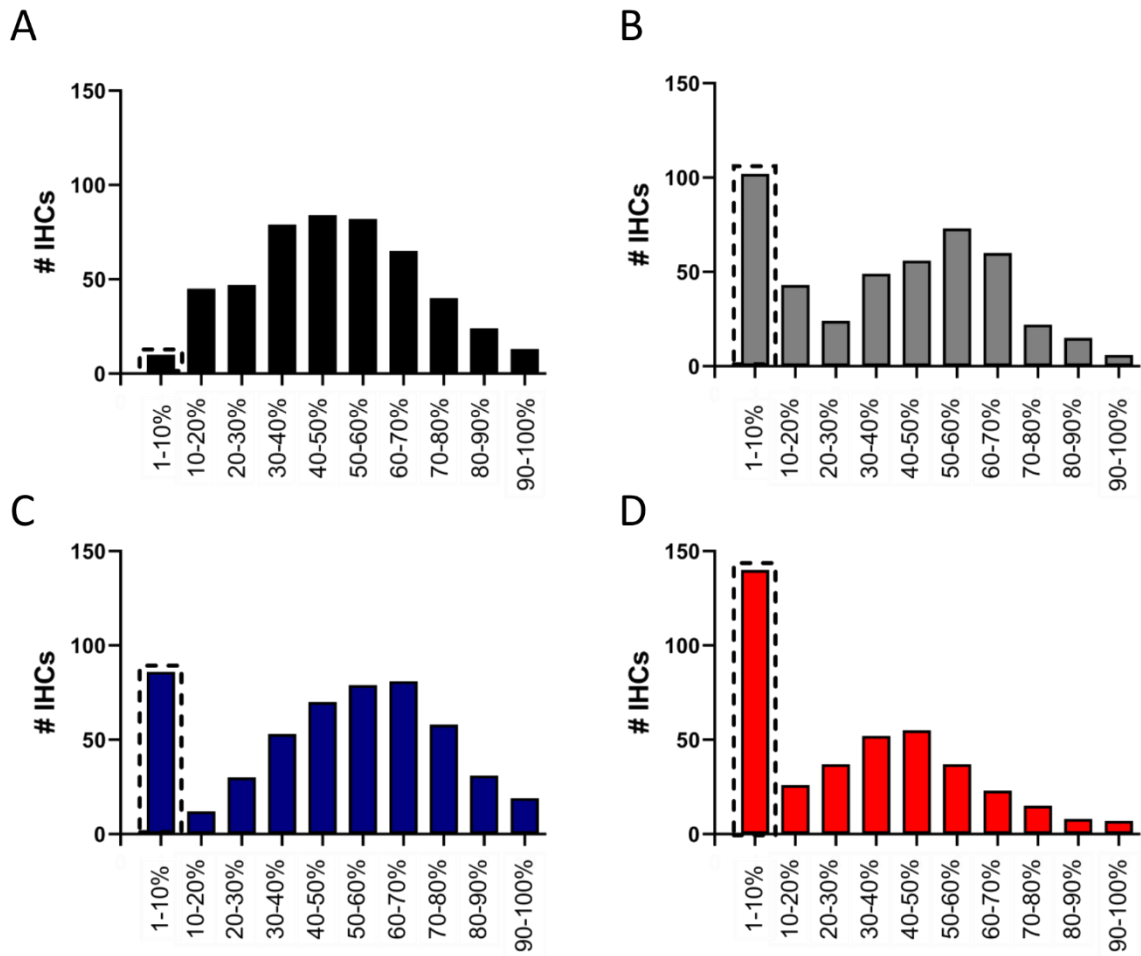


Figure 4. 4. Histogram plots showing the distribution of IHCs that had otoferlin knocked out.

A-D: histogram plots showing the distribution of IHCs from the normalised data. Dotted boxes around the 1-10% bars shows the change in the number of IHCs that had otoferlin knocked out at either one, two, three or four weeks post tamoxifen injection.

4.2.2. IHCs from otoferlin conditional knockout mice do not have a return of axosomatic efferent innervation

Otof^{fl/fl} Vglut3 cre^{+/-} mice had two tamoxifen injections from P10 and were left for four weeks to allow otoferlin to be knocked out of the IHCs and after four weeks around 35% of IHCs had otoferlin knocked out (Figure 4.3). To identify if there was a return of axosomatic efferent innervation on IHCs from *Otof^{fl/fl} Vglut3 cre^{+/-}* mice four weeks post injection, immunofluorescence and multichannel confocal microscopy were used to label otoferlin, the post-synaptic SK2 channels and the efferent pre-synaptic ChAT. Additionally, as a comparison to see if a non-tamoxifen inducible cre (conditional knockout) driving the knockout of otoferlin (*Otof^{fl/fl} Myo15 cre^{+/-}*). A full knockout model for otoferlin was not used for these experiments, as the rationale for using the *Otof^{fl/fl} Vglut3 cre^{+/-}* mice in the first place was to allow for postnatal innervation to fully mature before disrupting neurotransmitter release.

It was seen through immunolabelling performed by another lab member that otoferlin is beginning to be lost from IHCs at P8 in *Otof^{fl/fl} Myo15 cre^{+/-}* mice (Figure 4.5D-F) (Myo15 is expressed in IHCs from P4) and is fully lost from IHCs at P16 (Figure 4.5J-L). On the other hand, the IHCs from control *Otof^{fl/fl}* mice did not lose otoferlin at either P8 (Figure 4.5A-C) or P16 (Figure 4.5G-I). This indicates that a non-tamoxifen cre driver is much more efficient at knocking out otoferlin and therefore could result in efferent re-innervation of IHCs.

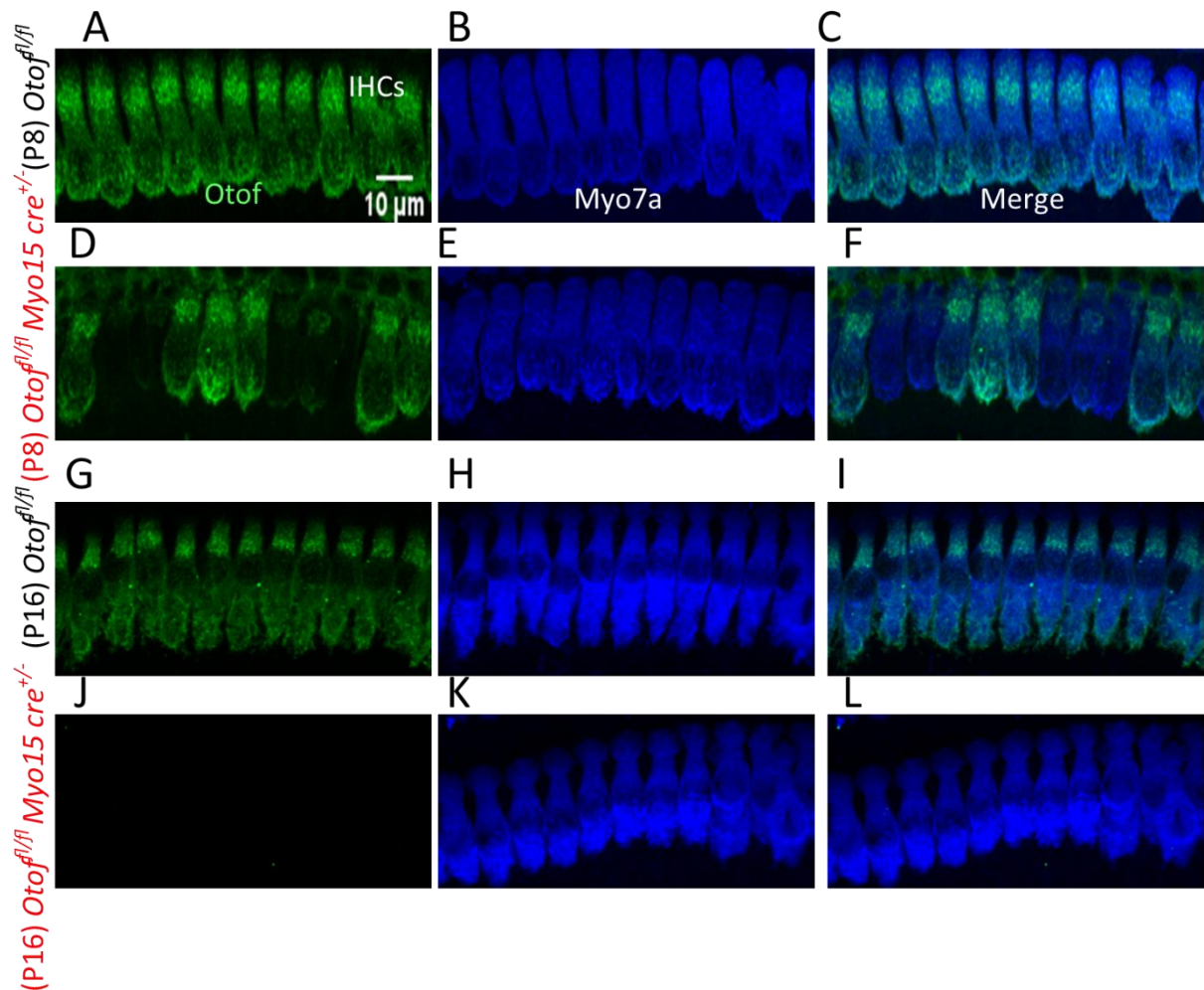


Figure 4. 5. IHCs from *Otof^{fl/fl}* *Myo15 cre^{+/-}* mice begin to lose otoferlin expression at P8 and is completely lost at P16.

A-L: maximum intensity projection images taken from confocal z-stack images of the apical coil of the cochlea. Antibodies against otoferlin (green) and myo7a (blue) were used to visualise the loss of otoferlin from IHCs and Myo7a was used as a hair cell marker. **A-C:** IHCs from control *Otof^{fl/fl}* do not lose expression of otoferlin at P8. **D-F:** IHCs from *Otof^{fl/fl}* *Myo15 cre^{+/-}* mice begin to lose expression of otoferlin from some IHCs in a field of view (~11-12 IHCs per field of view). **G-I:** at P16 IHCs continue to express otoferlin in control mice. **J-L:** IHCs from *Otof^{fl/fl}* *Myo15 cre^{+/-}* mice have all expression of otoferlin knocked out at P16. Scale bars: 10 μ m.

Figure 4.6A-C shows that IHCs from control *Otof^{fl/fl} Vglut3 cre^{-/-}* mice did not have otoferlin knocked out and did not re-express SK2 channels. Figure 4.5B shows a zoomed in IHC confirming that SK2 channels were not expressed, whereas Figure 4.5C visualises the IHCs from Figure 4.5A but rotated on the Z, Y plane, allowing the spatial location of any SK2 channels to be seen. The process of zooming into a single IHC and rotating the IHC images was applied to all images in Figure 4.5. Interestingly, Figure 4.6D-F revealed that IHCs that had otoferlin knocked out from *Otof^{fl/fl} Vglut3 cre^{+/-}* mice did not re-express SK2 channels. This data suggests that disrupting the neurotransmitter release in IHCs does not result in a return of axosomatic efferent innervation.

IHCs from control *Otof^{fl/fl}* mice at P50 did not have otoferlin knocked out of the IHCs and did not express SK2 channels (Figure 4.6G-I). Like the tamoxifen injected *Otof^{fl/fl} Vglut3 cre^{+/-}* mice, the IHCs from *Otof^{fl/fl} Myo15 cre^{+/-}* mice did not express SK2 channels at P50 (Figure 4.6J-L). From this data, it is likely that having a loss of otoferlin in IHCs does not drive the efferent re-innervation of the IHCs. Together, with the data from chapter 3, it is more likely that efferent re-innervation of IHCs is driven by impaired MET channels.

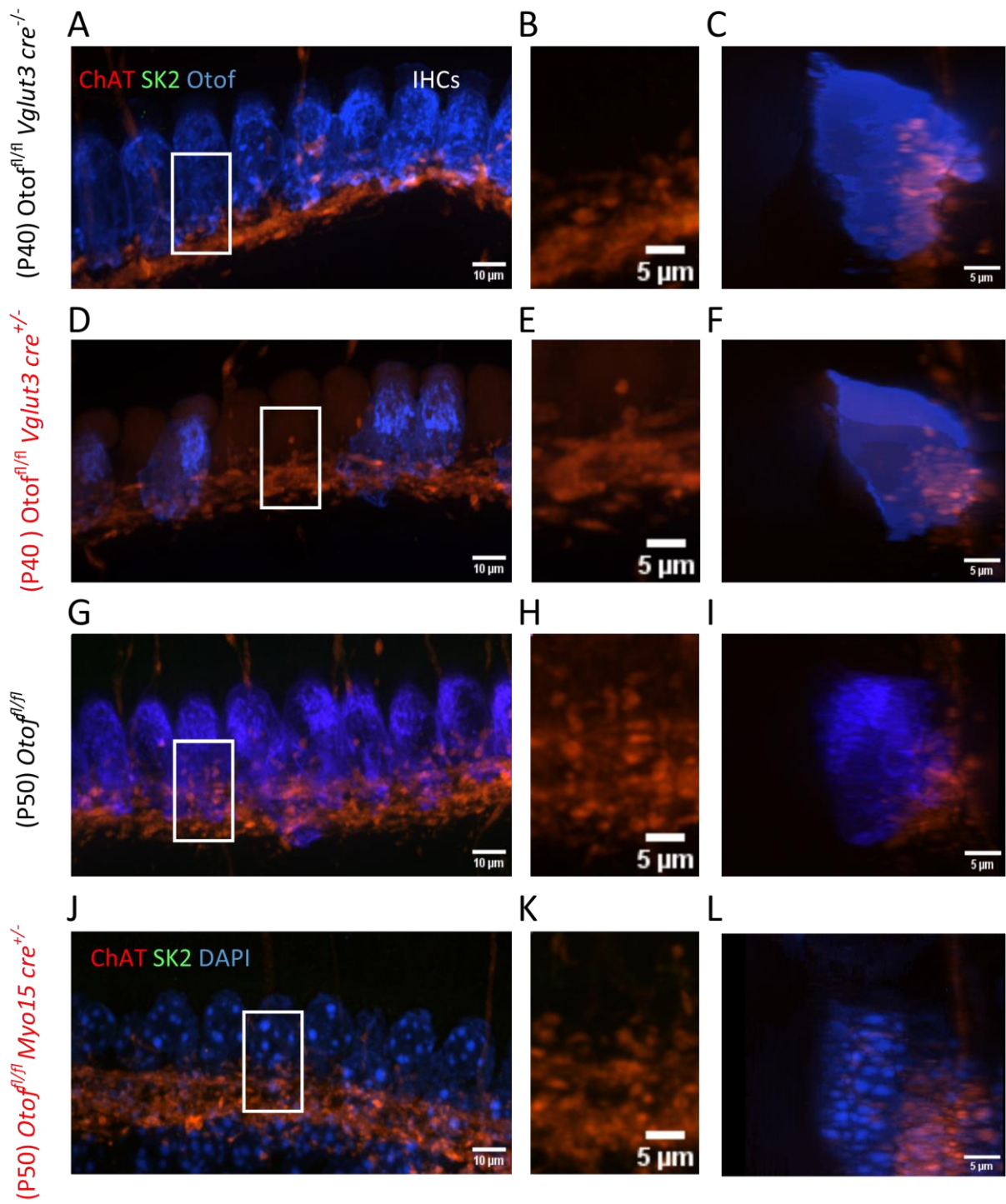


Figure 4. 6. IHCs from otoferlin conditional knockout mice do not have a return axosomatic efferent innervation.

A-L: maximum intensity projections of confocal z-stacks of the apical coil of the cochlea (85µm) at the 9-12 kHz region. IHCs were labelled for SK2 channels (green), otoferlin ((blue) **A-I**) or DAPI ((blue) **J-L**) as well as the efferent terminal markers ChAT (red). **A-C:** IHCs from control *Otof^{fl/fl} Vglut3 cre^{-/-}* mice that were injected with tamoxifen at P10 and left for four weeks did not lose the expression of otoferlin and did not express SK2 channels. **D-F:** some IHCs from *Otof^{fl/fl} Vglut3 cre^{+/-}* mice had otoferlin knocked out but did not re-express SK2 channels. **G-I:** IHCs from control *Otof^{fl/fl}* expressed otoferlin at P50 and did not re-express SK2 channels. **J-L:** IHCs from *Otof^{fl/fl} Myo15 cre^{+/-}* mice did not express otoferlin at P50, but did not re-express SK2 channels. Scale bars for the left column images: 10µm and for the middle and right column images: 5µm.

4.3. Discussion

In this chapter the characterisation of a tamoxifen inducible conditional knockout mouse model for otoferlin was shown. The *Otof^{fl/fl} Vglut3 cre^{+/-}* strain allowed for the temporal control of when to introduce the Cre recombinase to the IHCs, providing scope for how losing the expression of otoferlin at different time points during development could impact the IHCs.

This chapter has shown the initial steps taken to optimise the best age for tamoxifen injections to achieve the greatest knockout efficiency in the *Otof^{fl/fl} Vglut3 cre^{+/-}* mice and if the loss of otoferlin in IHCs induces a return of axosomatic efferent innervation. The overall aim of this chapter was to try and further investigate what drives the mechanism of efferent re-innervation in IHCs.

4.3.1. Tamoxifen injections from P10 induce the best knockout of otoferlin in IHCs

Tamoxifen inducible Cre mice allow for the conditional knockout of the target gene at any age chosen (Metzger et al., 1995, Feil et al., 1996, Feil et al., 2009), in theory this would allow for the knockout of otoferlin in adult mice if desired, and is advantageous over non-tamoxifen inducible Cre strains that take effect from the age at which the Cre driving gene is expressed (eg P2-4 in a *Myo15 cre* strain). Injections were initially performed when the *Otof^{fl/fl} Vglut3 cre^{+/-}* mice were P21, the age at which the innervation has fully matured during development (Johnson et al., 2011, Johnson et al., 2013a, Johnson et al., 2019). Results in Figure 4.1P-R show that very few IHCs lost the expression of otoferlin four weeks post tamoxifen injections and not all the IHCs expressed the *Vglut3 cre*. It is possible that as the mice get older the cochlea environment becomes more mature and the Cre expression is not as efficient compared to if the Cre was induced at earlier ages. Therefore mice were injected at P14, after the onset of hearing at P12 and close to the age at which IHCs lose the axosomatic efferent innervation during development (around P18-21) (Simmons et al., 1996, Glowatzki and Fuchs, 2000, Simmons, 2002).

When *Otof^{fl/fl} Vglut3 cre^{+/-}* mice were injected at P14 (Figure 4.1J-L) all the IHCs expressed td-tomato showing that the *Vglut3 cre* was expressed more efficiently when the mice were injected at younger ages. However, only a few of the IHCs had otoferlin knocked out.

To determine if injecting *Otof^{fl/fl} Vglut3 cre^{+/-}* mice earlier than P14 would lead to a greater number of IHCs with otoferlin knocked out, mice were injected at P10. The data revealed that seemingly more IHCs had otoferlin knocked out when mice were injected at P10 compared to P14. Therefore, P10 was the age at which mice were injected at for the subsequent experiments. Although more IHCs had a loss of otoferlin when mice were injected at P10, ultimately, a relatively low number of IHCs (around 35%) had otoferlin knocked out four weeks post injections. The rationale for using the tamoxifen inducible cre enabled for greater flexibility when inducing a knockout of the desired protein, however, the data in this chapter has revealed that in order to get a high efficiency, more optimisations would be required. Furthermore, due to time restraints during the PhD, the mice were only left for four weeks post injection and it may be that this is too short a time period to see a complete loss of otoferlin from IHCs, as the protein may have a long half-life.

4.3.2. Progressive loss of otoferlin in IHCs following tamoxifen injections

After identifying the best age for tamoxifen injections to be performed at, the next step was to investigate any variability in the length of time mice were left before being used for experiments. To investigate this, mice were left for one-four weeks after tamoxifen injections before immunolabelling was performed and quantified. As mentioned above, due to time restraints mice were not left longer than four weeks. The results in Figures 4.2 & 3 show that the conditional knockout of otoferlin from IHCs did not take place in a linear manner. Disparities were seen when comparing the two- and three-week post injection age groups, if the knockout rate of otoferlin was linear then the reduction in expression would be expected to decrease progressively from each age group, whilst the number of IHCs that had otoferlin knocked out would progressively increase during the same age groups. However, Figure 4.3A-D showed that at three weeks post tamoxifen injection there was not a significant difference in the number of IHCs that had otoferlin knocked out compared to at two weeks ($P = 0.39$,

Tukey's post-test, one-way ANOVA) (Figure 4.3D). To confirm these suggestions, it would require a greater number of mice to be used per condition to allow for the differences to be accounted for, before making definite conclusions on the knockout rate of otoferlin.

Currently, most literature reports that the difference in tamoxifen concentration induces large changes in target gene expression in different tissues, such as cardiac, epidermal, bone and in immune cell populations (Indra et al., 1999, Sohal et al., 2001, Zhang et al., 1996, Zhong et al., 2015, Chin et al., 2020, Donocoff et al., 2020). Moreover, some studies have successfully demonstrated that tamoxifen inducible conditional knockouts can be used to target the IHCs successfully (Zhang et al., 2012, Zhao et al., 2014). One study has utilised tamoxifen inducible *Vglut3* cre mouse lines to study the cochlea. This aim of the study was to induce an IHC cell specific knock-ins, and they reported that an increased number of IHCs expressed td tomato reporter lines when tamoxifen injections were performed at different ages (P2, P10, P30), with greater percentages reported compared to data from this chapter (Li et al., 2018). The differences between this study and the data reported in this chapter may be that tamoxifen inducible cre lines may be more efficient at producing knock-ins as opposed to knockouts. Additionally, very few studies have quantified the knockout rates of target genes after tamoxifen injections in different tissues.

There are multiple reasons as to why there was a different knockout rate in the IHCs from *Otof^{fl/fl} Vglut3 cre^{+/-}* mice at two- and three- weeks post injection. The first possibility could be down to a technical error during intraperitoneal injections, or if the tamoxifen had not been prepared efficiently, ensuring that all the tamoxifen had been sonicated and dispersed properly into the corn oil. However, other reasons for the knockout rate being variable and not linear could be down to how the tamoxifen would be expressed within the IHCs, it could be that IHCs located at different regions of the cochlea would have different metabolic demands and require more blood supply, which could potentially induce a faster rate of knockout compared to IHCs with a lower metabolic demand. When qualitatively examining any differences in the regions of the apical coil of the cochlea, there did not appear to be any preferential knockout of IHCs at either lower or higher frequencies of the apical coil (Figure 4.2). It would be informative in future studies to see if the knockout rate of otoferlin varies between the base and apex of the cochlea, similar to how the base develops around two days earlier than the apex (Mann and Kelley, 2011).

Comparing the knockout of otoferlin in the *Otof^{fl/fl} Vglut3 cre^{+/-}* mice compared to *Otof^{fl/fl} Myo15 cre^{+/-}* mice revealed that non tamoxifen cre drivers had a greater rate of otoferlin knockout, as well as a greater efficiency. As IHCs from *Otof^{fl/fl} Myo15 cre^{+/-}* mice had a complete loss of otoferlin by P16 (Figure 4.5G-I), it can be concluded that the tamoxifen inducible cre line has many positives in theory, however, the *Myo15 cre* is a better conditional knockout mouse model for otoferlin.

Furthermore, the data in this chapter is very preliminary, with only immunofluorescence experiments performed. Electrophysiology is essential to test the functionality of the IHCs and corroborate whether the immunolabelling images showing a loss of otoferlin expression is related to a physiological change in exocytosis. Unfortunately, due to time restraints these experiments were not able to be performed and need to be performed in the future. As there is a differential knockout rate of otoferlin in the *Otof^{fl/fl} Vglut3 cre^{+/-}* mice, with some IHCs showing a complete knockout, whereas others show a reduced expression of otoferlin. From this, it could be postulated that the IHCs would have multiple variable physiological phenotypes, depending on the amount of otoferlin that is knocked out.

Future work could also be to use molecular biology techniques to investigate the expression of otoferlin. For example, western blots and reverse transcription quantitative polymerase chain reactions (RT-qPCR) could be used to support the immunolabelling data.

4.3.3. The return of axosomatic efferent innervation on IHCs was not seen in otoferlin conditional knockout mice

Currently the return of axosomatic efferent synaptic contacts on IHCs has only been seen in age-related hearing loss mouse strains (Lauer et al., 2012, Zachary and Fuchs, 2015, Jeng et al., 2021) and mouse models with dysfunctional MET channels (Corns et al., 2018). Here, it is shown in two different otoferlin conditional knockout mouse models that the axosomatic efferent innervation did not return to IHCs. In the tamoxifen inducible *Otof^{fl/fl} Vglut3 cre^{+/-}* mice no expression of SK2 channels was seen in immunolabelling data four weeks post injection in IHCs that had otoferlin knocked out (Figure 4.6D-F). As mentioned previously, the lack of SK2 re-expression may be because leaving the mice for four weeks post injection was not a long enough period of time, and it may be necessary to leave it for longer in future

experiments. Secondly, in the *Otof^{fl/fl} Myo15 cre^{+/-}* conditional knockout of otoferlin there was also no expression of SK2 channels in IHCs at P50 (Figure 4.6J-L). As the IHCs *Myo7a^{fl/fl} Myo15 cre^{+/-}* mice showed re-innervation from P24 onwards but the *Otof^{fl/fl} Myo15 cre^{+/-}* mice did not show any re-innervation, it could be suggested that the loss of otoferlin is not sufficient to induce the re-innervation of IHCs and dysfunctional MET channels are what drives the re-innervation.

As mentioned above, no electrophysiology data was gathered for this chapter, therefore it is currently not known if the *Otof^{fl/fl} Vglut3 cre^{+/-}* mice have exocytosis release. Likewise, electrophysiology experiments would need to be used in the future to consolidate the immunofluorescence findings that there was no re-expression of SK2 channels or axosomatic efferent synapses. For example, perfusion of 40mM (high K⁺) KCl extracellular solution and 100μM acetylcholine could be used to confirm if there is expression α9α10 nAChRs or pre-synaptic efferent terminals.

Currently most studies researching the role of otoferlin and consequences of it being lost have been performed during development, demonstrating that otoferlin is essential for the maturation of the afferent ribbon synapses in IHCs as well as exocytosis (Yasunaga et al., 1999, Roux et al., 2006, Dulon et al., 2009, Heidrych et al., 2009, Johnson et al., 2009, Takago et al., 2019, Stalman et al., 2021). More recently there has been multiple studies exploring gene therapies as an approach to alleviate the hearing loss that is seen in otoferlin knockout mice (Akil et al., 2019, Al-Moyed et al., 2019, Rankovic et al., 2021), however, studies have not yet used a tamoxifen inducible cre to study the effects of knocking out otoferlin at a later stage of development. Additionally, mice with otoferlin knocked have profound deafness then auditory brainstem responses should be recorded at one-four weeks post injection to determine if the non-linear knockout of otoferlin in *Otof^{fl/fl} Vglut3 cre^{+/-}* has elevated hearing thresholds.

Chapter 5 - Increased immune response in the cochlea following the loss of Myo7a

5.1. Introduction

The final results chapter of this thesis was a side project that was performed along with the main focus of the study (Chapters 3 & 4). As mentioned briefly in the general introduction, there is a wide scope for immune studies to be performed within the cochlea and this chapter explores one of the current gaps in cochlea immune research.

For many years there was a dogma within hearing research that the cochlea was an immune privileged environment due to the presence of blood-labyrinth barriers (Juhn and Rybak, 1981, McCabe, 1989), however, this has since been disproven and revealed that the cochlea has a population of resident immune cells (Hirose et al., 2005). Immune cells and inflammation within the cochlea have been shown to have roles in both the physiology and pathophysiology of hearing and hearing loss (Ma et al., 2000, Wang et al., 2003, Fujioka et al., 2006, Keithley et al., 2008). In addition to resident immune cells, there are also monocytes that have been shown to infiltrate the cochlea from the circulation after acoustic trauma (Hirose et al., 2005, Tornabene et al., 2006, Tan et al., 2008), ototoxicity (Wang et al., 2003, Ladrech et al., 2007, Sato et al., 2010, Hirose and Sato, 2011, Kaur et al., 2015) as well as in induced hair cell death (Kaur et al., 2015) and these monocytes mature into macrophages. Macrophages are the most common resident immune cell within the cochlea and have roles in maintaining homeostasis and inflammation (Davies and Taylor, 2015, Ginhoux and Guilliams, 2016, Hoeffel and Ginhoux, 2018). Macrophages achieve their protective roles by detecting environmental changes and phagocytosing cells in the cochlea (Aderem and Underhill, 1999).

Resident macrophages and immune cells are located in multiple areas within the cochlea, predominantly the stria vascularis (Jabba et al., 2006, Ito et al., 2022), the spiral ganglion neurons (SGNs) (Kaur et al., 2015) and the osseous spiral lamina (OSL) of the modiolus (Wake et al., 2009, Hirose et al., 2017). Additionally macrophages are found in the basilar membrane (Yang et al., 2015, Frye et al., 2017, Frye et al., 2018) beneath the sensory epithelium and beneath the outer sulcus (Liu et al., 2018). However, in mice macrophages are only briefly found in the organ of Corti at birth and degenerate rapidly during early postnatal development (Hirose et al., 2005, Dong et al., 2018). It has been suggested that macrophages

cannot survive in the endolymph, the fluid that the organ of Corti is found in, due to the high potassium concentration (Warchol, 2019). Furthermore, macrophages have different morphologies in the normal and damaged cochlea. Typically, in the healthy cochlea macrophages have a ramified morphology (classified as a mature macrophage), with lots of dendritic extensions sensing the local environment. However, in the damaged cochlea the macrophages are often observed with an amoeboid morphology, which is because of monocytes (immature macrophages) being recruited/infiltrating to the cochlea via the bloodstream (Ladrech et al., 2007).

Macrophages role in inflammation has been explored in studies where cochlea insults occurred, such as noise exposure (Mizushima et al., 2017, He et al., 2020, Rai et al., 2020), ototoxic aminoglycosides (Wang et al., 2003, Ladrech et al., 2007, Sato et al., 2010, Hirose and Sato, 2011, Kaur et al., 2015), inducing cell death via diphtheria toxin injection (Kaur et al., 2015), ageing (Noble et al., 2019) and stress (Liu et al., 2018). What is more, macrophages have been shown responding and inducing inflammatory responses after tamoxifen injections induced the loss of OHCs (Xu et al., 2020). Studies have revealed that macrophages can either induce pro-inflammatory responses or anti-inflammatory responses depending on the chemokine and cytokine the macrophages release (Hough et al., 2022). Pro-inflammatory cytokines such as interleukin-1 β (IL-1 β), interleukin-6 (IL-6), tumour necrosis factor- α (TNF α) (Sato et al., 2002, Fujioka et al., 2006, Keithley et al., 2008), as well as the chemokines monocyte chemoattractant protein 1 (MCP-1/CCL2) and the fractalkine receptor (CX3CR1) along with its associated ligand CX3L1 (Sato et al., 2010) have all been shown to have their expression levels increase temporarily after cochlea insults. Moreover, macrophages have been implicated in protecting SGNs and help to reduce the degree of hearing loss, as shown in studies when fractalkine expression was impaired (Kaur et al., 2015, Kaur et al., 2018, Kaur et al., 2019).

Macrophage responses can also be seen in another form of inflammation, sterile inflammation. Sterile inflammation occurs in the absence of infection and microorganisms and is associated with intracellular contents of dying cells (damage-associated molecular patterns (DAMPs)) being recognised by inflammatory signalling receptors (Chen and Nuñez, 2010, Rock et al., 2010, Shen et al., 2013). In addition to DAMPs there are pattern recognition receptors (PRRs) that are activated by non-infectious stimuli and mediate sterile

inflammatory responses (Chen and Nuñez, 2010) by inducing macrophages to release pro-inflammatory cytokines and chemokines (Frye et al., 2019). Toll-like receptor 4 (Tlr4) is an example of a PRR that interacts with the endogenous molecules of damaged tissues (Vabulas et al., 2001) and upon binding to its ligands recruits adaptor molecules and activates multiple aspects of inflammatory pathways. Tlr4 activates inflammatory responses via the NF- κ B signalling pathway (Zhang and Ghosh, 2001, Kawai and Akira, 2007). Additionally, it was revealed that Tlr4 is constitutively expressed in the cochlea and its levels increase after acoustic insult or ototoxicity (Hirose et al., 2014), whilst Tlr4 has also been shown to be an upstream regulator of cochlea immune and inflammatory responses (Patel et al., 2013, Cai et al., 2014).

It is hypothesised that the *Myo7a^{fl/fl} Myo15 cre^{+/-}* mice could be a potential model for sterile inflammation and that the loss of Myo7a from IHCs and OHCs would result in an increased expression of PRRs such as Tlr4 which induces an inflammatory response within the cochlea. To visualise whether *Myo7a^{fl/fl} Myo15 cre^{+/-}* mice had an inflammatory response after the loss of Myo7a, the ionised calcium binding adapter molecule 1 (Iba1) (Imai et al., 1996, Okano et al., 2008) was used to label for the presence of macrophages. Iba1 is widely used in the literature to label for macrophages and microglia as it recognises both amoeboid and ramified macrophages (Fujioka et al., 2006). The findings from this preliminary project would reveal whether sterile inflammation can be triggered by genetic mutations in the cochlea and would open up new approaches to study inflammation, as well as to investigate if the inflammation is progressive, as opposed to a short-lived response to cochlea trauma. Currently there has been no literature reported on sterile inflammation in knockout mouse models of deafness in the cochlea and these findings would be the first reported observations.

5.2. Results

5.2.1. Changes in the number of macrophages in the cochlea after the loss of Myo7a

Immunofluorescence and confocal microscopy were used to image the apical coil of cochlea from *Myo7a^{fl/fl} Myo15 cre^{+/-}* and littermate control *Myo7a^{fl/fl}* mice at multiple ages following the loss of Myo7a and after the return of axosomatic efferent innervation returned to IHCs. The macrophage cell marker Iba1 was used to visualise the immune response in the apical coil of the cochlea and Myo7a was used to label the hair cells in control *Myo7a^{fl/fl}* mice as this would label both amoeboid and ramified macrophages.

Figure 5.1A shows the population of resident macrophages in the adult cochlea at P28, with the macrophages having a ramified morphology and located in the OSL as well as the outer sulcus regions. The number of macrophages were counted using the Segment.AI (Nikon Instruments) artificial intelligence that was trained on a subset of images, with each of the macrophage morphologies manually defined (see methods). There was an increased number of Iba1+ macrophages in *Myo7a^{fl/fl} Myo15 cre^{+/-}* mice at P28 (Figure 5.1B), particularly in the OSL. Figure 5.1C & E confirmed that there was no change in the resident macrophages with age in control *Myo7a^{fl/fl}* mice, as the Iba1+ macrophages appeared the same at P50 (Figure 5.1C) and P70 (Figure 5.1E) compared to P28 (Figure 5.1A). On the other hand, Figure 5.1D shows that the expression of Iba1+ macrophages seemingly remained elevated at P50 in *Myo7a^{fl/fl} Myo15 cre^{+/-}* mice. Interestingly, some of the macrophages in the outer sulcus had an amoeboid morphology, which indicates that some monocytes were infiltrating the cochlea. In P70 *Myo7a^{fl/fl} Myo15 cre^{+/-}* mice, there was an apparent increase in the number of amoeboid macrophages present in the outer sulcus region, as well as many macrophages in the OSL (Figure 5.1F).

A two-way ANOVA revealed that there was an age and genotype interaction that influenced the number of macrophages present in the apical coil of the cochlea ($F(5) = 20.85$, $P = 0.0037$,

two-way ANOVA). Moreover, there was a significant increase in the number of Iba1+ macrophages in the cochlea at both P50 and P70 in *Myo7a^{fl/fl} Myo15 cre^{+/-}* mice when compared to age matched control mice ($P = 0.0013$ & $P = 0.0428$, Šidák post-test, two-way ANOVA, respectively).

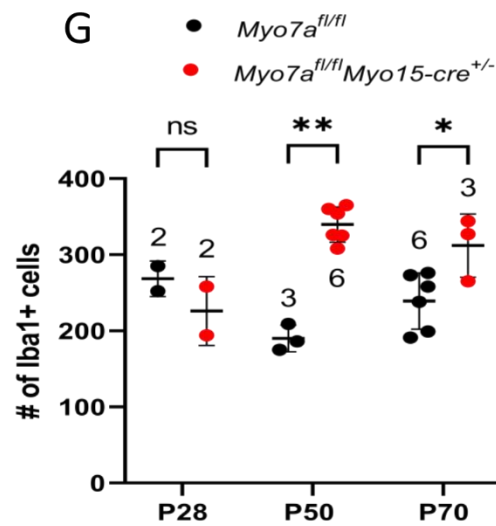
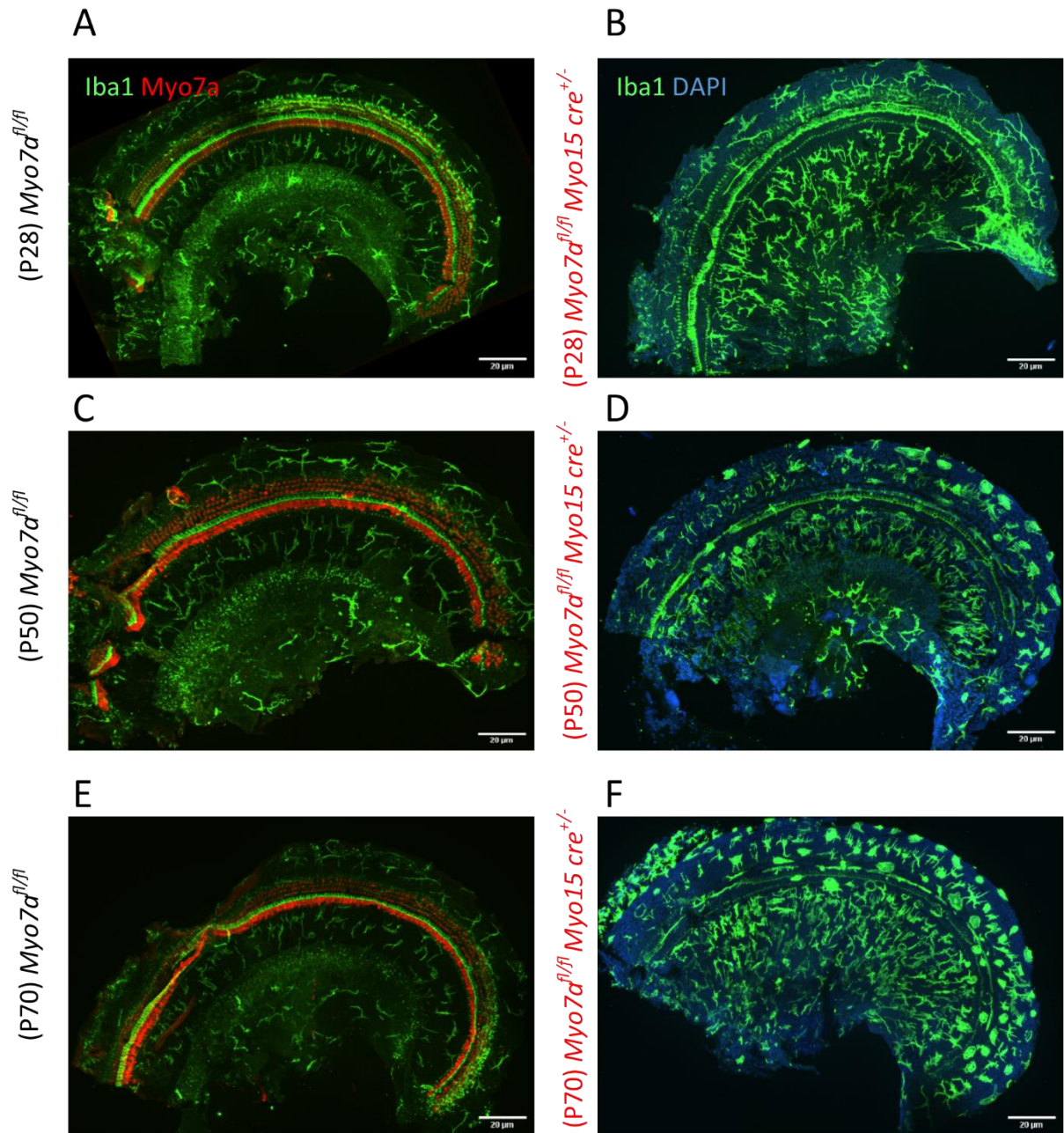


Figure 5. 1. The number of Iba1+ macrophages increase in *Myo7a^{fl/fl} Myo15 cre^{+/-}* mice with age.

A-F: maximum intensity projection images of confocal z-stack images showing the apical coil of the cochlea from control *Myo7a^{fl/fl}* and *Myo7a^{fl/fl} Myo15 cre^{+/-}* mice. Macrophages were labelled with Iba1 (green), hair cells were labelled with Myo7a (red) or DAPI (blue) for *Myo7a^{fl/fl} Myo15 cre^{+/-}*. **A:** resident macrophages in control *Myo7a^{fl/fl}* mice at P28 populate the OSL and the outer sulcus and have ramified morphology. **B:** more Iba1+ macrophages were in the OSL in *Myo7a^{fl/fl} Myo15 cre^{+/-}* mice at P28, with a ramified morphology. **C & E:** the population of resident macrophages remains unchanged in control *Myo7a^{fl/fl}* mice at P50 and P70. **D:** *Myo7a^{fl/fl} Myo15 cre^{+/-}* mice had more Iba1+ macrophages at P50 compared to control mice, amoeboid cells are seen in the outer sulcus. **F:** Iba1+ cells remained elevated in the OSL and outer sulcus at P70 in *Myo7a^{fl/fl}* mice. **G:** the number of Iba1+ macrophages increased at both P50 and P70 in *Myo7a^{fl/fl}* mice compared to age control mice at the same ages. The data points indicate measurements taken from different cochleae, with the numbers above the data points showing the number of mice used. Scale bars: 20µm. Averages are shown as the mean ± SD.

Figure 5.2A shows the resident macrophages in control *Myo7a^{fl/fl}* mice at 6 months remain similar to at earlier ages (Figure 5.1A, C & E) and have a ramified morphology. However, due to time restraints and availability of mice, this is only a qualitative observation. For quantitative analysis there would need to be repeats for the older age groups.

Conversely, the number of macrophages remained elevated in *Myo7a^{fl/fl} Myo15 cre^{+/-}* mice at 6 months of age (Figure 5.2B). Figure 5.2B also shows an apparent decrease in the number of amoeboid cells, suggesting that any amoeboid cells seen at P50 and P70 matured to have a ramified morphology. Interestingly, at 9 months of age the control *Myo7a^{fl/fl}* mice had an apparent (qualitative) increase in the Iba1+ macrophages cells (Figure 5.2C). Additionally, in *Myo7a^{fl/fl} Myo15 cre^{+/-}* mice that were 9 months of age, the population of Iba1+ macrophages seemed to have decreased compared to 6 months (Figure 5.2D). Figure 5.2D also shows that around half of the IHCs had died, indicating that it took around 7 months for the IHCs to die after they malfunction. It would have been interesting to find the exact time at which the IHCs begin to die, ideally, to visualise whether the macrophages are then responsible for phagocytosing and removing the dying IHCs or infiltrating the organ of Corti. However, in order to find the exact time point at which the IHCs die would require more repeats from additional mice, and it is possible that there is variation with each mice depending on external factors, or if the mice became sick.

As there was increase was seen in the number of Iba1+ macrophages in *Myo7a^{fl/fl} Myo15 cre^{+/-}* mice, the early onset age-related C57BL/6N were immunolabelled at 17 months, to determine if there was a progressive increase in the number of macrophages with age. Surprisingly, there was a small population of macrophages at 17 months of age in 6N mice, with most of the macrophages seen in the outer sulcus and very few in the OSL (Figure 5.2E). Moreover, the macrophages in the OSL did not have a particularly ramified morphology, whereas the cells were not quite amoeboid either, therefore it may be that there is an intermediate morphology that is observed here. The gene edited 6N-repaired mice were immunolabelled at 18 months and had a population of macrophages that appeared similar to the resident macrophages seen in control *Myo7a^{fl/fl}* mice (Figure 5.2F). Macrophages in 6N-repaired mice were found in both the OSL and the outer sulcus and displayed a ramified morphology.

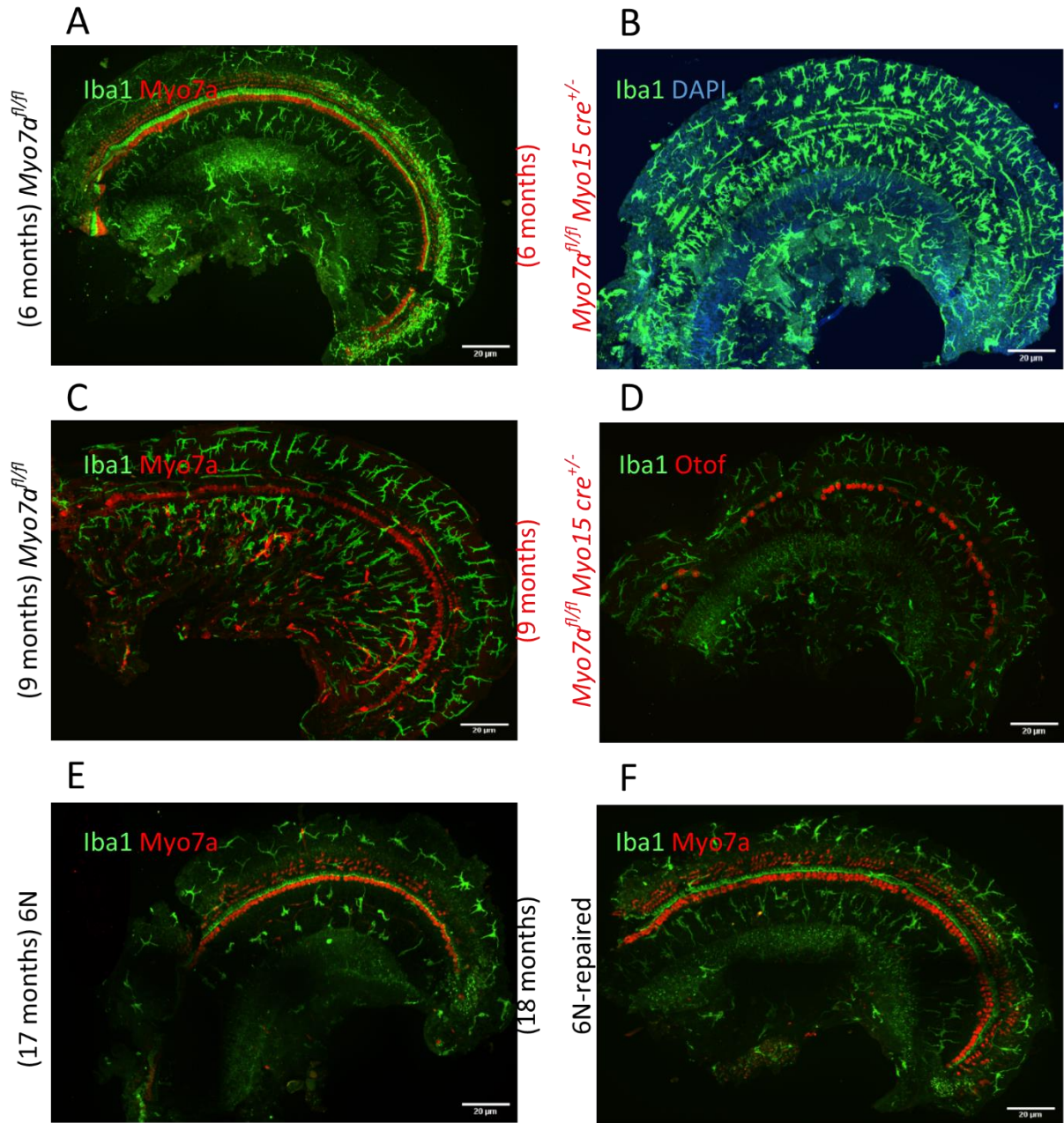


Figure 5. 2. Differences in inflammation between aged *Myo7a^{fl/fl} Myo15 cre^{+/-}* mice and aged 6N and 6N-repaired mice.

A-F: maximum intensity projection images of confocal z-stack images showing the apical coil of the cochlea from control *Myo7a^{fl/fl}* and *Myo7a^{fl/fl} Myo15 cre^{+/-}* mice. Macrophages were labelled with Iba1 (green), hair cells were labelled with Myo7a (red) or DAPI (blue) for *Myo7a^{fl/fl} Myo15 cre^{+/-}*, apart from **(D)** at 9 months when otoferlin (red) was used to label IHCs. **A:** the macrophage population within the apical coil of the cochlea at 6 months of age in the control *Myo7a^{fl/fl}* mice. Macrophages were ramified and populated the OSL and the outer sulcus. **B:** macrophages are densely populated in the OSL and outer sulcus regions in the cochlea of *Myo7a^{fl/fl} Myo15 cre^{+/-}* mice at 6 months. Most macrophages have a ramified morphology in all regions of the cochlea and there were no amoeboid macrophages seen. **C:** macrophages are found in the OSL and outer sulcus in control *Myo7a^{fl/fl}* mice at 9 months of age, with cells having a highly ramified morphology. **D:** the macrophages are less densely packed in the OSL and outer sulcus regions of the cochlea at 9 months of age and around half of the IHCs had died at this age. **E:** macrophages do not densely populate the OSL in the early onset age-related hearing loss 6N mice at 17 months of age. **F:** the resident macrophages expressed in the OSL and outer sulcus in 6N-repaired mice at 18 months of age and the expression of macrophages is similar to control *Myo7a^{fl/fl}* mice at 6 months of age (**A**). Scale bars: 20µm.

5.3. Discussion

This chapter has investigated how the number of macrophages changes in the apical coil of the cochlea following the loss of Myo7a in *Myo7a^{fl/fl} Myo15 cre^{+/-}* mice. Macrophages are the predominant resident immune cells found within the cochlea and have roles in homeostasis and inflammation (Aderem and Underhill, 1999). Therefore, by investigating the changes in macrophages this provided information as to whether a sterile inflammatory response occurred after a loss of Myo7a.

5.3.1. Macrophages numbers increase with age in *Myo7a^{fl/fl} Myo15 cre^{+/-}* mice

The number of macrophages was seen increasing with age in *Myo7a^{fl/fl} Myo15 cre^{+/-}* mice compared to control *Myo7a^{fl/fl}* mice (Figure 5.1). Although there were significant increases at P35, P50 and P70, there was no significant increase in macrophages at P28 in *Myo7a^{fl/fl} Myo15 cre^{+/-}* mice. This is likely due to the statistics being underpowered, with an N of 2 not being sufficient, and with an increase in N numbers this would improve the reliability of the statistical findings at P28. It is plausible that even with more N numbers at P28 there may be no statistical differences, if this were the case then it could be suggested that as the *Myo7a^{fl/fl} Myo15 cre^{+/-}* mice only have slight threshold shifts and are not fully deaf, then this prevents the heightened immune response.

For the quantification of the macrophage numbers, an AI was developed, which was trained by offering the software multiple images, with each of the macrophage morphologies manually defined. This was iteratively trained until the software would accurately identify each type of macrophage, as well as distinguishing any that were overlapping / on top of each other. The AI was the best method to quantify the macrophages, as manual counting would not have been as accurate, however, the major limitation to the AI was that a region of interest could not be defined and then accurately factored into the analysis. As macrophages are commonly found in the OSL and outer sulcus, these would be two defined ROIs to be used for each image, with a defined size and this would enable for accurate and reliable comparison. Unfortunately, at the time the software could not allow this to be used, therefore

the quantification was performed across the whole cochleae. Thus, as each cochlea dissection is slightly different, some may have a larger area compared to others, which would then impact the reliability of the quantification. In order to reliably quantify the number of macrophages in the future, a method must be determined within the analysis software to incorporate ROIs.

The macrophages were seen to have the typically ramified morphology at P28 (Figure 5.1B) in *Myo7a^{fl/fl} Myo15 cre^{+/-}* mice, which indicates that they were mature (Ladrech et al., 2007). However, at older ages there appeared to be an increase in the number of amoeboid macrophages (Figure 5.1D & F). It has been reported that macrophages with an amoeboid morphology are infiltrating monocytes which then mature into macrophages with a ramified morphology (Hirose et al., 2005). From this, it is possible that there was a delayed recruitment of monocytes to the cochlea after the IHCs MET channels are dysfunctional and there was a return of axosomatic efferent innervation. Previous studies have shown that the inflammatory responses to either noise-induced or ototoxic cochlea insults had an elevated number of macrophages for around two-weeks, after which the numbers returned to the resident macrophage population (Hirose et al., 2005, Sato et al., 2010, Hirose et al., 2014, Kaur et al., 2015). Interestingly, the number of macrophages remained elevated in *Myo7a^{fl/fl} Myo15 cre^{+/-}* mice for up to 6 months after the loss of Myo7a (Figure 4.2B) which suggests that there could be pro-inflammatory signals being released for up to 6 months. By 9 months of age the number of macrophages in the apical coil of the cochlea appeared to have decreased (Figure 5.2D) in *Myo7a^{fl/fl} Myo15 cre^{+/-}* mice, suggesting that after 6 months the inflammatory response decreased. The reason for this decrease in the number of macrophages at 9 months is not known, it may be that because there is some IHC loss there is a reduced expression of the activating factor (potentially Tlr4) stimulating the macrophage response. However, due to time restraints the Tlr4 immunolabelling experiments could not be performed to conclude this postulation. Additionally, more repeats would need to be done at older ages to quantify the changes in macrophage numbers, to identify whether the qualitative decrease seen in this chapter is representative.

The macrophages were investigated in the early onset age related hearing loss C57BL/6N mice and 6N-repaired mice (Figure 5.2E & F). Interestingly, in 6N mice there were very few macrophages seen in the apical coil of the cochlea, with the OSL having very few macrophages

present (Figure 5.2E). On the other hand, the 6N-repaired mice had a population of macrophages that appeared similar to control *Myo7a^{fl/fl}* mice at 6 months of age (Figure 5.2A). Studies have investigated the macrophage changes with ageing and reported increases in the number of macrophage in the cochlea (Noble et al., 2019, Seicol et al., 2022). Here, there are discrepancies compared to the reported literature in that there was seemingly a decrease in the number macrophages in the 6N mice at 17 months (Figure 5.2E). It is possible that the differences seen are due to different mouse models being used, as previous studies used the 'good' hearing strain CBA/CaJ (Sha et al., 2008, Ohlemiller et al., 2010). Additionally, it may be that using 17 month old mice was too long after the loss of hearing in these strains (which typically have lost their hearing by 12 months (Mianné et al., 2016)) and the immune response has already taken place and then declined, similar to the differences between the 6 and 9 month old *Myo7a^{fl/fl} Myo15 cre^{+/-}* mice. Therefore, future experiments should also look at 12 months old 6N and 6N-repaired mice.

It was hypothesised that the *Myo7a^{fl/fl} Myo15 cre^{+/-}* mice could be a model for sterile inflammation as there was no infection. In sterile inflammation it has been shown that PRRs, which mediate inflammatory responses are activated (Rock et al., 2010). Tlr4 is an example of a PRR, Tlr4 is upstream of the NF- κ B inflammatory pathway (Zhang and Ghosh, 2001), and is constitutively expressed in the cochlea (Hirose et al., 2014). Additionally, Tlr4 has been shown to have an increased expression after ototoxicity and noise-exposure (Patel et al., 2013). As the number of macrophages remained elevated at 6 months of age in *Myo7a^{fl/fl} Myo15 cre^{+/-}* mice it is possible that PRRs such as Tlr4 could have a prolonged increase in their expression, resulting in the number of macrophages remaining elevated. However, due to time restraints the investigation into changes in Tlr4 expression with age in *Myo7a^{fl/fl} Myo15 cre^{+/-}* mice could not be performed. However, it is hypothesised that the expression of Tlr4 will increase by P50 and remain until 6 months of age and may be responsible for the increased number of macrophages in the apical coil of the cochlea.

5.3.2. Future directions for investigating macrophages in sterile inflammation mouse models

There are multiple experiments that were not able to be performed in this study due to time restrictions and due to the investigations being a side project. Techniques could be used to corroborate the immunolabelling data, such as quantitative polymerase chain reaction (qPCR) and real time qPCR (RT-qPCR). These techniques could identify if there are any changes in the gene expression or RNA of PRRs in the control and *Myo7a^{fl/fl} Myo15 cre^{+/-}* mice. If there were to be changes in either PRRs such as Tlr4 or other genes involved in inflammatory pathways then RT-qPCR would reveal these, as well as being able to identify if there were any differences between the strains. The RT-qPCR data could then be compared to already published RT-PCR data that was performed in age-related hearing loss mice (Uraguchi et al., 2021). By comparing this to the age-related data, it could be identified if sterile inflammation in the cochlea has the same inflammatory pathways activated as in ageing, or if different inflammatory pathways become activated. RNA sequencing could also be performed in these mice at different ages, the advantage of RNA sequencing is that any changes in gene expression would be identified using this technique, as opposed to having to create specific primers for targets of interest in RT-qPCR. From this, it would enable the identification of a wide range of immune pathways that could be activating the inflammatory pathway, if it were to be that Tlr4 is not instigating the response.

Secondly, future studies could be performed in multiple age-related hearing loss strains (6J, 6N), as well as the late onset hearing loss strain C3H/HeJ to provide a better understanding of inflammatory responses during ageing. It would also be interesting to compare this to other conditional knockout strains, such as an Otoferlin knockout, to see if impairing the IHCs neurotransmitter release could also be a model of sterile inflammation, or if it would only be linked to impaired MET function.

Chapter 6 - General Discussion

The axosomatic efferent innervation returning to IHCs has previously been reported in early onset age-related hearing loss strains and strains where the MET channel is dysfunctional, amongst many other dysfunctions (Lauer et al., 2012, Zachary and Fuchs, 2015, Corns et al., 2018, Jeng et al., 2021). To further our understanding of the mechanistic changes that take place during the return of efferent innervation on IHCs, multiple conditional knockout mouse models targeting different core regions of the IHCs were used throughout this study.

One conditional knockout targeted *Myo7a*, resulting in it being lost from IHCs and OHCs. The absence of *Myo7a* from IHCs is detrimental to the MET channels in the hair bundles, resulting in reduced MET currents and the IHCs return to an immature like state (Corns et al., 2018). Additionally, the return of axosomatic efferent innervation was seen in *Myo7a^{fl/fl} Myo15 cre^{+/-}* mice, taking place around P33 (Corns et al., 2018), which is significantly earlier than in age-related hearing loss strains (after one year of age). Therefore, utilising the *Myo7a^{fl/fl} Myo15 cre^{+/-}* strain enabled the temporal mechanistic changes that take place as the efferent innervation returns to IHCs to be investigated. Secondly, to identify if the disrupting the neurotransmitter release from IHCs would result in the return of efferent innervation, the tamoxifen inducible conditional knockout mouse model for otoferlin was studied (*Otof^{fl/fl} Vglut3 cre^{+/-}* mice). Additionally, the non-tamoxifen inducible conditional knockout of otoferlin (*Otof^{fl/fl} Myo15 cre^{+/-}*) was also used during this study. Another conditional knockout mouse model disrupting the MET channels was investigated (*Ush1c^{fl/fl} Myo15 cre^{+/-}*), to confirm whether the axosomatic efferent innervation would return to IHCs if any MET dysfunctionality was present.

6.1. The return of axosomatic efferent innervation on IHCs is driven by MET dysfunction

This study revealed that the return of axosomatic efferent innervation returned to IHCs in *Myo7a^{fl/fl} Myo15 cre^{+/-}* mice from P24 onwards (Figure 3.2), which was 9 days earlier than previously reported (Corns et al., 2018). Interestingly, the post-synaptic SK2 channels were seen to be re-expressed in IHCs from *Myo7a^{fl/fl} Myo15 cre^{+/-}* mice at P24, prior to the return of the pre-synaptic efferent terminals. This finding supports the previous suggestion that the IHCs are driving the return of the axosomatic efferent innervation, by re-expressing the post-

synaptic machinery first. The responsiveness to ACh in the IHCs started to increase, whilst the IHCs begin to consistently return to an immature-like profile after P32. Together, this data indicates that the IHCs had an increased number of functional efferent synapses over time that was concurrent with the cells changing their biophysical profile.

In the second conditional knockout mouse model affecting the MET channel, the *Ush1c^{fl/fl} Myo15 cre^{+/-}*, IHCs expressed SK2 channels at P21, whereas control *Ush1c^{fl/fl}* mice did not (Figure 3.9). These results propose two different possibilities relating to the efferent innervation in this strain. Firstly, it could be that the innervation of IHCs in *Ush1c^{fl/fl} Myo15 cre^{+/-}* mice never matures properly. In development the axosomatic efferent innervation is lost from IHCs around P18, at a time when the cells no longer respond to ACh or express SK2 channels (Glowatzki and Fuchs, 2000, Katz et al., 2004, Marcotti et al., 2004). Therefore, by the *Ush1c^{fl/fl} Myo15 cre^{+/-}* mice expressing SK2 channels at P21 it could be that the disruption of the MET channel by knocking out the harmonin protein prevents the maturation of the IHCs innervation. Alternatively, the *Ush1c^{fl/fl} Myo15 cre^{+/-}* mice do have their innervation mature correctly, and that the SK2 channels seen at P21 were being re-expressed as part of the mechanism for the return of axosomatic efferent innervation.

However, when comparing the SK2 channel expression in *Ush1c^{fl/fl} Myo15 cre^{+/-}* mice at P21 compared to *Myo7a^{fl/fl} Myo15 cre^{+/-}* mice at P24, the *Ush1c^{fl/fl} Myo15 cre^{+/-}* mice had colocalising SK2 channels with ChAT efferent terminals (Figure 3.9). On the other hand, the SK2 channels expressed by IHCs from *Myo7a^{fl/fl} Myo15 cre^{+/-}* mice at P24 did not colocalise with efferent markers (Figure 3.2) and did not respond to perfusion of high K⁺ solution. A limitation of this conclusion is that only immunolabelling was performed in the *Ush1c^{fl/fl} Myo15 cre^{+/-}* mice in this study, however, it is likely that performing electrophysiology at P21 would reveal that the IHCs respond to ACh and high K⁺ as the SK2 channels colocalise with ChAT in at this age. As SK2 channels have been shown to be re-expressed by IHCs prior to efferent pre-synaptic terminals (Figure 3.2, (Jeng et al., 2021)), it can be postulated that the SK2 channels expressed by IHCs in *Ush1c^{fl/fl} Myo15 cre^{+/-}* mice at P21 is due to the improper maturation of efferent innervation, as opposed to the return of axosomatic efferent innervation. Further supporting this suggestion, it was reported by Corns et al., 2018 that the IHCs from *Ush1c^{fl/fl} Myo15 cre^{+/-}* mice never developed mature IHCs biophysical profiles, whilst their MET currents were abolished by P10, and the mice were shown to be deaf by P16.

Together with the efferent synapse immunolabelling data shown in this thesis, it is likely that the IHCs never mature their efferent innervation and the SK2 puncta seen at P21 are remnants of the immature innervation as opposed to re-innervation. To

The return of axosomatic efferent innervation to IHCs was not seen in either of the otoferlin conditional knockout strains (Figure 4.4). The tamoxifen inducible otoferlin knockout mice, *Otof^{fl/fl} Vglut3 cre^{+/-}* mice, were left for four-weeks after tamoxifen injections at P10 and P11. Throughout this time, about 35% of the IHCs had otoferlin completely knocked out, however, the IHCs did not express SK2 channels, indicating there was no return of axosomatic efferent synapses (Figure 4.4). It is possible that the re-innervation or re-expression of SK2 channels could take longer than the four-week time period investigated here, however, this was unable to be studied in this study due to time restraints. To determine whether the tamoxifen inducible cre driver could have affected any potential return of efferent innervation, the *Otof^{fl/fl} Myo15 cre^{+/-}* mice were also studied. By using the Myo15 cre, the knockout of otoferlin would be knocked out in a similar time frame as Myo7a and harmonin in the *Myo7a^{fl/fl} Myo15 cre^{+/-}* and *Ush1c^{fl/fl} Myo15 cre^{+/-}* mice. As shown in Figure 4.5, when the knockout of otoferlin was driven by Myo15 cre the IHCs had otoferlin completely knocked out by P16, as opposed to the differential knockout rate that was seen over a much longer time period in the tamoxifen inducible strain. Additionally, by using the *Otof^{fl/fl} Myo15 cre^{+/-}* mice this would reveal whether knocking out otoferlin at an earlier time point could induce efferent re-innervation of IHCs. Interestingly, there was no expression of SK2 channels in *Otof^{fl/fl} Myo15 cre^{+/-}* mice at P50 (Figure 4.6). From this data it can be concluded that the return of axosomatic efferent innervation on IHCs is driven by the MET channels becoming dysfunctional, and the disruption of neurotransmitter release at ribbon synapses in IHCs does not result in the efferent synapses returning to IHCs.

One of the major limitations to the otoferlin conditional knockout strains was that the exocytosis and neurotransmitter release of the IHCs was never functionally tested using electrophysiology during this study, due to time restraints. To make this conclusion stronger it is essential to first confirm that the exocytosis was impaired in the otoferlin knockout strains. Additionally, electrophysiology experiments would need to be performed to test whether the IHCs from the otoferlin conditional knockout mice respond to local perfusion of ACh, as well as if they respond when perfused with a high K⁺ solution to stimulate ACh release

from the efferent pre-synaptic terminal. These experiments would then provide more evidence showing that the IHCs from otoferlin conditional knockout mice do not re-express SK2 channels or become re-innervated by efferent fibres.

The finding that disrupting neurotransmitter release in IHCs does not result in efferent re-innervation is surprising. It was hypothesised that disrupting the neurotransmitter release in IHCs would result in the return of efferent innervation, similar to when the MET channels are dysfunctional. These findings lead to more questions for future work: would the disruption of other key processes in IHCs (such as knocking out $Ca_v1.3$ channels) result in the return of the efferent innervation? Moreover, would a constitutive knockout of otoferlin induce the efferent re-innervation? This question was not investigated during this study as the rationale for the experiments was to research the conditional knockouts for MET channel functionality or neurotransmitter release. If a constitutive knockout of otoferlin did result in efferent re-innervation, then this would be a very interesting finding and would require follow up investigation. However, the constitutive knockout of otoferlin would first need be investigated to ensure that the innervation of the IHCs matures properly in the absence of neurotransmitter release. There have been studies to show that the afferent synapse formation is affected during development in the constitutive knockout of otoferlin and this progressively deteriorates with age (Stalman et al., 2021). From these potential experiments it could confirm whether the return of axosomatic efferent innervation in IHCs is driven exclusively by the improper functioning of the MET channels, highlighting the crucial role of these channels.

6.2. Efferent synapses return to IHCs prior to a loss of afferent synapses

This is the first study to show that the re-innervation of IHCs occurs prior to the loss of afferent synapses (Figures 3.2, 3.7, 3.8). Previous studies have proposed that the re-innervation of IHCs was possible due to the loss of afferent synapses which results in type I SGN afferent fibre loss, leaving the LOC efferent fibres without any axodendritic synapses. This would subsequently enable the LOC fibres to re-innervate the IHCs (Lauer et al., 2012, Zachary and Fuchs, 2015, Corns et al., 2018, Jeng et al., 2021). However, the data in this study reveals that the IHCs become re-innervated before they lose their afferent synapses. It is possible that the re-innervation of the IHCs could accelerate the loss of afferent synapses. As the IHCs lose their

MET currents and return to immature phenotypes, there will likely be less stimulation of the afferent synapse, and this is potentially why there is a loss of afferent synapses. However, when the IHCs become re-innervated by the efferent fibres, with functional inhibitory synapses, it could be that this exacerbates the loss of the afferent synapses. Additionally, this data shows that the re-innervation of the IHCs can only take place after afferent fibre loss, as it was proposed that there would not be space on the IHC for axosomatic efferent innervation in the mature IHC (Lauer et al., 2012, Zachary and Fuchs, 2015, Corns et al., 2018, Jeng et al., 2021). These novel findings are interesting and raise more questions as to whether the efferent re-innervation of IHCs is a protective mechanism or not.

6.3. Is the returning efferent innervation a result of IHC and OHC dysfunction, or IHC dysfunction alone?

There remain many questions relating to the returning axosomatic efferent innervation on IHCs in both age-related hearing loss and in strains that have dysfunctional MET channels. Currently, all studies that have seen the return of efferent innervation have MET channel complications at some point, such as the *Cdh23^{ah1}* mutation in the early onset age-related hearing loss C57BL mice, as well as in the *Myo7a^{fl/fl} Myo15 cre^{+/-}* mice (Lauer et al., 2012, Zachary and Fuchs, 2015, Corns et al., 2018, Jeng et al., 2021). Moreover, in all these studies that demonstrated a return of axosomatic efferent innervation, both the IHCs and OHCs MET channels became dysfunctional. This raises the question as to whether both the IHCs and OHCs becoming dysfunctional is necessary for the return of axosomatic efferent innervation, or if just the IHCs becoming dysfunctional would result in the returning innervation. In this study, in the *Otof^{fl/fl} Vglut3 cre^{+/-}* mice there was not the return of axosomatic efferent innervation on IHCs, in part this result could suggest that impairing the function of the IHCs does not result in the return of efferent innervation. On the other hand, as it was shown that disrupting the release of neurotransmitter in IHCs does not result in the efferent innervation returning, future studies would be required to answer this question fully. The development of a conditional knockout of Myo7a on an IHC specific cre driver (such as otoferlin cre or Vglut cre) would result in dysfunctional MET channels, then, depending on whether the efferent innervation returned to IHCs or not would inform us as to whether dysfunctional IHC MET channels can induce the mechanism. An alternative approach could be to specifically

knockout *Myo7a* only in the OHCs, to do this an OHC specific cre driver would be required such as Prestin (or oncomodulin) cre. However, one of the studies using a prestin cre driver to specifically target OHCs is tamoxifen inducible (Fang et al., 2012). The efficiency of this tamoxifen inducible cre may be better than the *Otof^{fl/fl} Vglut3 cre^{+/-}* strain used in this study, however, it may be that the tamoxifen inducible cre lines do not result in re-innervation. Ideally, a non-tamoxifen inducible OHC specific cre would be used for future studies to be more comparative to this study.

6.4. Could neurotrophins be attracting efferent fibres to the IHCs?

Throughout development there are multiple neurotrophins that are involved with axon guidance and establishing the correct innervation for the cochlea hair cells, two key neurotrophins involved with efferent innervation are brain derived neurotrophic factor (BDNF) and neurotrophin-3 (NT-3) (Ernfors et al., 1995, Tessarollo et al., 2004, Blakley et al., 2020).

As the return of axosomatic efferent innervation on IHCs starts at about P24 in *Myo7a^{fl/fl} Myo15 cre^{+/-}* mice, it is possible that these developmental neurotrophins become re-expressed in order to guide the efferent fibres to the IHCs. As the IHCs re-express SK2 channels prior to efferent terminals contacting the IHCs, there may be an upregulation of NT-3 and/or BDNF at a similar time as the re-expression of SK2 channels.

Studies have revealed that the expression of BDNF and NT-3 have been upregulated in the cochlea to aid with the rearrangement of neuronal fibres in development (Wiechers et al., 1999, Fritsch et al., 2004), as well as after gene therapy to express BDNF or NT-3 in deaf mice (Wise et al., 2010). Therefore, to investigate if the expression of BDNF or NT-3 changes during the return of axosomatic efferent innervation, techniques such as RNA sequencing or RT-qPCR could be used. If there were to be an increased expression of these neurotrophins then it could be postulated that they are involved in attracting the efferent fibres to the IHCs during the return of axosomatic innervation.

6.5. What role is inflammation playing in hearing loss?

Studies have shown that inflammatory responses are seen after multiple types of cochlea insult, such as noise-induced, ototoxicity, diphtheria injections, ageing and stress (Wang et

al., 2003, Hirose et al., 2005, Tornabene et al., 2006, Ladrech et al., 2007, Hirose et al., 2014, Kaur et al., 2018, Hough et al., 2022). In these previous studies the inflammatory responses and increased number of macrophages was a temporary response, which typically lasted two-weeks. However, in the *Myo7a^{fl/fl} Myo15 cre^{+/-}* mice there was an increase in the number of macrophages that remained elevated until 6 months of age (Figure 5.1 & 5.2). The data suggests that the increased macrophage response was delayed after the IHCs had dysfunctional MET channels and the return of axosomatic efferent innervation. It would be interesting to investigate if the PRRs that initiate the inflammatory pathways become upregulated as the MET channels become dysfunctional, or as the efferent innervation returns. Alternatively, as the inflammatory response is seemingly delayed, it could be that the upregulation of PRRs might take place once the IHCs return to an immature like profile and the mice are deaf. As macrophages have been shown to be protective within the cochlea (Kaur et al., 2015, Kaur et al., 2018, Kaur et al., 2019), it could be suggested that the macrophage response in *Myo7a^{fl/fl} Myo15 cre^{+/-}* mice was a delayed attempt to limit damage in the cochlea, as a result of sterile inflammation.

Moreover, if experiments identified if the return of axosomatic efferent innervation is driven solely by IHC malfunction, or if both the IHCs and OHCs need to be malfunctioned for the innervation to return, this could lead to future inflammatory studies. If dysfunctional IHCs alone result in efferent innervation returning to IHCs, then it could be investigated to see if the macrophage response is the similar to the response seen in *Myo7a^{fl/fl} Myo15 cre^{+/-}* mice. If the response was similar and the mechanism of sterile inflammation initiated the same response, then it would demonstrate that the macrophages and inflammatory response in the cochlea is highly sensitive and responds to the malfunctioning of the IHCs.

6.6. Future work

This study has furthered our current understanding of the mechanistic changes that are driving the return of axosomatic efferent innervation in mice. However, there are experiments that could be performed to consolidate the findings discovered. For example, transmission electron microscopy could be performed in each of the conditional knockout strains used in this study to confirm either the return of axosomatic efferent innervation, or the lack of this innervation. One study that provided insight into the number of cochlea and

vestibular efferent fibres was achieved by using retrograde tracing (Warr, 1975). Subsequent studies have used the technique of tracing to determine how the innervation of the LOC and MOC fibres changes during development (Simmons, 2002). Therefore, by utilising the tracing techniques it would provide a definitive answer for whether it is the LOC or MOC fibres that are responsible for the axosomatic efferent innervation on IHCs. This question has partly been answered using immunofluorescence images to demonstrate that the LOC fibres are responsible for the returning innervation in age-related hearing loss strains (Jeng et al., 2021). There were limitations of this immunofluorescence imaging, in that there is no specific antibody for LOC fibres, therefore, a combination of different fibre markers was used to reach the conclusion that LOC fibres are responsible. Thus, by using tracing techniques this will allow the previous data to be consolidated and confirm that it is the LOC fibres returning to IHCs, or it would provide evidence that it is the MOC fibres responsible.

Currently all studies investigating the return of axosomatic efferent innervation have depolarised the efferent pre-synaptic terminals using a 40mM KCl extracellular solution (Zachary and Fuchs, 2015, Corns et al., 2018, Jeng et al., 2021). Future experiments could stimulate the efferent fibre directly using an electrode, instead of local perfusion of KCl solution, this would be more representative of *in vivo* stimulation. From this, any differences could be informative as to how the efferent synapses work upon electrical stimulation, as opposed to pharmacological stimulation.

There has been a focus on the changes to the peripheral auditory system for the return of axosomatic efferent innervation, therefore, future work could be to investigate any changes in different regions of the central auditory pathway. Regions such as the cochlear nucleus or inferior colliculus could be the focus of studies. In these regions there are multiple areas for potential research, such as investigating whether the inflammatory responses that are seen in the cochlea in mouse models with MET channel dysfunctions are similar in central auditory regions. It could be postulated that the microglia in the brain will respond to a changing environment as the mice become deaf. Moreover, as the return of axosomatic efferent innervation takes place in the cochlea, it could be that there are changes in the neurons and neuronal connections within the cochlear nucleus or inferior colliculus. If there were to be changes discovered, it would then be interesting to identify if any changes in the central auditory pathway occur prior to the return of axosomatic efferent innervation on IHCs, or

afterwards. Investigating the cochlear nucleus and inferior colliculus for inflammatory responses and neuronal population changes could also be performed in the age-related hearing loss strains that also have a return of axosomatic efferent innervation.

6.7. Conclusions

This study shows that the return of axosomatic efferent innervation on IHCs is driven by the IHCs. The IHCs from *Myo7a^{fl/fl} Myo15 cre^{+/-}* mice express the post-synaptic SK2 channels prior to the return of the pre-synaptic efferent terminals (Figures 3.2, 3.3, 3.4). Concurrent with the morphological and biophysical changes, the *Myo7a^{fl/fl} Myo15 cre^{+/-}* mice had progressive hearing loss (Figure 3.5). It was also shown in this study that the return of axosomatic efferent innervation is likely to be instigated by a loss of functional MET channels, but not when otoferlin is knocked out from IHCs (Figure 4.6). Additionally, this is the first study to show that the IHCs become re-innervated by efferent fibres before having a decrease in the number of afferent synapses (Figures 3.2, 3.7, 3.8).

Although this study has provided further understanding of the mechanism of axosomatic efferent innervation returning to IHCs, there are still important questions that are left unanswered. Firstly, is the mechanism of returning efferent innervation an inherent protective response from the IHCs upon the MET channels becoming dysfunctional? Additionally, if the mechanism is a protective response, does it help prevent the hearing loss that is seen, or does the returning efferent innervation actually exacerbate hearing loss?

References

- ADATO, A., MICHEL, V., KIKKAWA, Y., REINERS, J., ALAGRAMAM, K. N., WEIL, D., YONEKAWA, H., WOLFRUM, U., EL-AMRAOUI, A. & PETIT, C. 2004. Interactions in the network of Usher syndrome type 1 proteins. *Human Molecular Genetics*, 14, 347-356.
- ADEREM, A. & UNDERHILL, D. M. 1999. Mechanisms of phagocytosis in macrophages. *Annu Rev Immunol*, 17, 593-623.
- AHMED, Z. M., GOODYEAR, R., RIAZUDDIN, S., LAGZIEL, A., LEGAN, P. K., BEHRA, M., BURGESS, S. M., LILLEY, K. S., WILCOX, E. R., RIAZUDDIN, S., GRIFFITH, A. J., FROLENKOV, G. I., BELYANTSEVA, I. A., RICHARDSON, G. P. & FRIEDMAN, T. B. 2006. The tip-link antigen, a protein associated with the transduction complex of sensory hair cells, is protocadherin-15. *The Journal of neuroscience : the official journal of the Society for Neuroscience*, 26, 7022-7034.
- AHMED, Z. M., RIAZUDDIN, S., AHMAD, J., BERNSTEIN, S. L., GUO, Y., SABAR, M. F., SIEVING, P., RIAZUDDIN, S., GRIFFITH, A. J., FRIEDMAN, T. B., BELYANTSEVA, I. A. & WILCOX, E. R. 2003. PCDH15 is expressed in the neurosensory epithelium of the eye and ear and mutant alleles are responsible for both USH1F and DFNB23. *Human Molecular Genetics*, 12, 3215-3223.
- AHMED, Z. M., RIAZUDDIN, S., BERNSTEIN, S. L., AHMED, Z., KHAN, S., GRIFFITH, A. J., MORELL, R. J., FRIEDMAN, T. B. & WILCOX, E. R. 2001. Mutations of the protocadherin gene PCDH15 cause Usher syndrome type 1F. *American journal of human genetics*, 69, 25-34.
- AKIL, O., DYKA, F., CALVET, C., EMPTOZ, A., LAHLOU, G., NOUAILLE, S., BOUTET DE MONVEL, J., HARDELIN, J.-P., HAUSWIRTH, W. W., AVAN, P., PETIT, C., SAFIEDDINE, S. & LUSTIG, L. R. 2019. Dual AAV-mediated gene therapy restores hearing in a DFNB9 mouse model. *Proceedings of the National Academy of Sciences*, 116, 4496-4501.
- AKIL, O., SEAL, R. P., BURKE, K., WANG, C., ALEMI, A., DURING, M., EDWARDS, R. H. & LUSTIG, L. R. 2012. Restoration of hearing in the VGLUT3 knockout mouse using virally mediated gene therapy. *Neuron*, 75, 283-93.
- AL-MOYED, H., CEPEDA, A. P., JUNG, S., MOSER, T., KÜGLER, S. & REISINGER, E. 2019. A dual-AAV approach restores fast exocytosis and partially rescues auditory function in deaf otoferlin knock-out mice. *EMBO Mol Med*, 11.

- ALAGRAMAM, K. N., YUAN, H., KUEHN, M. H., MURCIA, C. L., WAYNE, S., SRISAILPATHY, C. R. S., LOWRY, R. B., KNAUS, R., VAN LAER, L., BERNIER, F. P., SCHWARTZ, S., LEE, C., MORTON, C. C., MULLINS, R. F., RAMESH, A., VAN CAMP, G., HAGEMEN, G. S., WOYCHIK, R. P. & SMITH, R. J. H. 2001. Mutations in the novel protocadherin PCDH15 cause Usher syndrome type 1F. *Human Molecular Genetics*, 10, 1709-1718.
- ALTSCHULER, R. A., HUFFMAN, D. W., REEKS, K. A. & FEX, J. 1985. Localization of dynorphin B-like and alpha-neoendorphin-like immunoreactivities in the guinea pig organ of Corti. *Hearing Research*, 17, 249-258.
- ALTSCHULER, R. A., REEKS, K. A., FEX, J. & HOFFMAN, D. W. 1988. Lateral olivocochlear neurons contain both enkephalin and dynorphin immunoreactivities: immunocytochemical co-localization studies. *Journal of Histochemistry & Cytochemistry*, 36, 797-801.
- ALVARADO, J. C., FUENTES-SANTAMARÍA, V., GABALDÓN-ULL, M. C., BLANCO, J. L. & JUÍZ, J. 2014. Wistar rats: a forgotten model of age-related hearing loss. *Frontiers in Aging Neuroscience*, 6, 29.
- ALVARADO, J. C., FUENTES-SANTAMARÍA, V., GABALDÓN-ULL, M. C., JAREÑO-FLORES, T., MILLER, J. M. & JUIZ, J. M. 2016. Noise-Induced “Toughening” Effect in Wistar Rats: Enhanced Auditory Brainstem Responses Are Related to Calretinin and Nitric Oxide Synthase Upregulation. *Frontiers in Neuroanatomy*, 10, 19.
- ALVARADO, J. C., FUENTES-SANTAMARÍA, V., GABALDÓN-ULL, M. C. & JUIZ, J. M. 2018. An Oral Combination of Vitamins A, C, E, and Mg(++) Improves Auditory Thresholds in Age-Related Hearing Loss. *Front Neurosci*, 12, 527.
- ALVARADO, J. C., FUENTES-SANTAMARÍA, V., GABALDÓN-ULL, M. C. & JUIZ, J. M. 2019. Age-Related Hearing Loss Is Accelerated by Repeated Short-Duration Loud Sound Stimulation. *Frontiers in neuroscience*, 13, 77-77.
- ALVARADO, J. C., FUENTES-SANTAMARÍA, V., MELGAR-ROJAS, P., VALERO, M. L., GABALDÓN-ULL, M. C., MILLER, J. M. & JUIZ, J. M. 2015. Synergistic effects of free radical scavengers and cochlear vasodilators: a new otoprotective strategy for age-related hearing loss. *Front Aging Neurosci*, 7, 86.
- ANDERSON, D. W., PROBST, F. J., BELYANTSEVA, I. A., FRIDELL, R. A., BEYER, L., MARTIN, D. M., WU, D., KACHAR, B., FRIEDMAN, T. B., RAPHAEL, Y. & CAMPER, S. A. 2000. The

- motor and tail regions of myosin XV are critical for normal structure and function of auditory and vestibular hair cells. *Human Molecular Genetics*, 9, 1729-1738.
- APPENRODT, P. & KROS, C. J. Single-channel recordings of large conductance Ca²⁺-activated K⁺ channels from guinea-pig inner hair cells. 1997 1997. CAMBRIDGE UNIV PRESS 40 WEST 20TH STREET, NEW YORK, NY 10011-4211, P147-P147.
- ARNOLD, T., OESTREICHER, E., EHRENBERGER, K. & FELIX, D. 1998. GABA(A) receptor modulates the activity of inner hair cell afferents in guinea pig cochlea. *Hear Res*, 125, 147-53.
- ART, J. J., CRAWFORD, A. C., FETTIPLACE, R. & FUCHS, P. A. 1985. Efferent modulation of hair cell tuning in the cochlea of the turtle. *J Physiol*, 360, 397-421.
- ART, J. J., FETTIPLACE, R. & FUCHS, P. A. 1984. Synaptic hyperpolarization and inhibition of turtle cochlear hair cells. *J Physiol*, 356, 525-50.
- ASHMORE, J. 2008. Cochlear Outer Hair Cell Motility. *Physiological Reviews*, 88, 173-210.
- ASHMORE, J. F. 1987. A fast motile response in guinea-pig outer hair cells: the cellular basis of the cochlear amplifier. *J Physiol*, 388, 323-47.
- ASSAD, J. A., SHEPHERD, G. M. G. & COREY, D. P. 1991. Tip-link integrity and mechanical transduction in vertebrate hair cells. *Neuron*, 7, 985-994.
- BAHLOUL, A., MICHEL, V., HARDELIN, J.-P., NOUAILLE, S., HOOS, S., HOUDUSSE, A., ENGLAND, P. & PETIT, C. 2010. Cadherin-23, myosin VIIa and harmonin, encoded by Usher syndrome type I genes, form a ternary complex and interact with membrane phospholipids. *Human Molecular Genetics*, 19, 3557-3565.
- BAILEY, G. P. & SEWELL, W. F. 2000. Calcitonin gene-related peptide suppresses hair cell responses to mechanical stimulation in the *Xenopus* lateral line organ. *J Neurosci*, 20, 5163-9.
- BARCLAY, M., RYAN, A. F. & HOUSLEY, G. D. 2011. Type I vs type II spiral ganglion neurons exhibit differential survival and neuritogenesis during cochlear development. *Neural Development*, 6, 33.
- BARED, A., OUYANG, X., ANGELI, S., DU, L. L., HOANG, K., YAN, D. & LIU, X. Z. 2010. Antioxidant enzymes, presbycusis, and ethnic variability. *Otolaryngology--head and neck surgery : official journal of American Academy of Otolaryngology-Head and Neck Surgery*, 143, 263-268.

- BASNER, M., BABISCH, W., DAVIS, A., BRINK, M., CLARK, C., JANSSEN, S. & STANSFELD, S. 2014. Auditory and non-auditory effects of noise on health. *The Lancet*, 383, 1325-1332.
- BECKER, L., SCHNEE, M. E., NIWA, M., SUN, W., MAXEINER, S., TALAEI, S., KACHAR, B., RUTHERFORD, M. A. & RICCI, A. J. 2018. The presynaptic ribbon maintains vesicle populations at the hair cell afferent fiber synapse. *Elife*, 7.
- BELYANTSEVA, I. A., BOGER, E. T. & FRIEDMAN, T. B. 2003. Myosin XVa localizes to the tips of inner ear sensory cell stereocilia and is essential for staircase formation of the hair bundle. *Proceedings of the National Academy of Sciences*, 100, 13958.
- BEURG, M., FETTIPLACE, R., NAM, J.-H. & RICCI, A. J. 2009a. Localization of inner hair cell mechanotransducer channels using high-speed calcium imaging. *Nature Neuroscience*, 12, 553-558.
- BEURG, M., FETTIPLACE, R., NAM, J. H. & RICCI, A. J. 2009b. Localization of inner hair cell mechanotransducer channels using high-speed calcium imaging. *Nat Neurosci*, 12, 553-8.
- BEURG, M., XIONG, W., ZHAO, B., MÜLLER, U. & FETTIPLACE, R. 2015. Subunit determination of the conductance of hair-cell mechanotransducer channels. *Proceedings of the National Academy of Sciences*, 112, 1589.
- BEUTNER, D. & MOSER, T. 2001. The presynaptic function of mouse cochlear inner hair cells during development of hearing. *Journal of Neuroscience*, 21, 4593-4599.
- BHATTACHARYYA, T. K. & DAYAL, V. S. 1989. Influence of age on hair cell loss in the rabbit cochlea. *Hear Res*, 40, 179-83.
- BILODEAU-MERCURE, M., LORTIE, C. L., SATO, M., GUITTON, M. J. & TREMBLAY, P. 2015. The neurobiology of speech perception decline in aging. *Brain Structure and Function*, 220, 979-997.
- BLAKLEY, B. W., SEAMAN, M. & ALENEZI, A. 2020. Brain-derived nerve growth factor in the cochlea – a reproducibility study. *Journal of Otolaryngology - Head & Neck Surgery*, 49, 37.
- BOLZ, H., VON BREDERLOW, B., RAMÍREZ, A., BRYDA, E. C., KUTSCHE, K., NOTHWANG, H. G., SEELIGER, M., CABRERA, M. D. C. S., VILA, M. C., MOLINA, O. P., GAL, A. & KUBISCH, C. 2001. Mutation of CDH23, encoding a new member of the cadherin gene family, causes Usher syndrome type 1D. *Nature Genetics*, 27, 108-112.

- BORK, J. M., PETERS, L. M., RIAZUDDIN, S., BERNSTEIN, S. L., AHMED, Z. M., NESS, S. L., POLOMENO, R., RAMESH, A., SCHLOSS, M., SRISAILPATHY, C. R., WAYNE, S., BELLMAN, S., DESMUKH, D., AHMED, Z., KHAN, S. N., KALOUSTIAN, V. M., LI, X. C., LALWANI, A., BITNER-GLINDZICZ, M., NANCE, W. E., LIU, X. Z., WISTOW, G., SMITH, R. J., GRIFFITH, A. J., WILCOX, E. R., FRIEDMAN, T. B. & MORELL, R. J. 2001. Usher syndrome 1D and nonsyndromic autosomal recessive deafness DFNB12 are caused by allelic mutations of the novel cadherin-like gene CDH23. *American journal of human genetics*, 68, 26-37.
- BORON, W. F. & BOULPAEP, E. L. 2012. *Medical Physiology, 2e Updated Edition: with STUDENT CONSULT Online Access*, Saunders.
- BOWL, M. R. & DAWSON, S. J. 2015. The Mouse as a Model for Age-Related Hearing Loss - A Mini-Review. *Gerontology*, 61, 149-157.
- BOËDA, B., EL-AMRAOUI, A., BAHLOUL, A., GOODYEAR, R., DAVIET, L., BLANCHARD, S., PERFETTINI, I., FATH, K. R., SHORTE, S., REINERS, J., HOUDUSSE, A., LEGRAIN, P., WOLFRUM, U., RICHARDSON, G. & PETIT, C. 2002. Myosin VIIa, harmonin and cadherin 23, three Usher I gene products that cooperate to shape the sensory hair cell bundle. *The EMBO journal*, 21, 6689-6699.
- BOËDA, B., WEIL, D. & PETIT, C. 2001. A specific promoter of the sensory cells of the inner ear defined by transgenesis. *Human Molecular Genetics*, 10, 1581-1589.
- BRANDT, A., KHIMICH, D. & MOSER, T. 2005. Few CaV1.3 channels regulate the exocytosis of a synaptic vesicle at the hair cell ribbon synapse. *The Journal of neuroscience : the official journal of the Society for Neuroscience*, 25, 11577-11585.
- BRANDT, A., STRIESSNIG, J. & MOSER, T. 2003. CaV1.3 channels are essential for development and presynaptic activity of cochlear inner hair cells. *The Journal of neuroscience : the official journal of the Society for Neuroscience*, 23, 10832-10840.
- BROWN, M. C. 1987. Morphology of labeled efferent fibers in the guinea pig cochlea. *J Comp Neurol*, 260, 605-18.
- BROWN, M. C. 2014. Single-unit labeling of medial olivocochlear neurons: the cochlear frequency map for efferent axons. *Journal of neurophysiology*, 111, 2177-2186.
- BROWN, M. C. & NUTTALL, A. L. 1984. Efferent control of cochlear inner hair cell responses in the guinea-pig. *J Physiol*, 354, 625-46.

- BROWN, M. C., NUTTALL, A. L. & MASTA, R. I. 1983. Intracellular recordings from cochlear inner hair cells: effects of stimulation of the crossed olivocochlear efferents. *Science*, 222, 69-72.
- BROWN, S. D. & STEEL, K. P. 1994. Genetic deafness--progress with mouse models. *Human Molecular Genetics*, 3, 1453-1456.
- BROWNELL, W. E. 1983. Observation on a motile response in isolated outer hair cells. *Mechanisms of Hearing*. Monash University Press, Clayton, Australia.
- BROWNELL, W. E., BADER, C. R., BERTRAND, D. & DE RIBAUPIERRE, Y. 1985. Evoked mechanical responses of isolated cochlear outer hair cells. *Science*, 227, 194.
- BRUCE, L. L., CHRISTENSEN, M. A. & FRITZSCH, B. 1997. Electron microscopic differentiation of directly and transneuronally transported Dil and applications for studies of synaptogenesis. *Journal of Neuroscience Methods*, 73, 107-112.
- BRUCE, L. L., CHRISTENSEN, M. A. & WARR, W. B. 2000. Postnatal development of efferent synapses in the rat cochlea. *Journal of Comparative Neurology*, 423, 532-548.
- C KOHRMAN, D., WAN, G., CASSINOTTI, L. & CORFAS, G. 2020. Hidden Hearing Loss: A Disorder with Multiple Etiologies and Mechanisms. *Cold Spring Harbor perspectives in medicine*, 10, a035493.
- CABERLOTTO, E., MICHEL, V., FOUCHER, I., BAHLOUL, A., GOODYEAR, R. J., PEPERMANS, E., MICHALSKI, N., PERFETTINI, I., ALEGRIA-PRÉVOT, O., CHARDENOUX, S., DO CRUZEIRO, M., HARDELIN, J.-P., RICHARDSON, G. P., AVAN, P., WEIL, D. & PETIT, C. 2011a. Usher type 1G protein sans is a critical component of the tip-link complex, a structure controlling actin polymerization in stereocilia. *Proceedings of the National Academy of Sciences*, 108, 5825.
- CABERLOTTO, E., MICHEL, V., FOUCHER, I., BAHLOUL, A., GOODYEAR, R. J., PEPERMANS, E., MICHALSKI, N., PERFETTINI, I., ALEGRIA-PRÉVOT, O., CHARDENOUX, S., DO CRUZEIRO, M., HARDELIN, J.-P., RICHARDSON, G. P., AVAN, P., WEIL, D. & PETIT, C. 2011b. Usher type 1G protein sans is a critical component of the tip-link complex, a structure controlling actin polymerization in stereocilia. *Proceedings of the National Academy of Sciences*, 108, 5825-5830.
- CAI, Q., VETHANAYAGAM, R. R., YANG, S., BARD, J., JAMISON, J., CARTWRIGHT, D., DONG, Y. & HU, B. H. 2014. Molecular profile of cochlear immunity in the resident cells of the organ of Corti. *J Neuroinflammation*, 11, 173.

- CHABA 1988. Speech understanding and aging. *Journal of the Acoustical Society of America*, 83, 859-895.
- CHEN, G. Y. & NUÑEZ, G. 2010. Sterile inflammation: sensing and reacting to damage. *Nature Reviews Immunology*, 10, 826-837.
- CHEUNG, E. L. & COREY, D. P. 2006. Ca²⁺ changes the force sensitivity of the hair-cell transduction channel. *Biophys J*, 90, 124-39.
- CHIN, H. J., LEE, S.-Y. & LEE, D. 2020. Tamoxifen-inducible cardiac-specific Cre transgenic mouse using VIPR2 intron. *Laboratory Animal Research*, 36, 31.
- CHOE, Y., MAGNASCO, M. O. & HUDSPETH, A. J. 1998. A model for amplification of hair-bundle motion by cyclical binding of Ca²⁺ to mechanoelectrical-transduction channels. *Proc Natl Acad Sci U S A*, 95, 15321-6.
- CHRISTENSEN, K., FREDERIKSEN, H. & HOFFMAN, H. J. 2001. Genetic and environmental influences on self-reported reduced hearing in the old and oldest old. *J Am Geriatr Soc*, 49, 1512-7.
- CHURCH, M. W. & SHUCARD, D. W. 1986. Age-Related Hearing Loss in BDF1 Mice as Evidenced by the Brainstem Auditory Evoked Potential¹. *Audiology*, 25, 363-372.
- CLARK, W. W. & BOHNE, B. A. 1999. Effects of noise on hearing. *Jama*, 281, 1658-9.
- CLAUSE, A., KIM, G., SONNTAG, M., WEISZ, C. J., VETTER, D. E., RÚBSAMEN, R. & KANDLER, K. 2014. The precise temporal pattern of prehearing spontaneous activity is necessary for tonotopic map refinement. *Neuron*, 82, 822-35.
- CLAUSE, A., LAUER, A. M. & KANDLER, K. 2017. Mice Lacking the Alpha9 Subunit of the Nicotinic Acetylcholine Receptor Exhibit Deficits in Frequency Difference Limens and Sound Localization. *Front Cell Neurosci*, 11, 167.
- CODY, A. R. & RUSSELL, I. J. 1987. The response of hair cells in the basal turn of the guinea-pig cochlea to tones. *The Journal of physiology*, 383, 551-569.
- COREY, D. P. & HUDSPETH, A. J. 1979. Ionic basis of the receptor potential in a vertebrate hair cell. *Nature*, 281, 675-677.
- COREY, D. P. & HUDSPETH, A. J. 1983. Kinetics of the receptor current in bullfrog saccular hair cells. *The Journal of neuroscience : the official journal of the Society for Neuroscience*, 3, 962-976.
- CORNS, L. F., BARDHAN, T., HOUSTON, O., OLT, J., HOLLEY, M. C., MASETTO, S., JOHNSON, S. L. & MARCOTTI, W. 2014a. Chapter 6 - Functional Development of Hair Cells in the

- Mammalian Inner Ear. In: ROMAND, R. & VARELA-NIETO, I. (eds.) *Development of Auditory and Vestibular Systems*. San Diego: Academic Press.
- CORNS, L. F., JOHNSON, S. L., KROS, C. J. & MARCOTTI, W. 2014b. Calcium entry into stereocilia drives adaptation of the mechano-electrical transducer current of mammalian cochlear hair cells. *Proceedings of the National Academy of Sciences*, 111, 14918.
- CORNS, L. F., JOHNSON, S. L., ROBERTS, T., RANATUNGA, K. M., HENDRY, A., CERIANI, F., SAFIEDDINE, S., STEEL, K. P., FORGE, A., PETIT, C., FURNESS, D. N., KROS, C. J. & MARCOTTI, W. 2018. Mechanotransduction is required for establishing and maintaining mature inner hair cells and regulating efferent innervation. *Nature Communications*, 9, 4015.
- CRAWFORD, A. C., EVANS, M. G. & FETTIPLACE, R. 1989. Activation and adaptation of transducer currents in turtle hair cells. *The Journal of Physiology*, 419, 405-434.
- CRAWFORD, A. C., EVANS, M. G. & FETTIPLACE, R. 1991. The actions of calcium on the mechano-electrical transducer current of turtle hair cells. *J Physiol*, 434, 369-98.
- CROWE, S. J., GUILD, S. R. & POLVOGT, L. M. 1934. Observations on the pathology of high-tone deafness. *The Journal of Nervous and Mental Disease*, 80, 480.
- CRUICKSHANKS, K. J., KLEIN, R., KLEIN, B. E., WILEY, T. L., NONDAHL, D. M. & TWEED, T. S. 1998a. Cigarette smoking and hearing loss: the epidemiology of hearing loss study. *Jama*, 279, 1715-9.
- CRUICKSHANKS, K. J., WILEY, T. L., TWEED, T. S., KLEIN, B. E., KLEIN, R., MARES-PERLMAN, J. A. & NONDAHL, D. M. 1998b. Prevalence of hearing loss in older adults in Beaver Dam, Wisconsin. The Epidemiology of Hearing Loss Study. *Am J Epidemiol*, 148, 879-86.
- DALLOS, P. 2008. Cochlear amplification, outer hair cells and prestin. *Current Opinion in Neurobiology*, 18, 370-376.
- DALLOS, P. & HARRIS, D. 1978. Properties of auditory nerve responses in absence of outer hair cells. *J Neurophysiol*, 41, 365-83.
- DALTON, D. S., CRUICKSHANKS, K. J., KLEIN, R., KLEIN, B. E. & WILEY, T. L. 1998. Association of NIDDM and hearing loss. *Diabetes Care*, 21, 1540-4.

- DARROW, K. N., SIMONS, E. J., DODDS, L. & LIBERMAN, M. C. 2006. Dopaminergic innervation of the mouse inner ear: evidence for a separate cytochemical group of cochlear efferent fibers. *J Comp Neurol*, 498, 403-14.
- DAVIES, L. C. & TAYLOR, P. R. 2015. Tissue-resident macrophages: then and now. *Immunology*, 144, 541-8.
- DE GRAAF, E. L., VERMEIJ, W. P., DE WAARD, M. C., RIJKSEN, Y., VAN DER PLUIJM, I., HOOGENRAAD, C. C., HOEIJMAKERS, J. H., ALTELAAR, A. F. & HECK, A. J. 2013. Spatio-temporal analysis of molecular determinants of neuronal degeneration in the aging mouse cerebellum. *Mol Cell Proteomics*, 12, 1350-62.
- DELANO, P. H., ELGUEDA, D., HAMAME, C. M. & ROBLES, L. 2007. Selective attention to visual stimuli reduces cochlear sensitivity in chinchillas. *J Neurosci*, 27, 4146-53.
- DELPAT, B., MICHEL, V., GOODYEAR, R., YAMASAKI, Y., MICHALSKI, N., EL-AMRAOUI, A., PERFETTINI, I., LEGRAIN, P., RICHARDSON, G., HARDELIN, J.-P. & PETIT, C. 2004. Myosin XVa and whirlin, two deafness gene products required for hair bundle growth, are located at the stereocilia tips and interact directly. *Human Molecular Genetics*, 14, 401-410.
- DOLAN, D. F. & NUTTALL, A. L. 1988. Masked cochlear whole-nerve response intensity functions altered by electrical stimulation of the crossed olivocochlear bundle. *The Journal of the Acoustical Society of America*, 83, 1081-1086.
- DOMINIK, O., MARLIES, K., CHRISTIAN, D. & BERND, F. 2003. Resting Potential and Submembrane Calcium Concentration of Inner Hair Cells in the Isolated Mouse Cochlea Are Set by KCNQ-Type Potassium Channels. *The Journal of Neuroscience*, 23, 2141.
- DONG, Y., ZHANG, C., FRYE, M., YANG, W., DING, D., SHARMA, A., GUO, W. & HU, B. H. 2018. Differential fates of tissue macrophages in the cochlea during postnatal development. *Hear Res*, 365, 110-126.
- DONOCOFF, R. S., TETELOSHVILI, N., CHUNG, H., SHOULSON, R. & CREUSOT, R. J. 2020. Optimization of tamoxifen-induced Cre activity and its effect on immune cell populations. *Scientific Reports*, 10, 15244.
- DUBLIN, W. B. 1976. The Combined Correlated Audiohistogram: Incorporation of the Superior Ventral Cochlear Nucleus. *Annals of Otology, Rhinology & Laryngology*, 85, 813-819.

- DULON, D. & LENOIR, M. 1996. Cholinergic responses in developing outer hair cells of the rat cochlea. *Eur J Neurosci*, 8, 1945-52.
- DULON, D., SAFIEDDINE, S., JONES, S. M. & PETIT, C. 2009. Otoferlin is critical for a highly sensitive and linear calcium-dependent exocytosis at vestibular hair cell ribbon synapses. *J Neurosci*, 29, 10474-87.
- ECHTELER, S. M. 1992. Developmental segregation in the afferent projections to mammalian auditory hair cells. *Proceedings of the National Academy of Sciences*, 89, 6324.
- EHRET, G. 1983. Development of hearing and response behavior to sound stimuli: behavioral studies. In: ROMAND, R. (ed.) *Development of the Auditory and Vestibular Systems*. New York: Academic Press.
- ELGOYHEN, A. B., JOHNSON, D. S., BOULTER, J., VETTER, D. E. & HEINEMANN, S. 1994. $\alpha 9$: An acetylcholine receptor with novel pharmacological properties expressed in rat cochlear hair cells. *Cell*, 79, 705-715.
- ELGOYHEN, A. B., VETTER, D. E., KATZ, E., ROTHLIN, C. V., HEINEMANN, S. F. & BOULTER, J. 2001. $\alpha 10$: a determinant of nicotinic cholinergic receptor function in mammalian vestibular and cochlear mechanosensory hair cells. *Proceedings of the National Academy of Sciences of the United States of America*, 98, 3501-3506.
- ELGOYHEN, A. B., WEDEMEYER, C. & N. DI GUILMI, M. 2018. Efferent Innervation to the Cochlea. In: KANDLER, K. (ed.). Oxford University Press.
- ELLIOTT, S. J. & SHERA, C. A. 2012. The cochlea as a smart structure. *Smart materials & structures*, 21, 64001-64001.
- EMADI, G., RICHTER, C.-P. & DALLOS, P. 2004. Stiffness of the Gerbil Basilar Membrane: Radial and Longitudinal Variations. *Journal of Neurophysiology*, 91, 474-488.
- ERNFORS, P., VAN DE WATER, T., LORING, J. & JAENISCH, R. 1995. Complementary roles of BDNF and NT-3 in vestibular and auditory development. *Neuron*, 14, 1153-64.
- ERWAY, L. C., WILLOTT, J. F., ARCHER, J. R. & HARRISON, D. E. 1993. Genetics of age-related hearing loss in mice: I. Inbred and F1 hybrid strains. *Hearing Research*, 65, 125-132.
- EVANS, M. G. 1996. Acetylcholine activates two currents in guinea-pig outer hair cells. *The Journal of Physiology*, 491, 563-578.
- EYBALIN, M. 1993. Neurotransmitters and neuromodulators of the mammalian cochlea. *Physiological Reviews*, 73, 309-373.

- EYBALIN, M., CAICEDO, A., RENARD, N., RUEL, J. & PUEL, J.-L. 2004. Transient Ca²⁺-permeable AMPA receptors in postnatal rat primary auditory neurons. *European Journal of Neuroscience*, 20, 2981-2989.
- EYBALIN, M., RENARD, N., AURE, F. & SAFIEDDINE, S. 2002. Cysteine-string protein in inner hair cells of the organ of Corti: synaptic expression and upregulation at the onset of hearing. *Eur J Neurosci*, 15, 1409-20.
- FANG, J., ZHANG, W. C., YAMASHITA, T., GAO, J., ZHU, M. S. & ZUO, J. 2012. Outer hair cell-specific prestin-CreERT2 knockin mouse lines. *Genesis*, 50, 124-31.
- FANG, Q., INDZHYKULIAN, A. A., MUSTAPHA, M., RIORDAN, G. P., DOLAN, D. F., FRIEDMAN, T. B., BELYANTSEVA, I. A., FROLENKOV, G. I., CAMPER, S. A. & BIRD, J. E. 2015. The 133-kDa N-terminal domain enables myosin 15 to maintain mechanotransducing stereocilia and is essential for hearing. *Elife*, 4.
- FEIL, R., BROCARD, J., MASCREZ, B., LEMEURE, M., METZGER, D. & CHAMBON, P. 1996. Ligand-activated site-specific recombination in mice. *Proc Natl Acad Sci U S A*, 93, 10887-90.
- FEIL, R., WAGNER, J., METZGER, D. & CHAMBON, P. 1997. Regulation of Cre recombinase activity by mutated estrogen receptor ligand-binding domains. *Biochem Biophys Res Commun*, 237, 752-7.
- FEIL, S., VALTCHEVA, N. & FEIL, R. 2009. Inducible Cre mice. *Methods Mol Biol*, 530, 343-63.
- FELIX, D. & EHRENBERGER, K. 1992. The efferent modulation of mammalian inner hair cell afferents. *Hear Res*, 64, 1-5.
- FERNANDEZ, K. A., JEFFERS, P. W. C., LALL, K., LIBERMAN, M. C. & KUJAWA, S. G. 2015. Aging after noise exposure: acceleration of cochlear synaptopathy in "recovered" ears. *The Journal of neuroscience : the official journal of the Society for Neuroscience*, 35, 7509-7520.
- FETONI, A. R., PICCIOTTI, P. M., PALUDETTI, G. & TROIANI, D. 2011. Pathogenesis of presbycusis in animal models: A review. *Experimental Gerontology*, 46, 413-425.
- FETTIPLACE, R. & HACKNEY, C. M. 2006. The sensory and motor roles of auditory hair cells. *Nature Reviews Neuroscience*, 7, 19-29.
- FETTIPLACE, R. & KIM, K. X. 2014. The physiology of mechano-electrical transduction channels in hearing. *Physiol Rev*, 94, 951-86.

- FLOCK, A. & RUSSELL, I. J. 1973. The post-synaptic action of efferent fibres in the lateral line organ of the burbot *Lota lota*. *The Journal of physiology*, 235, 591-605.
- FRANK, M. M. & GOODRICH, L. V. 2018. Talking back: Development of the olivocochlear efferent system. *Wiley Interdiscip Rev Dev Biol*, 7, e324.
- FRANSEN, E., LEMKENS, N., VAN LAER, L. & VAN CAMP, G. 2003. Age-related hearing impairment (ARHI): environmental risk factors and genetic prospects. *Exp Gerontol*, 38, 353-9.
- FREDELIUS, L. & RASK-ANDERSEN, H. 1990. The role of macrophages in the disposal of degeneration products within the organ of corti after acoustic overstimulation. *Acta Oto-Laryngologica*, 109, 76-82.
- FRITZSCH, B., TESSAROLLO, L., COPPOLA, E. & REICHARDT, L. F. 2004. Neurotrophins in the ear: their roles in sensory neuron survival and fiber guidance. *Prog Brain Res*, 146, 265-78.
- FRYE, M. D., RYAN, A. F. & KURABI, A. 2019. Inflammation associated with noise-induced hearing loss. *J Acoust Soc Am*, 146, 4020.
- FRYE, M. D., YANG, W., ZHANG, C., XIONG, B. & HU, B. H. 2017. Dynamic activation of basilar membrane macrophages in response to chronic sensory cell degeneration in aging mouse cochleae. *Hear Res*, 344, 125-134.
- FRYE, M. D., ZHANG, C. & HU, B. H. 2018. Lower level noise exposure that produces only TTS modulates the immune homeostasis of cochlear macrophages. *J Neuroimmunol*, 323, 152-166.
- FUJIOKA, M., KANZAKI, S., OKANO, H. J., MASUDA, M., OGAWA, K. & OKANO, H. 2006. Proinflammatory cytokines expression in noise-induced damaged cochlea. *J Neurosci Res*, 83, 575-83.
- FUKUI, H., WONG, H. T., BEYER, L. A., CASE, B. G., SWIDERSKI, D. L., DI POLO, A., RYAN, A. F. & RAPHAEL, Y. 2012. BDNF gene therapy induces auditory nerve survival and fiber sprouting in deaf *Pou4f3* mutant mice. *Scientific Reports*, 2, 838.
- FURMAN, A. C., KUJAWA, S. G. & LIBERMAN, M. C. 2013. Noise-induced cochlear neuropathy is selective for fibers with low spontaneous rates. *J Neurophysiol*, 110, 577-86.
- FURNESS, D. N. & HACKNEY, C. M. 1985. Cross-links between stereocilia in the guinea pig cochlea. *Hear Res*, 18, 177-88.

- FURNESS, D. N., KATORI, Y., NIRMAL KUMAR, B. & HACKNEY, C. M. 2008. The dimensions and structural attachments of tip links in mammalian cochlear hair cells and the effects of exposure to different levels of extracellular calcium. *Neuroscience*, 154, 10-21.
- GALAMBOS, R. 1956. Suppression of auditory nerve activity by stimulation of efferent fibers to cochlea. *J Neurophysiol*, 19, 424-37.
- GATES, G. A. 2012. Central Presbycusis: An Emerging View. *Otolaryngology–Head and Neck Surgery*, 147, 1-2.
- GATES, G. A., COUROPMITREE, N. N. & MYERS, R. H. 1999. Genetic associations in age-related hearing thresholds. *Arch Otolaryngol Head Neck Surg*, 125, 654-9.
- GATES, G. A., MILLS, D., NAM, B. H., D'AGOSTINO, R. & RUBEL, E. W. 2002. Effects of age on the distortion product otoacoustic emission growth functions. *Hear Res*, 163, 53-60.
- GATES, G. A. & MILLS, J. H. 2005. Presbycusis. *The Lancet*, 366, 1111-1120.
- GATES, G. A., SCHMID, P., KUJAWA, S. G., NAM, B. & D'AGOSTINO, R. 2000. Longitudinal threshold changes in older men with audiometric notches. *Hear Res*, 141, 220-8.
- GIBSON, F., WALSH, J., MBURU, P., VARELA, A., BROWN, K. A., ANTONIO, M., BEISEL, K. W., STEEL, K. P. & BROWN, S. D. M. 1995. A type VII myosin encoded by the mouse deafness gene shaker-1. *Nature*, 374, 62-64.
- GIFFORD, M. L. & GUINAN, J. J., JR. 1987. Effects of electrical stimulation of medial olivocochlear neurons on ipsilateral and contralateral cochlear responses. *Hear Res*, 29, 179-94.
- GILLESPIE, P. G., WAGNER, M. C. & HUDSPETH, A. J. 1993. Identification of a 120 kd hair-bundle myosin located near stereociliary tips. *Neuron*, 11, 581-594.
- GINHOUX, F., GRETER, M., LEBOEUF, M., NANDI, S., SEE, P., GOKHAN, S., MEHLER, M. F., CONWAY, S. J., NG, L. G., STANLEY, E. R., SAMOKHVALOV, I. M. & MERAD, M. 2010. Fate mapping analysis reveals that adult microglia derive from primitive macrophages. *Science*, 330, 841-5.
- GINHOUX, F. & GUILLIAMS, M. 2016. Tissue-Resident Macrophage Ontogeny and Homeostasis. *Immunity*, 44, 439-449.
- GLOWATZKI, E. & FUCHS, P. A. 2000. Cholinergic Synaptic Inhibition of Inner Hair Cells in the Neonatal Mammalian Cochlea. *Science*, 288, 2366.

- GLOWATZKI, E. & FUCHS, P. A. 2002. Transmitter release at the hair cell ribbon synapse. *Nature Neuroscience*, 5, 147-154.
- GOMAN, A. M., REED, N. S. & LIN, F. R. 2017. Addressing Estimated Hearing Loss in Adults in 2060. *JAMA otolaryngology-- head & neck surgery*, 143, 733-734.
- GOODYEAR, R. J., MARCOTTI, W., KROS, C. J. & RICHARDSON, G. P. 2005. Development and properties of stereociliary link types in hair cells of the mouse cochlea. *Journal of Comparative Neurology*, 485, 75-85.
- GOUTMAN, J. D., FUCHS, P. A. & GLOWATZKI, E. 2005. Facilitating efferent inhibition of inner hair cells in the cochlea of the neonatal rat. *J Physiol*, 566, 49-59.
- GRANT, L., YI, E. & GLOWATZKI, E. 2010. Two modes of release shape the postsynaptic response at the inner hair cell ribbon synapse. *J Neurosci*, 30, 4210-20.
- GRATI, M. H. & KACHAR, B. 2011. Myosin VIIa and sans localization at stereocilia upper tip-link density implicates these Usher syndrome proteins in mechanotransduction. *Proceedings of the National Academy of Sciences of the United States of America*, 108, 11476-11481.
- GRATTON, M. A., SCHMIEDT, R. A. & SCHULTE, B. A. 1996. Age-related decreases in endocochlear potential are associated with vascular abnormalities in the stria vascularis. *Hearing Research*, 102, 181-190.
- GRATTON, M. A., SCHULTE, B. A. & SMYTHE, N. M. 1997a. Quantification of the stria vascularis and strial capillary areas in quiet-reared young and aged gerbils. *Hear Res*, 114, 1-9.
- GRATTON, M. A., SMYTH, B. J., LAM, C. F., BOETTCHER, F. A. & SCHMIEDT, R. A. 1997b. Decline in the endocochlear potential corresponds to decreased Na,K-ATPase activity in the lateral wall of quiet-aged gerbils. *Hear Res*, 108, 9-16.
- GRILLET, N., XIONG, W., REYNOLDS, A., KAZMIERCZAK, P., SATO, T., LILLO, C., DUMONT, R. A., HINTERMANN, E., SCZANIECKA, A., SCHWANDER, M., WILLIAMS, D., KACHAR, B., GILLESPIE, P. G. & MÜLLER, U. 2009. Harmonin mutations cause mechanotransduction defects in cochlear hair cells. *Neuron*, 62, 375-387.
- GROFF, J. A. & LIBERMAN, M. C. 2003. Modulation of Cochlear Afferent Response by the Lateral Olivocochlear System: Activation Via Electrical Stimulation of the Inferior Colliculus. *Journal of Neurophysiology*, 90, 3178-3200.

- GUINAN, J. J., JR. 2006. Olivocochlear efferents: anatomy, physiology, function, and the measurement of efferent effects in humans. *Ear Hear*, 27, 589-607.
- GUINAN, J. J., RYUGO, D. K., FAY, R. R. & POPPER, A. N. 2011. Auditory and vestibular efferents.
- GUINAN, J. J. & STANKOVIC, K. M. 1996. Medial efferent inhibition produces the largest equivalent attenuations at moderate to high sound levels in cat auditory-nerve fibers. *The Journal of the Acoustical Society of America*, 100, 1680-1690.
- GUINAN JR, J. J., WARR, W. B. & NORRIS, B. E. 1983. Differential olivocochlear projections from lateral versus medial zones of the superior olivary complex. *Journal of Comparative Neurology*, 221, 358-370.
- HANSEN, C. C. & RESKE-NIELSEN, E. 1965. Pathological Studies in Presbycusis: Cochlear and Central Findings in 12 Aged Patients. *Archives of Otolaryngology*, 82, 115-132.
- HARRISON, R. V. & EVANS, E. F. 1979. Cochlear fibre responses in guinea pigs with well defined cochlear lesions. *Scand Audiol Suppl*, 83-92.
- HE, D. Z. & DALLOS, P. 1999. Development of acetylcholine-induced responses in neonatal gerbil outer hair cells. *J Neurophysiol*, 81, 1162-70.
- HE, D. Z. Z., EVANS, B. N. & DALLOS, P. 1994. First appearance and development of electromotility in neonatal gerbil outer hair cells. *Hearing Research*, 78, 77-90.
- HE, W., YU, J., SUN, Y. & KONG, W. 2020. Macrophages in Noise-Exposed Cochlea: Changes, Regulation and the Potential Role. *Aging Dis*, 11, 191-199.
- HEIDRYCH, P., ZIMMERMANN, U., KUHN, S., FRANZ, C., ENGEL, J., DUNCKER, S. V., HIRT, B., PUSCH, C. M., RUTH, P., PFISTER, M., MARCOTTI, W., BLIN, N. & KNIPPER, M. 2009. Otoferlin interacts with myosin VI: implications for maintenance of the basolateral synaptic structure of the inner hair cell. *Human Molecular Genetics*, 18, 2779-2790.
- HENRY, K. R. & CHOLE, R. A. 1980. Genotypic Differences in Behavioral, Physiological and Anatomical Expressions of Age-Related Hearing Loss in the Laboratory Mouse: Original Papers Travaux originaux. *Audiology*, 19, 369-383.
- HICKOK, G., HOUDE, J. & RONG, F. 2011. Sensorimotor Integration in Speech Processing: Computational Basis and Neural Organization. *Neuron*, 69, 407-422.
- HICKOK, G. & POEPEL, D. 2007. The cortical organization of speech processing. *Nature Reviews Neuroscience*, 8, 393-402.

- HIROSE, K., DISCOLO, C. M., KEASLER, J. R. & RANSOHOFF, R. 2005. Mononuclear phagocytes migrate into the murine cochlea after acoustic trauma. *J Comp Neurol*, 489, 180-94.
- HIROSE, K., LI, S. Z., OHLEMILLER, K. K. & RANSOHOFF, R. M. 2014. Systemic lipopolysaccharide induces cochlear inflammation and exacerbates the synergistic ototoxicity of kanamycin and furosemide. *J Assoc Res Otolaryngol*, 15, 555-70.
- HIROSE, K., RUTHERFORD, M. A. & WARCHOL, M. E. 2017. Two cell populations participate in clearance of damaged hair cells from the sensory epithelia of the inner ear. *Hearing Research*, 352, 70-81.
- HIROSE, K. & SATO, E. 2011. Comparative analysis of combination kanamycin-furosemide versus kanamycin alone in the mouse cochlea. *Hearing Research*, 272, 108-116.
- HOEFFEL, G. & GINHOUX, F. 2018. Fetal monocytes and the origins of tissue-resident macrophages. *Cell Immunol*, 330, 5-15.
- HOLT, J. R. & COREY, D. P. 2000. Two mechanisms for transducer adaptation in vertebrate hair cells. *Proceedings of the National Academy of Sciences of the United States of America*, 97, 11730-11735.
- HOSSAIN, W. A., ANTIC, S. D., YANG, Y., RASBAND, M. N. & MOREST, D. K. 2005. Where is the spike generator of the cochlear nerve? Voltage-gated sodium channels in the mouse cochlea. *J Neurosci*, 25, 6857-68.
- HOUGH, K., VERSCHUUR, C. A., CUNNINGHAM, C. & NEWMAN, T. A. 2022. Macrophages in the cochlea; an immunological link between risk factors and progressive hearing loss. *Glia*, 70, 219-238.
- HOUSLEY, G. D. & ASHMORE, J. F. 1992. Ionic currents of outer hair cells isolated from the guinea-pig cochlea. *The Journal of Physiology*, 448, 73-98.
- HOWARD, J. & HUDSPETH, A. J. 1987. Mechanical relaxation of the hair bundle mediates adaptation in mechano-electrical transduction by the bullfrog's saccular hair cell. *Proc Natl Acad Sci U S A*, 84, 3064-8.
- HOWARTH, A. & SHONE, G. R. 2006. Ageing and the auditory system. *Postgraduate Medical Journal*, 82, 166.
- HRIBERNIK, M. & VOLAVŠEK, M. 2016. Ear and Temporal Bone. In: VOLAVŠEK, M. (ed.) *Head and Neck Pathology*. Cham: Springer International Publishing.

- HU, Y., ZHOU, L.-Q., LU, H.-T., YUAN, K. & GONG, S.-S. 2015. Excitotoxic effects of glutamate on cochlear organotypic cultures. *Journal of Huazhong University of Science and Technology [Medical Sciences]*, 35, 117-121.
- HUANG, L.-C., BARCLAY, M., LEE, K., PETER, S., HOUSLEY, G. D., THORNE, P. R. & MONTGOMERY, J. M. 2012. Synaptic profiles during neurite extension, refinement and retraction in the developing cochlea. *Neural development*, 7, 38-38.
- HUANG, L.-C., THORNE, P. R., HOUSLEY, G. D. & MONTGOMERY, J. M. 2007. Spatiotemporal definition of neurite outgrowth, refinement and retraction in the developing mouse cochlea. *Development*, 134, 2925.
- HUMPHRIES, C., LIEBENTHAL, E. & BINDER, J. R. 2010. Tonotopic organization of human auditory cortex. *Neuroimage*, 50, 1202-11.
- HUNTER, K. P. & WILLOTT, J. F. 1987a. Aging and the auditory brainstem response in mice with severe or minimal presbycusis. *Hear Res*, 30, 207-18.
- HUNTER, K. P. & WILLOTT, J. F. 1987b. Aging and the auditory brainstem response in mice with severe or minimal presbycusis. *Hearing Research*, 30, 207-218.
- IMAI, Y., IBATA, I., ITO, D., OHSAWA, K. & KOHSAKA, S. 1996. A Novel Gene in the Major Histocompatibility Complex Class III Region Encoding an EF Hand Protein Expressed in a Monocytic Lineage. *Biochemical and Biophysical Research Communications*, 224, 855-862.
- INDRA, A. K., WAROT, X., BROCARD, J., BORNERT, J.-M., XIAO, J.-H., CHAMBON, P. & METZGER, D. 1999. Temporally-controlled site-specific mutagenesis in the basal layer of the epidermis: comparison of the recombinase activity of the tamoxifen-inducible Cre-ERT and Cre-ERT2 recombinases. *Nucleic Acids Research*, 27, 4324-4327.
- INGHAM, N. J., PEARSON, S. & STEEL, K. P. 2011. Using the auditory brainstem response (ABR) to determine sensitivity of hearing in mutant mice. *Current Protocols in Mouse Biology*, 1, 279-287.
- ITO, T., KURATA, N. & FUKUNAGA, Y. 2022. Tissue-Resident Macrophages in the Stria Vascularis. *Front Neurol*, 13, 818395.
- JABBA, S. V., OELKE, A., SINGH, R., MAGANTI, R. J., FLEMING, S., WALL, S. M., EVERETT, L. A., GREEN, E. D. & WANGEMANN, P. 2006. Macrophage invasion contributes to degeneration of stria vascularis in Pendred syndrome mouse model. *BMC Med*, 4, 37.

- JACOBSON, M., KIM, S., ROMNEY, J., ZHU, X. & FRISINA, R. D. 2003. Contralateral suppression of distortion-product otoacoustic emissions declines with age: a comparison of findings in CBA mice with human listeners. *Laryngoscope*, 113, 1707-13.
- JAFARI, Z., KOLB, B. E. & MOHAJERANI, M. H. 2019. Age-related hearing loss and tinnitus, dementia risk, and auditory amplification outcomes. *Ageing Research Reviews*, 56, 100963.
- JAHN, H. M., KASAKOW, C. V., HELFER, A., MICHELY, J., VERKHRATSKY, A., MAURER, H. H., SCHELLER, A. & KIRCHHOFF, F. 2018. Refined protocols of tamoxifen injection for inducible DNA recombination in mouse astroglia. *Scientific Reports*, 8, 5913.
- JENG, J.-Y., CARLTON, A. J., JOHNSON, S. L., BROWN, S. D. M., HOLLEY, M. C., BOWL, M. R. & MARCOTTI, W. 2021. Biophysical and morphological changes in inner hair cells and their efferent innervation in the ageing mouse cochlea. *The Journal of Physiology*, 599, 269-287.
- JENG, J.-Y., CERIANI, F., OLT, J., BROWN, S. D. M., HOLLEY, M. C., BOWL, M. R., JOHNSON, S. L. & MARCOTTI, W. 2020a. Pathophysiological changes in inner hair cell ribbon synapses in the ageing mammalian cochlea. *The Journal of Physiology*, n/a.
- JENG, J.-Y., JOHNSON, S. L., CARLTON, A. J., DE TOMASI, L., GOODYEAR, R. J., DE FAVERI, F., FURNESS, D. N., WELLS, S., BROWN, S. D. M., HOLLEY, M. C., RICHARDSON, G. P., MUSTAPHA, M., BOWL, M. R. & MARCOTTI, W. 2020b. Age-related changes in the biophysical and morphological characteristics of mouse cochlear outer hair cells. *The Journal of Physiology*, 598, 3891-3910.
- JERGER, J., CHMIEL, R., STACH, B. & SPRETNJAK, M. 1993. Gender affects audiometric shape in presbycusis. *J Am Acad Audiol*, 4, 42-9.
- JOHNSON, K. R., ERWAY, L. C., COOK, S. A., WILLOTT, J. F. & ZHENG, Q. Y. 1997. A major gene affecting age-related hearing loss in C57BL/6J mice. *Hearing Research*, 114, 83-92.
- JOHNSON, K. R., ZHENG, Q. Y. & ERWAY, L. C. 2000. A Major Gene Affecting Age-Related Hearing Loss Is Common to at Least Ten Inbred Strains of Mice. *Genomics*, 70, 171-180.
- JOHNSON, S. L., ADELMAN, J. P. & MARCOTTI, W. 2007. Genetic deletion of SK2 channels in mouse inner hair cells prevents the developmental linearization in the Ca²⁺ dependence of exocytosis. *The Journal of Physiology*, 583, 631-646.

- JOHNSON, S. L., CERIANI, F., HOUSTON, O., POLISHCHUK, R., POLISHCHUK, E., CRISPINO, G., ZORZI, V., MAMMANO, F. & MARCOTTI, W. 2017. Connexin-Mediated Signaling in Nonsensory Cells Is Crucial for the Development of Sensory Inner Hair Cells in the Mouse Cochlea. *J Neurosci*, 37, 258-268.
- JOHNSON, S. L., ECKRICH, T., KUHN, S., ZAMPINI, V., FRANZ, C., RANATUNGA, K. M., ROBERTS, T. P., MASETTO, S., KNIPPER, M., KROS, C. J. & MARCOTTI, W. 2011. Position-dependent patterning of spontaneous action potentials in immature cochlear inner hair cells. *Nature Neuroscience*, 14, 711-717.
- JOHNSON, S. L., FRANZ, C., KNIPPER, M. & MARCOTTI, W. 2009. Functional maturation of the exocytotic machinery at gerbil hair cell ribbon synapses. *The Journal of Physiology*, 587, 1715-1726.
- JOHNSON, S. L., KENNEDY, H. J., HOLLEY, M. C., FETTIPLACE, R. & MARCOTTI, W. 2012. The Resting Transducer Current Drives Spontaneous Activity in Prehearing Mammalian Cochlear Inner Hair Cells. *The Journal of Neuroscience*, 32, 10479.
- JOHNSON, S. L., KUHN, S., FRANZ, C., INGHAM, N., FURNESS, D. N., KNIPPER, M., STEEL, K. P., ADELMAN, J. P., HOLLEY, M. C. & MARCOTTI, W. 2013a. Presynaptic maturation in auditory hair cells requires a critical period of sensory-independent spiking activity. *Proceedings of the National Academy of Sciences*, 110, 8720.
- JOHNSON, S. L. & MARCOTTI, W. 2008. Biophysical properties of CaV1.3 calcium channels in gerbil inner hair cells. *The Journal of physiology*, 586, 1029-1042.
- JOHNSON, S. L., MARCOTTI, W. & KROS, C. J. 2005. Increase in efficiency and reduction in Ca²⁺ dependence of exocytosis during development of mouse inner hair cells. *The Journal of physiology*, 563, 177-191.
- JOHNSON, S. L., SAFIEDDINE, S., MUSTAPHA, M. & MARCOTTI, W. 2019. Hair Cell Afferent Synapses: Function and Dysfunction. *Cold Spring Harb Perspect Med*, 9.
- JOHNSON, S. L., WEDEMEYER, C., VETTER, D. E., ADACHI, R., HOLLEY, M. C., ELGOYHEN, A. B. & MARCOTTI, W. 2013b. Cholinergic efferent synaptic transmission regulates the maturation of auditory hair cell ribbon synapses. *Open biology*, 3, 130163-130163.
- JOHNSSON, L.-G. & HAWKINS, J. E. 1972. Sensory and Neural Degeneration with Aging, as Seen in Microdissections of the Human Inner Ear. *Annals of Otology, Rhinology & Laryngology*, 81, 179-193.

- JUHN, S. K. & RYBAK, L. P. 1981. Labyrinthine barriers and cochlear homeostasis. *Acta Otolaryngol*, 91, 529-34.
- KACHAR, B., PARAKKAL, M., KURC, M., ZHAO, Y. & GILLESPIE, P. G. 2000. High-resolution structure of hair-cell tip links. *Proceedings of the National Academy of Sciences of the United States of America*, 97, 13336-13341.
- KANTARDZHIEVA, A., LIBERMAN, M. C. & SEWELL, W. F. 2013. Quantitative analysis of ribbons, vesicles, and cisterns at the cat inner hair cell synapse: correlations with spontaneous rate. *J Comp Neurol*, 521, 3260-71.
- KATAOKA, Y. & OHMORI, H. 1994. Activation of glutamate receptors in response to membrane depolarization of hair cells isolated from chick cochlea. *J Physiol*, 477 (Pt 3), 403-14.
- KATZ, E., ELGOYHEN, A. B., GÓMEZ-CASATI, M. E., KNIPPER, M., VETTER, D. E., FUCHS, P. A. & GLOWATZKI, E. 2004. Developmental regulation of nicotinic synapses on cochlear inner hair cells. *The Journal of neuroscience : the official journal of the Society for Neuroscience*, 24, 7814-7820.
- KAUR, T., CLAYMAN, A. C., NASH, A. J., SCHRADER, A. D., WARCHOL, M. E. & OHLEMILLER, K. K. 2019. Lack of Fractalkine Receptor on Macrophages Impairs Spontaneous Recovery of Ribbon Synapses After Moderate Noise Trauma in C57BL/6 Mice. *Frontiers in Neuroscience*, 13.
- KAUR, T., OHLEMILLER, K. K. & WARCHOL, M. E. 2018. Genetic disruption of fractalkine signaling leads to enhanced loss of cochlear afferents following ototoxic or acoustic injury. *J Comp Neurol*, 526, 824-835.
- KAUR, T., ZAMANI, D., TONG, L., RUBEL, E. W., OHLEMILLER, K. K., HIROSE, K. & WARCHOL, M. E. 2015. Fractalkine Signaling Regulates Macrophage Recruitment into the Cochlea and Promotes the Survival of Spiral Ganglion Neurons after Selective Hair Cell Lesion. *The Journal of Neuroscience*, 35, 15050.
- KAWAI, T. & AKIRA, S. 2007. Signaling to NF-kappaB by Toll-like receptors. *Trends Mol Med*, 13, 460-9.
- KAWASE, T., DELGUTTE, B. & LIBERMAN, M. C. 1993. Antimasking effects of the olivocochlear reflex. II. Enhancement of auditory-nerve response to masked tones. *J Neurophysiol*, 70, 2533-49.

- KAZMIERCZAK, P., SAKAGUCHI, H., TOKITA, J., WILSON-KUBALEK, E. M., MILLIGAN, R. A., MÜLLER, U. & KACHAR, B. 2007. Cadherin 23 and protocadherin 15 interact to form tip-link filaments in sensory hair cells. *Nature*, 449, 87-91.
- KEEN, E. C. & HUDSPETH, A. J. 2006. Transfer characteristics of the hair cell's afferent synapse. *Proceedings of the National Academy of Sciences of the United States of America*, 103, 5537-5542.
- KEITHLEY, E. M. 2019. Pathology and mechanisms of cochlear aging. *Journal of neuroscience research*.
- KEITHLEY, E. M., WANG, X. & BARKDULL, G. C. 2008. Tumor necrosis factor alpha can induce recruitment of inflammatory cells to the cochlea. *Otol Neurotol*, 29, 854-9.
- KENNEDY, H. J., EVANS, M. G., CRAWFORD, A. C. & FETTIPLACE, R. 2003. Fast adaptation of mechano-electrical transducer channels in mammalian cochlear hair cells. *Nat Neurosci*, 6, 832-6.
- KHIMICH, D., NOUVIAN, R., PUJOL, R., TOM DIECK, S., EGNER, A., GUNDELFINGER, E. D. & MOSER, T. 2005. Hair cell synaptic ribbons are essential for synchronous auditory signalling. *Nature*, 434, 889-894.
- KIANG, N. Y., RHO, J. M., NORTHROP, C. C., LIBERMAN, M. C. & RYUGO, D. K. 1982. Hair-cell innervation by spiral ganglion cells in adult cats. *Science*, 217, 175-7.
- KIM, H., KIM, M., IM, S.-K. & FANG, S. 2018. Mouse Cre-LoxP system: general principles to determine tissue-specific roles of target genes. *Laboratory Animal Research*, 34, 147.
- KIRKWOOD, N. K. & KROS, C. J. Rapid photorelease of calcium augments the fast potassium conductance of guinea-pig inner hair cells. 1997 1997. CAMBRIDGE UNIV PRESS 40 WEST 20TH STREET, NEW YORK, NY 10011-4211, P127-P127.
- KOBRINA, A., SCHRODE, K. M., SCREVEN, L. A., JAVAID, H., WEINBERG, M. M., BROWN, G., BOARD, R., VILLAVISANIS, D. F., DENT, M. L. & LAUER, A. M. 2020. Linking anatomical and physiological markers of auditory system degeneration with behavioral hearing assessments in a mouse (*Mus musculus*) model of age-related hearing loss. *Neurobiol Aging*, 96, 87-103.
- KROS, C. J., MARCOTTI, W., VAN NETTEN, S. M., SELF, T. J., LIBBY, R. T., BROWN, S. D. M., RICHARDSON, G. P. & STEEL, K. P. 2002. Reduced climbing and increased slipping adaptation in cochlear hair cells of mice with *Myo7a* mutations. *Nature Neuroscience*, 5, 41-47.

- KROS, C. J., RUPPERSBERG, J. P. & RÜSCH, A. 1998. Expression of a potassium current in inner hair cells during development of hearing in mice. *Nature*, 394, 281-284.
- KROS, C. J., RUSCH, A. & RICHARDSON, G. P. 1992. Mechano-electrical transducer currents in hair cells of the cultured neonatal mouse cochlea. *Proceedings of the Royal Society of London. Series B: Biological Sciences*, 249, 185-193.
- KUBISCH, C., SCHROEDER, B. C., FRIEDRICH, T., LÜTJOHANN, B., EL-AMRAOUI, A., MARLIN, S., PETIT, C. & JENTSCH, T. J. 1999. KCNQ4, a novel potassium channel expressed in sensory outer hair cells, is mutated in dominant deafness. *Cell*, 96, 437-46.
- KUJAWA, S. G. & LIBERMAN, M. C. 2006. Acceleration of age-related hearing loss by early noise exposure: evidence of a misspent youth. *The Journal of neuroscience : the official journal of the Society for Neuroscience*, 26, 2115-2123.
- KUJAWA, S. G. & LIBERMAN, M. C. 2009. Adding insult to injury: cochlear nerve degeneration after "temporary" noise-induced hearing loss. *J Neurosci*, 29, 14077-85.
- KUJAWA, S. G. & LIBERMAN, M. C. 2015. Synaptopathy in the noise-exposed and aging cochlea: Primary neural degeneration in acquired sensorineural hearing loss. *Hear Res*, 330, 191-9.
- LADRECH, S., LENOIR, M., RUEL, J. & PUEL, J.-L. 2003. Microtubule-associated protein 2 (MAP2) expression during synaptic plasticity in the guinea pig cochlea. *Hearing Research*, 186, 85-90.
- LADRECH, S., WANG, J., SIMONNEAU, L., PUEL, J.-L. & LENOIR, M. 2007. Macrophage contribution to the response of the rat organ of Corti to amikacin. *Journal of Neuroscience Research*, 85, 1970-1979.
- LAUER, A. M., FUCHS, P. A., RYUGO, D. K. & FRANCIS, H. W. 2012. Efferent synapses return to inner hair cells in the aging cochlea. *Neurobiology of Aging*, 33, 2892-2902.
- LEE, F.-S., MATTHEWS, L. J., DUBNO, J. R. & MILLS, J. H. 2005. Longitudinal Study of Pure-Tone Thresholds in Older Persons. *Ear and Hearing*, 26.
- LEE, K.-Y. 2013. Pathophysiology of age-related hearing loss (peripheral and central). *Korean journal of audiology*, 17, 45-49.
- LEFÈVRE, G., MICHEL, V., WEIL, D., LEPELLETIER, L., BIZARD, E., WOLFRUM, U., HARDELIN, J.-P. & PETIT, C. 2008. A core cochlear phenotype in USH1 mouse mutants implicates

- fibrous links of the hair bundle in its cohesion, orientation and differential growth. *Development*, 135, 1427.
- LELLI, A., ASAI, Y., FORGE, A., HOLT, J. R. & GÉLÉOC, G. S. 2009. Tonotopic gradient in the developmental acquisition of sensory transduction in outer hair cells of the mouse cochlea. *J Neurophysiol*, 101, 2961-73.
- LI, C., SHU, Y., WANG, G., ZHANG, H., LU, Y., LI, X., LI, G., SONG, L. & LIU, Z. 2018. Characterizing a novel vGlut3-P2A-iCreER knockin mouse strain in cochlea. *Hearing Research*, 364, 12-24.
- LI, H. S. & BORG, E. 1991. Age-related loss of auditory sensitivity in two mouse genotypes. *Acta Oto-Laryngologica*, 111, 827-834.
- LIBERMAN, L. D. & LIBERMAN, M. C. 2019. Cochlear efferent innervation is sparse in humans and decreases with age. *The Journal of Neuroscience*, 3004-18.
- LIBERMAN, L. D., WANG, H. & LIBERMAN, M. C. 2011. Opposing gradients of ribbon size and AMPA receptor expression underlie sensitivity differences among cochlear-nerve/hair-cell synapses. *The Journal of neuroscience : the official journal of the Society for Neuroscience*, 31, 801-808.
- LIBERMAN, M. C. 1980. Morphological differences among radial afferent fibers in the cat cochlea: An electron-microscopic study of serial sections. *Hearing Research*, 3, 45-63.
- LIBERMAN, M. C. 1982a. Single-Neuron Labeling in the Cat Auditory Nerve. *Science*, 216, 1239-1241.
- LIBERMAN, M. C. 1982b. The cochlear frequency map for the cat: Labeling auditory-nerve fibers of known characteristic frequency. *The Journal of the Acoustical Society of America*, 72, 1441-1449.
- LIBERMAN, M. C. 1990. Effects of chronic cochlear de-efferentation on auditory-nerve response. *Hear Res*, 49, 209-23.
- LIBERMAN, M. C. 2017. Noise-induced and age-related hearing loss: new perspectives and potential therapies. *F1000Research*, 6, 927-927.
- LIBERMAN, M. C. & BROWN, M. C. 1986. Physiology and anatomy of single olivocochlear neurons in the cat. *Hearing Research*, 24, 17-36.
- LIBERMAN, M. C. & KIANG, N. Y. 1978. Acoustic trauma in cats. Cochlear pathology and auditory-nerve activity. *Acta Otolaryngol Suppl*, 358, 1-63.

- LIBERMAN, M. C. & KUJAWA, S. G. 2017. Cochlear synaptopathy in acquired sensorineural hearing loss: Manifestations and mechanisms. *Hear Res*, 349, 138-147.
- LIN, F. R., FERRUCCI, L., METTER, E. J., AN, Y., ZONDERMAN, A. B. & RESNICK, S. M. 2011. Hearing loss and cognition in the Baltimore Longitudinal Study of Aging. *Neuropsychology*, 25, 763.
- LIU, W., MOLNAR, M., GARNHAM, C., BENAVIDES, H. & RASK-ANDERSEN, H. 2018. Macrophages in the Human Cochlea: Saviors or Predators—A Study Using Super-Resolution Immunohistochemistry. *Frontiers in Immunology*, 9.
- LIU, X.-Z., WALSH, J., MBURU, P., KENDRICK-JONES, J., COPE, M. J. T., STEEL, K. P. & BROWN, S. D. 1997a. Mutations in the myosin VIIA gene cause non-syndromic recessive deafness. *Nature genetics*, 16, 188-190.
- LIU, X.-Z., WALSH, J., TAMAGAWA, Y., KITAMURA, K., NISHIZAWA, M., STEEL, K. P. & BROWN, S. D. M. 1997b. Autosomal dominant non-syndromic deafness caused by a mutation in the myosin VIIA gene. *Nature Genetics*, 17, 268-269.
- LIU, X. Z. & YAN, D. 2007. Ageing and hearing loss. *The Journal of Pathology*, 211, 188-197.
- LOSS, A. O. H. 2019. *Facts and figures on hearing loss* [Online]. Available: <https://www.actiononhearingloss.org.uk/about-us/our-research-and-evidence/facts-and-figures/> [Accessed 18th November 2019].
- LYON, M. F. & SEARLE, A. G. 1989. *Genetic variants and strains of the laboratory mouse*, Oxford University Press.
- MA, C., BILLINGS, P., HARRIS, J. P. & KEITHLEY, E. M. 2000. Characterization of an experimentally induced inner ear immune response. *Laryngoscope*, 110, 451-6.
- MAGUPALLI, V. G., SCHWARZ, K., ALPADI, K., NATARAJAN, S., SEIGEL, G. M. & SCHMITZ, F. 2008. Multiple RIBEYE-RIBEYE interactions create a dynamic scaffold for the formation of synaptic ribbons. *The Journal of neuroscience : the official journal of the Society for Neuroscience*, 28, 7954-7967.
- MAISON, S. F., EMESON, R. B., ADAMS, J. C., LUEBKE, A. E. & LIBERMAN, M. C. 2003. Loss of α CGRP Reduces Sound-Evoked Activity in the Cochlear Nerve. *Journal of Neurophysiology*, 90, 2941-2949.
- MAISON, S. F. & LIBERMAN, M. C. 2000. Predicting vulnerability to acoustic injury with a noninvasive assay of olivocochlear reflex strength. *The Journal of neuroscience : the official journal of the Society for Neuroscience*, 20, 4701-4707.

- MAISON, S. F., LUEBKE, A. E., LIBERMAN, M. C. & ZUO, J. 2002. Efferent protection from acoustic injury is mediated via alpha9 nicotinic acetylcholine receptors on outer hair cells. *J Neurosci*, 22, 10838-46.
- MAKARY, C. A., SHIN, J., KUJAWA, S. G., LIBERMAN, M. C. & MERCHANT, S. N. 2011. Age-related primary cochlear neuronal degeneration in human temporal bones. *J Assoc Res Otolaryngol*, 12, 711-7.
- MANDELL, J. W., TOWNES-ANDERSON, E., CZERNIK, A. J., CAMERON, R., GREENGARD, P. & DE CAMILLI, P. 1990. Synapsins in the vertebrate retina: absence from ribbon synapses and heterogeneous distribution among conventional synapses. *Neuron*, 5, 19-33.
- MANN, Z. F. & KELLEY, M. W. 2011. Development of tonotopy in the auditory periphery. *Hearing Research*, 276, 2-15.
- MARCOTTI, W., GÉLÉOC, G. S., LENNAN, G. W. & KROS, C. J. 1999. Transient expression of an inwardly rectifying potassium conductance in developing inner and outer hair cells along the mouse cochlea. *Pflugers Arch*, 439, 113-22.
- MARCOTTI, W., JOHNSON, S. L., HOLLEY, M. C. & KROS, C. J. 2003a. Developmental changes in the expression of potassium currents of embryonic, neonatal and mature mouse inner hair cells. *The Journal of physiology*, 548, 383-400.
- MARCOTTI, W., JOHNSON, S. L. & KROS, C. J. 2004. A transiently expressed SK current sustains and modulates action potential activity in immature mouse inner hair cells. *The Journal of physiology*, 560, 691-708.
- MARCOTTI, W., JOHNSON, S. L., RUSCH, A. & KROS, C. J. 2003b. Sodium and calcium currents shape action potentials in immature mouse inner hair cells. *The Journal of physiology*, 552, 743-761.
- MARCOTTI, W., JOHNSON, S. L., RUSCH, A. & KROS, C. J. 2003c. Sodium and calcium currents shape action potentials in immature mouse inner hair cells. *J Physiol*, 552, 743-61.
- MARCOTTI, W. & KROS, C. J. 1999. Developmental expression of the potassium current $I_{K,n}$ contributes to maturation of mouse outer hair cells. *The Journal of physiology*, 520 Pt 3, 653-660.
- MATERN, M., VIJAYAKUMAR, S., MARGULIES, Z., MILON, B., SONG, Y., ELKON, R., ZHANG, X., JONES, S. M. & HERTZANO, R. 2017. Gfi1Cre mice have early onset progressive

hearing loss and induce recombination in numerous inner ear non-hair cells.

Scientific reports, 7, 1-13.

MATSUBARA, A., LAAKE, J. H., DAVANGER, S., USAMI, S. & OTTERSEN, O. P. 1996.

Organization of AMPA receptor subunits at a glutamate synapse: a quantitative immunogold analysis of hair cell synapses in the rat organ of Corti. *The Journal of neuroscience : the official journal of the Society for Neuroscience*, 16, 4457-4467.

MCCABE, B. F. 1989. Autoimmune inner ear disease: therapy. *Am J Otol*, 10, 196-7.

MCFADDEN, S. L. & WILLOTT, J. F. 1994. Responses of inferior colliculus neurons in C57BL/6J

mice with and without sensorineural hearing loss: Effects of changing the azimuthal location of an unmasked pure-tone stimulus. *Hearing Research*, 78, 115-131.

MELGAR-ROJAS, P., ALVARADO, J. C., FUENTES-SANTAMARÍA, V. & JUIZ, J. M. 2015. Cellular

Mechanisms of Age-Related Hearing Loss. In: MILLER, J., LE PRELL, C. G. & RYBAK, L. (eds.) *Free Radicals in ENT Pathology*. Cham: Springer International Publishing.

METZGER, D., CLIFFORD, J., CHIBA, H. & CHAMBON, P. 1995. Conditional site-specific

recombination in mammalian cells using a ligand-dependent chimeric Cre recombinase. *Proc Natl Acad Sci U S A*, 92, 6991-5.

MEYER, A. C., FRANK, T., KHIMICH, D., HOCH, G., RIEDEL, D., CHAPOCHNIKOV, N. M., YARIN,

Y. M., HARKE, B., HELL, S. W., EGNER, A. & MOSER, T. 2009. Tuning of synapse number, structure and function in the cochlea. *Nature Neuroscience*, 12, 444-453.

MIANNÉ, J., CHESSUM, L., KUMAR, S., AGUILAR, C., CODNER, G., HUTCHISON, M., PARKER,

A., MALLON, A.-M., WELLS, S., SIMON, M. M., TEBOUL, L., BROWN, S. D. M. & BOWL, M. R. 2016. Correction of the auditory phenotype in C57BL/6N mice via CRISPR/Cas9-mediated homology directed repair. *Genome Medicine*, 8, 16.

MICHALSKI, N., GOUTMAN, J. D., AUCLAIR, S. M., BOUTET DE MONVEL, J., TERTRAIS, M.,

EMPTOZ, A., PARRIN, A., NOUAILLE, S., GUILLON, M., SACHSE, M., CIRIC, D., BAHLOUL, A., HARDELIN, J.-P., SUTTON, R. B., AVAN, P., KRISHNAKUMAR, S. S.,

ROTHMAN, J. E., DULON, D., SAFIEDDINE, S. & PETIT, C. 2017. Otoferlin acts as a Ca(2+) sensor for vesicle fusion and vesicle pool replenishment at auditory hair cell ribbon synapses. *eLife*, 6, e31013.

MICHANSKI, S., SMALUCH, K., STEYER, A. M., CHAKRABARTI, R., SETZ, C., OESTREICHER, D.,

FISCHER, C., MÖBIUS, W., MOSER, T., VOGL, C. & WICHMANN, C. 2019. Mapping

- developmental maturation of inner hair cell ribbon synapses in the apical mouse cochlea. *Proc Natl Acad Sci U S A*, 116, 6415-6424.
- MIKAELIAN, D. & RUBEN, R. J. 1965. Development of Hearing in the Normal Cba-J Mouse: Correlation of Physiological Observations with Behavioral Responses and with Cochlear Anatomy. *Acta Oto-Laryngologica*, 59, 451-461.
- MILLS, D. M. & SCHMIEDT, R. A. 2004. Metabolic presbycusis: differential changes in auditory brainstem and otoacoustic emission responses with chronic furosemide application in the gerbil. *J Assoc Res Otolaryngol*, 5, 1-10.
- MIZUSHIMA, Y., FUJIMOTO, C., KASHIO, A., KONDO, K. & YAMASOBA, T. 2017. Macrophage recruitment, but not interleukin 1 beta activation, enhances noise-induced hearing damage. *Biochemical and Biophysical Research Communications*, 493, 894-900.
- MOGLIE, M. J., FUCHS, P. A., ELGOYHEN, A. B. & GOUTMAN, J. D. 2018. Compartmentalization of antagonistic Ca²⁺ signals in developing cochlear hair cells. *Proc Natl Acad Sci U S A*, 115, E2095-e2104.
- MOSER, T. & BEUTNER, D. 2000. Kinetics of exocytosis and endocytosis at the cochlear inner hair cell afferent synapse of the mouse. *Proceedings of the National Academy of Sciences*, 97, 883.
- MOSER, T., BRANDT, A. & LYSAKOWSKI, A. 2006. Hair cell ribbon synapses. *Cell Tissue Res*, 326, 347-59.
- MOSER, T., GRABNER, C. P. & SCHMITZ, F. 2019. Sensory Processing at Ribbon Synapses in the Retina and the Cochlea. *Physiological Reviews*, 100, 103-144.
- MULROW, C. D., AGUILAR, C., ENDICOTT, J. E., VELEZ, R., TULEY, M. R., CHARLIP, W. S. & HILL, J. A. 1990. Association between hearing impairment and the quality of life of elderly individuals. *J Am Geriatr Soc*, 38, 45-50.
- NIEDER, P. & NIEDER, I. 1970a. Antimasking effect of crossed olivocochlear bundle stimulation with loud clicks in guinea pig. *Experimental Neurology*, 28, 179-188.
- NIEDER, P. & NIEDER, I. 1970b. Stimulation of Efferent Olivocochlear Bundle causes Release from Low Level Masking. *Nature*, 227, 184-185.
- NIEDZIELSKI, A. S. & WENTHOLD, R. J. 1995. Expression of AMPA, kainate, and NMDA receptor subunits in cochlear and vestibular ganglia. *The Journal of neuroscience : the official journal of the Society for Neuroscience*, 15, 2338-2353.

- NIWA, M., YOUNG, E. D., GLOWATZKI, E. & RICCI, A. J. 2021. Functional subgroups of cochlear inner hair cell ribbon synapses differently modulate their EPSC properties in response to stimulation. *Journal of Neurophysiology*, 125, 2461-2479.
- NOBLE, K. V., LIU, T., MATTHEWS, L. J., SCHULTE, B. A. & LANG, H. 2019. Age-Related Changes in Immune Cells of the Human Cochlea. *Front Neurol*, 10, 895.
- OATMAN, L. C. 1976. Effects of visual attention on the intensity of auditory evoked potentials. *Experimental Neurology*, 51, 41-53.
- OHLEMILLER, K. K. 2006. Contributions of mouse models to understanding of age- and noise-related hearing loss. *Brain Research*, 1091, 89-102.
- OHLEMILLER, K. K., DAHL, A. R. & GAGNON, P. M. 2010. Divergent aging characteristics in CBA/J and CBA/CaJ mouse cochleae. *Journal of the Association for Research in Otolaryngology*, 11, 605-623.
- OHMORI, H. 1985. Mechano-electrical transduction currents in isolated vestibular hair cells of the chick. *The Journal of physiology*, 359, 189-217.
- OKANO, T., NAKAGAWA, T., KITA, T., KADA, S., YOSHIMOTO, M., NAKAHATA, T. & ITO, J. 2008. Bone marrow-derived cells expressing Iba1 are constitutively present as resident tissue macrophages in the mouse cochlea. *J Neurosci Res*, 86, 1758-67.
- OLIVER, D., KLÖCKER, N., SCHUCK, J., BAUKROWITZ, T., RUPPERSBERG, J. P. & FAKLER, B. 2000. Gating of Ca²⁺-Activated K⁺ Channels Controls Fast Inhibitory Synaptic Transmission at Auditory Outer Hair Cells. *Neuron*, 26, 595-601.
- OTTE, J., SCHUNKNECHT, H. F. & KERR, A. G. 1978. Ganglion cell populations in normal and pathological human cochleae. Implications for cochlear implantation. *Laryngoscope*, 88, 1231-46.
- OUDA, L., PROFANT, O. & SYKA, J. 2015. Age-related changes in the central auditory system. *Cell and Tissue Research*, 361, 337-358.
- PAN, B., GÉLÉOC, G. S., ASAI, Y., HORWITZ, G. C., KURIMA, K., ISHIKAWA, K., KAWASHIMA, Y., GRIFFITH, A. J. & HOLT, J. R. 2013. TMC1 and TMC2 are components of the mechanotransduction channel in hair cells of the mammalian inner ear. *Neuron*, 79, 504-515.
- PAN, L., YAN, J., WU, L. & ZHANG, M. 2009. Assembling stable hair cell tip link complex via multidentate interactions between harmonin and cadherin 23. *Proceedings of the National Academy of Sciences of the United States of America*, 106, 5575-5580.

- PANGRŠIČ, T., LASAROW, L., REUTER, K., TAKAGO, H., SCHWANDER, M., RIEDEL, D., FRANK, T., TARANTINO, L. M., BAILEY, J. S., STRENZKE, N., BROSE, N., MÜLLER, U., REISINGER, E. & MOSER, T. 2010. Hearing requires otoferlin-dependent efficient replenishment of synaptic vesicles in hair cells. *Nature Neuroscience*, 13, 869-876.
- PARHAM, K. 1997. Distortion product otoacoustic emissions in the C57BL/6J mouse model of age-related hearing loss. *Hearing Research*, 112, 216-234.
- PATEL, M., HU, Z., BARD, J., JAMISON, J., CAI, Q. & HU, B. H. 2013. Transcriptome characterization by RNA-Seq reveals the involvement of the complement components in noise-traumatized rat cochleae. *Neuroscience*, 248, 1-16.
- PATUZZI, R. B. & THOMPSON, M. L. 1991. Cochlear efferent neurones and protection against acoustic trauma: protection of outer hair cell receptor current and interanimal variability. *Hear Res*, 54, 45-58.
- PAULER, M., SCHUKNECHT, H. F. & THORNTON, A. R. 1986. Correlative studies of cochlear neuronal loss with speech discrimination and pure-tone thresholds. *Arch Otorhinolaryngol*, 243, 200-6.
- PAULER, M., SCHUKNECHT, H. F. & WHITE, J. A. 1988. Atrophy of the stria vascularis as a cause of sensorineural hearing loss. *Laryngoscope*, 98, 754-9.
- PERKINS, R. E. & MOREST, D. K. 1975. A study of cochlear innervation patterns in cats and rats with the Golgi method and Nomarski optics. *Journal of Comparative Neurology*, 163, 129-158.
- PICKLES, J. O., COMIS, S. D. & OSBORNE, M. P. 1984. Cross-links between stereocilia in the guinea pig organ of Corti, and their possible relation to sensory transduction. *Hear Res*, 15, 103-12.
- PLATZER, J., ENGEL, J., SCHROTT-FISCHER, A., STEPHAN, K., BOVA, S., CHEN, H., ZHENG, H. & STRIESSNIG, J. 2000. Congenital deafness and sinoatrial node dysfunction in mice lacking class D L-type Ca²⁺ channels. *Cell*, 102, 89-97.
- PROBST, F. J., FRIDELL, R. A., RAPHAEL, Y., SAUNDERS, T. L., WANG, A., LIANG, Y., MORELL, R. J., TOUCHMAN, J. W., LYONS, R. H., NOBEN-TRAUTH, K., FRIEDMAN, T. B. & CAMPER, S. A. 1998. Correction of Deafness in *shaker-2* Mice by an Unconventional Myosin in a BAC Transgene. *Science*, 280, 1444.

- PUJOL, R., LAVIGNE-REBILLARD, M. & LENOIR, M. 1998. Development of Sensory and Neural Structures in the Mammalian Cochlea. *In*: RUBEL, E. W., POPPER, A. N. & FAY, R. R. (eds.) *Development of the Auditory System*. New York, NY: Springer New York.
- PURVES, D., AUGUSTINE, G. J., FITZPATRICK, D., KATZ, L. C., LAMANTIA, A.-S., MCNAMARA, J. O. & WILLIAMS, S. M. 2001. *Neuroscience. 2nd Edition*, Sunderland (MA), Sinauer Associates.
- RABINOWITZ, P. 2012. Noise-induced hearing loss: scientific advances.
- RAI, V., WOOD, M. B., FENG, H., SCHABLA, N. M., TU, S. & ZUO, J. 2020. The immune response after noise damage in the cochlea is characterized by a heterogeneous mix of adaptive and innate immune cells. *Sci Rep*, 10, 15167.
- RAMADAN, H. H. & SCHUKNECHT, H. F. 1989. Is there a conductive type of presbycusis? *Otolaryngol Head Neck Surg*, 100, 30-4.
- RANCK JR, J. B. 1981. Extracellular stimulation. *Electrical stimulation research techniques*. Elsevier.
- RANKOVIC, V., VOGL, C., DÖRJE, N. M., BAHADER, I., DUQUE-AFONSO, C. J., THIRUMALAI, A., WEBER, T., KUSCH, K., STRENZKE, N. & MOSER, T. 2021. Overloaded Adeno-Associated Virus as a Novel Gene Therapeutic Tool for Otoferlin-Related Deafness. *Frontiers in Molecular Neuroscience*, 13.
- RASMUSSEN, G. L. 1946. The olivary peduncle and other fiber projections of the superior olivary complex. *J Comp Neurol*, 84, 141-219.
- RICCI, A. J., CRAWFORD, A. C. & FETTIPLACE, R. 2000. Active hair bundle motion linked to fast transducer adaptation in auditory hair cells. *J Neurosci*, 20, 7131-42.
- RICCI, A. J. & FETTIPLACE, R. 1998. Calcium permeation of the turtle hair cell mechanotransducer channel and its relation to the composition of endolymph. *The Journal of physiology*, 506 (Pt 1), 159-173.
- RICHARDSON, G. P. & PETIT, C. 2019. Hair-Bundle Links: Genetics as the Gateway to Function. *Cold Spring Harbor Perspectives in Medicine*, 9.
- ROBERTSON, D. & GUMMER, M. 1985. Physiological and morphological characterization of efferent neurones in the guinea pig cochlea. *Hearing Research*, 20, 63-77.
- ROCK, K. L., LATZ, E., ONTIVEROS, F. & KONO, H. 2010. The sterile inflammatory response. *Annu Rev Immunol*, 28, 321-42.

- ROMAND, R. 1983. Development of the cochlea. In: ROMAND, R. (ed.) *Development of the Auditory and Vestibular Systems.*: New York: Academic Press.
- ROUX, I., SAFIEDDINE, S., NOUVIAN, R., GRATI, M. H., SIMMLER, M.-C., BAHLOUL, A., PERFETTINI, I., LE GALL, M., ROSTAING, P., HAMARD, G., TRILLER, A., AVAN, P., MOSER, T. & PETIT, C. 2006. Otoferlin, Defective in a Human Deafness Form, Is Essential for Exocytosis at the Auditory Ribbon Synapse. *Cell*, 127, 277-289.
- ROUX, I., WERSINGER, E., MCINTOSH, J. M., FUCHS, P. A. & GLOWATZKI, E. 2011. Onset of Cholinergic Efferent Synaptic Function in Sensory Hair Cells of the Rat Cochlea. *The Journal of Neuroscience*, 31, 15092.
- RUEL, J., BOBBIN, R. P., VIDAL, D., PUJOL, R. & PUEL, J. L. 2000. The selective AMPA receptor antagonist GYKI 53784 blocks action potential generation and excitotoxicity in the guinea pig cochlea. *Neuropharmacology*, 39, 1959-1973.
- RUEL, J., CHEN, C., PUJOL, R., BOBBIN, R. P. & PUEL, J. L. 1999. AMPA-preferring glutamate receptors in cochlear physiology of adult guinea-pig. *The Journal of physiology*, 518 (Pt 3), 667-680.
- RUEL, J., EMERY, S., NOUVIAN, R., BERSOT, T., AMILHON, B., VAN RYBROEK, J. M., REBILLARD, G., LENOIR, M., EYBALIN, M., DELPRAT, B., SIVAKUMARAN, T. A., GIROS, B., EL MESTIKAWY, S., MOSER, T., SMITH, R. J. H., LESPERANCE, M. M. & PUEL, J.-L. 2008. Impairment of SLC17A8 Encoding Vesicular Glutamate Transporter-3, VGLUT3, Underlies Nonsyndromic Deafness DFNA25 and Inner Hair Cell Dysfunction in Null Mice. *The American Journal of Human Genetics*, 83, 278-292.
- RUEL, J., WANG, J., REBILLARD, G., EYBALIN, M., LLOYD, R., PUJOL, R. & PUEL, J. L. 2007. Physiology, pharmacology and plasticity at the inner hair cell synaptic complex. *Hear Res*, 227, 19-27.
- RUSSELL, I. J. & SELICK, P. M. 1977. Tuning properties of cochlear hair cells. *Nature*, 267, 858-860.
- RYAN, A. & DALLOS, P. 1975. Effect of absence of cochlear outer hair cells on behavioural auditory threshold. *Nature*, 253, 44-6.
- SAFIEDDINE, S., EL-AMRAOUI, A. & PETIT, C. 2012. The Auditory Hair Cell Ribbon Synapse: From Assembly to Function. *Annual Review of Neuroscience*, 35, 509-528.
- SAFIEDDINE, S. & EYBALIN, M. 1992. Triple Immunofluorescence Evidence for the Coexistence of Acetylcholine, Enkephalins and Calcitonin Gene-related Peptide

- Within Efferent (Olivocochlear) Neurons of Rats and Guinea-pigs. *European Journal of Neuroscience*, 4, 981-992.
- SAFIEDDINE, S. & WENTHOLD, R. J. 1997. The glutamate receptor subunit delta1 is highly expressed in hair cells of the auditory and vestibular systems. *J Neurosci*, 17, 7523-31.
- SAFIEDDINE, S. & WENTHOLD, R. J. 1999. SNARE complex at the ribbon synapses of cochlear hair cells: analysis of synaptic vesicle- and synaptic membrane-associated proteins. *Eur J Neurosci*, 11, 803-12.
- SAHLEY, T. L., KALISH, R. B., MUSIEK, F. E. & HOFFMAN, D. W. 1991. Effects of opioid drugs on auditory evoked potentials suggest a role of lateral olivocochlear dynorphins in auditory function. *Hear Res*, 55, 133-42.
- SAHLY, I., EL-AMRAOUI, A., ABITBOL, M., PETIT, C. & DUFIER, J. L. 1997. Expression of myosin VIIA during mouse embryogenesis. *Anat Embryol (Berl)*, 196, 159-70.
- SALVI, R., DING, D., JIANG, H., CHEN, G.-D., GRECO, A., MANOHAR, S., SUN, W. & RALLI, M. 2018. Hidden Age-Related Hearing Loss and Hearing Disorders: Current Knowledge and Future Directions. *Hearing, balance and communication*, 16, 74-82.
- SATO, E., SHICK, H. E., RANSOHOFF, R. M. & HIROSE, K. 2010. Expression of fractalkine receptor CX3CR1 on cochlear macrophages influences survival of hair cells following ototoxic injury. *J Assoc Res Otolaryngol*, 11, 223-34.
- SATOH, H., FIRESTEIN, G. S., BILLINGS, P. B., HARRIS, J. P. & KEITHLEY, E. M. 2002. Tumor Necrosis Factor- α , an Initiator, and Etanercept, an Inhibitor of Cochlear Inflammation. *The Laryngoscope*, 112, 1627-1634.
- SCHMITZ, F., KÖNIGSTORFER, A. & SÜDHOF, T. C. 2000. RIBEYE, a Component of Synaptic Ribbons: A Protein's Journey through Evolution Provides Insight into Synaptic Ribbon Function. *Neuron*, 28, 857-872.
- SCHROTT-FISCHER, A., KAMMEN-JOLLY, K., SCHOLTZ, A., RASK-ANDERSEN, H., GLUECKERT, GT, R & EYBALIN, M. 2007. Efferent neurotransmitters in the human cochlea and vestibule. *Acta Oto-Laryngologica*, 127, 13-19.
- SCHUKNECHT, H. F. 1955. Presbycusis. *The Laryngoscope*, 65, 402-419.
- SCHUKNECHT, H. F. 1964. Further Observations On the Pathology of Presbycusis. *Archives of Otolaryngology*, 80, 369-382.

- SCHUKNECHT, H. F. & GACEK, M. R. 1993. Cochlear pathology in presbycusis. *Ann Otol Rhinol Laryngol*, 102, 1-16.
- SCHULTE, B. A. & SCHMIEDT, R. A. 1992. Lateral wall Na, K-ATPase and endocochlear potentials decline with age in quiet-reared gerbils. *Hearing Research*, 61, 35-46.
- SCHWANDER, M., KACHAR, B. & MÜLLER, U. 2010. Review series: The cell biology of hearing. *The Journal of cell biology*, 190, 9-20.
- SEAL, R. P., AKIL, O., YI, E., WEBER, C. M., GRANT, L., YOO, J., CLAUSE, A., KANDLER, K., NOEBELS, J. L., GLOWATZKI, E., LUSTIG, L. R. & EDWARDS, R. H. 2008. Sensorineural deafness and seizures in mice lacking vesicular glutamate transporter 3. *Neuron*, 57, 263-275.
- SEICOL, B. J., LIN, S. & XIE, R. 2022. Age-Related Hearing Loss Is Accompanied by Chronic Inflammation in the Cochlea and the Cochlear Nucleus. *Front Aging Neurosci*, 14, 846804.
- SELF, T., MAHONY, M., FLEMING, J., WALSH, J., BROWN, S. D. & STEEL, K. P. 1998. Shaker-1 mutations reveal roles for myosin VIIA in both development and function of cochlear hair cells. *Development*, 125, 557.
- SENDIN, G., BULANKINA, A. V., RIEDEL, D. & MOSER, T. 2007. Maturation of Ribbon Synapses in Hair Cells Is Driven by Thyroid Hormone. *The Journal of Neuroscience*, 27, 3163.
- SENFTEN, M., SCHWANDER, M., KAZMIERCZAK, P., LILLO, C., SHIN, J.-B., HASSON, T., GÉLÉOC, G. S. G., GILLESPIE, P. G., WILLIAMS, D., HOLT, J. R. & MÜLLER, U. 2006. Physical and Functional Interaction between Protocadherin 15 and Myosin VIIa in Mechanosensory Hair Cells. *The Journal of Neuroscience*, 26, 2060.
- SERGEYENKO, Y., LALL, K., LIBERMAN, M. C. & KUJAWA, S. G. 2013. Age-related cochlear synaptopathy: an early-onset contributor to auditory functional decline. *J Neurosci*, 33, 13686-94.
- SERVICES, H. L. 2022. *How the ear works* [Online]. [Accessed 27/09/2022 2022].
- SHA, S.-H., KANICKI, A., DOOTZ, G., TALASKA, A. E., HALSEY, K., DOLAN, D., ALTSCHULER, R. & SCHACHT, J. 2008. Age-related auditory pathology in the CBA/J mouse. *Hearing Research*, 243, 87-94.
- SHEN, H., KREISEL, D. & GOLDSTEIN, D. R. 2013. Processes of Sterile Inflammation. *The Journal of Immunology*, 191, 2857.

- SHONE, G., ALTSCHULER, R. A., MILLER, J. M. & NUTTALL, A. L. 1991. The effect of noise exposure on the aging ear. *Hearing Research*, 56, 173-178.
- SIEMENS, J., KAZMIERCZAK, P., REYNOLDS, A., STICKER, M., LITTLEWOOD-EVANS, A. & MÜLLER, U. 2002. The Usher syndrome proteins cadherin 23 and harmonin form a complex by means of PDZ-domain interactions. *Proceedings of the National Academy of Sciences of the United States of America*, 99, 14946-14951.
- SIEMENS, J., LILLO, C., DUMONT, R. A., REYNOLDS, A., WILLIAMS, D. S., GILLESPIE, P. G. & MÜLLER, U. 2004. Cadherin 23 is a component of the tip link in hair-cell stereocilia. *Nature*, 428, 950-955.
- SIMMONS, D. D. 1994. A transient afferent innervation of outer hair cells in the postnatal cochlea. *Neuroreport*, 5, 1309-12.
- SIMMONS, D. D. 2002. Development of the inner ear efferent system across vertebrate species. *J Neurobiol*, 53, 228-50.
- SIMMONS, D. D., MANSDORF, N. B. & KIM, J. H. 1996. Olivocochlear innervation of inner and outer hair cells during postnatal maturation: Evidence for a waiting period. *Journal of Comparative Neurology*, 370, 551-562.
- SKIPPER, J. I., DEVLIN, J. T. & LAMETTI, D. R. 2017. The hearing ear is always found close to the speaking tongue: Review of the role of the motor system in speech perception. *Brain and Language*, 164, 77-105.
- SLEPECKY, N. B. 1996. Structure of the Mammalian Cochlea. *In: DALLOS, P., POPPER, A. N. & FAY, R. R. (eds.) The Cochlea*. New York, NY: Springer New York.
- SMITH, C. A. & SJÖSTRAND, F. S. 1961. Structure of the nerve endings on the external hair cells of the guinea pig cochlea as studied by serial sections. *Journal of Ultrastructure Research*, 5, 523-556.
- SOBKOWICZ, H. M., AUGUST, B. K. & SLAPNICK, S. M. 2004. Synaptic arrangements between inner hair cells and tunnel fibers in the mouse cochlea. *Synapse*, 52, 299-315.
- SOBKOWICZ, H. M. & EMMERLING, M. R. 1989. Development of acetylcholinesterase-positive neuronal pathways in the cochlea of the mouse. *J Neurocytol*, 18, 209-24.
- SOBKOWICZ, H. M., ROSE, J. E., SCOTT, G. E. & SLAPNICK, S. M. 1982. Ribbon synapses in the developing intact and cultured organ of Corti in the mouse. *The Journal of Neuroscience*, 2, 942.

- SOBKOWICZ, H. M., ROSE, J. E., SCOTT, G. L. & LEVENICK, C. V. 1986. Distribution of synaptic ribbons in the developing organ of Corti. *Journal of neurocytology*, 15, 693-714.
- SOBKOWICZ, H. M., SLAPNICK, S. M. & AUGUST, B. K. 2002. Differentiation of spinous synapses in the mouse organ of Corti. *Synapse*, 45, 10-24.
- SOHAL, D. S., NGHIEM, M., CRACKOWER, M. A., WITT, S. A., KIMBALL, T. R., TYMITZ, K. M., PENNINGER, J. M. & MOLKENTIN, J. D. 2001. Temporally Regulated and Tissue-Specific Gene Manipulations in the Adult and Embryonic Heart Using a Tamoxifen-Inducible Cre Protein. *Circulation Research*, 89, 20-25.
- SPICER, S. S. & SCHULTE, B. A. 2005. Pathologic changes of presbycusis begin in secondary processes and spread to primary processes of strial marginal cells. *Hearing Research*, 205, 225-240.
- SPINELLI, K. J. & GILLESPIE, P. G. 2009. Bottoms up: transduction channels at tip link bases. *Nature Neuroscience*, 12, 529-530.
- SPOENDLIN, H. 1972. Innervation Densities of the Cochlea. *Acta Oto-Laryngologica*, 73, 235-248.
- SPONGR, V. P., FLOOD, D. G., FRISINA, R. D. & SALVI, R. J. 1997. Quantitative measures of hair cell loss in CBA and C57BL/6 mice throughout their life spans. *J Acoust Soc Am*, 101, 3546-53.
- SPRINZL, G. M. & RIECHELMANN, H. 2010. Current Trends in Treating Hearing Loss in Elderly People: A Review of the Technology and Treatment Options – A Mini-Review. *Gerontology*, 56, 351-358.
- STALMANN, U., FRANKE, A. J., AL-MOYED, H., STRENZKE, N. & REISINGER, E. 2021. Otoferlin Is Required for Proper Synapse Maturation and for Maintenance of Inner and Outer Hair Cells in Mouse Models for DFNB9. *Frontiers in Cellular Neuroscience*, 15.
- STAMATAKI, S., FRANCIS, H. W., LEHAR, M., MAY, B. J. & RYUGO, D. K. 2006. Synaptic alterations at inner hair cells precede spiral ganglion cell loss in aging C57BL/6J mice. *Hearing Research*, 221, 104-118.
- STEEL, K. P. 1995. INHERITED HEARING DEFECTS IN MICE. *Annual Review of Genetics*, 29, 675-701.
- STEEL, K. P. & BARKWAY, C. 1989. Another role for melanocytes: their importance for normal stria vascularis development in the mammalian inner ear. *Development*, 107, 453-63.

- STEEL, K. P. & BOCK, G. R. 1983. Hereditary Inner-Ear Abnormalities in Animals: Relationships With Human Abnormalities. *Archives of Otolaryngology*, 109, 22-29.
- STEEL, K. P. & BROWN, S. D. M. 1996. Genetics of deafness. *Current Opinion in Neurobiology*, 6, 520-525.
- STEPANYAN, R. & FROLENKOV, G. I. 2009. Fast adaptation and Ca²⁺ sensitivity of the mechanotransducer require myosin-XVa in inner but not outer cochlear hair cells. *The Journal of neuroscience : the official journal of the Society for Neuroscience*, 29, 4023-4034.
- STRENZKE, N., CHAKRABARTI, R., AL-MOYED, H., MULLER, A., HOCH, G., PANGRSIC, T., YAMANBAEVA, G., LENZ, C., PAN, K. T., AUGÉ, E., GEISS-FRIEDLANDER, R., URLAUB, H., BROSE, N., WICHMANN, C. & REISINGER, E. 2016. Hair cell synaptic dysfunction, auditory fatigue and thermal sensitivity in otoferlin Ile515Thr mutants. *Embo j*, 35, 2519-2535.
- SUGA, F. & LINDSAY, J. R. 1976. Histopathological observations of presbycusis. *Ann Otol Rhinol Laryngol*, 85, 169-84.
- TABERNER, A. M. & LIBERMAN, M. C. 2005. Response Properties of Single Auditory Nerve Fibers in the Mouse. *Journal of Neurophysiology*, 93, 557-569.
- TAKAGO, H., OSHIMA-TAKAGO, T. & MOSER, T. 2019. Disruption of Otoferlin Alters the Mode of Exocytosis at the Mouse Inner Hair Cell Ribbon Synapse. *Frontiers in Molecular Neuroscience*, 11, 492.
- TAKEUCHI, S., ANDO, M. & KAKIGI, A. 2000. Mechanism generating endocochlear potential: role played by intermediate cells in stria vascularis. *Biophysical journal*, 79, 2572-2582.
- TAN, B. T., LEE, M. M. & RUAN, R. 2008. Bone-marrow-derived cells that home to acoustic deafened cochlea preserved their hematopoietic identity. *J Comp Neurol*, 509, 167-79.
- TARANDA, J., MAISON, S. F., BALLESTERO, J. A., KATZ, E., SAVINO, J., VETTER, D. E., BOULTER, J., LIBERMAN, M. C., FUCHS, P. A. & ELGOYHEN, A. B. 2009. A Point Mutation in the Hair Cell Nicotinic Cholinergic Receptor Prolongs Cochlear Inhibition and Enhances Noise Protection. *PLOS Biology*, 7, e1000018.

- TASAKI, I., DAVIS, H. & ELDREDGE, D. H. 1954. Exploration of Cochlear Potentials in Guinea Pig with a Microelectrode. *The Journal of the Acoustical Society of America*, 26, 765-773.
- TAVANAI, E. & MOHAMMADKHANI, G. 2017. Role of antioxidants in prevention of age-related hearing loss: a review of literature. *Eur Arch Otorhinolaryngol*, 274, 1821-1834.
- TERREROS, G., JORRATT, P., AEDO, C., ELGOYHEN, A. B. & DELANO, P. H. 2016. Selective Attention to Visual Stimuli Using Auditory Distractors Is Altered in Alpha-9 Nicotinic Receptor Subunit Knock-Out Mice. *J Neurosci*, 36, 7198-209.
- TESSAROLLO, L., COPPOLA, V. & FRITZSCH, B. 2004. NT-3 replacement with brain-derived neurotrophic factor redirects vestibular nerve fibers to the cochlea. *J Neurosci*, 24, 2575-84.
- TILNEY, L. G., TILNEY, M. S. & DEROSIER, D. J. 1992. Actin Filaments, Stereocilia, and Hair Cells: How Cells Count and Measure. *Annual Review of Cell Biology*, 8, 257-274.
- TOM DIECK, S., ALTROCK, W. D., KESSELS, M. M., QUALMANN, B., REGUS, H., BRAUNER, D., FEJTOVÁ, A., BRACKO, O., GUNDELFINGER, E. D. & BRANDSTÄTTER, J. H. 2005. Molecular dissection of the photoreceptor ribbon synapse: physical interaction of Bassoon and RIBEYE is essential for the assembly of the ribbon complex. *The Journal of cell biology*, 168, 825-836.
- TORNABENE, S. V., SATO, K., PHAM, L., BILLINGS, P. & KEITHLEY, E. M. 2006. Immune cell recruitment following acoustic trauma. *Hear Res*, 222, 115-24.
- TRITSCH, N. X., RODRÍGUEZ-CONTRERAS, A., CRINS, T. T., WANG, H. C., BORST, J. G. & BERGLES, D. E. 2010. Calcium action potentials in hair cells pattern auditory neuron activity before hearing onset. *Nat Neurosci*, 13, 1050-2.
- TRUNE, D. R., KEMPTON, J. B. & MITCHELL, C. 1996. Auditory function in the C3H/HeJ and C3H/HeSnJ mouse strains. *Hear Res*, 96, 41-5.
- TU, N. C. & FRIEDMAN, R. A. 2018. Age-related hearing loss: Unraveling the pieces. *Laryngoscope investigative otolaryngology*, 3, 68-72.
- TURUNEN-TAHERI, S., WETTERGREN, L., SWANEPOEL, D. & JOHNSON, A.-C. 2017. *Hearing health care in Kenya; a regional field study*.
- URAGUCHI, K., MAEDA, Y., TAKAHARA, J., OMICHI, R., FUJIMOTO, S., KARIYA, S., NISHIZAKI, K. & ANDO, M. 2021. Upregulation of a nuclear factor-kappa B-interacting immune

- gene network in mice cochleae with age-related hearing loss. *PLOS ONE*, 16, e0258977.
- USAMI, S., MATSUBARA, A., FUJITA, S., SHINKAWA, H. & HAYASHI, M. 1995. NMDA (NMDAR1) and AMPA-type (GluR2/3) receptor subunits are expressed in the inner ear. *Neuroreport*, 6, 1161-4.
- UZIEL, A., ROMAND, R. & MAROT, M. 1981. Development of cochlear potentials in rats. *Audiology*, 20, 89-100.
- V. BÉKÉSY, G. 1952. DC resting potentials inside the cochlear partition. *The Journal of the Acoustical Society of America*, 24, 72-76.
- VABULAS, R. M., AHMAD-NEJAD, P., DA COSTA, C., MIETHKE, T., KIRSCHNING, C. J., HÄCKER, H. & WAGNER, H. 2001. Endocytosed HSP60s use toll-like receptor 2 (TLR2) and TLR4 to activate the toll/interleukin-1 receptor signaling pathway in innate immune cells. *J Biol Chem*, 276, 31332-9.
- VAN EYKEN, E., VAN CAMP, G., FRANSEN, E., TOPSAKAL, V., HENDRICKX, J. J., DEMEESTER, K., VAN DE HEYNING, P., MÄKI-TORKKO, E., HANNULA, S., SORRI, M., JENSEN, M., PARVING, A., BILLE, M., BAUR, M., PFISTER, M., BONACONSA, A., MAZZOLI, M., ORZAN, E., ESPESO, A., STEPHENS, D., VERBRUGGEN, K., HUYGHE, J., DHOOGHE, I., HUYGEN, P., KREMER, H., CREMERS, C. W. R. J., KUNST, S., MANNINEN, M., PYYKKÖ, I., LACAVALA, A., STEFFENS, M., WIENKER, T. F. & VAN LAER, L. 2007a. Contribution of the N-acetyltransferase 2 polymorphism NAT2*6A to age-related hearing impairment. *Journal of medical genetics*, 44, 570-578.
- VAN EYKEN, E., VAN CAMP, G. & VAN LAER, L. 2007b. The Complexity of Age-Related Hearing Impairment: Contributing Environmental and Genetic Factors. *Audiology and Neurotology*, 12, 345-358.
- VERPY, E., LEIBOVICI, M., ZWAENEPOEL, I., LIU, X.-Z., GAL, A., SALEM, N., MANSOUR, A., BLANCHARD, S., KOBAYASHI, I., KEATS, B. J. B., SLIM, R. & PETIT, C. 2000. A defect in harmonin, a PDZ domain-containing protein expressed in the inner ear sensory hair cells, underlies Usher syndrome type 1C. *Nature Genetics*, 26, 51-55.
- VETTER, D. E. & MUGNAINI, E. 1992. Distribution and dendritic features of three groups of rat olivocochlear neurons. A study with two retrograde cholera toxin tracers. *Anat Embryol (Berl)*, 185, 1-16.

- VILJANEN, A., ERA, P., KAPRIO, J., PYYKKÖ, I., KOSKENVUO, M. & RANTANEN, T. 2007. Genetic and environmental influences on hearing in older women. *J Gerontol A Biol Sci Med Sci*, 62, 447-52.
- VON BÉKÉSY, G. & WEVER, E. G. 1960. Experiments in hearing.
- WAKE, H., MOORHOUSE, A. J., JINNO, S., KOHSAKA, S. & NABEKURA, J. 2009. Resting microglia directly monitor the functional state of synapses in vivo and determine the fate of ischemic terminals. *J Neurosci*, 29, 3974-80.
- WALLHAGEN, M. I., STRAWBRIDGE, W. J., COHEN, R. D. & KAPLAN, G. A. 1997. An increasing prevalence of hearing impairment and associated risk factors over three decades of the Alameda County Study. *Am J Public Health*, 87, 440-2.
- WALTON, J. P., FRISINA, R. D. & MEIERHANS, L. R. 1995. Sensorineural hearing loss alters recovery from short-term adaptation in the C57BL/6 mouse. *Hearing Research*, 88, 19-26.
- WANG, A., LIANG, Y., FRIDELL, R. A., PROBST, F. J., WILCOX, E. R., TOUCHMAN, J. W., MORTON, C. C., MORELL, R. J., NOBEN-TRAUTH, K., CAMPER, S. A. & FRIEDMAN, T. B. 1998. Association of Unconventional Myosin *MYO15* Mutations with Human Nonsyndromic Deafness *DFNB3*. *Science*, 280, 1447.
- WANG, H. C., LIN, C. C., CHEUNG, R., ZHANG-HOOKS, Y., AGARWAL, A., ELLIS-DAVIES, G., ROCK, J. & BERGLES, D. E. 2015. Spontaneous Activity of Cochlear Hair Cells Triggered by Fluid Secretion Mechanism in Adjacent Support Cells. *Cell*, 163, 1348-59.
- WANG, J. & PUEL, J.-L. 2020. Presbycusis: An Update on Cochlear Mechanisms and Therapies. *Journal of clinical medicine*, 9, 218.
- WANG, X., TRUONG, T., BILLINGS, P. B., HARRIS, J. P. & KEITHLEY, E. M. 2003. Blockage of immune-mediated inner ear damage by etanercept. *Otol Neurotol*, 24, 52-7.
- WANGEMANN, P. 2002. K⁺ cycling and the endocochlear potential. *Hearing Research*, 165, 1-9.
- WANGEMANN, P. & SCHACHT, J. 1996. Springer Handbook of Auditory Research: The Cochlea.
- WARCHOL, M. E. 2019. Interactions between Macrophages and the Sensory Cells of the Inner Ear. *Cold Spring Harb Perspect Med*, 9.
- WARR, W. B. 1975. Olivocochlear and vestibular efferent neurons of the feline brain stem: Their location, morphology and number determined by retrograde axonal transport

- and acetylcholinesterase histochemistry. *Journal of Comparative Neurology*, 161, 159-181.
- WARR, W. B., BOCHE, J. B. & NEELY, S. T. 1997. Efferent innervation of the inner hair cell region: origins and terminations of two lateral olivocochlear systems. *Hear Res*, 108, 89-111.
- WARR, W. B. & GUINAN, J. J. 1979. Efferent innervation of the organ of corti: two separate systems. *Brain Research*, 173, 152-155.
- WEDEMEYER, C., VATTINO, L. G., MOGLIE, M. J., BALLESTERO, J., MAISON, S. F., DI GUILMI, M. N., TARANDA, J., LIBERMAN, M. C., FUCHS, P. A., KATZ, E. & ELGOYHEN, A. B. 2018. A Gain-of-Function Mutation in the $\alpha 9$ Nicotinic Acetylcholine Receptor Alters Medial Olivocochlear Efferent Short-Term Synaptic Plasticity. *J Neurosci*, 38, 3939-3954.
- WEIL, D., BLANCHARD, S., KAPLAN, J., GUILFORD, P., GIBSON, F., WALSH, J., MBURU, P., VARELA, A., LEVILLIERS, J., WESTON, M. D. & ET AL. 1995. Defective myosin VIIA gene responsible for Usher syndrome type 1B. *Nature*, 374, 60-1.
- WEIL, D., EL-AMRAOUI, A., MASMOUDI, S., MUSTAPHA, M., KIKKAWA, Y., LAINÉ, S., DELMAGHANI, S., ADATO, A., NADIFI, S., ZINA, Z. B., HAMEL, C., GAL, A., AYADI, H., YONEKAWA, H. & PETIT, C. 2003. Usher syndrome type I G (USH1G) is caused by mutations in the gene encoding SANS, a protein that associates with the USH1C protein, harmonin. *Human Molecular Genetics*, 12, 463-471.
- WELL, D., BLANCHARD, S., KAPLAN, J., GUILFORD, P., GIBSON, F., WALSH, J., MBURU, P., VARELA, A., LEVILLIERS, J., WESTON, M. D., KELLEY, P. M., KIMBERLING, W. J., WAGENAAR, M., LEVI-ACOBAS, F., LARGET-PIET, D., MUNNICH, A., STEEL, K. P., BROWN, S. D. M. & PETIT, C. 1995. Defective myosin VIIA gene responsible for Usher syndrome type 1B. *Nature*, 374, 60-61.
- WIECHERS, B., GESTWA, G., MACK, A., CARROLL, P., ZENNER, H. P. & KNIPPER, M. 1999. A changing pattern of brain-derived neurotrophic factor expression correlates with the rearrangement of fibers during cochlear development of rats and mice. *J Neurosci*, 19, 3033-42.
- WILLOTT, J. F. 1986. Effects of aging, hearing loss, and anatomical location on thresholds of inferior colliculus neurons in C57BL/6 and CBA mice. *J Neurophysiol*, 56, 391-408.

- WILLOTT, J. F. & BROSS, L. S. 1990. Morphology of the octopus cell area of the cochlear nucleus in young and aging C57BL/6J and CBA/J mice. *J Comp Neurol*, 300, 61-81.
- WILLOTT, J. F., ERWAY, L. C., ARCHER, J. R. & HARRISON, D. E. 1995. Genetics of age-related hearing loss in mice. II. Strain differences and effects of caloric restriction on cochlear pathology and evoked response thresholds. *Hearing Research*, 88, 143-155.
- WINSLOW, R. L. & SACHS, M. B. 1987. Effect of electrical stimulation of the crossed olivocochlear bundle on auditory nerve response to tones in noise. *J Neurophysiol*, 57, 1002-21.
- WISE, A. K., HUME, C. R., FLYNN, B. O., JEELALL, Y. S., SUHR, C. L., SGRO, B. E., O'LEARY, S. J., SHEPHERD, R. K. & RICHARDSON, R. T. 2010. Effects of localized neurotrophin gene expression on spiral ganglion neuron resprouting in the deafened cochlea. *Mol Ther*, 18, 1111-22.
- WONG, A. B., JING, Z., RUTHERFORD, M. A., FRANK, T., STRENZKE, N. & MOSER, T. 2013. Concurrent maturation of inner hair cell synaptic Ca²⁺ influx and auditory nerve spontaneous activity around hearing onset in mice. *The Journal of neuroscience : the official journal of the Society for Neuroscience*, 33, 10661-10666.
- WRIGHT, A., DAVIS, A., BREDBERG, G., ULEHLOVA, L. & SPENCER, H. 1987. Hair cell distributions in the normal human cochlea. *Acta Otolaryngol Suppl*, 444, 1-48.
- WU, Y.-C., RICCI, A. J. & FETTIPLACE, R. 1999. Two Components of Transducer Adaptation in Auditory Hair Cells. *Journal of Neurophysiology*, 82, 2171-2181.
- XIONG, W., YU, S., LIU, K. & GONG, S. 2020. Loss of cochlear ribbon synapses in the early stage of aging causes initial hearing impairment. *Am J Transl Res*, 12, 7354-7366.
- XU, K., CHEN, S., XIE, L., QIU, Y., BAI, X., LIU, X. Z., ZHANG, H. M., WANG, X. H., JIN, Y., SUN, Y. & KONG, W. J. 2020. Local Macrophage-Related Immune Response Is Involved in Cochlear Epithelial Damage in Distinct Gjb2-Related Hereditary Deafness Models. *Front Cell Dev Biol*, 8, 597769.
- YANG, W., VETHANAYAGAM, R. R., DONG, Y., CAI, Q. & HU, B. H. 2015. Activation of the antigen presentation function of mononuclear phagocyte populations associated with the basilar membrane of the cochlea after acoustic overstimulation. *Neuroscience*, 303, 1-15.
- YASUNAGA, S., GRATI, M., COHEN-SALMON, M., EL-AMRAOUI, A., MUSTAPHA, M., SALEM, N., EL-ZIR, E., LOISELET, J. & PETIT, C. 1999. A mutation in OTOF, encoding otoferlin, a

- FER-1-like protein, causes DFNB9, a nonsyndromic form of deafness. *Nat Genet*, 21, 363-9.
- ZACHARY, S. P. & FUCHS, P. A. 2015. Re-Emergent Inhibition of Cochlear Inner Hair Cells in a Mouse Model of Hearing Loss. *The Journal of Neuroscience*, 35, 9701.
- ZAMPINI, V., JOHNSON, S. L., FRANZ, C., LAWRENCE, N. D., MÜNKNER, S., ENGEL, J., KNIPPER, M., MAGISTRETTI, J., MASETTO, S. & MARCOTTI, W. 2010. Elementary properties of CaV1.3 Ca(2+) channels expressed in mouse cochlear inner hair cells. *The Journal of physiology*, 588, 187-199.
- ZHANG, D. S., PIAZZA, V., PERRIN, B. J., RZADZINSKA, A. K., PO CZATEK, J. C., WANG, M., PROSSER, H. M., ERVASTI, J. M., COREY, D. P. & LECHENE, C. P. 2012. Multi-isotope imaging mass spectrometry reveals slow protein turnover in hair-cell stereocilia. *Nature*, 481, 520-4.
- ZHANG, G. & GHOSH, S. 2001. Toll-like receptor-mediated NF-kappaB activation: a phylogenetically conserved paradigm in innate immunity. *J Clin Invest*, 107, 13-9.
- ZHANG, Y., RIESTERER, C., AYRALL, A. M., SABLITZKY, F., LITTLEWOOD, T. D. & RETH, M. 1996. Inducible site-directed recombination in mouse embryonic stem cells. *Nucleic Acids Res*, 24, 543-8.
- ZHAO, B., WU, Z., GRILLET, N., YAN, L., XIONG, W., HARKINS-PERRY, S. & MÜLLER, U. 2014. TMIE is an essential component of the mechanotransduction machinery of cochlear hair cells. *Neuron*, 84, 954-967.
- ZHENG, J., SHEN, W., HE, D. Z. Z., LONG, K. B., MADISON, L. D. & DALLOS, P. 2000. Prestin is the motor protein of cochlear outer hair cells. *Nature*, 405, 149-155.
- ZHONG, Z. A., SUN, W., CHEN, H., ZHANG, H., LAY, Y. E., LANE, N. E. & YAO, W. 2015. Optimizing tamoxifen-inducible Cre/loxp system to reduce tamoxifen effect on bone turnover in long bones of young mice. *Bone*, 81, 614-619.
- ÜNAL, M., TAMER, L., DOĞRUER, Z. N., YILDIRIM, H., VAYISOĞLU, Y. & ÇAMDEVIREN, H. 2005. N-Acetyltransferase 2 Gene Polymorphism and Presbycusis. *The Laryngoscope*, 115, 2238-2241.